T182
50601
50601
4
540
KON
CENTRAL LIBRARY
TEZPUR UNIVERSITY
Accession No. 50601
Date 14/6/12
CENTRAL LIBRARY, T. U
ACC. NO. T 182

STUDIES ON CARBON FILLED π - CONJUGATED POLYMERS AND THEIR APPLICATIONS

A thesis submitted
in partial fulfillment of the requirements for the degree of

Doctor of Philosophy

By

Surajit Konwer

Registration No.025 of 2010

School of Science and Technology

Department of Chemical Sciences

Tezpur University

Napaam, Tezpur - 784028

Assam, India

April, 2011

Dedicated to my Parents

with love and gratitude

Studies on carbon filled π-conjugated polymers and their applications

ABSTRACT

The present thesis deals with synthesis, characterization and evaluation of optical, thermal, electrical and electrochemical properties of carbon filled polyaniline and polypyrrole composites. A considerable effort has been devoted to the synthesis of polymer composites with special emphasis on the improved electrical and electrochemical properties for possible application in chemical sensor and super capacitor application. The influence of carbon fillers and effect of temperature on electrical properties of the composites are also reported. The contents of the thesis have been compiled into five chapters.

Chapter 1 deals with the general introduction on π-conjugated polymers and different carbon fillers, their importance, history and various fields of applications. Brief reviews on different properties of π-conjugated polymers with special emphasis to optical, electrical, electrochemical properties have been described in this chapter. This chapter also focuses the scopes and objectives along with the plans of work of the present investigation.

Chapter 2 reports the synthesis and characterization of carbon fillers viz. expanded graphite and graphene oxide from natural graphite flake. The synthesis of polyaniline and polypyrrole composites with various carbon fillers have also been discussed in this chapter. The polymer composites were prepared by in-situ chemical polymerization and characterized by FTIR, XRD, TGA, SEM and TEM analysis.

Chapter 3 describes the thermal, optical, electrical and electrochemical properties of the carbon filled π-conjugated polyaniline and polypyrrole composites. Thermal and optical properties of the synthesized polymer composites were investigated by TGA and UV-vis study. The thermal properties of the composites were much improved after incorporation of the carbon filler compared to the pristine polymer. The current-voltage relationship, dc electrical conductivity of the polymer composites are thoroughly studied in this chapter. The influence of carbon fillers like graphite, EG and GO on the

reduction potential / oxidation potentials of the polyaniline and polypyrrole composites are also discussed in this chapter. Furthermore, band gap of polymer composites were measured electrochemically and compared with optical method.

Chapter 4 includes the study of sensor and super capacitor application of the synthesized polymer composites. Polyaniline/graphene oxide composite has been applied as methanol gas sensing material. The sensing properties of expanded graphite filled polyaniline and polypyrrole composites for volatile organic compounds have also been described in this chapter. The changes in resistivity of polymer composite on exposure to various concentration of vapour are discussed in this chapter. The study of capacitance behaviour of synthesized polypyrrole/graphite, polyaniline/graphene oxide composites has also been reported in this chapter.

Chapter 5, the last chapter of the thesis includes the concluding remarks, highlights of the findings and future scopes of the present investigation. The synthesized polymer composites show improved thermal stability than the pristine polymer. The dc electrical conductivity of the synthesized polymer composites dramatically increases compared to the pure polymer with the increase in carbon fillers and temperature as well. The composites show gratifying reversible electrochemical response to intaking charge capacity almost unchanged even upto 150^{th} cycles. Considering their high conductivities and reversible electrochemical properties, it appears that the polymer composites have potential for application in sensors and super capacitor electrodes.

DECLARATION BY THE CANDIDATE

The thesis entitled "***Studies on carbon filled π-conjugated polymers and their applications***" is being submitted to Tezpur University in partial fulfillment for the award of the degree of Doctor of Philosophy in *Chemical Sciences* is a record of bonafide research work accomplished by me under the supervision of Prof. S. K. Dolui.

All helps received from various sources have been duly acknowledged.

No part of this thesis has been submitted elsewhere for award of any other degree.

Surajit Konwer

Date: 27/04/11

Surajit Konwer

Place: Tezpur

Department of Chemical Sciences
Tezpur University
Assam, India

TEZPUR UNIVERSITY

(A Central University established by an Act of Parliament)
Napaam, Tezpur-784028
DISTRICT: SONITPUR:: ASSAM:: INDIA

Ph: 03712-267004(O) 9957198489(m) Fax: 03712-267006 email: dolui@tezu.ernetin

CERTIFICATE OF THE PRINCIPAL SUPERVISOR

This is to certify that the thesis entitled "***Studies on carbon filled π-conjugated polymers and their applications***" submitted to the School of *Science and Technology*, Tezpur University in partial fulfillment for the award of the degree of Doctor of Philosophy in the Department of Chemical Sciences is a record of research work carried out by ***Mr. Surajit Konwer*** under my supervision and guidance.

All help received by him from various sources have been duly acknowledged.

No part of this thesis has been submitted elsewhere for award of any other degree.

Date: 27 April 2011

Place: Tezpur

S. K. Dolui
Professor
Department of Chemical Sciences
School of Science and Technology
Tezpur University
Assam, India

TEZPUR UNIVERSITY

(A Central University established by an Act of Parliament)

Napaam, Tezpur-784028

DISTRICT: SONITPUR:: ASSAM:: INDIA

Ph: 03712-267004(O) 9957198489(m) Fax: 03712-267006 email: adm@tezu.ernet.in

Certificate of the External Examiner and ODEC

This is to certify that the thesis entitled "***Studies on carbon filled π-conjugated polymers and their applications***" submitted by **Mr. Surajit Konwer** to Tezpur University in the Department of Chemical Sciences under the school of Science and Technology in partial fulfillment of the requirement for the award of the degree of Doctor of Philosophy in Chemical Sciences has been examined by us on _____ and found to be satisfactory.

Signature of:

Principal Supervisor *External Examiner*

Associate Supervisor

Co-Supervisor

Date: _____

Preface

Conjugated polymers (CPs) are valuable material for scientists to design electronic devices like light emitting diode (LED) to generate light, photovoltaic cell to generate power, sensor to detect materials etc. The advancement made in this field is so rapid that almost every day a new polymer or a modification of existing polymer is appearing in the journals.

CPs offer several advantages over inorganic and organic molecules such as flexibility, relative ease of processing by common techniques (spin and blade coating, ink – jet printing), or the ability to architect a compound for efficient energy conversion in solar cells. A large number of different classes of conjugated polymers have been developed such as polyaniline (PA), polypyrroles (PPy), poly(N-vinylcarbazole)s, poly(fluorene)s, poly(p-phenylene vinylenes), and poly(thiophenes) etc. Amongst the various π-conjugated polymers the greater part of this work has centred on PA and PPy mainly because of their rather straightforward preparation methods, reasonably stable in air, good electrochemical properties and thermal stability. Both the polymers also show their capability to store electrical charges which can be recovered upon demand.

In many instances polymers need to fulfil contradictory demands which are not possible with a single polymer or a mere physical blend of two polymers. The principal problem encountered with the potential utilization of virgin CPs like PA, PPy, etc. is their poor processability and the lake of essential mechanical properties. Attempts have been made earlier to incorporate plastics or rubber with CPs in order to improve the processability of the said mixed material without losing the mechanical properties. To overcome these drawbacks, some filler are incorporated into these polymer matrices to form composite materials.

The present thesis deals with synthesis, characterization and evaluation of optical, thermal, electrical and electrochemical properties of carbon filled polyaniline and polypyrrole composites. A considerable effort has been devoted to the synthesis of polymer composites with special emphasis on the improved electrical and electrochemical properties for possible application in sensor and super capacitors. The influence of carbon fillers and effect of temperature on electrical properties of the composites are also reported.

We hope that this study contributes a little knowledge to the rapidly advancing field of carbon filled π-conjugated polymers and also opens up the possibilities of further research on the subject.

This research was carried out in the Department of Chemical Sciences, Tezpur University with financial assistance from the Board of Research in Nuclear Science (BRNS), Department of Atomic Energy (DAE) and under sponsored research scheme.

Surajit Konwer

Acknowledgement

I express my deep gratitude and respects to my guide Prof. S. K. Dolui for his keen interest and valuable guidance, strong motivation constant encouragement and freedom for work during the course of the work. I thank him from the bottom of my heart for introducing me to the science of electrically conducting π-conjugated polymer.

With a deep sense of gratitude I would like to thank Late Prof. Dolon Konwer for his kind advice, support and constant inspiration.

I am grateful to all the faculty members of Department of Chemical Sciences for their help and suggestions.

I wish my sincere thanks to my entire lab colleague Jatin, Binod, Anamika, Lakhya, Muhsina, Isha, Amar, Monalisha, Chandramika, Dhaneswar and Pranab and wish to thank all my friends for their cooperation during entire work period.

My special thanks to my friend Rana, Sunanta, Pratim, Shreemoyee, Ankur, Uday, Kandarpa, Kamal and Ratan for their timely help in many situations.

I gratefully acknowledged Mrs. Sutapa Dolui and Swapnil Dolui for their constant encouragement, hospitality and warmth.

My heartfelt thank goes to the technical staff, for instrumental and library facilities throughout the study. Special thanks also goes to office staff, Chemical Sciences Department. I would like to thank Jose and Anjali, NEHU, Shilling for TEM analysis.

I am grateful to Board of Research in Nuclear Science (BRNS) and Department of Atomic Energy (DAE) for funding the projects to complete this research.

Finally, I thank the authorities of Tezpur University for granting me the permission to do this work.

Last but not least, I would like to thank my parents and all my family members for their blessing, love, constant encouragement, inspiration and support throughout my studies to fulfill my dream.

Surajit Konwer

Contents

Abstract			**i**
Preface			**vi**
Acknowledgement			**viii**
Table of Contents			**ix**
List of Tables			**xi**
List of Figures			**xii**
List of Schemes			**xv**
Abbreviations			**xvi**
Chapter 1:	**Introduction**		
	1.1	Conjugated polymers	1
	1.2	Doping of conjugated polymers	5
	1.3	Types of Conducting Polymers	8
	1.4	Properties of π-Conjugated Polymers	26
	1.5	Application of Conducting Polymers	34
	1.6	Research Background and Challenges (Scopes and Objectives)	38
		References	41
Chapter 2:	**Synthesis and characterization of carbon filled π-conjugated polymers**		
	2.1	Introduction	60
	2.2	Materials	60
	2.3	Synthesis and Modification of Pi-Conjugated Polymer	60
	2.4	Instrumentations	65
	2.5	Results and discussions	66
	2.6	Conclusions	91
		References	93

Chapter 3: Study of electrochemical and optical properties of conjugated polymers

3.1	Introduction	96
3.2	Materials	96
3.3	Instrumentations	96
3.4	Results and Discussion	100
3.5	Conclusions	132
	References	134

Chapter 4: Sensors Application and Capacitance Behaviour of Carbon Filled π-Conjugated Polymers

4.1	Introduction	136
4.2.	Materials	136
4.3.	Experimental	136
4.4	Carbon Filled π-Conjugated Polymer as Gas Sensor	137
4.5	Capacitance Behaviour of Carbon Filled π-Conjugated Polymers	150
4.6	Conclusions	155
	References	157

Chapter 5: Conclusion and future scopes

5.1	Conclusions	161
5.2	Future Scope of the Present Investigation	164
	List of publications	165

List of Tables

Chapter	Table	Title	
2	2.1-2.5	FTIR assignment of graphite, EG, GO, PA, and PPy composites	69-75
	2.6-2.7	XRD data of PA and PPy composites	77-79
Chapter 3	3.1-3.6	Conductivity of polymer composites at various Temperatures	111-119
	3.7-3.13	Electrochemical data of polymer composites	122-128
	3.14-3.15	Electrochemical and optical band gap of polymer composites	129

List of Figures

Chapter	Figure	Title	
1	1.1	Formation σ and π molecular orbital from two sp^2 hybridized carbon atoms	2
	1.2	Chemical structure of some conjugated polymers	3
	1.3	Chart of typical conductivities of some metals and doped conjugated polymers	4
	1.4	Graphite lattice showing the ABAB stacking of carbon layers	19
	1.5	Atomic structures of CNTs (a) an armchair and (b) a ziz-zag nanotubes	20
	1.6	Schematic models for the microstructure of activated carbon fibers	21
	1.7	Graphene: mother of all graphitic forms	22
	1.8	Collection of energy states of metal, semiconductor and graphite	23
	1.9	Defects in conjugated chains: a "physical-chemical dictionary	29
	1.10	The energy level scheme for the soliton and polarons	30
	1.11	A voltammogram of an ideal system for forward scan	31
	1.12	Colour tuning in π-conjugated polymers	33
Chapter 2	2.1-2.7	FTIR spectra of graphite, EG, GO and polymer composites	68-75
	2.8-2.10	XRD of graphite, EG, GO polymer composites	76-78
	2.11-2.17	SEM images of Graphite, EG, GO polymer composites	79-83
	2.18-2.20	TEM images of GO, PA/GO, PPy/GO and	

		SMA-PA/G core-shell composite	84-85
	2.21-2.29	TGA of polymer composites	86-91
Chapter	3.1	Two-probe set up	99
3	3.2	Diagram of the Four-probe set-up	100
	3.3	Circuit of the four probe resistivity measurements	101
	3.4	The complete electrochemical setup	102
	3.5-3.10	UV-vis spectra of polymer composites	103-107
	3.11-3.17	I–V plot of polymer composites composite	108-111
	3.18-3.26	Conductivity of polymer composites	113-120
	3.27	Measurement of onset in CV	122
	3.28-3.34	CV of polymer composites	123-129
	3.35-3.41	CV (repeated cycle) of polymer composites	130-132
Chapter	4.1	Gas sensor set – up	138
4	4.2	Response curves of (a) pure PA and PA/GO exposed to saturated vapours of methanol at different concentrations (b) 100 (c) 200 (d) 300 and (e) 500 ppm	140
	4.3	Response curves of PA/GO composite exposed to saturated vapours of (a) ethanol and (b) propanol	141
	4.4	Selectivity of PA/GO composite	142
	4.5	DFT optimized geometry of the bare polymer and methanol showing the possibility of H-bonding	142
	4.6-4.7	Actual response curves of (a) PA and (b) PA/GO with various concentrations of methanol vapours	143
	4.8	FTIR spectra of (a) GO, (b) PA, (c) PA/GO in air and (d) PA/GO with methanol	144
	4.9	Response curves of (a) pure PA and PA/GO exposed to saturated vapours of acetone at (b) 100, (c) 200 and (d) 300 concentration	145

4.10	Response curves of (a) pure PA and PA/EG Exposed to saturated vapours of chloroform at (b) 100, (c) 200 and (d) 300 ppm concentrations	146
4.11	Response curves of (a) pure PA and PA/EG Exposed to carbon tetrachloride at (b) 100, (c) 200 and (d) 300 ppm concentrations	148
4.12	Detection limit of PA/EG against the gas concentration (a) acetone, (b) carbon tetrachloride and (c) chloroform	149
4.13	Selectivity of PA/EG composite with 300 ppm concentration VOCs	149
4.14	Geometrical structure of supercapacitor fabrication	151
4.15	CV of (a) pure PPy, (b) PPy/GO (5%) and (c) PPy/GO (10%) pellet electrode at scan rate 50 mV/s	152
4.16	Galvanostatic discharge curve, (a) pure PPy, (b) PPy/GO (5%) and (c) PPy/GO (10%) pellet electrode at current 2mA	153
4.17	CV of (a) pure PA, (b) PA/EG (5%) and (c) PA/EG (10%) pellet electrode at scan rate, 50 mV/s	154
4.18	Galvanostatic discharge curve of (a) pure PPy, (b) PA/EG (5%) and (c) PA/EG (10%) pellet electrode at current 2mA	155

List of Schemes

Chapter	Scheme	Title	
1	1.1	Doping of polyaniline	6
	1.2	Various oxidation states of polyaniline	11
	1.3	Synthesis of PA by oxidative coupling method	12
	1.4	Electrochemical synthesis of Polyaniline	14
	1.5	Possible structure of PPy	15
	1.6	Reaction scheme for PPy chemical synthesis	16
	1.7	Mechanism for the electropolymerization of pyrrole	17
	1.8	Polyphthalocyanines, an example of organometallic polymeric conductors	24
	1.9	Aromatic heterocyclic polyimide	25
	1.10	One electron band model for electrical conduction	28
Chapter 2	2.1	Illustration of the process of preparation of PA/EG composite	66
	2.2	Interactions between PA and GO	67
	2.3	Schematic representation of the formation of the core-shell composite particles	67
Chapter 4	4.1	Schematic representation depicting interaction of methanol vapours with PA/GO composite	141
	4.2	Schematic representation of the proposed hydrogen bonding interaction between acetone vapour and PA	145
	4.3	Schematic representation of the proposed hydrogen bonding interaction between chloroform vapour and PA	147
	4.4	Schematic representation of the proposed hydrogen bonding interaction between carbon tetrachloride vapour and PA	148

Abbreviations used in the thesis

Ani	Aniline
APS	Ammonium per sulphate
ATP	Adenosine tri phosphate
CNT	Carbon nanotube
CP	Conjugated polymer
CV	Cyclic voltammogram
DNAQ	1,5-dinitroantraquinone
DFT	Density Functional Theory
EG	Expanded Graphite
FTIR	Fourier Transform Infra-red Spectroscopy
GGA	Generalized Gradient Approximation
GIC	Graphite intercalated compound
GR	Graphene
GO	Graphene oxide
GRIM	Grignard Metathesis
HOMO	Highest Occupied Molecular Orbital
ITO	Indium tin oxide
LED	Light Emitting Diode
LUMO	Lowest Unoccupied Molecular Orbital
MWCNT	Multi-walled Carbon nanotube
MEH-PPV	2-methoxy-5-(2'-ethylhexyloxy)-*p*-phenylene vinylene
MIS	metal/insulator/semiconductor
NMP	N-methyl pyrrolidone
PA	Polyaniline
PA/G	Polyaniline/graphite
PA/EG	Polyaniline/expanded graphite
PA/G	Polyaniline/graphene oxide
Py	Pyrrole

PPy	Polypyrrole
PPy/G	Polypyrrole/graphite
PPy/EG	Polypyrrole/expanded graphite
SCE	Saturated Calomel Electrode
SEM	Scanning Electron Microscopy
SMA	Styrene-methyl acrylate
SMA-/PA/G	Polystyrene-co-methyl acrylate -polyaniline/graphite
TNF	2,4,7-trinitrofluorenone
THF	Tetra hydro furan
TEM	Transmission Electron Microscopy
TGA	Thermogravimetric Analysis
UV-vis	Ultra Violet-visible
VOC	Volatile organic compound
XRD	X-ray Diffraction

Symbols used in the thesis:

Å	Armstrong
°C	degree centigrade
cm	centimetre
eV	Electron volt
F	Faraday
g	gram
h	hour
L	liter
M	mole
mA	milliampere
mL	milliliter
min	minute
kV	kilovolt
ppm	perts per million
S	Siemen
w	weight
vol	volume
V	volt
α	alpha
λ	lamda
θ	theta

Chapter 1

Introduction

1.1 Conjugated Polymers

Right from preparing daily commodities to sophisticated and artificial heart valve, polymers provide solutions to almost all deeds in our life. Till the other day, heat resistant, electrically conducting, ferromagnetic, semiconducting and superconducting polymers were a dream, but today, all these miracles are coming true, at least on laboratory scale and a few of them have also been commercialized.

Conjugated polymers (CPs) consisting of an alternating single bond and double bond structure along the polymer backbone exhibit semiconducting behaviour. Today, CPs represent one of the most highly progressive fields of polymer research and mesmerize much importance in light emitting diode,[1-5] super capacitors,[6-15] batteries,[16-19] photovoltaic cell,[20-23] sensors[24-29] etc. This is particularly exciting because it creates a new field of research and a number of opportunities on the boundary between chemistry and condensed-matter physics. The CPs possess a relatively large number of delocalized π-electrons, a fairly large energy gap exists between the valence band and the conducting band (greater than 1 eV). Thus these polymers are considered to be semi-conducting. The electronic configuration of CPs is fundamentally different where the chemical bonding leads to one unpaired electron per carbon atom (**Figure 1.1**). The carbon orbitals are in sp^2 hybridized and the orbitals of successive carbon atoms along the backbone overlap, leads to electron delocalization of the polymer. This electronic delocalization provides the highway for charge mobility along the backbone of the polymer chain. Therefore, the electronic structure in CPs is determined by the chain symmetry, i.e. the number and kind of atoms within the repeated unit, with the result that such polymers can exhibit semiconducting or even metallic properties.

Electrically conducting polymers are designated as the fourth generation of polymeric materials. Since Shirakawa, Heeger and MacDiarmid discovered that polyacetylene can reach extremely high electronic conductivities,[30, 31] the field of CPs has attracted the interest of thousands of scientists and researchers. Much of the combined research efforts of industrial, academic and government researchers have been directed toward developing CP based materials that are mechanically and electronically stable for end use applications, easily processible, can be produced at a low cost. Many interesting

conducting polymers polyanilines (PA), polypyrroles (PPy), polythiophenes, polyphenylenes and poly(*p*-phenylene vinylene)s have attracted the most attention.

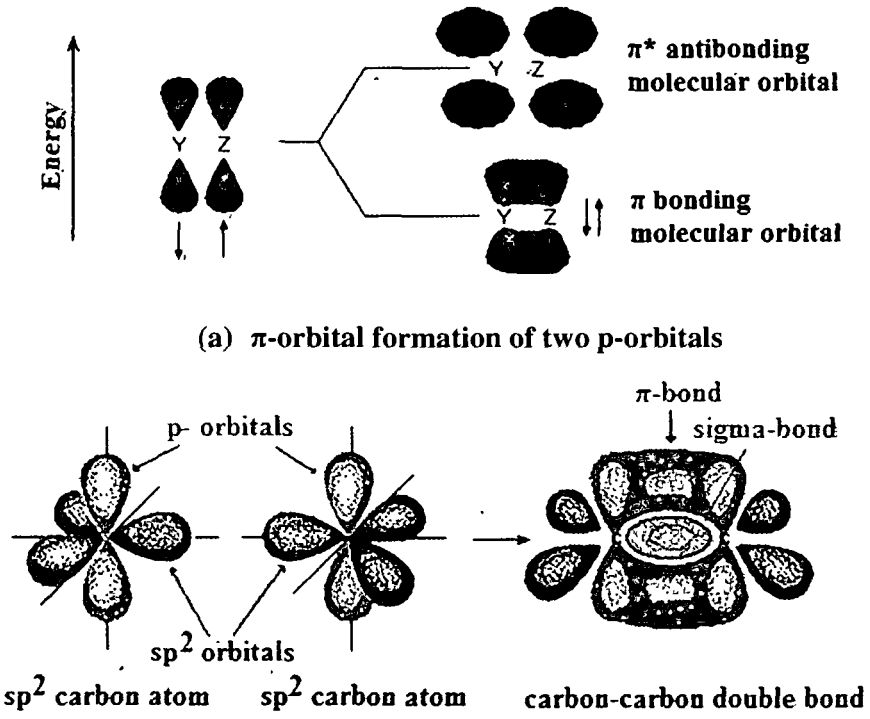

Figure 1.1 Formation σ and π molecular orbital from two sp^2 hybridized carbon atoms

In order to make the CPs electronically conductive, it is necessary to introduce some mobile carriers into the conjugated system; this is achieved by oxidation or reduction reactions and the insertion of counter ions (called 'doping'). Dedoped CPs are semiconductors with band gaps ranging from 1 eV to several eV. Therefore their room temperature conductivities are very low, typically 10^{-8} S/cm or lower. However, by doping, conductivity can be increased by many orders of magnitude. The highest value of conductivity reported to date has been obtained in iodine-doped polyacetylene (>10^5 S/cm). **Figure 1.2** shows the structure of some CPs in their neutral insulating form.

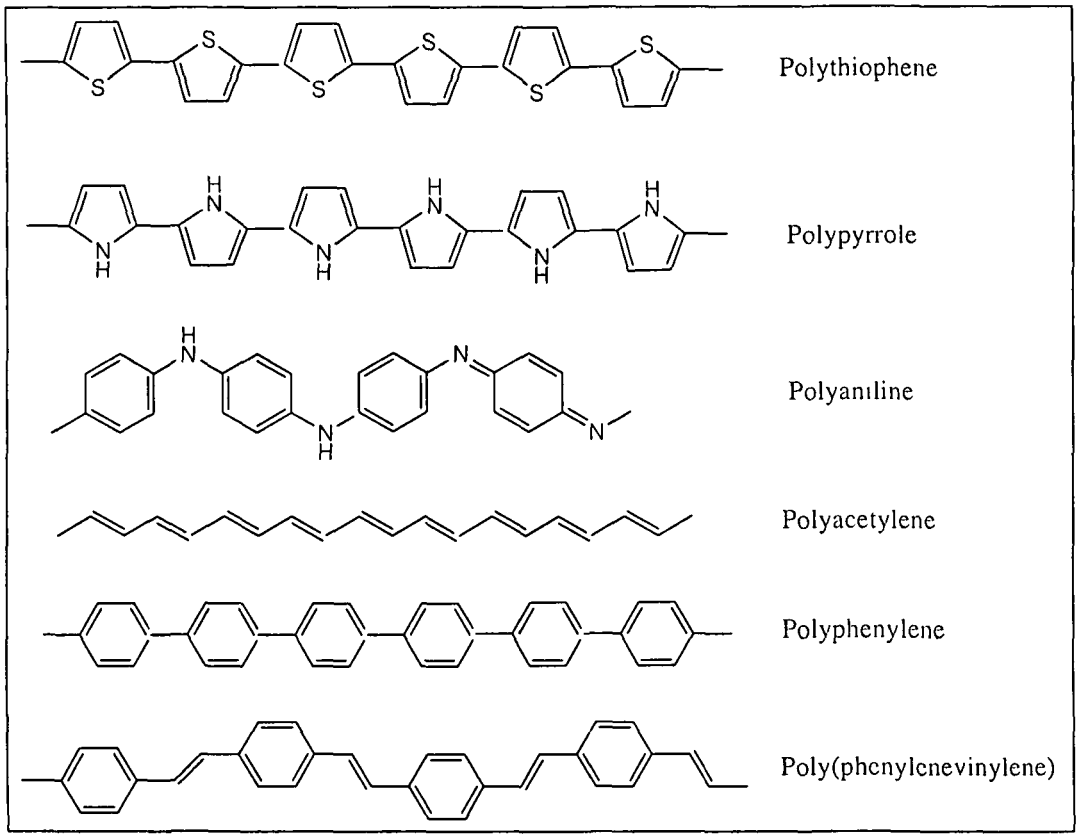

Figure 1.2 Chemical structure of some conjugated polymers

The predicted theoretical limit for the electrical conductivity of doped polymers was about 2×10^7 S/cm, more than an order of magnitude higher than that of copper. In general, the electrical conductivity of insulators is typically less than 10^{-14} S/cm. For semi-insulating or semiconductive materials the range is 10^{-14} to ~10^2 S/cm whereas for semi-metals and metals it is greater than 10^2 S/cm with a maximum value of ~10^{10} S/cm. Conductivity of some materials including some CPs,[30-32] are shown in **Figure 1.3**.

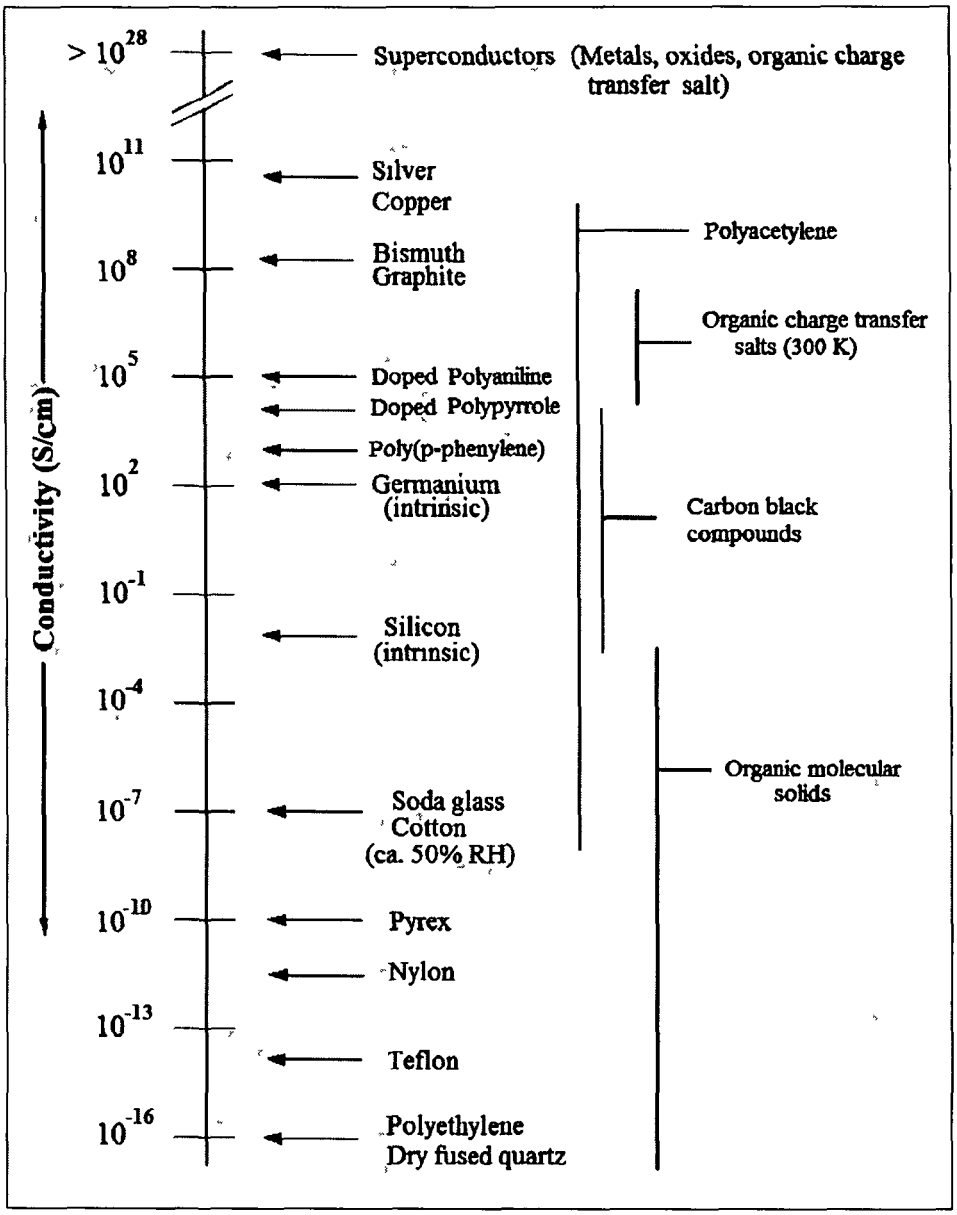

Figure 1. 3 Chart of typical conductivities of some metals and doped conjugated polymers[33, 34]

In the year 1979, scientist Su, Schrieffer, and Heeger had proposed a theoretical model describing conductivity in doped CPs,[35, 36] and a collection of new polymers had been synthesized, including the luminescent polymer poly (p-phenylene).[37] Additionally, in the same year it was discovered that these materials could also be electrochemically doped to achieve a conductive state, and that this process was reversible.[38] In the 1980's and 1990's the research focus tended to be on demonstrating the usefulness of

semiconducting and conducting polymers in a broad range of applications. Organic field-effect transistors,[39] electrochromic devices,[40] actuators,[41] supercapacitors,[6-15] sensors,[24-29] and several other applications based on CPs all made their appearance in the late 1980's to till date.[42-47] In recent researches the demand for electrically conducting polymers in the electronics industry by using high loading of conductive powders such as graphite,[48-50] Carbon nanotubes (CNTs),[51-53] graphene,[54-56] Titanium di-oxide (TiO_2),[57-59] Zinc oxide (ZnO)[60-61] etc. with the polymer matrix.

1.2 Doping of Conjugated Polymers

The conjugated polymers can become highly electrically conductive after some structural modification process called "doping". Doping can be simply regarded as the insertion or ejection of electrons which results in dramatic changes in the electronic, electrical, magnetic, optical, and structural properties of the CPs. There is a distinct difference in between the doping of polymeric semiconductors and conventional (or inorganic) semiconductors. In case of inorganic semiconductors, on incorporation of specific dopant, n-type or p-type in ppm level, only lattice becomes highly distorted due to their three dimensional crystal lattice. The dopant is distributed along specific crystal orientations in specific sites on a repetitive basis. Whereas in CPs, the doping involves random dispersion or aggregation of dopants in molar concentrations in the disordered structure of entangled chains of the CPs. In addition, the incorporation of dopants in the quasi one dimensional polymer systems considerably disturbs the chain order leading to reorganization of the polymer. Doping process is reversible, and it produces the original polymer with little or no degradation of the polymer backbone. Doping of CPs mainly leads to the formation of conjugation defects, viz. solitons, polarons or bipolarons in the polymer chain. On the other hand, doping of inorganic semiconductors can produces either holes in the valence band or electrons in the conduction band. The conductivity in CPs mostly depends on carrier mobility, nature and concentration of dopants, homogeneity of doping, crystallinity and morphology of polymers.

In the doped state, the backbone of a conducting polymer consists of a delocalized π - system. In the undoped state, the polymer may have a conjugated backbone which is retained in a modified form after doping, or it may have a nonconjugated backbone, as in

polyaniline (leucoemeraldine base form), which becomes truly conjugated only after protonic acid doping which is shown in the **Scheme 1.1**.

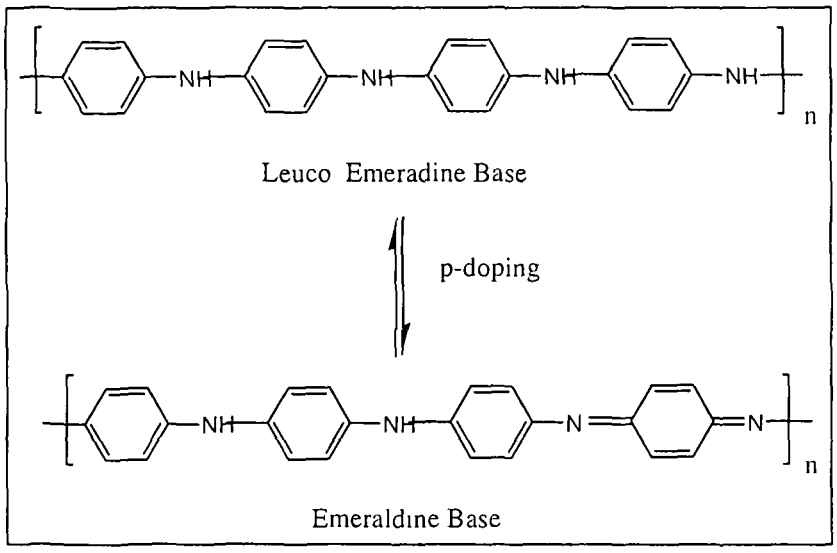

Scheme 1.1 Doping of polyaniline

1.2.1 Different types of Doping

Redox doping

All CPs viz. PA, PPy, polythiophene, etc. undergo p or n- redox doping by chemical and electrochemical processes during which the number of electrons associated with the polymer backbone changes. The p-doping of CPs occurs by partial oxidation of the π-backbone of the polymer. It was first discovered by treating trans - $(CH)_x$ with an oxidizing agent such as iodine.[62, 63] The n-doping of CPs is a partial reduction of the π-backbone of the conjugated system which was also discovered using trans - $(CH)_x$ by treating it with a reducing agent such as sodium naphthalide.

Photo doping

When trans - $(CH)_x$ is exposed to radiation of energy greater than its band gap, electrons are promoted across the gap and polymer undergoes "photo-doping".

Charge injection doping

Charge injection doping is most conveniently carried out using a metal/insulator/semiconductor configuration involving a metal and a conducting polymer

separated by a thin layer of a high dielectric strength insulator. Application of an appropriate potential across the structure can give rise to a surface charge layer. The resulting charges in the polymer, for example, $(CH)_x$ or poly (3-hexylthiophene) are present without any associated dopant ion.

Non redox doping

This type of doping differs from redox doping is that the number of electrons associated with the polymer backbone does not change during the doping process. The energy levels are rearranged during doping. The emeraldine base form of PA was the first example of the doping of an organic polymer to a highly conductive regime by non-redox type doping.

1.2.2 Types of Doping Agents

Dopants may be classified as-

(a) Neutral dopants: iodine (I_2), bromine (Br_2), AsF_2, sodium (Na), potassium (K), Sulphuric acid (H_2SO_4), ferric chloride ($FeCl_3$) etc. Neutral dopants are converted into negative or positive ions with or without chemical modifications during the process of doping.

(b) Ionic dopants: $LiClO_4$, $FeClO_4$, CF_3SO_3Na, $BuNClO_4$ etc. Ionic dopants are either oxidized or reduced by an electron transfer with the polymer and the counter ion remains with the polymer to make the system neutral.

(c) Organic dopants: CF_3COOH, CF_3SO_3Na, p-$CH_3C_6H_4SO_3H$ etc. Organic dopants are anionic dopants, generally incorporated into polymers from aqueous electrolytes during anodic deposition of the polymer.

(d) *Polymeric dopants:* Poly(*p*-styrene sulfonic acid) (PSSA), poly(2-acrylamido-2-methyl-1-propane sulfonic acid) (PAMPS) etc. Polymer dopants are functionalized polymer electrolytes containing amphiphilic anions.

1.2.3 Doping Techniques

The doping of CPs can be done by adding chemical reactants to oxidize or reduce the system so that the electrons are pushed into the conjugated system. There are so many

methods by which of doping in CPs can be done. These are - chemical doping, electrochemical doping, gaseous doping, solution doping, self doping, radiation induced doping and Ion exchange doping.

The chemical and electrochemical doping techniques are the two primary methods of doping a conductive polymer, both of which use an oxidation-reduction process. However, gaseous, solution and electrochemical doping methods are widely used because of their convenience and low cost.

Chemical doping can be carried out in two ways, either exposing a polymer to an oxidant such as iodine or bromine or the polymer can also be exposed to a reducing agent. The chemical doping is less common than the other methods, and normally this method involves alkali metals.

Electrochemical doping involves suspending a polymer-coated, working electrode in an electrolyte solution in which the polymer is insoluble along with separate counter and reference electrodes. An electrical potential difference is created between the electrodes that cause a charge and the appropriate counter ion from the electrolyte to enter the polymer in the form of electron addition (i.e., n-doping) or removal (i.e., p-doping). Electrochemical n-doping is common in research, because it is easier to exclude oxygen from a solvent in a sealed container.

In gaseous doping process, the polymers are exposed to the vapour of the dopant under vacuum. The level of dopant concentrations in polymers may be easily controlled by temperature, vacuum and time of exposure.

Solution doping involves the use of a solvent in which all the products of doping are soluble. Polar solvents such as acetonitrile, tetrahydrofuran, nitro methane are used as solvents. The polymer is treated with dopant solutions.

1.3 Types of Conducting Polymers

On the basis of conduction mechanism that renders electrical conductivity to polymers the π-conjugated polymers can be classified in to different types-

1.3.1 Inherently conducting polymers.

1.3.2 Conducting polymer composites

1.3.3 Organometallic polymeric conductors

1.3.4 Polymeric charge transfer complexes

Brief description of the conducting materials have been given here but as present study deals with the carbon filled π-conjugated polymer composites and inherently conducting polymers , mainly PA and PPy, so detail discussion have been done for these types of conducting materials.

1.3.1 Inherently Conducting Polymers

Research in the field of inherently conducting polymers started nearly three decades ago when Shirakawa, MacDiarmid and Heeger found dramatic increase in the electrical conductivity of polyacetylene films when exposed to iodine vapor. From this breakthrough, many small conjugated molecules were found to polymerize, producing CPs, which were either insulating or semiconducting in the oxidized or doped state. The electronic properties of CPs are due to the presence of π-electrons, the wave functions of which are delocalized over large portions of polymer chain when the molecular structure of the backbone is planar. Hence it is necessary that there are no torsion angles at the bonds, which would decrease the delocalization of the π-electron system.

Features, which differentiate, CPs from conventional polymers are as follows:

- Band gap Eg (electronic band gap) is small (~ 1 to 3.5 eV) with corresponding low excitations and semiconducting behavior.
- Can be oxidized or reduced through charge transfer reactions with atomic or molecular dopant species.
- Net charge carrier mobilities in the conducting state are large enough and because of this high electrical conductivity are observed.
- Quasi particle, which under certain conditions, may move relatively freely through the material.

The electrical and optical properties of these kinds of materials depend on the electronic structure and on the chemical nature of the repeated units. The electronic conductivity is proportional to both density and the drift mobility of the charged carriers. The carrier drift mobility is defined as the ratio of the drift velocity to the electric field and reflects the ease with which carriers are propagated. To enhance the electrical conductivity of polymers, an increase in the carrier mobility and the density of the charge carriers is

required. Since the present work deals with conducting polymers, PA and PPy, a brief history of these materials is given here.

1.3.1.1 Polyaniline (PA)

Among all conducting polymers PA has a special representation because of its diverse, but unique properties and potential applications in several fields of technology. The conducting polymer, PA is known for it's ease of synthesis, environmental stability and easy to dope by protonic acids. PA is a typical phenylene based polymer having a chemically flexible –NH group in a polymer chain flanked either side by a phenylene ring. It can also be defined as the simple 1, 4-coupling product of monomeric aniline molecule. The protonation, deprotonation and various other physico-chemical properties of PA is due to the presence of the –NH- group. The first report on the production of PA was in the year 1862 when Letheby used a platinum electrode during the anodic oxidation of aniline in a solution containing sulfuric acid and obtained a dark-green precipitate.[64] This green powdery material soon became known as 'aniline black'. Green and Woodhead[65] performed the first organic synthesis and classification of intermediate products in the "aniline black" formation and five different aniline octamers were identified and named as leucoemeraldine base, protoemeraldine, emeraldine, nigraniline and pernigraniline. These names are still used, indicating various oxidation states of PA (**Scheme 1.2**). There are several reports of PA found in the literature over the decades about the structure and constitutional aspect of aniline polymerization. In the year 1968, Surville et al. reported the proton exchange and redox properties with the influence of water on the conductivity of PA[66]. However, interest in PA was generated only after the fundamental discovery in 1977 that iodine doped polyacetylene gives metallic conductivity which triggered research interest in new organic conducting materials.[67] PA exists in four main oxidation states viz. Leucoemeraldine base, Emeraldine base, Emeraldine salt and Pernigraniline.

Schematic representations for various oxidation states of PA are given in the **Scheme 1.2**.

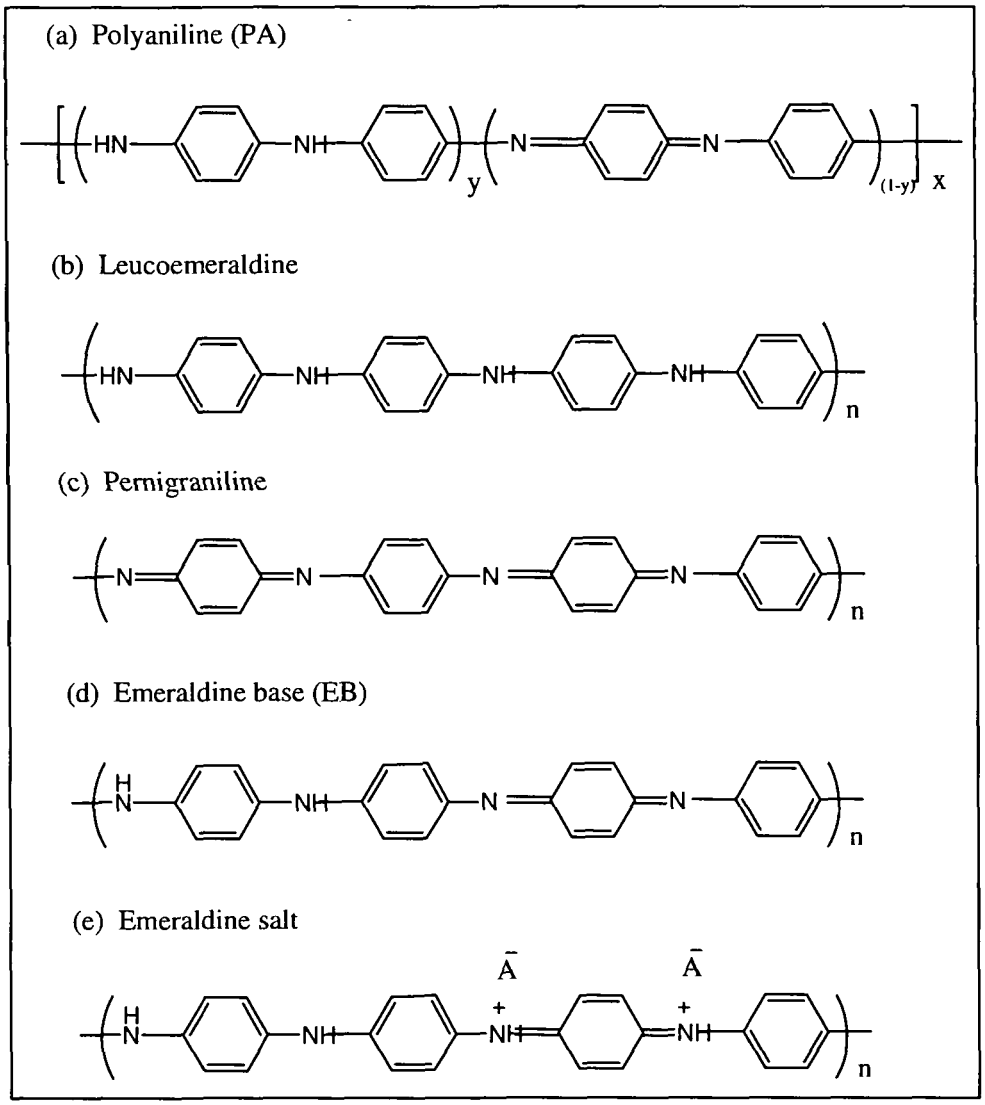

Scheme 1.2 Various oxidation states of polyaniline

PA is a unique polymer because it can exist in a variety of structures depending on the ratio of benzenoid and quinoid structure in the general formula of the polymer.[68,69] The electronic properties of PA can reversibly be controlled by protonation as well as by redox doping. Therefore, PA could be visualized as a mixed oxidation state polymer composed of benzenoid and quinoid repeat units (**Scheme 1.2 a**). Depending upon the oxidation state of nitrogen atoms which exist as amine or imine functional group, PA can adopt various structures in several oxidation states, leucoemeraldine, pernigraniline, emeraldine base. The protonated form is the conducting emeraldine salt.

Synthesis of PA

The most widely accepted methods for synthesis of PA are chemical oxidative polymerization method and electrochemical methods. Chemical oxidative method is preferred over electrochemical polymerization because of its cost effectiveness and bulk quantity of the polymer that can be prepared during the onset of a reaction.

Chemical Synthesis

Synthesis of PA by chemical oxidative route involves the use of either hydrochloric or sulfuric acid in the presence of ammonium per-sulfate or potassium per-sulfate as the oxidizing agent in the aqueous medium. The principal function of the oxidant is to withdraw a proton from an aniline molecule, without forming a strong co-ordination bond either with the substrate / intermediate or with the final product (**Scheme 1.3**). However smaller quantity of oxidant is used to avoid oxidative degradation of the polymer formed. The propagation of polymer chains proceeds by oxidation and coupling (growth) process between the growing chain (as an oxidant) and aniline (as a reductant) with addition of monomer to the chain end.[70] The high concentration of a strong oxidant, $(NH_4)_2S_2O_8$ or $K_2S_2O_8$ at the initial stage of the polymerization enables the fast oxidation of polymer and finally exist in the oxidized form.

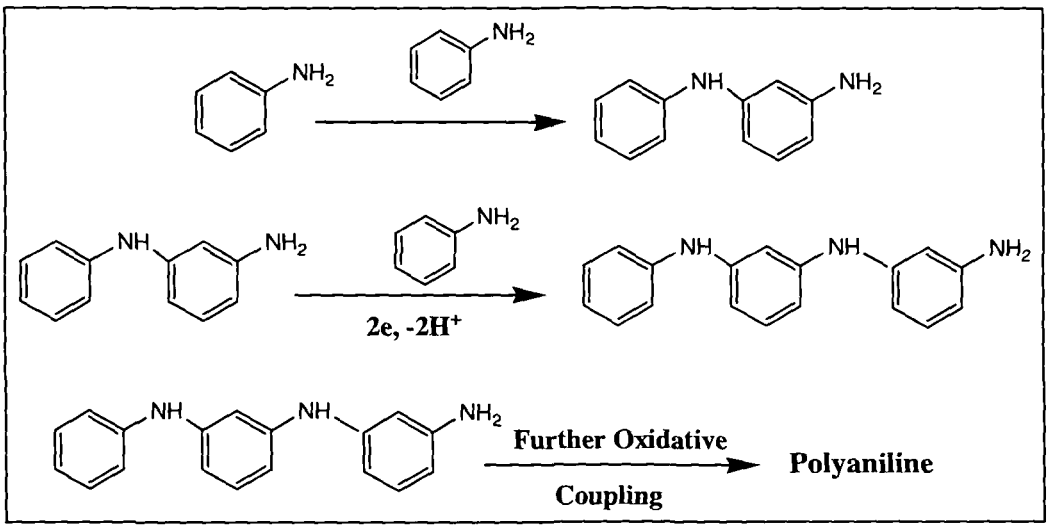

Scheme 1.3 Synthesis of polyaniline by oxidative coupling method

Armes et al.[71a] had studied the polymerization of aniline at 20°C using, $(NH_4)_2S_2O_8$ as an oxidant, where they reported the effect of the oxidant/monomer initial mole ratio.

The conductivity, yield, elemental composition and degree of oxidation of the resulting polymer were independent of the oxidant/monomer ratio when its value was below 1.15. Asturias et al.[71b] studied the influence of the atmosphere (viz air and argon) on the degree of oxidation of PA, using $(NH_4)_2S_2O_8$ as the initiator. Cao et al.[72] reported the commonly employed procedure for protonation of polyemeraldine salt i.e., stirring of PA powder with concentrated aqueous HCl solution, leading to the significant degradation of PA. Pron et al.[73] had synthesized PA with four different oxidizing agents and at different aniline:oxidant ratios and compared the electrical conductivity and the reaction yield. They reported that the redox potential of the oxidant is not a mandatory parameter in the chemical oxidative polymerization of aniline.

Electrochemical Synthesis

In electrochemical synthesis of PA (**Scheme 1.4**), anodic oxidation of aniline is carried out on an inert metallic electrode using two main modes: potentiostatic or galvanostatic. However, several studies have been carried out with other electrode materials such as iron, aluminum and aluminum alloys. In this method, the potential is fixed or cycled with the value of the applied potential being in range of 0.7 to 1.2 V (vs. saturated calomel electrode potential, SCE) and sweeping potential limits -0.2V to +1.0V vs. SCE. The scan rates most commonly used are in the range of 10 to 100 mV s^{-1} at the constant current in the range of 1-10 mA.

PA was first synthesized electrochemically by oxidative polymerization of aniline monomer by Letheby[65] in 1862 when he observed the growth of a blue-green powdery pigment on a platinum anode during electrolysis of solution of aniline in sulphuric acid. But the detailed study of PA took almost one century from the discovery when Mohilner et al. carried out the first systematic study in 1962.[74] They found that the oxidation of aniline takes place through a free radical mechanism leading to the octamer emeraldine as the major product. Their conclusion was based on the reaction kinetics and comparison of the properties of chemically synthesized emeraldine to the electrochemical product. When the researchers have been exposed that the aromatic amine, pyrrole, thiophene, furan, indole and benzene can be polymerized anodically to conducting film, the major interest in the electrochemistry of PA was generated. Electrochemically prepared PA is the preferred

CENTRAL LIBRARY, T. U.
ACC. NO. T 182

method to obtain a clean and better ordered polymer thin film. Noufi et al.[75] reported the preparation of PA in an aqueous solution using a platinum electrode by cycling the potential between –0.2 to 0.8V vs. SCE. The physicochemical properties of PA films cast from organic solvent like NMP are reported by Kang et al.[76] Shaolin et al.[77] had reported that the conductivity of PA films synthesized in presence of NaCl salt is about 30 times higher than that the PA films prepared without NaCl. Chen and Lee investigated the structure and doping behavior of PA films plasticized with NMP.[78] Lux had reported the various properties of conducting polyaniline in his review article.[79]

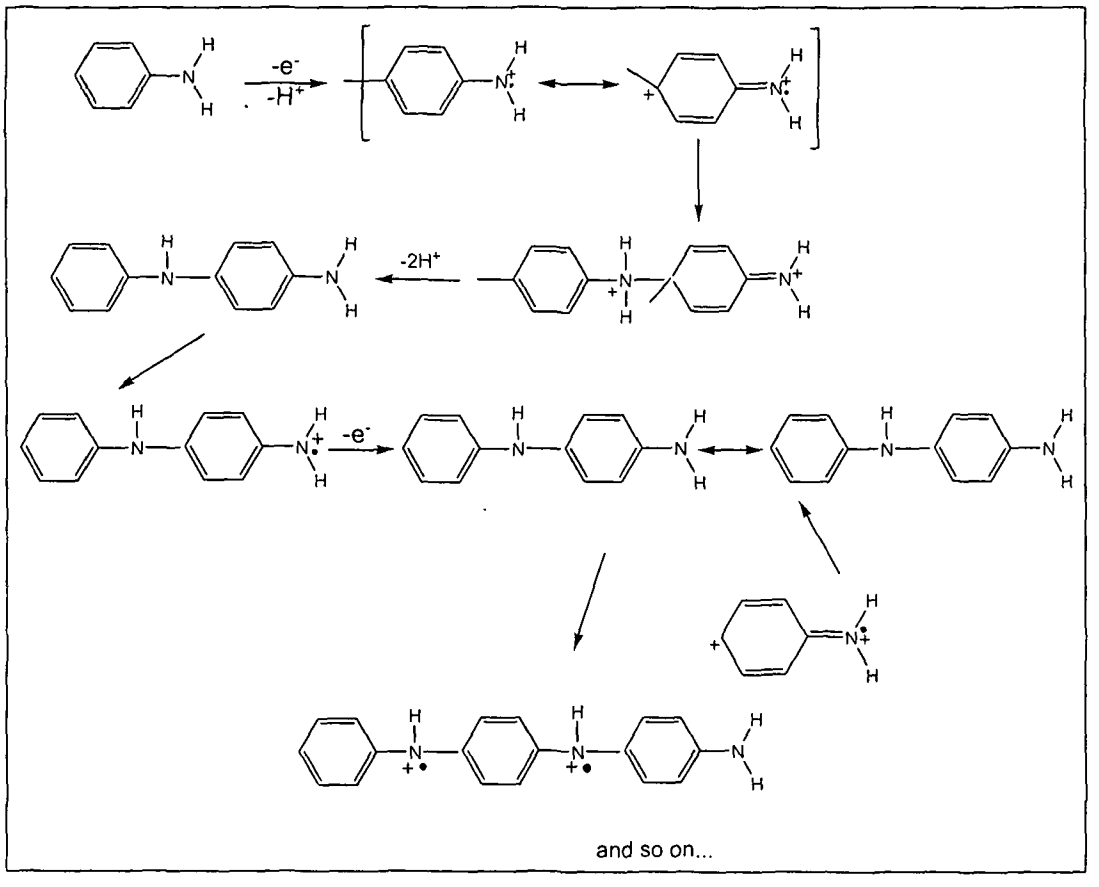

Scheme 1.4 Electrochemical synthesis of Polyaniline

1.3.1.2 Polypyrrole (PPy)

Among known conducting polymers PPy is most frequently used in the commercial applications due to its

- Straightforward preparation methods,

- Reasonable stability in air,
- Good electrochemical properties
- High conductivity and thermal stability and
- The possibility of forming homopolymers or composites with optimal mechanical properties.

PPy is known for its stability in the oxidized state and interesting redox properties. Conducting PPy can be prepared by various methods such as chemical, electrochemical, vapor phase etc. The possible structures of PPy are shown in the **Scheme 1.5** below.

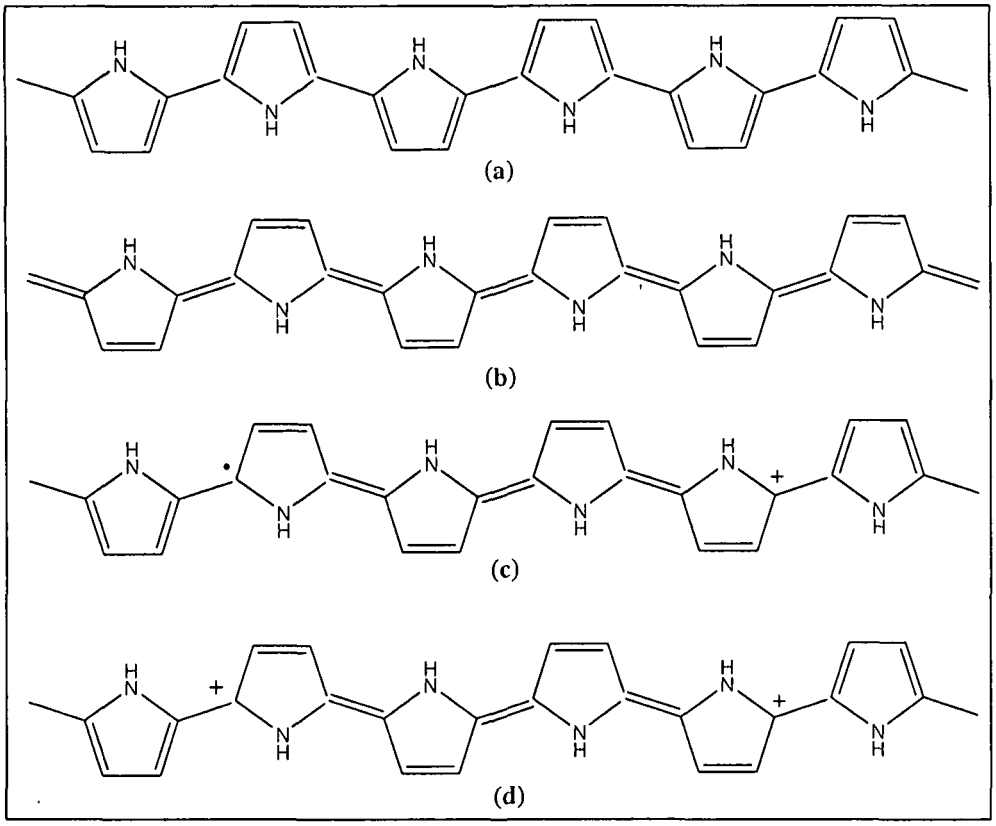

Scheme 1.5 Possible structure of PPy showing (a) non degenerated aromatic configuration, (b) quinoid configuration, (c) a polaron defects and (b) a bipolaron defects

Chemical Synthesis

PPy known as "pyrrole black" in conductive form was first found on the sides of pyrrole container, which was polymerized by spontaneous polymerization in air and chemical oxidative polymerization.[80] Chemical polymerization of pyrrole was first

reported in the year 1916 by Angeli et al. They synthesized PPy by the oxidation of pyrrole with H_2O_2. PPy powder as obtained was amorphous in nature and was known as pyrrole black. Generally, pyrrole black have been prepared in presence of various oxidizing agents like H_2O_2, PbO_2, Quinones or O_3. The materials thus obtained by this method are mainly insulating in nature with room temperature conductivity 10^{-10} to 10^{-11} S/cm, but after subjecting to doping with halogenic electron acceptor, the conductivity rises to 10^{-5} S/cm.[81] The low conductivity of PPy prepared from acid or peroxide initiators is associated with the high degree of saturation of the pyrrole rings in the polymer.

One of the great advantages of PPy from synthetic point of view is its low oxidation potential of the pyrrole monomer. Pyrrole is one of the most easily oxidized monomer and hence a variety of oxidizing agents are available for preparing PPy. Commonly used oxidants for pyrrole polymerization are oxidative transition metal ions. Various oxidizing agents such as $FeCl_3$, $Fe(NO_3)_3$, $Fe(SO_4)_3$, $K_3Fe(CN)_6$, $CuCl_2$ etc. have been employed to polymerize pyrrole with conductivity between 10^{-5} to 200 S/cm. $FeCl_3$ is the most commonly used oxidizing agent for the synthesis of highly conducting PPy. The general reaction scheme for PPy synthesis is given below (**Scheme 1.6**).

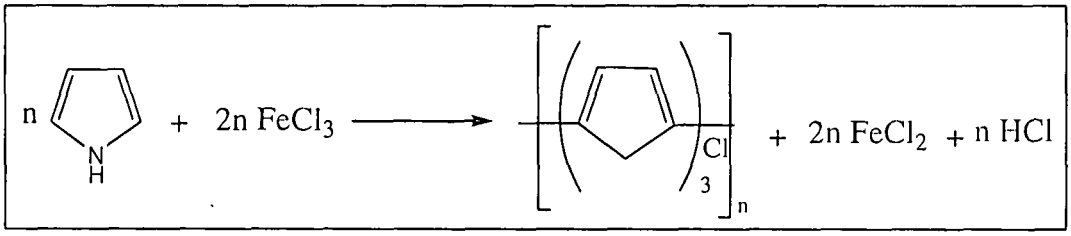

Scheme 1.6 Reaction scheme for PPy chemical synthesis

Hsing et al. proposed this type of similar mechanism in the year 1983.[82] The reaction would be initiated by the cationic radical $C_4H_5^{\cdot+}$, which coordinates with the other pyrrole units.

Electrochemical Synthesis

Generally electrochemically PPy films are prepared by the electro-oxidation of pyrrole in one compartment cell equipped with platinum working electrode, gold wire counter electrode and SCE as the reference electrode. A wide variety of solvents and electrolytes can be used as the electrical resistance of the solution is high and the

nucleophilicity does not interfere with the polymerization reaction. The reaction mechanism for the electrochemical synthesis of PPy is given in the **Scheme 1.7**. The selecting electrolyte solution should be highly dissociative and slightly acidic. Films of various thicknesses can be prepared by changing the current density. As the electrical potential needed to oxidize the monomer is higher than the charging (or doping) of the formed polymer, the polymer is directly obtained in the conducting state.

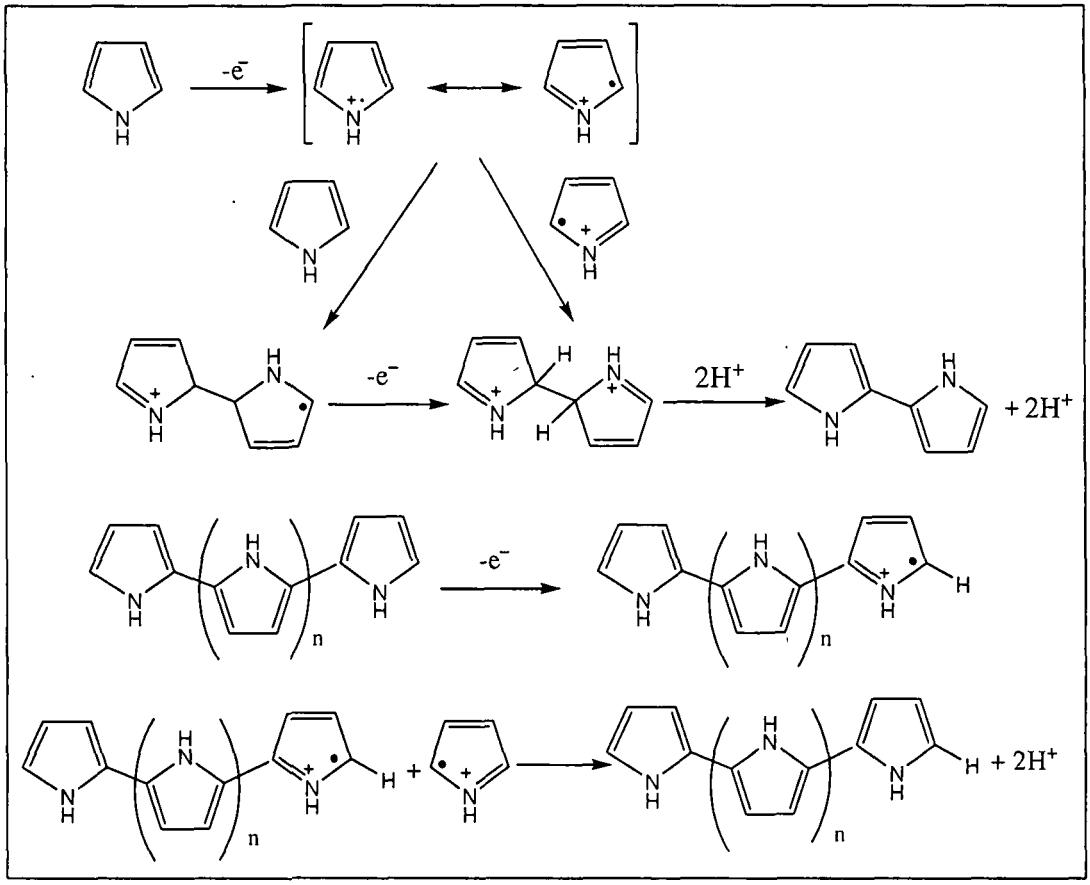

Scheme 1.7 Mechanism for the electropolymerization of pyrrole

Dall'Ollio in 1968 first electrochemically synthesized PPy by the electrochemical oxidative polymerization of pyrrole monomer in aqueous sulphuric acid on Pt electrode. This was the first experiment to produce a conducting polymeric material and showed conductivity of 8 S/cm. According to Diaz et al., the electrochemical synthesis of PPy film proceeds via the oxidation of pyrrole at the platinum electrode to produce an unstable π-radical cation which then reacts with the neighboring pyrrole species.[83] Cyclic voltammograms of this solution shows an irreversible peak for the oxidation of pyrrole at

+1.2V vs. SCE. The mechanism of the overall reaction for the formation of fully aromatized product is very complicated and involves series of oxidation and deprotonation steps.

1.3.2 Conducting Polymer Composites

Conducting polymer composites are mixture or blends of conductive fillers and polymers. Electrically conductive π-conjugated polymer composites served as an inexpensive approach to obtain conductive materials for applications where metals are not suitable. The conductivity and mechanical properties can easily be tailored by incorporation of different types, grades, amount of conductive fillers. The choices of conductive fillers are very wide, such as metal particles, carbon black, carbon fiber, carbon nanotubes, graphite and graphene. The undeniable benefits of conductive composites over intrinsic conductive polymers improve a significant research thrust in development of different conductive composites. Conductive polymer composites are widely used for a large range of applications. The present work deals with conducting carbon fillers, a brief history of these materials is given here.

1.3.2.1 Carbon Filled π-Conjugated Polymers

Carbon is the lightest element in Group IV in the periodic table with some unique properties. At ambient conditions, sp^2 bonded graphite[85] is the ground state phase of carbon. The pure structure of graphite lattice consists of hexagonal net planes of carbon stacked along the c-axis in a staggered array usually denoted as ABAB...(**Figure 1.4**). Graphite is one of the widely studied carbon fillers due to its unique properties like good conductivity,[86-89] better adsorption capability and low cost compared to other fillers.

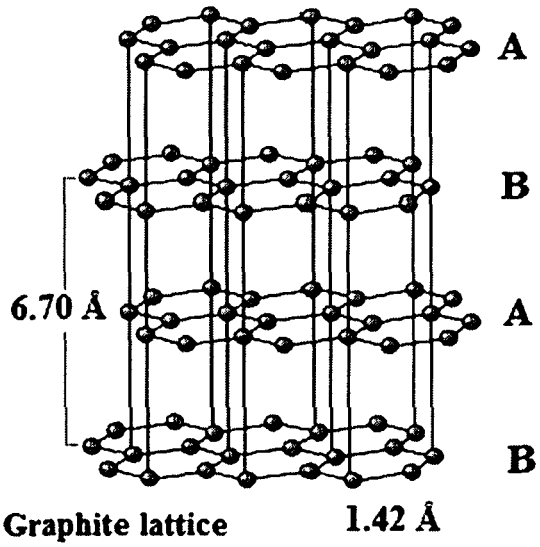

Figure 1.4 Graphite lattice showing the ABAB stacking of carbon layers[90]

Graphite has been widely used as electronically conducting filler for preparing conducting polymer/graphite composites in the last decade.[91-98] When graphite was used as filler in the preparation of conductive polymer composites, the factors influencing their electrical conductivity, such as the structure and size of graphite particles, polymer types, temperature, pressure, applied electrical current and voltages, etc. have been studied.[99-103] The electrical conductivity of graphite is 10^4 S/cm at ambient temperature as high as carbon fibers. Park et al. reported the capacitance properties of graphite/polypyrrole composite electrode prepared by chemical polymerization of pyrrole on graphite fiber and show specific capacitance of about 400 F/g and a Coulombic efficiency of 96–99%.[104] Recently Cakar et al.[105] showed that conducting poly (ether amide)/graphite composite can be used as a sensor element to detect chloroform and chlorobenzene.

Much attention has recently been focused on the small carbon clusters, since the discovery of fullerenes in 1985 by Kroto et al.[106] and of CNTs in 1991 by Iijima.[107] The quasi one-dimensional CNTs have captured the attention of researchers worldwide due to their unusual mechanical, electronic, and adsorptive properties as well as their good chemical stability. These features of CNTs make them attractive candidates in nanoscale device applications. The CNTs are cylindrical structures based on the hexagonal lattice of carbon atoms that forms crystalline graphite. **Figure 1.5** shows the two types of CNTs called armchair and zigzag nanotubes depending on how the two- dimensional graphene

sheet is "rolled up".[108] The CNTs are tube like structures having diameter (10^{-9} m) and many microns in length, which easily form bundles. They entangle together in the solid state is giving rise to a highly complex network. However, due to strong inter-tube van der Waals interactions, CNTs show lack of solubility and are difficult to manipulate in any solvent. Hence applications using the materials have been limited.

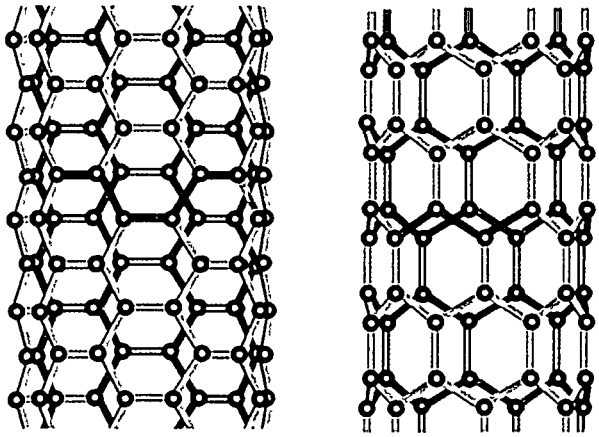

Figure 1.5 Atomic structures of CNTs (a) an armchair and (b) a ziz-zag nanotubes

The extraordinary properties of CNTs make them very promising and favourable as fillers for fabrication of a new class of polymeric heterostructures. In CNTs-polymer composites, chemical functionalization is used to enhance the nanotube-polymer interface. Functionalized nanotubes are also typically easier to disperse in organic solvents and water which can improve the dispersion and homogeneity of the CNTs within the polymer. There are different methods by which CNT-conducting polymers composites can be synthesized, depending on the desired applications. The most widely accepted methods are chemical oxidative polymerization method and electrochemical methods. Tzong-Ming Wu et al. reported synthesis of doped PA in its emeraldine salt form with carboxylic groups containing multi-walled CNTs (MWCNT) via in situ polymerization.[109] S. Hrapovic reported preparation of polymer/CNT composite materials and their applications for enzyme entrapment.[110] Moreover, CNTs have been predicted as excellent filler for polymer on improving the electrical conductivity. Recently, obvious progress has been made in designing and fabricating PA/CNTs composites.[51-53, 111-118] Gupta et al. reported the electrochemical polymerization of PA/single-walled CNTs composites and studied the

capacitor behaviour of the composites in acid system with the highest specific capacitance of 463 F/g obtained for 73 wt.% PA[119] and the highest specific capacitance value of 500 F/g for the MWCNT/PA composite film containing MWCNT of 0.8 wt.%. Khomenko et al.[120] reported composite materials containing 20 wt.% of MWCNTs and 80 wt.% of chemically formed PA and PPy for supercapacitor electrodes and found capacitance 90 F/g for PPy/MWCNTs and 360 F/g for PA/MWCNTs. Dong et al.[121] reported the synthesis of PA/MWCNTs composites by in situ chemical oxidative polymerization and studied for supercapacitors behaviour (328 F/g) of the composites in neutral system ($NaNO_3$).

Carbon fibers (CF) (**Figure 1.6**) represent an important class of graphite-related carbon fillers. CF can be synthesized by using the various precursors, but each produces fibers with different cross-sectional morphologies. The preferred orientation of the fiber axes for all CFs is close to an in-plane direction of a graphene layer. This fact accounts for the high mechanical strength of these fibers. Most commercial CFs exploit the great strength of carbon materials under tension, which is achieved when the CFs are prepared from a polymer precursor, such as polyacrylonitrile, while fibers prepared from a mesophase pitch liquid crystal precursor are used for high modulus (stiffness) application.

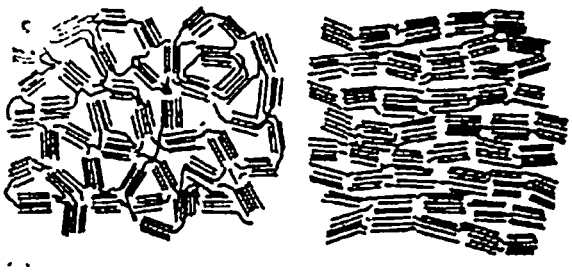

Figure 1.6 Schematic models for the microstructure of activated carbon fibers

In the recent years graphene has become one of the most exciting topic of research[122] not only out of academic curiosity but also with potential applications in mind. It is a two-dimensional material, composed of layers of carbon atoms forming six membered rings. Graphene is the mother of all graphitic forms including zero dimensional fullerenes, one-dimensional carbon nanotubes and three-dimensional graphite (**Figure 1.7**). Although CNTs are formed through the rolling of graphene sheets, but the properties (e.g., electrical conductivity and mechanical strength) of these two are quite different.

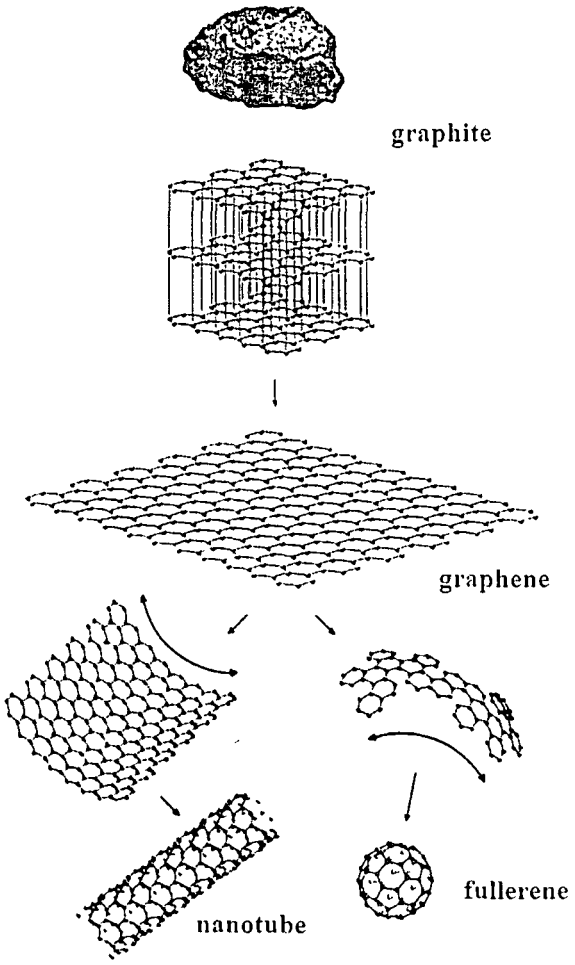

Figure 1.7 Graphene: mother of all graphitic forms

Graphene is the first essentially two-dimensional material ever made. Being the thinnest piece of matter in the world is just one of many superlatives that can be applied to graphene. It is also the strongest material known, about 100 times stronger than steel. Since a sheet of graphene is only one atom thick, it is also transparent, and therefore it may play a role in the development of new material. Some of the most interesting features of this graphene material, from the point of view of future applications, have to do with its electrical properties. Electricity flows quickly through graphene and without losing much energy along the way. It is relatively easy to fabricate, makes graphene a candidate for replacing or enhancing the integrated circuits that fill our computers today. When mixed into plastics, graphene can turn them into conductors of electricity while making them

more heat resistant and mechanically robust. This resilience can be utilized in new super strong materials, which are also thin, elastic and lightweight. For the discovery of this new class of two-dimensional materials, the Nobel Prize in 2010 for physics goes to *Andre Geim* and *Konstantin Novoselov*.[123, 124]

To exploit the potential of graphene-based polymer materials for electronic devices, supercapacitor applications, etc. recent researches have been mainly focused on this type of materials. Wang et al. prepared a graphene/PA composite by in-situ anodic electro-polymerization of aniline on graphene paper, and electrochemical capacitance was achieved 233 F/g.[125] Recently Yan et al. reported a simple process to synthesis the composite of graphene doped with PA using in situ polymerization and showed maximum specific capacitance of 1046 F/g at a scan rate of 1 mV/s.

Electrical properties of a material depend on the separation between the collections of energy states that are filled by electrons (red) and the additional "conduction" states that are empty and available for electrons to hop into (light blue) as shown in **Figure 1.8**. Metals conduct electricity easily because there are so many electrons with easy access to adjacent conduction states. In semiconductors, electrons need an energy boost from light or an electrical field to jump the gap to the first available conduction state.

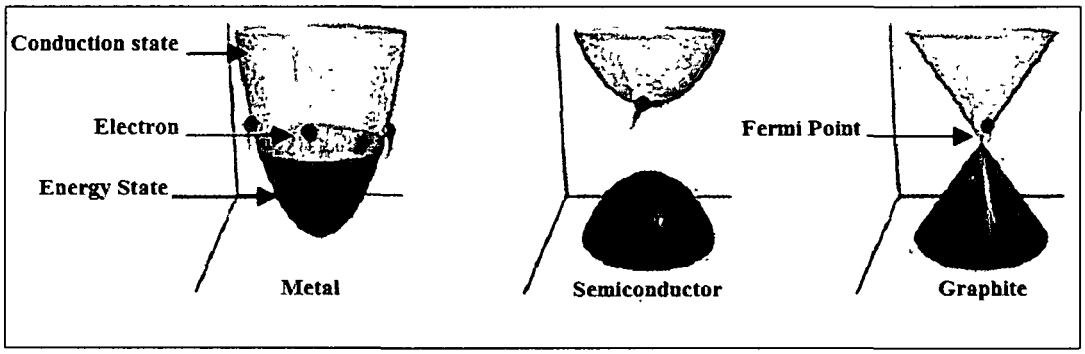

Figure 1.8 Collection of energy states of metal, semiconductor and graphite[126]

Graphite is a semimetal that just barely conducts, because without these external boosts, only a few electrons can access the narrow path to a conduction state. The electrical conductivity of the compound is decided by the volume fraction of the filler. A transition from insulating to non-insulating behavior is generally observed when volume fraction of conductive filler in the mixture reaches a threshold of about 25%. The various polymers,

which have been used as major matrix, are typically Nylon, polyvinylchloride, high density polyethylene, PA, PPy, polythiophene, etc.

1.3.3 Organometallic Polymeric Conductors

These types of conducting materials are obtained by adding organometallic groups to polymer molecules. In this type of materials the d- orbital of metal may overlap π-orbitals of the organic structure and thereby increases the electron delocalization. The d-orbital may also bridge adjacent layers in crystalline polymers to give conducting property to it.

Metallophthalocyanines and their polymers fall in this class of polymeric material (**Scheme 1.8**). These polymers have extensively conjugated structures. The bridge transition metal complexes form one of the stable systems exhibiting intrinsic electrical conductivities, without external oxidative doping. Polyferrocenylene is also an example of this type of polymer. These materials possess strong potential for future applications such as molecular wires, antistatic foils, fibers and in xerography.

Swager's et al. has reported the investigation of an organometallic polymeric series of polythiophene-tris (bipyridyl) ruthenium (II) ($Ru(bipy)_3$) hybrid materials.[127,128] These polymers were synthesized by the electrochemical polymerization of $Ru(bipy)_3$ derivatives that were appended with bithienyl moieties. The highest electrical conductivity of these types of polymers was reported 3.3×10^{-3} S/cm.[129]

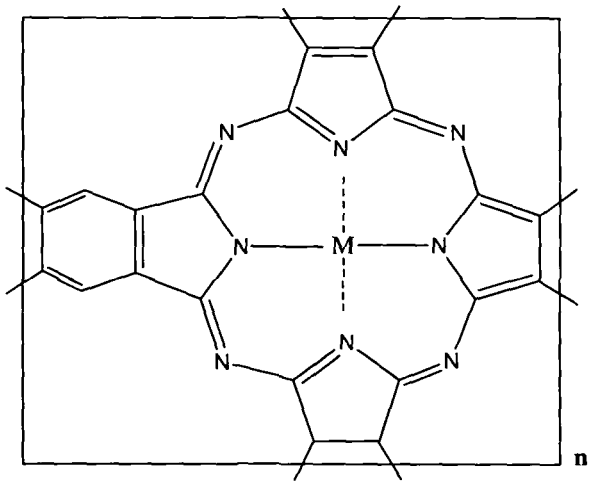

Scheme 1.8 Polyphthalocyanines, an example of organometallic polymeric conductors

1.3.4 Polymeric Charge Transfer Complexes

Polymeric charge transfer complexes are formed when acceptor like molecules are added to the insulating polymers. A polymer which contains a charge transfer complex consists of two different types of monomers, a donor and an acceptor (**Scheme 1.9**). The donor is like a rich man with more money than he knows what to do with. It has plenty of electrons to go around because of its nitrogen groups. The acceptor, then, is like a mooching houseguest. Its carbonyl groups, like our houseguest's many vices of gambling, drinking and such, suck away its electron density. The donor doesn't mind supporting the acceptor, in fact, with the acceptor around, the donor looks better. So the donor lends some of its electrons to the acceptor, holding them tightly together.[130]

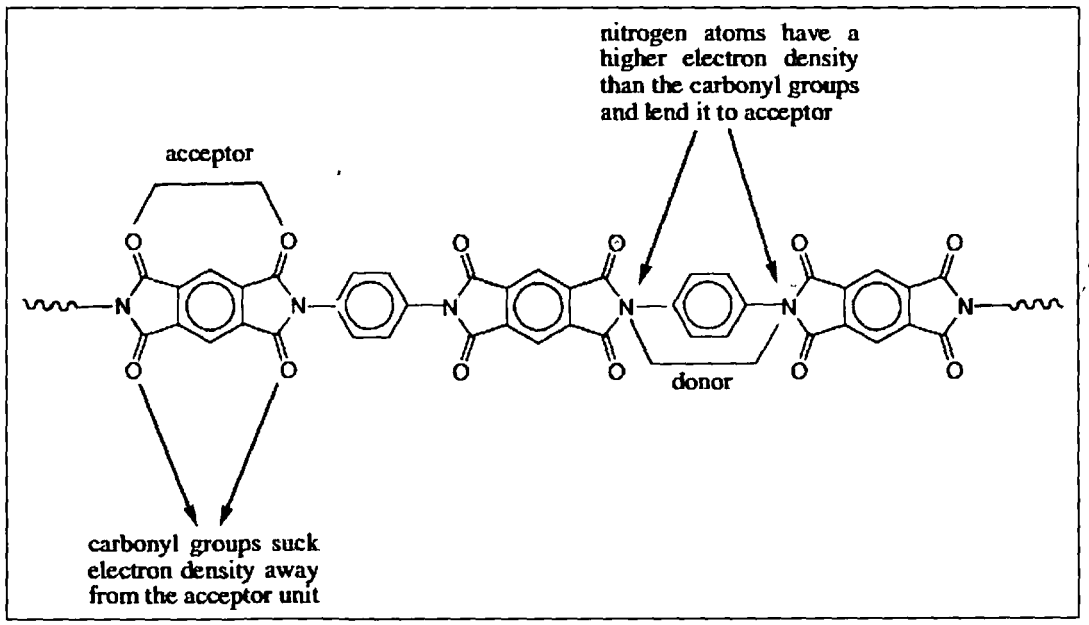

Scheme 1.9 Aromatic heterocyclic polyimide

There are many charge transfer complexes reported in the literature[131, 132] e.g, study of charge photogeneration in binary and ternary blends of a conjugated polymer poly[2-methoxy-5-(2'-ethylhexyloxy)-*p*-phenylene vinylene] (MEH-PPV), with three organic acceptors: 2,4,7-trinitrofluorenone (TNF), 1,5-dinitroantraquinone (DNAQ), and C_{60}.[133] Sergey et al. reported a study of MEH-PPV/acceptor blends with DNAQ and TNF, showing considerable optical absorption below 2 eV.[134] Singh et al. reported electrical properties of the polymer composites based on charge-transfer complex of phenothiazine–iodine in polystyrene and the conductivity was found 2.72×10^{-12} S/cm.[135] The reason for

the conductivity in polymeric charge transfer complexes and radical ion salts are still somewhat unclear. It is likely that in polymeric charge transfer complexes, the donor - acceptor interaction promotes orbital overlap, which contributes to alter molecular arrangements and enhanced electron delocalization.

1.4 Properties of π-Conjugated Polymers

A large number of different classes of CPs has been developed, e.g., poly(acetylene)s, poly(p-phenylene)s, PPy, PA, poly(phenylenevinylenes), poly(carbazole)s, poly(flourene)s, poly(thiophene)s. The early interest of CPs was to study their electrical conductivity and their corresponding electronic structure. Highest values reported up to now for the electrical conductivity of doped polymers are 8 x 10^5 S/cm.[136, 137] The different path breaking application oriented discovery of CPs gave the opportunities to analyze their properties. The development of soluble CPs has led to significant improvement in their properties.

Charge carrier mobility of CPs was reported as high as 10 cm^2/Vs.[138] As per our knowledge, excellent on/off ratios in polymer based FETs was found up to 10^7.[139] Polymer based photovoltaic cell with record power conversion efficiencies up to 5 % were accounted till to date.[140] Recently polymer light emitting diodes (LEDs) can sustain 400 cd/m^2 of luminance for over 1,98,000 hours for green LEDs and 62,000 hours for blue LEDs.[141] To date, polymer LEDs have been demonstrated with emission wavelengths from the ultraviolet to near infrared,[142] external quantum efficiency 10% photons/electrons.[143] For light emitting polymers, poly(phenylenevinylenes) and its derivatives are still the leading materials for green LEDs, the larger band gap PFs are the blue –light emitting polymers and polythiophenes and its derivatives are remembered for red and almost all visible light emitting polymer materials.[144]

1.4.1 Electronic properties of π-Conjugated Polymers

The electronic properties of CPs depend on the electronic band structure. If the bands are filled or empty, then no conduction occurs. If the band gap is small compared with thermal excitation energies, electrons are excited to the conduction band and thus

conductivity increases. When the band gap is too wide, thermal excitation is insufficient to excite electrons to the conduction band resulting insulating properties.

For electrical properties of the CPs, the essential feature is that it provides bands of delocalized molecular orbitals, the π-bands, within which the full range of semiconductor and metal behaviour can be achieved through control of the degree of filling. To explain the conduction phenomena, it is proposed that when an electron is removed from the top of the valence band by oxidation, a vacancy (hole or radical cation) is created. Partial delocalization occurs over several monomer units instead of complete delocalization which results the structurally deformed monomer units. The energy level associated with the radical cation represents a destabilized bonding orbital and thus has a higher energy than that of the valence band. A radical cation that is partially delocalized over some polymer segment is called a 'polaron'. A dication or 'bipolaron' has two charges associated with the localized polymer segment. Thus, low oxidation levels yield polarons and higher oxidation levels give the bipolarons. Both polarons and bipolarons are mobile and can move along the polymeric chain by the rearrangement of the double and single bonds in the conjugated system that occurs in an electric field.

For the electrical conduction the most widely used model is one-electron band model as shown in **Scheme 1.10.** When two identical atoms each having a half filled orbital are brought together closely enough for their orbitals to overlap, the two orbitals interact to produce two new orbitals, one of lower energy and one of higher energy. The magnitude of this energy difference is determined by the extent of orbital overlap. The two electrons go into the lower energy orbital is a bonding orbital and the high energy orbital is an antibonding orbital.

CPs in the undoped state possess one p_z electron per site, thus giving occupation of one half of the molecular orbitals within the manifold. All these polymers show an energy gap (Eg) between filled, π states (for bonding) and empty, π* states (for antibonding) so that semiconducting behaviour is observed. The semiconducting gap or energy gap, which is the energy separation between π and π* states, ranges from around 1 eV for poly (isothionaphthene), 1.5 eV for polyacetylene, to 3 eV for poly (p-phenylene).[145] The size of this gap is directly related to the magnitude of the alternation of bond lengths along the chain. All conjugated polymers, such as PA, PTh, PPy, poly (p-phenylene) etc. except

polyacetylene, show a preferred sense of bond alternation. For these polymers the ground-state geometry is the so-called aromatic configuration, with long bonds between rings, and an aromatic structure within the ring. The other sense of bond alternation gives the quinoidal configuration, with shortened bonds between rings, and a quinoidal structure in the ring.[146, 147]

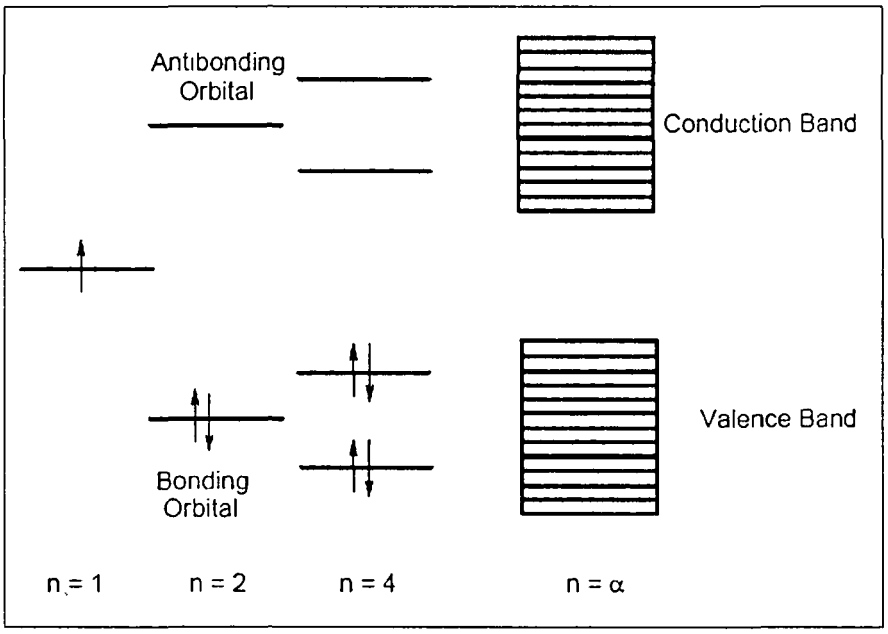

Scheme 1.10 One electron band model for electrical conduction

The electronic excited states are described by three frequently used physical terms namely soliton, polaron and bipolaron[148] as shown in **Figure 1.9**. Soliton, sometime called as conjugational defect, is lone electron created in the polymer backbone during the synthesis of conductive polymer, in very low concentration. Conjugational defect is a misfit in the bond alternation so that two single bonds will touch. The soliton is a zero energy state of the chain with a energy level lying at the centre of the energy gap between the band states. Soliton can be generated in pairs, as soliton and antisoliton. Three methods were used to generate additional solitons - chemical doping, photogeneration and charge injection. When an electron is accepted by the dopant anion it forms a carbocation (positive charge) and when a free radical is formed during the chemical doping (oxidation) of the polymer chain, it is known as radical cation or polaron[149]. Both the soliton and polaron can be neutral or charged (positively or negatively) as shown in **Figure 1.10**. The

charge coupled to the surrounding (induced) lattice distortion to lower the total electronic energy is known as polaron with a charge $-e$ and spin = ½.

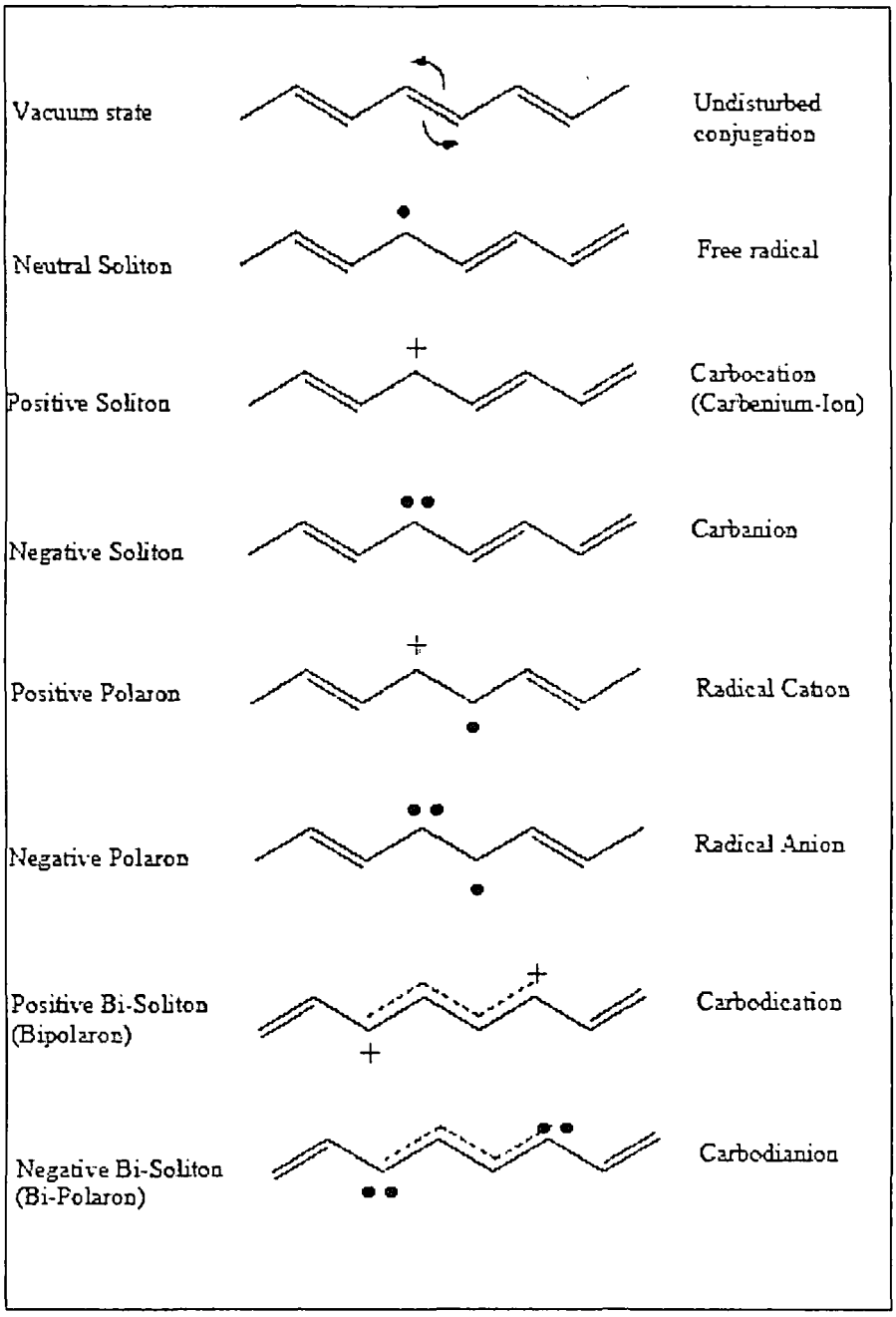

Figure 1.9 Defects in conjugated chains: a "physical – chemical dictionary"[149]

A bipolaron consist of two coupled polarons with charge = $2e$ and spin = 0. Where the different states of occupancy of the soliton level have unusual combinations of spins and charge[150]:

(i) The singly occupied, neutral soliton has *zero* charge but has spin ½,

(ii) The doubly occupied soliton has charge $-e$ and spin *zero* and

(iii) Unoccupied soliton has charge +e and spin *zero*

Bipolarons are not created directly but must form by the coupling of pre-existing polarons or possibly by addition of charge to pre-existing polarons.[151-153]

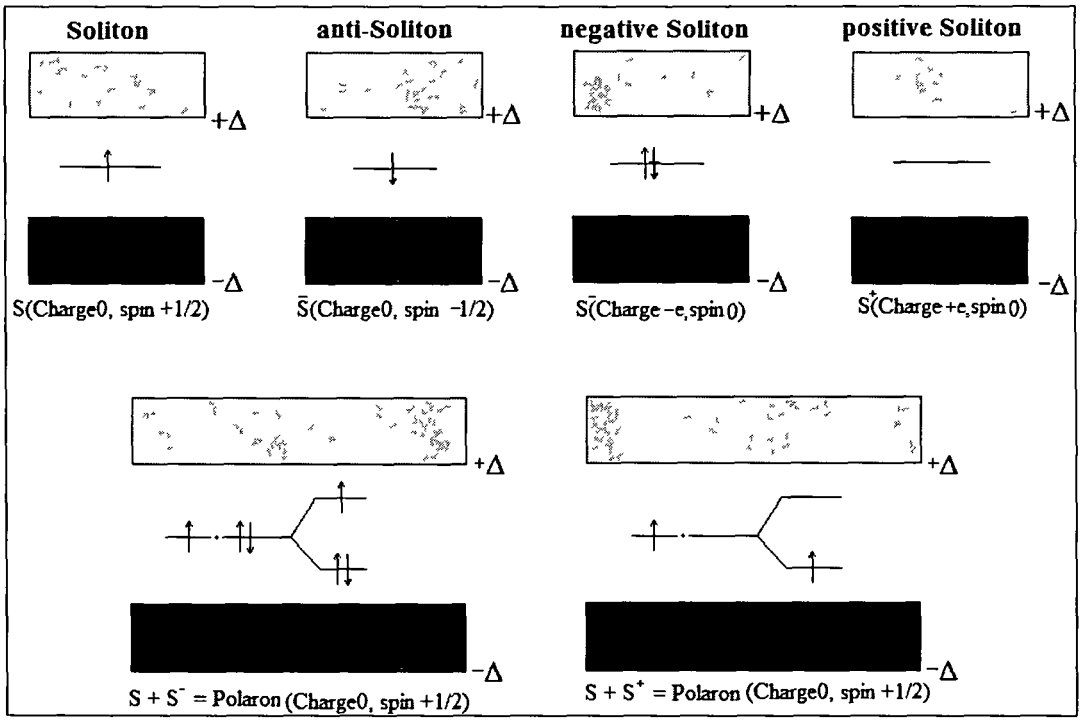

Figure 1.10 The energy level scheme for the soliton and polarons

1.4.2 Electrochemical Properties

Elcterochemical properties can be studied through cyclic voltammetric method. In cyclic voltammetry (CV), the potential is increased linearly from an initial potential to a peak potential and back to the initial potential again, while the current response is measured (**Figure 1.11**). For freely diffusing species, as the potential is increased, easily oxidized species near the electrode surface react, and a current response is measured.

When the direction of the scan is reversed, the oxidized species near the electrode surface are reduced, and again a current response is measured.

The electrochemical properties of conjugated polymers offer the information of oxidation and reduction potential, and stability of synthesized polymer. Moreover, it gives the range of electrochemical potential window which is essential for end use application. The oxidation potential is a measure of how much energy is needed to withdraw electrons from the highest occupied molecular orbital (HOMO) level of polymer and the reduction potential is at the same time a characteristic of the lowest unoccupied molecular orbital (LUMO) level. Therefore, the onset oxidation and reduction potentials are closely related to the energies of the HOMO and LUMO levels of polymer and thus can provide important information regarding the magnitude of the energy gap.[154, 155]

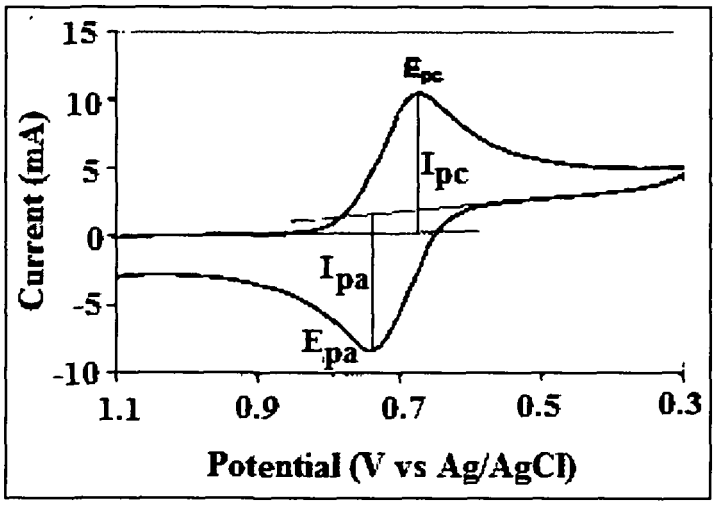

Figure 1.11 A voltammogram of an ideal system for forward scan

The oxidation and reduction potential of CPs films increases with increasing alkyl side chain length. Introduction of an electron donating group, such as an alkoxy or alkyl thio –group results in reducing band gaps, lowering oxidation potentials and stabilizing of conducting state. Fluoroalkyl substituents on the polymer backbone lead to a higher oxidation potential. Electron withdrawing substituents in CPs lower the HOMO and LUMO energies and increase the electron affinity of the polymer.[156-167]

1.4.3 Optical Properties

The mean conjugation length of the CP is related to the maximum wavelength of both absorption and emission spectra. The first electronic transition of undoped polythiophene (PTh) lies between 300 and 500 nm. As the number of thiophenes increase, both the absorption and emission wavelengths increase due to larger conjugation lengths.

Band gap and colour tuning

As the colour of the emitted light depends on the band gap of the π-π^* transition which is a function of polymeric structure, modifications of the above will affect the band gap and consequently the emitted colour. Usually, PThs emit orange-red light, consistent with their band gap of ca. 2 eV.[168] The PTh emission colour directly depends on the effective conjugation length determined by the twist angle between the thiophene units. Theory predicts a large change in the band gap of PTh depending on the torsion angle between thiophene units. The difference in the band gap of fully planar and 90° twisted PThs is calculated to be 1.7 eV. Although the emission of the substituted PThs is not predictable due to the interaction of several other factors (steric effects, regioregularity, electronic effects, substituents effects, intermolecular interaction-aggregation, side-chain crystallinity).[169, 170] The full visible region, i.e., from blue to red color can be achieved by controlling the conjugation length in polythiophenes.[171] The conjugation length is modified by adding different substituents on the repeating unit, imposing continuous steric torsions of the main chain.[172-175] The larger substituents give a large dihedral angle between the rings, and short conjugation along the polymer backbone is achieved, resulting in blue shifted emission. In the case of Poly (3-(4-octyl phenyl)thiophene)(I), Poly(2-(3-(4-octylphenyl)thiophene-2-yl)thiophene)(II), Poly(3-yclohexylthiophene)(III), Poly(3-cyclohexyl-4-methylthiophene)(IV), steric hindrance offers a blue(IV), green (III), orange (II) and red (I) emission (**Figure 1.12**).[176] Other approaches to tune the emission colour of polythiophene are the preparation of completely coplanar systems with controlled inclusion of head-to-tail dyads or the preparation of alternating block copolymers.

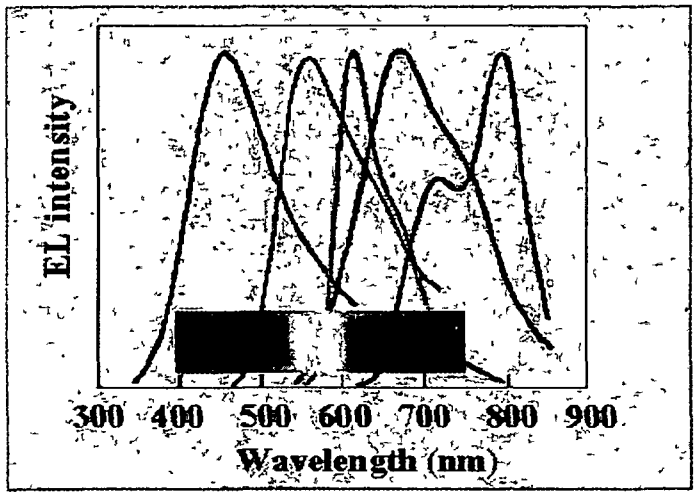

Figure 1.12 Colour tuning in π-conjugated polymers

1.4.4 Solubility of conjugated polymers

From the very beginning, CPs have been found as insoluble and intractable due to their rigid backbone. It was an important goal in basic research as in application-oriented material science to develop techniques by which they could be processed.

A number of general techniques have been developed for improving the solubility of the polymers.[177-182] These include the following

i) Copolymerization
ii) Chain flexibility incorporation
iii) Polymer blending
iv) Chain substitution

Copolymerization

The rigidity of the conjugated chain may be reduced and thereby its solubility improved by copolymerization technique. Block copolymerization of 3- methyl thiophene and methyl methacrylate produces polymers soluble in THF. Poly (3-octylthiophene –co-N-(3-thenyl)-4-amino-2-nitrophenol) develops polymer highly soluble in solvents such as THF, chlorinated solvents, dioxane, toluene, etc.[183] Block copolymers containing thiophene units of several lengths alternating with aliphatic spacers and polyesters have been found to be highly soluble polymers.

Chain Flexibility Incorporation

Chain flexibility can be improved by incorporation of flexible centres or flexible linkages like sulphur, nitrogen, phosphorous etc. in the side chain. Polymers of 3-(ethylmercapto)- and 3,4-bis(ethylmercapto)thiophenes are soluble in common organic solvents such as methylene chloride, chloroform, and THF.

Polymer Blending

Blending of rigid conducting polymers with processable polymers is reported to have improved solubility. The success of blends depends on the mutual adhesion or compatibility of the polymers.

Chain Substitution

Appropriate chain substitution leads to enhanced solubility due to reduction of close packing of the chains in the crystal lattice. Substitution of a long alkyl chain as the side groups gives rise to a soluble CPs. The introduction of alkyl groups longer than butyl yields the materials soluble in common organic solvents. For example, replacement of a long alkyl sulfonate group in the 3- position of the thiophene molecule leads to a water soluble polythiophene. Alkoxy side groups on polythiophenes backbone increase the solubility of the polymer. Short alkoxy chains on polythiophenes lead to insoluble materials but long chain alkoxy substituents led to large increase in solubility. Polythiophene derivatives with fluoroalkyl, ether, hydroxyl, carboxylic acid, amide, urethane groups in side chain have improved the solubility. The presence of bulky phenyl, cyclohexyl substituents in polythiophene makes it soluble in typical organic solvents.

1.5 Application of Conducting Polymers

There are two main groups of applications for organic conducting polymers. The first group utilizes their conductivity as its main property. The second group utilizes their electroactivity. The two groups of applications are briefly described below:

Group I: These applications just use the conductivity of the polymers. The polymers are used because of either their lightweight, biological compatibility for ease of manufacturing

or cost. This group includes Electrostatic materials, Conducting adhesives, Electromagnetic shielding, Printed circuit boards, artificial nerves, antistatic clothing, active electronics (diodes, transistors), and aircraft structures. By coating an insulator with a very thin layer of conducting polymer it is possible to prevent the build up of static electricity. This is particularly important where such a discharge is undesirable. Such a discharge can be dangerous in an environment with flammable gases and liquids and also in the explosives industry.

Conducting adhesives: By placing monomer between two conducting surfaces and allowing it to polymerize it is possible to stick them together. This is a conductive adhesive and is used to stick conducting objects together and allow an electric current to pass through them.

Electromagnetic shielding: Many electrical devices, particularly computers, generate electromagnetic radiation, often radio and microwave frequencies. This can cause malfunctions in nearby electrical devices. The plastic casing used in many of these devices is transparent to such radiation. By coating the inside of the plastic casing with a conductive surface this radiation can be absorbed.

Printed circuit boards: Many electrical appliances use printed circuit boards. These are copper coated epoxy-resins. The copper is selectively etched to produce conducting lines used to connect various devices. These devices are placed in holes cut into the resin. In order to get a good connection the holes need to be lined with a conductor. Copper has been used but the coating method, electroless copper plating, has several problems. This process is being replaced by the polymerization of a conducting plastic. If the board is etched with potassium permanganate solution a thin layer of manganese dioxide is produced only on the surface of the resin. This will then initiate polymerisation of a suitable monomer to produce a layer of conducting polymer.

Artificial nerves: Conducting polymers are smart materials that can mimic biological systems and can be used as components of artificial nerves, electronic noses/tongues, drug-release-and-delivering systems, and artificial muscles. Due to the biocompatibility of some conducting polymers they may be used to transport small electrical signals through the body, i.e. act as artificial nerves.

Aircraft structures: Modern planes and spacecraft are often made with lightweight composites. This makes them vulnerable to damage from lightning bolts. By coating aircraft with a conducting polymer the electricity can be directed away from the vulnerable internals of the aircraft.

Group II: This group utilizes the electroactivity character of the materials. Molecular electronics, electrical displays, chemical, biochemical and thermal sensors, rechargeable batteries, drug release systems, optical computers, ion exchange membranes, electromechanical actuators, photovoltaic cell etc covers into this group.

Sensors: The potential application of conducting polymers in chemical and biological sensors or as gas sensors worldwide in the recent years because of the electrical conductivity of conducting polymers varies in the presence of different substances. In its simplest form, a sensor consists of a planar interdigital electrode coated with conducting polymer thin film. If a particular vapour is absorbed by the film and affects the conductivity, its presence may be detected as a conductivity change. In 1986, interdigited electrodes covered by a PPy layer have been tested by Miasik et al.[184] Radhakrishnan et al. had used phthalocyanine incorporated conducting polymers viz. PA, PPy and polythiophene as sensor materials for detecting NO_2 gas.[185] Contractor et al. had reported the use of electrochemically prepared PA film for urea sensors. The same group is working on biosensors based on conducting polymer also.[186, 187]

Rechargeable batteries: A rechargeable battery or storage battery is a group of one or more electrochemical cells. Batteries were one of the first areas where conducting polymers promised to have a commercial impact. Conducting polymer batteries were investigated by leading companies like BASF/VARTA and Allied Signal.[188] A number of conducting polymers such as polyacetylene, polyaniline and other polyheterocycles have been used as electrode materials for rechargeable batteries. Bridgestone has already marketed a button sized battery using polyaniline and lithium.

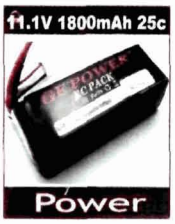

Electrochromic devices: The phenomenon of electrochromism can be defined as the change of the optical properties of a material due to the action of an electric field. The field reversal allows the return to the original state. CPs that can be repeatedly driven from insulating to conductive state electrochemically with high contrast in color are promising materials for electrochromic device technology. CPs have an electronic band structure. The energy gap between the valence band and the conduction band determines the intrinsic optical properties of the polymers. The colour changes elicited by doping are due to the modification of the polymer band electronic structure. The electrochromic materials first drew interest in large area display panels. In architecture electrochromic devices are used to control the sun energy crossing a window. In automotive industry rearview mirrors are a good application for electrochromic system. With oxidation, polypyrrole turns from yellow to black whereas polythiophene turns from red to blue.

Electromechanical Actuators: Conducting polymers also change volume depending on their oxidation state. Therefore it is possible for conducting polymers to convert electrical energy into mechanical work. Conducting polymer actuators were proposed by Baughmann et al.[189] Oxidation induced strain of PA[190] and PPy based actuators has been reported.[191] The first self contained actuators were reported by MacDiarmid et al. in 1994.[192]

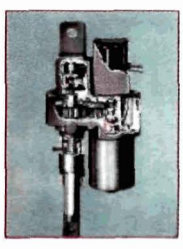

Drug release systems: Another application for conducting polymers is controlled release devices. Ions can be selectively released, as well as biologically active ions such as adenosine 5- triphosphate (ATP) and Heparin.[193-198] Principle used in this application is potential dependence ion transport which is an interesting way to deliver ionic drugs to certain biological systems. One can deliver selective ions depending on the requirement.

Catalyst: Conducting polymers show redox property, therefore these are expected to behave as redox catalyst. Several reports have been found in the literature on modification of conducting polymers and their use as catalyst for small organic molecules. Conducting polymers in their various oxidation states interconvert each other, which permits to construct redox cycle for catalytic reactions. The catalytic activity has been revealed to be controlled by doping. Coordination of transition metals to the nitrogen atoms (in case of PA and PPy) affords the complexes, in which transition metals are considered to interact through a π-conjugated chain. The characteristics of π- conjugated polymers are reflected on the complexes, which are expected to provide a novel catalytic system.

1.6 Research Background and Challenges (Scopes and Objectives)

Pi-conjugated polymer composites with various conductive fillers have recently attracted much attention. They can exhibit significant levels of electrical conductivity suitable for use in electronic devices, rechargeable batteries, functional electrodes, electrochromic devices, sensors, and so on. The principal problem encountered with the potential utilization of virgin CPs like PA, PPy, etc. is their poor processability and the lake of essential mechanical properties. The scientist attempted earlier to incorporate plastics or rubber with CPs in order to improve the processability of the said mixed material without losing the electrical properties.[199] To overcome these drawbacks, some filler are incorporated into these polymer matrices to form composite materials.[200-203] In the recent researches intensive studies have been devoted to the synthetic methodology, structure characterization, stability, electrical and electrochemical properties of CPs. Among the various π-conjugated polymers the greater part of the work on heterocyclic CPs has centred on PA and PPy mainly because of their rather straightforward preparation methods, reasonably stable in air, good electrochemical properties and thermal stability.

They exhibit a wide range of conductivities (10^{-3}-10^{3} S/cm) depending on the functionality and substitution pattern of the monomer and the nature of the counter ion or dopant.[204,205] Both the polymers show their capability to store electrical charges which can be recovered upon demand. For these reasons PA and PPy can be considered as a good candidate for super-capacitors.[206-208]

Graphite, which is naturally abundant and low cost, has widely been used as electronically conducting filler in preparing conducting polymer composites.[90-97] In most of the cases relatively large quantities of graphite are required to reach a critical percolation value. Large amount of graphite concentration is always leading to the poor mechanical property of the composite materials.[209] To overcome this problem the concept of expanded graphite (EG) has been extensively employed. EG is produced from graphite flakes intercalated with concentrated H_2SO_4 followed by rapid thermal treatment which could lead expansion upto several hundred times of the original volume. This expansion splits up the graphite sheet into nanoplates with a very high aspect ratio.[210] The graphite intercalation compounds may provide a possible source for nanocomposite formation with polymers. It is also well known that EG is much lighter, and has a higher specific surface area than carbon powder and carbon nanotubes.[211]

Recently, graphene oxide (GO), a two-dimensional nanosheet of covalently bonded carbon atoms bearing various oxygen functional groups (e.g. hydroxyl, epoxide, and carbonyl groups) on their basal planes and edges, has received a rapidly growing research interest.[212-216] Meanwhile, these oxygen-containing groups impart GO sheets with the function of strong interaction with polar small molecules or polymers to form GO intercalated or exfoliated composites. The thermal stability and electrical properties of polymers could be greatly improved by the incorporation of GO nanosheets.[216-223] Therefore, the potential of using GO-based materials for various applications such as supercapacitor, sensor etc. have attracted much attention very recently.[224-226]

In the present thesis, a considerable effort has been devoted to the synthesis of π-conjugated polymers with special emphasis on the improved electrical and electrochemical properties. The following objectives have been set for the thesis:

Objectives of the present investigation:

- Preparation of expanded graphite and graphene oxide from natural graphite flake and their characterization by FTIR, XRD SEM and TEM analysis.
- Preparation of graphite/expanded graphite/ graphite-oxide filled polyaniline and polypyrrole composites by in-situ polymerization and their characterization by UV-vis, FTIR, XRD, SEM, and TEM analysis.
- Investigation of the electrical, electrochemical and thermal properties of the synthesized polymer composites.
- Application of the prepared polymer composites as capacitor and toxic gas sensor.
- To study the structure – property relationship of conjugated polymer composites for end use application.

References

1. Burroughes, J. H. *et al.* Light-emitting diodes based on conjugated polymers, *Nature* **347,** 539-541 (1990)
2. Hide, F.; Kozodoy, P.; DenBaars, S. P.; Heeger, A. J. White light from InGaN/conjugated polymer hybrid light-emitting diodes, *Appl. Phys. Lett.* **70,** 2664-2666 (1997)
3. Carter, S. A.; Angelopoulos, M.; Karg, S.; Brock, P. J.; Scott, J. C. Polymeric anodes for improved polymer light-emitting diode performance, *Appl. Phys. Lett.* **70,** 2067-2669 (1997)
4. Towns, C. R.; Grizzi, I.; Roberts, M.; Wehrum, A. Conjugated polymer-based light emitting diodes, *J. Lumin.* **122,** 976-979 (2007)
5. Yang, R.; Wu, H.; Cao, Y.; Bazan, G. C. Control of cationic conjugated polymer performance in light emitting diodes by choice of counterion, *J. Am. Chem. Soc.* **128,** 14422-14423 (2006)
6. Mastragostino, M.; Arbizzani, C.; Soavi, F. Polymer-based supercapacitors, *J. Power Sources.* **97,** 812-815 (2001)
7. Frackowiak, E.; Khomenko, V.; Jurewicz, K.; Lota, K.; B´eguin, F. Supercapacitors based on conducting polymers/nanotubes composites, *J. Power Sources* **153,** 413-418 (2006)
8. Yan, J. *et al.* Preparation of a graphene nanosheet/polyaniline composite with high specific capacitance, *Carbon* **48,** 487-493 (2010)
9. Dong, B.; He, B. L.; Xu, C. L.; Li, H. L. Preparation and electrochemical characterization of polyaniline/multi-walled carbon nanotubes composites for supercapacitor, *Mater. Sci. Eng., B* **143,** 7-13 (2007)
10. Zhang, K.; Zhang, L. L.; Zhao, X. S.; Wu, J. Graphene/Polyaniline Nanofiber Composites as Supercapacitor Electrodes, *Chem. Mater.* **22,** 1392-1401 (2010)
11. Sen, P.; De, A. Electrochemical performances of poly(3,4-ethylenedioxythiophene)–$NiFe_2O_4$ nanocomposite as electrode for supercapacitor, *Electrochim. Acta* **55,** 4677-4684 (2010)
12. Wang, H.; Hao, Q.; Yang, X.; Lu, L.; Wang, X. Graphene oxide doped polyaniline for supercapacitors, *Electrochem. Commun.* **11,** 1158-1161 (2009)

13. Arbizzani, C.; Mastragostino, M.; Meneghello, L. Polymer-based redox supercapacitors: A comparative study, *Electrochim. Acta* **41,** 21-26 (1996)

14. Chen, L.; Yuan, C.; Gao, B.; Chen, S.; Zhang, X. Microwave-assisted synthesis of organic–inorganic poly(3,4-ethylenedioxythiophene)/$RuO_2 \cdot xH_2O$ nanocomposite for supercapacitor, *J. Solid State Electrochem.* **13,** 1925-1933 (2009)

15. Vaillant, J.; Lira-Cantu, M.; Cuentas-Gallegos, K.; Casañ-Pastor, N.; Gómez-Romero, P. Chemical synthesis of hybrid materials based on PAni and PEDOT with polyoxometalates for electrochemical supercapacitors, *Prog. Solid State Chem.* **34,** 147-159 (2006)

16. Veeraraghavan, B.; Paul, J.; Haran, B.; Popov, B. Study of polypyrrole graphite composite as anode material for secondary lithium-ion batteries, *J. Power Sources* **109,** 377-387 (2002)

17. Kwang, S. R.; Kim, K. M.; Hong, Y. S.; Park, Y. J.; Chang, S. H. The polyaniline electrode doped with Li salt and protonic acid in lithium secondary battery, *Bull. Korean Chem. Soc.* **23,** 1144-1148 (2002)

18. Ryu, K. S.; Jeong, S. K.; Joo, J. ; Kim, K. M. Polyaniline doped with dimethyl sulfate as a nucleophilic dopant and its electrochemical properties as an electrode in a lithium secondary battery and a redox supercapacitor, *J. Phys. Chem. B* **111,** 731-739 (2007)

19. Ghanbari, K.; Mousavi, M. F.; Shamsipur, M.; Karami, H. Synthesis of polyaniline/graphite composite as a cathode of Zn-polyaniline rechargeable battery, *J. Power Sources* **170,** 513-519 (2007)

20. Coakley, K. M.; McGehee, M. D. Conjugated polymer photovoltaic cells, *Chem. Mater.* **16,** 4533-4542 (2004)

21. Li, G. *et al.* High-efficiency solution processable polymer photovoltaic cells by self-organization of polymer blends, *Nat. Mat.* **4,** 864-868 (2005)

22. Kim, M. S. *et al.* Flexible conjugated polymer photovoltaic cells with controlled heterojunctions fabricated using nanoimprint lithography, *Appl. Phys. Lett.* **90,** 123113-123116 (2007)

23. Pokhrel, B.; Kamrupi, I. R.; Maiti, J.; Adhikari, B.; Dolui, S. K. Synthesis, characterization, and photovoltaic properties of poly(3-Phenyl azomethine Alkylthiophene) polymers, *J. Electron. Mater.* **40,** 149-156 (2011)

24. Chithra lekha, P.; Balaji, M.; Subramanian, S.; Pathinettam, D. P. Sensing properties of polyoxomolybdate doped polyaniline nanomaterials for oxidising and reducing volatile organic compounds, *Curr. Appl. Phys.* **10,** 457-467 (2010)

25. Jung, Y. S.; Jung, W. C.; Tuller, H. L.; Ross, C. A. Nanowire conductive polymer gas sensor patterned using self-assembled block copolymer lithography, *Nano Lett.* **8,** 3776-3780 (2008)

26. Esser, B.; Swager, T. M. Detection of ethylene gas by fluorescence turn-on of a conjugated polymer, *Angew. Chem., Int. Ed.* **49,** 8872-8875 (2010)

27. Ince, F. G. *et al.* Fabrication of plasma polymerized polythiophene and polypyrrole thin films as chloroform vapor sensors, *J. Optoelectron. Adv. Mater.* **11,** 1182-1185 (2009)

28. Liu, X.; Fan, Q.; Huang, W. DNA biosensors based on water-soluble conjugated polymers, *Biosens. Bioelectron.* **26,** 2154-2164 (2011)

29. Feng, J.; Li, Y.; Yang, M. Conjugated polymer-grafted silica nanoparticles for the sensitive detection of TNT, *Sens. Actuators, B* **145,** 438-443 (2010)

30. Chiang, C. K. *et al.* Electrical conductivity in doped polyacetylene, *Phys. Rev. Lett.* **39,** 1098-1101 (1977)

31. Shirakawa, H.; Louis, E. J.; MacDiarmid, A. G.; Chiang, C. K.; Heeger, A. J. Synthesis of electrically conducting organic polymers: halogen derivatives of polyacetylene, *J. Chem. Soc.,Chem. Comm.* 578-580 (1977)

32. Shirakawa, H. The discovery of polyacetylene film: the dawning of an era of conducting polymers (Nobel lecture), *Angew. Chem., Int. Ed.* **40,** 2575-2580 (2001)

33. Blythe, T.; Bloor, D. *Electrical Properties of Polymers* (United State of America, Cambridge University Press, New York, 2005)

34. Freund, M. S.; Deore, B. A. *Self-doped conducting polymers* (John Wiley and Sons Ltd, 2007)

35. Su, W. P.; Shrieffer, J. R.; Heeger, A. J. Solitons in polyacetylene, *Phys. Rev. Lett.* **42,** 1698-1701 (1979)

36. Su, W. P.; Shrieffer, J. R.; Heeger, A. J. Soliton excitations in polyacetylene, *Phys. Rev. B* **22,** 2099-2111 (1980)

37. Ivory, D. M. *et al.* Highly conducting charge-transfer complexes of poly(p-phenylene), *J. Chem. Phys.* **71,** 1506-1507 (1979)

38. Nigrey, P. J.; MacDiarmid, A. G.; Heeger, A. J. Electrochemistry of polyacetylene, $(CH)_x$: electrochemical doping of $(CH)_x$ films, *J. Chem. Soc., Chem. Commun.* 594-595 (1979)

39. Burroughes, J. H.; Jones, C. A.; Friend, R. H. New semiconductor device physics in polymer diodes and transistors, *Nature* **335,** 137-141 (1988)

40. Yildiz, U. H. *et al.* A new soluble conducting polymer and its electrochromic devices, *J. Polym. Sci., Part A: Polym. Chem.* **44,** 2215-2225 (2006)

41. MacDiarmid, A. G.; Zhang, W. Electrochemistry of conjugated polymers and electrochemical applications, *MRS Bulletin* **22,** 24-28 (1997)

42. Katz, H. E.; Huang, J. Thin-film organic electronic devices, *Annu. Rev. Mater. Res.* **39,** 71-92 (2009)

43. Sun, Q.; Li, Y.; Pei, Q. Polymer light-emitting electrochemical cells for high-efficiency low-voltage electroluminescent devices, *J. Display Technol.* **3,** 211-224 (2007)

44. Burroughes, J. H. *et al.* Light-emitting diodes based on conjugated polymers, *Nature* **347,** 539-541 (1990)

45. Snook, G. A.; Kao, P.; Best, A. S. Conducting-polymer-based supercapacitor devices and electrodes, *J. Power Sources* **196,** 1-12 (2011)

46. Xu, X.; Zhang, H.; Liu, X.; Zhuang, Q.; Han, Z. Synthesis and photoluminescence stability of non-conjugated polymers based on fluorene and benzoxazole, *Eur. Polym. J.* **46,** 528-534 (2010)

47. Metz, P.; Alici, G.; Spinks, G. M. A finite element model for bending behaviour of conducting polymer electromechanical actuators, *Sens. Actuators, A* **130,** 1-11 (2006)

48. Sengupta, R.; Bhattacharya, M.; Bandyopadhyay, S.; Bhowmick, A. K. A review on the mechanical and electrical properties of graphite and modified graphite reinforced polymer composites, *Prog. Polym. Sci.* **36,** 638-670 (2011)

49. Tung, N. T.; Khai, T. V.; Lee, H.; Sohn, D. The effects of dopant on morphology formation in polyaniline graphite nanoplatelet composite, *Synth. Met.* **161,** 177-182 (2011)

50. Causin, V.; Marega, C.; Marigo, A.; Ferrara, G.; Ferraro, A. Morphological and structural characterization of polypropylene/conductive graphite nanocomposites, *Eur. Polym. J.* **42,** 3153-3161 (2006)

51. Spitalsky, Z.; Tasis, D.; Papagelis, K.; Galiotis, C. Carbon nanotube–polymer composites: Chemistry, processing, mechanical and electrical properties, *Prog. Polym. Sci.* **35,** 357-401 (2010)

52. Bauhofer, W.; Kovacs, J. Z. A review and analysis of electrical percolation in carbon nanotube polymer composites, *Comp. Sci. Tech.* **69,** 1486-1498 (2009)

53. Zeng, Y. *et al.* Increasing the electrical conductivity of carbon nanotube/polymer composites by using weak nanotube–polymer interactions, *Carbon* **48,** 3551-3558 (2010)

54. Kuilla, T. *et al.* Recent advances in graphene based polymer composites, *Prog. Polym. Sci.* **35,** 1350-1375 (2010)

55. Potts, J. R.; Dreyer, D. R.; Bielawski, C. W.; Ruoff, R. S. Graphene-based polymer nanocomposites, *Polymer* **52,** 5-25 (2011)

56. Vadukumpully, S.; Paul, J.; Mahanta, N.; Valiyaveettil, S. Flexible conductive graphene/poly(vinyl chloride) composite thin films with high mechanical strength and thermal stability, *Carbon* **49,** 198-205 (2011)

57. Vats, T. *et al.* Comparison of photostability, optical and structural properties of TiO_2/conjugated polymer hybrid composites prepared via different methods, *Thin Solid Films* **519,** 1100-1105 (2010)

58. Gurunathan, K.; Trivedi, D. C. Studies on polyaniline and colloidal TiO_2 composites, *Mater. Lett.* **45,** 262-268 (2000)

59. Min, S. X.; Wang, F.; Feng, L.; Tong, Y. C.; Yang, Z. R. Synthesis and photocatalytic activity of TiO_2/conjugated polymer complex nanoparticles, *Chin. Chem. Lett.* **19,** 742-746 (2008)

60. Chang, C. J.; Tsai, M. H.; Hsu, Y. H.; Tuan, C. S. Morphology and optoelectronic properties of ZnO rod array/conjugated polymer hybrid films, *Thin Solid Films* **516,** 5523-5526 (2008)

61. Jetson, R.; Yin, K.; Donovan, K.; Zhu, Z. Effects of surface modification on the fluorescence properties of conjugated polymer/ZnO nanocomposites, *Mat. Chem. Phys.* **124,** 417-421 (2010)

62. Chiang, C. K. *et al.* Electrical conductivity in doped polyacetylene, *Phys. Rev. Lett.* **39,** 1098-1101 (1977)

63. Chiang, C. K. *et al.* Synthesis of highly conducting films of derivatives of polyacetylene (CH)x, *J. Am. Chem. Soc.* **100,** 1013-1015 (1978)

64. Letheby, H. On the production of a blue substance by the electrolysis of sulphate of aniline, *J. Chem. Soc.* **15,** 161-163 (1862)

65. M S Cho et al. An electroactive conducting polymer actuator based on NBR/RTIL solid polymer electrolyte, *Smart Mater. Struct.* **16,** 237-240 (2007)

66. Surville, R. D; Josefowicz, M.; Yu, L. T.; Pepichon, J.; Buvet, R. Electrochemical chains using protolytic organic semiconductors, *Electrochim. Acta* **13,** 1451-1458 (1968)

67. Shirakawa, H.; Louis, E. J.; Macdiarmid, A. G.; Chiang C. K.; Heeger, A. J. Synthesis of electrically conducting organic polymers: Halogen derivatives of polyacetylene, (CH)x, *J. Chem. Soc., Chem. Commun.* 578-580 (1977)

68. Epstein, A. J. *Conductive Polymers and Plastics In Industrial Applications.* (Norwich, New York, Plastics Design Library, 1999)

69. Bredas, J. L.; Silbey, R. *Conjugated Polymers: The Novel Science and Technology of Highly Conducting and Nonlinear Optically Active Materials:* (Kluwer, Netherlands, 1991)

70. Gospodinova, N.; Terlemezyan, L. Conducting polymers prepared by oxidative polymerization: polyaniline, *Prog. Polym. Sci.* **23,** 1443-1484 (1998)

71. Armes, S. P.; Miller, J. F. Optimum reaction conditions for the polymerization of aniline in aqueous solution by ammonium persulphate, *Synth. Met.* **22,** 385-393 (1988)

72. Cao, Y.; Andreatta, A.; Heeger, A. J.; Smith, P. Influence of chemical polymerization conditions on the properties of polyaniline, *Polymer* **30,** 2305-2311 (1989)

73. Pron, A.; Genoud, F.; Menarod, C.; Nechtstein, M. The effect of the oxidation conditions on the chemical polymerization of polyaniline, *Synth. Met.* **24,** 193-201 (1988)

74. Trivedi, D.C. *Handbook of Organic Conductive Molecules and Polymers* (John Wiley, London, 1997)

75. Noufi, R.; Nozik, A. J.; White, J.; Warren, L. F. Enhanced stability of photoelectrodes with electrogenerated polyaniline films, *J. Electrochem. Soc.* **129,** 2261-2265 (1982)

76. Kang, E. T. *et al.* Surface studies of chemically processed polyaniline films, *Synth. Met.* **53,** 333-345 (1993)

77. Mu, S.; Kan, J. The effect of salts on the electrochemical polymerization of aniline, *Synth. Met.* **92,** 149-155 (1998)

78. Chen, S. A.; Lee, H. T. Polyaniline plasticized with 1-methyl-2-pyrrolidone: structure and doping behavior, *Macromolecules* **26,** 3254-3261 (1993)

79. Lux, F. Properties of electronically conductive polyaniline - A comparison between well-known literature data and some recent experimental findings, *Polymer* **35,** 2915-2936 (1994)

80. Nalwa H.S. *Handbook of Advanced Electronic and Photonic Materials and Devices* (Academic Press, London, 2001)

81. Nalawa, H. S.; Dalton, L. R.; Schmidt, W. F.; Rabe, J. G. Electrical and optical studies of chemically synthesized polypyrrole, *Polym. Commun.* **27,** 240-242 (1985)

82. Hsing, C. F.; Kovacic, P.; Khoury, I. A. Oligomers from biphenyl, biphenyl-d_{10}, or *p*-terphenyl with aluminium chloride-cupric chloride: Mechanism, ESR, and conductivity, *J. Polym. Sci., Part A: Polym. Chem.* **21,** 457-466 (1983)

83. Qian, R.; Qiu, J.; Shen D. Conducting polypyrrole electrochemically prepared from aqueous solutions, *Synth. Met,* **18,** 13-18 (1987)

84. Diaz, A. F.; Kanazawa, K. K.; Gardini, G. P. Electrochemical polymerization of pyrrole, *J. Chem. Soc., Chem. Commun.* 635-636 (1979)

85. Yoshimura, S.; Chang, R. P. H. *Supercarbon-Synthesis, Properties and Applications* (Springer-Verlag, Berlin, Heidelberg, 1998)

86. Chen, G.; Wu, C.; Weng, W.; Wu, D.; Yan, W. Preparation of polystyrene/graphite nanosheet composite, *Polymer* **44**, 1781–1784 (2003)

87. Calixto, C. M. F. *et al.* Development of graphite-polymer composites as electrode materials, *Mater. Res.* **10,** 109-114 (2007)

88. Park, J. H.; Ko, J. M.; Park, O. O.; Kim, D. W. Capacitance properties of graphite/polypyrrole composite electrode prepared by chemical polymerization of pyrrole on graphite fiber, *J. Power Sources* **105,** 20-25 (2002)

89. Chen, G. H.; Wu, D. J.; Weng, W. G.; Yan, W. L. Preparation of polymer/graphite conducting nanocomposite by intercalation polymerization, *J. Appl. Polym. Sci.* **82,** 2506-2513 (2001)

90. Zabel, H.; Solin, S. A. *Graphite Intercalation Compounds I—Structure and Dynamics* (Springer-Verlag, Berlin, Heidelberg, New York, 1990)

91. Bourdo, S. E., Viswanathan, T. Graphite/Polyaniline (GP) composites: Synthesis and characterization, *Carbon* **43,** 2983-2988 (2005)

92. Xiao, P., Xiao, M.; Liu, P. G.; Gong, K. C. Direct synthesis of a polyaniline-intercalated graphite oxide nanocomposite, *Carbon* **38,** 626-628 (2000)

93. Du, X. S.; Xiao, M.; Meng, Y. Z. Facile synthesis of highly conductive polyaniline/graphite nanocomposites, *Eur. Polym. J.* **40,** 1489-1493 (2004)

94. Chen, G. H.; Wu, C. L.; Weng, W. G.; Wu, D. J.; Yan, W. L. Preparation of polystyrene/graphite nanosheet composite, *Polymer* **44,** 1781-1784 (2003)

95. Xiao, P.; Xiao, M.; Gong, K. Preparation of exfoliated graphite/polystyrene composite by polymerization-filling technique, *Polymer* **42,** 4813-4816 (2001)

96. Xiao, M.; Sun, L.; Liu, J.; Li, Y.; Gong, K. Synthesis and properties of polystyrene/graphite nanocomposites, *Polymer* **43,** 2245-2248 (2002)

97. Wang, W. P.; Pan, C. Y. Synthesis and characterizations of poly(ethylene oxide) methyl ether grafted on the expanded graphite with isocyanate groups, *Eur. Polym. J.* **40,** 543-548 (2004)

98. Zheng, G.; Wu, J.; Wang, W.; Pan, C. Characterizations of expanded graphite/polymer composites prepared by in situ polymerization, *Carbon* **42,** 2839-2847 (2004)

99. Liu, P.; Xiao, P.; Xiao, M.; Gong, K. Synthesis of poly (vinyl acetate)-intercalated graphite oxide by an in situ intercalative polymerization, *Chin. J. Polym. Sci.* **18,** 413-418 (2000)

100. Chen, G. H. *et al.* Investigation on the nano-dispersion of graphite into polymer matrix, *Acta. Polym. Sin.* **6,** 803-806 (2001)

101. Celzard A.; McRae, E.; Furdin, G.; Mareche, J. F. Conduction mechanisms in some graphite - polymer composites: the effect of a direct-current electric field, *J. Phys.: Condens. Matter.* **9,** 2225-2237 (1997)

102. Dawson, J. C.; Adkins, C. J. Conduction mechanisms in carbon-loaded composites, *J. Phys.: Condens. Matter.* **8,** 8321-8338 (1996)

103. Zou, J. F.; Yu, Z. Z.; Pan, Y. X.; Fang, X. P.; Ou, Y. C. Conductive mechanism of polymer/graphite conducting composites with low percolation threshold, *J. Polym. Sci., Part B: Polym. Phys.* **40,** 954-963 (2002)

104. Park, J. H.; Ko, J. M.; Park, O. O.; Kim, D. W. Capacitance properties of graphite/polypyrrole composite electrode prepared by chemical polymerization of pyrrole on graphite fiber, *J. Power Sources* **105,** 20-25 (2002)

105. Cakar, F.; Moroglu, M. R.; Cankurtaran, H.; Karaman, F. Conducting poly(ether imide)–graphite composite for some solvent vapors sensing application, *sens. Actuators, B* **145,** 126-132 (2010)

106. Kroto, H. W.; Heath, J. R.; O'Brien, S. C.; Curl, R. F.; Smalley, R. E. C_{60}: Buckminsterfullerene, *Nature* **318,** 162-163 (1985)

107. Iijima, S. Helical microtubules of graphitic carbon, *Nature* **354,** 56-58 (1991)

108. Dekker, C. Carbon nanotubes as molecular quantum wires, *Physics Today* **55,** 22-28 (1999)

109. Wu, T. M.; Lin, Y. W.; Liao, C. S. Preparation and characterization of polyaniline/multi-walled carbon nanotube composites, *Carbon* **43,** 734-740 (2005)

110. Hrapovic, S.; Male, K. B.; Liu, Y.; Luong, J. H. T. Preparation of polymer-carbon nanotube composite materials and their applications for enzyme entrapment, *Anal. Lett.* **41,** 278-288 (2008)

111. Cochet, M. *et al.* Synthesis of a new polyaniline/nanotube composite: "*in-situ*" polymerization and charge transfer through site-selective interaction, *Chem. Commun.* 1450-1451 (2001)

112. Huang, J. E.; Li, X. H.; Xu, J. C.; Li, H. L. Well-dispersed single-walled carbon nanotube/ polyaniline composite films, *Carbon* **41,** 2731-2736 (2003)

113. Wei, Z.; Wan, M.; Lin, T.; Dai, L. Polyaniline nanotubes doped with sulfonated carbon nanotubes made via a self-assembly process, *Adv. Mater.* **15,** 136–139 (2003)

114. Zhang, X.; Zhang, J.; Wang, R.; Liu, Z. Cationic surfactant directed polyaniline/CNT nanocables: synthesis, characterization, and enhanced electrical properties, *Carbon* **42,** 1455-1461 (2004)

115. Baibarac, M.; Baltog, I.; Godon, C.; Lefrant, S.; Chauvet, O. Covalent functionalization of single-walled carbon nanotubes by aniline electrochemical polymerization, *Carbon* **42,** 3143-3152 (2004)

116. Santhosh, P.; Gopalan, A.; Lee, K. P. Gold nanoparticles dispersed polyaniline grafted multiwall carbon nanotubes as newer electrocatalysts: Preparation and performances for methanol oxidation, *J. Catal.* **238,** 177-185 (2006)

117. Wu, G.; Li, L.; Li, J. H.; Xu, B. Q. Methanol electrooxidation on Pt particles dispersed into PANI/SWNT composite films, *J. Power Sources* **155,** 118-127 (2006)

118. Gupta, V.; Miura, N. Influence of the microstructure on the supercapacitive behavior of polyaniline/single-wall carbon nanotube composites, *J. Power Sources* **157,** 616-620 (2006)

119. Gupta, V.; Miura, N. Polyaniline/single-wall carbon nanotube (PANI/SWCNT) composites for high performance supercapacitors, *Electrochim. Acta* **52,** 1721–1726 (2006)

120. Khomenko,V.; Frackowiak, E.; Béguin, F. Determination of the specific capacitance of conducting polymer/nanotubes composite electrodes using different cell configurations, *Electrochim. Acta* **50,** 2499-2506 (2005)

121. Dong, B.; He, B. L.; Xu, C. L.; Li, H. L. Preparation and electrochemical characterization of polyaniline/multi-walled carbon nanotubes composites for supercapacitor, *Mater. Sci. Eng., B* **143,** 7-13 (2007)

122. Geim, A. K.; Novoselov, K. S. The rise of graphene, *Nat. Mater.* **6,** 183-191 (2007)

123. http://www.raremetalblog.com/2010/10/the-london-ree-report-graphene-and-supercapicors, (accessed on 04.04.2011)

124. http://nobelprize.org/nobel_prizes/physics/laureates/2010/press.html, (accessed on 04.04.2011)

125. Wang, D. W. *et al.* Fabrication of graphene/polyaniline composite paper via in situ anodic electropolymerization for high-performance flexible electrode, *ACS Nano* **3,** 1745-1752 (2009)

126. Collins, P. G.; Avouris, P. *Nanotubes for electronics* (Scientific American, December, 2000)

127. Zhu, S. S.; Swager, T. M. Design of conducting redox polymers: A polythiophene-$Ru(bipy)_3$;$^{n\oplus}$Hybrid Material, *Adv. Mater.* **8,** 497-500 (1996)

128. Zhu, S. S.; Kingsborough, R. P.; Swager, T. M. Conducting redox polymers: investigations of polythiophene–$Ru(bpy)_3^{n+}$ hybrid materials, *J. Mater. Chem.* **9,** 2123- 2131 (1999)

129. Ofer, D.; Crooks, R. M.; Wrighton, M. S. Potential dependence of the conductivity of highly oxidized polythiophenes, polypyrroles, and polyaniline: finite windows of high conductivity, *J. Am. Chem. Soc.* **112,** 7869-7879 (1990)

130. http://pslc.ws/macrog/imide.htm, (accessed on 04.04.2011)

131. Peredereeva, S. I.; Orlov, I. G.; Cherkashin, M. I. Polymeric charge-transfer complexes, *Russ. Chem. Rev.* **44,** 295-305 (1975)

132. Palaniappan, S.; Sathyanarayana, D. N. Polymeric charge-transfer complexes: a study by electronic absorption spectroscopy, *Polymer* **31,** 1401-1405 (1990)

133. Bakulin, A. A.; Martyanov, D.; Paraschuk, D. Y.; Loosdrecht, P. H. M.; Pshenichnikov, M. S. Charge-transfer complexes of conjugated polymers as

intermediates in charge photogeneration for organic photovoltaics, *Chem. Phys. Lett.* **482,** 99-104 (2009)

134. Zapunidy, S.A. *et al.* Approaches to low-bandgap polymer solar cells: Using polymer charge-transfer complexes and fullerene metallocomplexes, *Pure Appl. Chem.* **80,** 2151-2161 (2008)

135. Singh, R. A.; Gupta, R. K.; Singh, S. K. Preparation and characterization of polymer composites based on charge-transfer complex of phenothiazine–iodine in polystyrene, *Bull. Mater. Sci.* **28,** 423-429 (2005)

136. Heeger, A. J.; Kivelson, S.; Schrieffer, J. R.; Su, W. P. Solitons in conducting polymers, *Rev. Mod. Phys.* **60,** 781-850 (1988)

137. Burroughes, J.H. *et al.* Light-emitting diodes based on conjugated polymers, *Nature* **347,** 539-541 (1990)

138. Dimitrakopoulos, C. D.; Malenfant, P. R. L. Organic thin film transistors for Large area electronics, *Adv. Mater.***14,** 99-117 (2002)

139. Ong, B. S.; Wu, Y.; Liu, P.; Gardner, S. High-performance semiconducting polythiophenes for organic thin-film transistors, *J. Am. Chem. Soc.***126,** 3378-3379 (2004)

140. Gunes, S.; Neugebauer, H.; Sariciftci, N. S. Conjugated polymer-based organic solar cells, *Chem. Rev.***107,** 1324-1338 (2007)

141. http://en.wikipedia.org/wiki/PLED (accessed on 04.04.2011)

142. Grimsdale, A. C.; Chan, K. L.; Martin, R. E.; Jokisz, P. G.; Holmes, A. B. Synthesis of light-emitting conjugated polymers for applications in electroluminescent devices, *Chem. Rev.* **109,** 897-1091 (2009)

143. Gong, X.; Robinson, M. R.; Ostrowski, J. C.; Bazan, G. C.; Heeger, A. J. High-efficiency polymer-based electrophosphorescent devices, *Adv. Mater.* **14,** 581-585 (2002)

144. Perepichka, I. F.; Perepichika, D. F.; Meng, H.; Wudl, F. Light-emitting polythiophenes, *Adv. Mater.* **17,** 2281-2305 (2005)

145. Friend, R.H. Conductive polymer II - from science to application, *Rapra Review Reports* **6,** 3-18 (1993)

146. Fesser, K.; Bishop, A. R.; Campbell, D. K. Optical absorption from polaron in a model of polyacetylene, *Phys. Rev. B.* **27,** 4804-4825 (1983)

147. Billingham, N.C.; Calvert, P.D. *Advances In Polymer Science 90* (Springer-Verlag, New York, Heidelberg, 1989)

148. Roth, S. Introduction to the physics of conducting polymers, *Mater. Sci. Forum.* **21,** 1-12 (1987)

149. Zuo, F.; Angelopolous, M.; MacDiarmid, A. G.; Epstein, A. J. Transport studies of protonated emeraldine polymer: a granular polymeric metal system, *Phys. Rev. B.* **36,** 3475-3478 (1987)

150. Roth, S. *One-Dimensional Metals: Physics and Materials Science* (VCH Weinheim, Germany, 1995)

151. Trivedi, D. C. *Handbook of Organic Conductive Molecules and Polymers: Vol. 2. Conductive Polymers: Synthesis and Electrical Properties.* (John Wiley, England, 1997)

152. Cataldo, F.; Maltese, P. Synthesis of alkyl and N-alkyl-substituted polyanilines: A study on their spectral properties and thermal stability, *Eur. Polym. J.* **38,** 1791-1803 (2002)

153. Luzny, W.; Kaniowski, T.; Pron, A. Structural and transport properties of thermally processable conducting polymer: Polyaniline protonated with diphenyl phosphate, *Polymer* **39,** 475-483 (1998)

154. Bredas, J. L.; Silbey, R. Bourdreaux, D. S.; Chance, R. R. Chain-length dependence of electronic and electrochemical properties of conjugated systems: polyacetylene, polyphenylene, polythiophene, and polypyrrole, *J. Am. Chem. Soc.* **105,** 6555-6559 (1983)

155. Hu, X.; Xu, L. Structure and properties of 3-alkoxy substituted polythiophene synthesized at low temperature, *Polymer* **41,** 9147-9154 (2000)

156. Fichou, D. Structural order in conjugated oligothiophenes and its implications on opto-electronic devices, *J. Mater. Chem.* **10,** 571-588 (2000)

157. Leclerc, M.; Faid, K. Electrical and optical properties of processable polythiophene derivatives: Structure-property relationships, *Adv. Mater.* **9,** 1087-1094 (1997)

158. Anderson, M. R.; Beggren, M.; Inganas, O.; Gustafsson, G. Electroluminescence from substituted poly(thiophenes)-from blue to nearinfrared, *Macromolecules* **28,** 7525-7529 (1995)

159. Andersson, M. R. *et al.* Substituted polythiophenes designed for optoclectronic devices and conductors, *J. Mater. Chem.* **9,** 1933-1940 (1999)

160. Pomerantz, M.; Yang, H.; Cheng, Y. Poly(alkyl thiophene-3-carboxylates). synthesis and characterization of polythiophenes with a carbonyl group directly attached to the ring, *Macromolecules* **28,** 5706-5708 (1995)

161. Pomerantz, M.; Chang, Y.; Kasim, R. K.; Elsenbaumer, R. L. Poly(alkyl thiophene-3-carboxylates). Synthesis, properties and electroluminescence studies of polythiophenes containing a carbonyl group directly attached to the ring, *J.Mater. Chem.* **9,** 2155-2163 (1999)

162. Lanzi, M.; Bizzarri, P. C.; Paganin, L.; Cesari, G. Highly processable esterfunctionalized polythiophenes as valuable multifunctional and postfunctionalizable conjugated polymers, *Eur. Polym. J.* **43,** 72-83 (2007)

163. Murphy, A.R. *et al.* Synthesis, characterization, and field-effect transistor performance of carboxylate-functionalized polythiophenes with increased air stability, *Chem. Mater.* **17,** 4892-4899 (2005)

164. Kang, T. K.; Kim, J. Y.; Kim, K. J.; Lee, C.; Rhee, S. B. Photoluminescence properties of various polythiophene derivates, *Synth. Met.* **69,** 377-378 (1995)

165. Lee, C.; Kim, K. J.; Rhee, S. B. The effects of ester substitution and alkyl chain length on the properties of poly(thiophene)s, *Synth. Met.* **69,** 295-296 (1995)

166. Lee, S.; Hong, S. I.; Lee, C.; Rhee, S. B.; Kang, T. J. Luminescence study of poly(3-alkyl ester thiophene)s, *Mol. Cryst. Liq. Cryst.* **295,** 19-22 (1997)

167. Bolognesi, A.; Botta, C.; Geng, Z.; Flores, C.; Denti, L. Modified poly(3-alkylthiophene) for LED preparation, *Synth. Met.* **71,** 2191-2192 (1995)

168. Perepichka, I. F.; Perepichika, D. F.; Meng, H.; Wudl, F. Light-emitting polythiophenes, *Adv. Mater.* **17,** 2281-2305 (2005)

169. Chan, H. S. O.; Ng, S. C. Synthesis, characterization and applications of thiophene-based functional polymers, *Prog. Polym. Sci.* **23,** 1167-1231 (1998)

170. Somanathan, N.; Radhakrishnan, S. Optical properties of functionalized polythiophenes, *Int. J. Mod. Phys. B* **19,** 4645-4676 (2005)

171. Akcelrud, L. Electroluminescent polymers, *Prog. Polym. Sci.* **28,** 875-962 (2003)

172. Anderson, M. R. *et al.* Substituted polythiophenes designed for optoelectronic devices and conductors, *J. Mater. Chem.* **9,** 1933-1940 (1999)

173. Pomerantz, M.; Yang, H.; Cheng, Y. Poly(alkyl thiophene-3-carboxylates). Synthesis and characterization of polythiophenes with a carbonyl group directly attached to the ring, *Macromolecules* **28,** 5706-5708 (1995)

174. Pomerantz, M.; Chang. Y.; Kasim, R. K.; Elsenbaumer, R. L. Poly(alkyl thiophene-3-carboxylates). Synthesis, properties and electroluminescence studies of polythiophenes containing a carbonyl group directly attached to the ring, *J. Mater. Chem.* **9,** 2155-2163 (1999)

175. Lanzi, M.; Bizzarri, P. C.; Paganin, L.; Cesari, G. Highly processable ester-functionalized polythiophenes as valuable multifunctional and post-functionalizable conjugated polymers, *Eur. Polym. J.* **43,** 72-83 (2007)

176. Anderson, M. R. *et al.* Electroluminescence from substituted poly(thiophenes): from blue to near-infrared, *Macromolecules* **28,** 7525-7529 (1995)

177. Hu, X.; Xu, L. Structure and properties of 3-alkoxy substituted polythiophene synthesized at low temperature, *Polymer* **41,** 9147-9154 (2000)

178. Leclerc, M.; Faid, K. Electrical and optical properties of processable polythiophene derivatives: Structure-property relationships, *Adv. Mater.* **9,** 1087-1094 (1997)

179. Zhao, X.; Hu, X.; Gan, L. H. Photoluminescent behavior of poly(3-hexylthiophene) derivatives with a high azobenzene content in the side chains, *Polym. Adv. Technol.* **16,** 370-377 (2005)

180. Daoust, V.; Leclerc, M. Structure-property relationships in alkoxy-substituted polythiophenes, *Macromolecules* **24,** 455-459 (1991)

181. Lanzi, M.; Bizzarri, P. C.; Paganin, L.; Cesari, G. Highly processable esterfunctionalized polythiophenes as valuable multifunctional and postfunctionalizable conjugated polymers, *Eur. Polym. J.* **43,** 72-83 (2007)

182. Chittibabu, K. G.; Li, L.; Kamath, M.; Kumar, J.; Tripathy, S. K. Synthesis and properties of a novel polythiophene derivative with a side-chain NLO chromophore, *Chem. Mater.* **6,** 475-480 (1994)

183. J. R. Lakowitz, (Ed.): Principles of fluorescence spectroscopy, (Kluwer Academic, New York, 1999)

184. Miasik, J.; Hopper, A.; Tofield, B. Conducting polymer gas sensors, *J. Chem. Soc. Faraday Trans.1* **82,** 1117-1126 (1986)

185. Radhakrishnan, S.; Deshpande, S. D. Conducting polymers functionalized with phthalocyanine as nitrogen dioxide sensors, *Sensors* **2,** 185-194 (2002)

186. Kanungo, M.; Kumar, A.; Contractor, A. Q. Studies on electropolymerization of aniline in the presence of sodium dodecyl sulfate and its application in sensing urea, *J. Electroanal. Chem.* **528,** 46-56 (2002)

187. Contractor, A. Q. *et al.* Conducting polymer-based biosensors, *Electrochim. Acta.* **39,** 1321-1324 (1994)

188. Shacklette, L. W.; Jow, T. R.; Maxfield, M.; Hatami, R. High energy density batteries derived from conductive polymers, *Synth. Met.* **28,** 655-662 (1989)

189. Baughmann, R. H. Conducting polymer artificial muscles, *Synth. Met.* **78,** 339-353 (1996)

190. Herod, T. E.; Schlenoff, J. B. Doping-induced strain in polyaniline: stretchoelectrochemistry, *Chem. Mater.* **5,** 951-955 (1993)

191. Hara, S.; Zama, T.; Takashima, W.; Kaneto, K. TFSI-doped polypyrrole actuator with 26% strain, *J. Mater. Chem.* **14,** 1516-1517 (2004)

192. McDiarmid, A. G., Kaneto, K.; Saito, H.; Min. Y.; Electromechanical actuators using polyaniline-polyaniline films, *Polymeric Materials Science and Engineering,* **71,** 713-727 (1994)

193. Champagne, S. D.; Reynolds, J. R.; Pomerantz, M. Charge- and ion-transport properties of polypyrrole/poly(styrenesulfonate): poly(3-octylthiophene) bilayers, *Chem. Mater.* **7,** 277-283 (1995)

194. Reynolds, J. R.; Pyo, M.; Qui, Y. J. Cation and anion dominated ion transport during electrochemical switching of polypyrrole controlled by polymer-ion interactions, *Synth. Met.* **55,** 1388-1395 (1993)

195. Pyo, M.; Reynolds, J. R. Dual ion transport during electrochemical switching of conducting polymer bilayers, *J. Chem Soc. Chem.Commun.* 258-260 (1993)

196. Pyo, M.; Reynolds, J. R. Poly(pyrrole adenosine 5'-triphosphate) (PP-ATP) and conducting polymer bilayers for transport of biologically active ions, *Synth. Met.* 71, 2233-2236 (1995)

197. Pyo, M.; Maeder, G.; Kennedy, R. T.; Reynolds, J. R. Controlled release of biological molecules from conducting polymer modified electrodes. The potential dependent release of adenosine 5'-triphosphate from poly(pyrrole adenosine 5'-triphosphate) films, *J. Electroanal.Chem.* **368,** 329-332 (1994)

198. Banerjee, P. Electrically conductive interpenetrating network composites of polyaniline and carboxymethylcellulose, *Eur. Polym. J.* **34,** 1557-1560 (1998)

199. Lee, T. W.; Park, O. O.; Kim, J. J.; Hong, J. M.; Kim, Y. C. Efficient photoluminescence and electroluminescence from environmentally stable polymer/clay nanocomposites, *Chem. Mater.* **13,** 2217-2222 (2001)

200. Gangopadhyay, R.; De, A. Conducting polymer nanocomposites: a brief overview, *Chem. Mater.* **12,** 608-622 (2000)

201. Yuan, L. *et al.* Synthesis and characterization of SnO_2–polypyrrole composite for lithium-ion battery, *J. Power Sources* **174,** 1183-1187 (2007)

202. Migahed, M. D.; Fahmy, T.; Ishra, M.; Barakat, A. Preparation, characterization, and electrical conductivity of polypyrrole composite films, *Polym. Test.* **23,** 361-365 (2004)

203. Kassim, A.; Mahmud, H. N. M. E.; Yee, L. M.; Hanipah, N. Electrochemical preparation and characterization of polypyrrole-polyethylene glycol conducting polymer composite films, *Pac. J. Sci. Techno.* **7,** 103-107 (2006)

204. da Cruz, A. G. B.; Wardell, J. L.; Rocco, A. M. A novel material obtained by electropolymerization of polypyrrole doped with $[Sn(dmit)_3]^{2-}$, [tris(1,3-dithiole-2-thione-4,5-dithiolato)-stannate]$^{2-}$, *Synth. Met.* **156,** 396-404 (2006)

205. Yang, C.; Liu, P. Polypyrrole/conductive mica composites: Preparation, characterization, and application in supercapacitor, *Synth. Met.* **160,** 768-773 (2010)

206. Wang, J.; Xu, Y.; Chen, X.; Sun, X. Capacitance properties of single wall carbon nanotube/polypyrrole composite films, *Compos. Sci. Technol.* **67,** 2981-2985 (2007)

207. Dione, G.; Dieng, M. M.; Aaron, J. J.; Cachet, H.; Cachet, C. New composite electrodes made of polypyrrole and graphite: Construction, optimization and characterization, *J. Power Sources* **170,** 441-449 (2007)

208. Zhao, Y. F.; Xiao, M.; Wang, S. J.; Ge, X. C.; Meng, Y. Z. Preparation and properties of electrically conductive PPS/expanded graphite nanocomposites, *Compos. Sci. Tech.* **67,** 2528-2534 (2007)

209. Dhakate, S. R.; Sharma, S.; Borah, M.; Mathur, R. B.; Dhami, T. L. Development and Characterization of Expanded Graphite-Based Nanocomposite as Bipolar Plate for Polymer Electrolyte Membrane Fuel Cells (PEMFCs), *Energy Fuels* **22,** 3329-3334 (2008)

210. Chen, G.; Weng, W.; Wu, D.; Wu, C. PMMA/graphite nanosheets composite and its conducting properties, *Eur. Polym. J.* **39,** 2329-2335 (2003)

211. Geim, A. K.; Novoselov, K. S. The rise of graphene, *Nat. Mater.* **6,** 183-191 (2007)

212. Wu, J.; Pisula, W.; Mullen, K. Graphene as potential material for electronics, *Chem. Rev.* **107,** 718-747 (2007)

213. Bunch, J. S. *et al.* Electromechanical resonators from graphene sheets, *Science* **315,** 490-493 (2007)

214. Dikin, D. A. *et al.* Preparation and characterization of graphene oxide paper, *Nature* **448,** 457-460 (2007)

215. Wang, X.; Zhi, L.; Mullen, K. Transparent, conductive graphene electrodes for dye-sensitized solar cells, *Nano. Lett.* **8,** 323-327 (2008)

216. Matsuo, Y.; Tahara, K.; Sugie, Y. Structure and thermal properties of poly(ethylene oxide)-intercalated graphite oxide, *Carbon* **35,** 113-120 (1997)

217. Liu, P.; Gong, K.; Xiao, P.; Xiao, M. Preparation and characterization of poly(vinyl acetate)-intercalated graphite oxide nanocomposite, *J. Mater. Chem.* **10,** 933-935 (2000)

218. Xu, J. *et al.* Thermal analysis of poly(vinyl alcohol)/graphite oxide intercalated composites, *Polym. Degrad. Stab.* **73,** 29-31 (2001)

219. Kai, W. H.; Hirota, Y.; Hua, L.; Inoue, Y. Thermal and mechanical properties of a poly(epsilon-caprolactone)/graphite oxide composite, *J. Appl. Polym. Sci.* **107,** 1395-1400 (2008)

220. Kotov, N. A.; Dekany, I.; Fendler, J. H. Ultrathin graphite oxide– polyelectrolyte composites prepared by self-assembly: transition between conductive and non-conductive states, *Adv. Mater.* **8,** 637-641 (1996)

221. Cassagneau, T.; Fendler, J. H. High density rechargeable lithium– ion batteries self-assembled from graphite oxide nanoplatelets and polyelectrolytes, *Adv. Mater.* **10,** 877-881(1998)

222. Kovtyukhova, N. I. *et al.* Layer-by-layer assembly of ultrathin composite films from micron-sized graphite oxide sheets and polycations, *Chem. Mater.* **11,** 771-778 (1999)

223. Wu, J. *et al.* Conducting film from graphite oxide nanoplatelets and poly(acrylic acid) by layer-by-layer self-assembly, *Langmuir* **24,** 4800-4805 (2008)

224. Yan, J. *et al.* Preparation of graphene nanosheet/polyaniline composite with high specific capacitance, *Carbon* **48,** 487-493 (2010)

225. Brownson, D. A. C.; Kampouris, D. K.; Banks, C. E. An overview of graphene in energy production and storage applications, *J. Power Sources* **196,** 4873-4885 (2011)

226. Li, Y.; Li, X.; Dong, C.; Qi, J.; Han, X. A graphene oxide-based molecularly imprinted polymer platform for detecting endocrine disrupting, *Carbon* **48,** 3427-3433 (2010)

Chapter 2

Synthesis and Characterization

2.1 Introduction

The present investigation deals with the synthesis and modification of pi-conjugated polymers with different carbon fillers and their characterization. Generally, functional conjugated polymers are prepared through electrochemical and chemical polymerization methods.[1-6] The limitation in producing large amount of polymers by electrochemical process has restricted its utility. Therefore, chemical polymerization methods have attained popularity for synthesizing the large scale and soluble polymer. The chemical polymerization methods include oxidative coupling, Yamamoto coupling, McCullough method, Grignard Metathesis method, Reike method, Suzuki and Still method.[7-12]

In this study, polyaniline (PA) and polypyrrole (PPy) are chosen as bare conjugated polymers. Graphite, expanded graphite (EG) and graphene oxide (GO) filled PA and PPy composites have been prepared by *in-situ* chemical method. The synthesized polymer composites were characterized by FTIR, XRD, UV-visible, SEM and TEM analysis. Thermal properties of the polymers were studied using TGA technique.

2.2 Materials

Aniline, pyrrole and graphite powder (20 μm) were obtained from Aldrich Co. and used as received. Ferric chloride ($FeCl_3$), Hydrogen peroxide (H_2O_2), Lithium percholate ($LiClO_4$), potassium permanganate ($KMnO_4$)) and potassium persulphate ($K_2S_2O_8$) were obtained from Merck and used as received. All the solvents were distilled before use. For all purposes, double distilled water was used.

2.3 Synthesis and modification of π-conjugated polymers

2.3.1 Chemical synthesis of π-conjugated polymers

Synthesis of conducting polymer involves the oxidation of the monomer viz. aniline and pyrrole with oxidizing agents such as $K_2S_2O_8$ or $FeCl_3$ in acidic medium.

The part of this chapter is published in

J. Appl. Polym. Sci. 116, 1138–1145 (2010);

Mater. Chem. Phys. 124, 738–743 (2010);

J. Mater. Sci. Mater. Elect. (Accepted, 2011);

Mater. Chem. Phys. (Accepted, 2011)

Solvents used for the polymerization reaction is distilled water or methanol. Detailed procedure for the synthesis is given below.

i) Synthesis of Polyaniline

Polyaniline was synthesized by chemical oxidation polymerization of aniline using $K_2S_2O_8$ as an oxidizing agent. In a three-necked round-bottomed flask 0.1 mol of aniline was dissolved in 50 mL 1M HCl solution. The solution was cooled (0 – 5 °C) in a salt/ice mixture. An aqueous solution of 25 mL (0.125 mol) of $K_2S_2O_8$ was added very slowly to the aniline solution while the temperature was maintained in a range close to 0 – 5 °C with vigorous stirring for 2 h. The monomer - initiator molar ratio was maintained at 4 : 5 for the standard preparation of PA.[13] The reaction mixture was then allowed to stir at 30 °C for another 6 h. The solid precipitate of PA–HCl salt was first collected from the reaction mixture by filtration and washed thoroughly with 1M HCl and then distilled water followed by ethanol. The filtrate was dried at room temperature in vacuum.

ii) Synthesis of Polypyrrole

The polymer has been prepared using a standard procedure described elsewhere.[14] In the chemical polymerization of pyrrole, $FeCl_3$ was used as oxidizing agent. Reaction was carried out in the methanol medium. In a three-necked round-bottomed flask 2.5 M $FeCl_3$ was taken in 20 ml methanol. The solution was cooled to 0-5 °C by salt/ice mixture. The monomer pyrrole was added dropwise to the reaction mixture and vigorously stirring for 6h. Here the monomer to $FeCl_3$ ratio was maintained at 2.33:1 molar ratio. The reaction was carried out at the temperature range of 0- 5 °C for 24 hours. The polymer so obtained is filtered, washed with distilled water followed by methanol until the solution became colourless and dried in vacuum.

2.3.2 Preparation of carbon filler

(i) Preparation of Expanded Graphite

EG was prepared by the chemical oxidation method described elsewhere.[15] The natural graphite flake of size –50 + 100 BS mesh was dried at 75 °C in vacuum oven for 10 h to remove the moisture. It was then mixed with concentrated H_2SO_4 and HNO_3 in a volume ratio 3:1 for 10–15 h to form graphite intercalated compound (GIC) where HNO_3 serves as an oxidizer and H_2SO_4 as an intercalant. The mixture was stirred to get the uniform intercalation of each flake. After filtration the flakes were washed with

distilled water until the pH level of the solution reached upto 7 (neutral). After washing, the flakes were dried at temperature 60 °C in a vacuum oven for 5 h. GIC was rapidly expanded in between temperature 800-900 °C within 10–20 s in muffle furnace to form EG.

(ii) Preparation of Graphene oxide

GO was synthesized from natural graphite by a modified Hummers method described elsewhere.[16] In a 500 mL beaker, 5 g of graphite and 2.5 g of $NaNO_3$ were mixed with 120 mL of concentrated H_2SO_4. The mixture was stirred for 30 min at the temperature range of 0-5 °C. During stirring 15 g of $KMnO_4$ was slowly added to the suspension and the temperature was maintained to below 20 °C. After addition of $KMnO_4$ the reaction mixture was stirred at 30 °C until the mixture became pasty, and the colour turned into light brownish. Finally 150 mL of distilled water was slowly added to the past - with vigorous stirring. The diluted yellow colour suspension was again stirred at 98 °C for 24 h. Finally 50 mL of 30% H_2O_2 was added. The whole reaction mixture was centrifuged and washed with 1.5 M HCl followed by distilled water for 8-10 times. Finally, the mixture was filtered to get the gray coloured GO sheets.

2.3.3 Preparation of carbon filled π-conjugated polymers

(i) Preparation of polyaniline/graphite (PA/G) composites

PA/G composites were synthesized by *in-situ* polymerization technique. In a 250 mL three necked flask, 0.10mol of aniline was dissolved in 50mL of 0.1M HCl, and different concentration (0.2%, 0.5%, and 1.0% w/v) of graphite powder was dispersed in the aniline solutions. A solution of 0.05 mol of $K_2S_2O_8$ in 50 mL of 0.1M HCl was added dropwise under vigorous stirring. Initial polymerization reaction was carried out at 0-5°C for 2 h and the further polymerization was carried out at room temperature (27 °C) for another 2 h. The precipitate of PA/G composites were first washed with 0.1M HCl followed by a 250ml of ethanol. The polymer composites were finally dried under vacuum.

(ii) Preparation of polypyrrole/graphite (PPy/G) composites

In a 250 mL three-necked round-bottomed flask, 2.5 M $FeCl_3$ was taken in 20ml methanol and different concentration (0.25, 0.5 and 1.0 % w/v) of graphite was dispersed in methanol with constant stirring. Then pyrrole was added slowly to the

mixture in 2.33:1 molar ratio with2.5 M $FeCl_3$ at a temperature range close to 0-5 °C under vigorous stirring for 6h. The polymer so obtained is filtered, washed with water and methanol until the solution became colourless and dried in vacuum.

(iii) ***Preparation of polyaniline/expanded graphite (PA/EG) composites***

EG powder was washed with a solution of NaOH (2 mol/L) at 40°C for 2 h to improve its surface functional group. The EG (0.25, 0.50, and 1.0 wt.%) and 0.1 mol of aniline were added to 25 mL of 1.5 M HCl solution. The mixture was cooled (0-5 °C) in a salt-ice mixture and sonicated for 1 h. Then, 40 mL of 0.125 mol $K_2S_2O_8$ solution was slowly added to the mixture with stirring for 6 h and allowed to stir at the ambient temperature for another 24 h. After filtration, the precipitates were washed with distilled water and alcohol repeatedly to remove unreacted monomer and unabsorbed EG particles. The solid was then dried in vacuum at the ambient temperature for 24 h.

(iv) ***Preparation of polypyrrole/expanded graphite (PPy/EG) composites***

EG powder was washed with a solution of NaOH (2 mol/L) at 40°C for 2 h to improve its surface conformation. In a 250 mL three-necked round-bottomed flask, 2.5 M $FeCl_3$ was taken in 20 ml methanol and 0.25%, 0.50% and 1.0% EG particles (w/v) were also dispersed in methanol. The mixture was cooled (0-5 °C) in a salt-ice mixture and sonicated for 1 h. Then pyrrole was added slowly to the mixture in 2.33:1 molar ratio with2.5 M $FeCl_3$ at a temperature range close to 0-5 °C under vigorous stirring for 6h. The polymer so obtained is filtered, washed with water and methanol until the solution became colourless and dried in vacuum.

(v) ***Preparation of polyaniline/graphene oxide (PA/GO)***

The PPy/GO composites were prepared by *in-situ* polymerization involving pyrrole and GO. In a 250 mL three-necked round-bottomed flask, different concentration (0.25, 0.50, and 1.0 % w/v) of GO was dispersed in 50 mL of methanol by ultrasonication for 30 min. Conversely, pyrrole (0.2 M) was dissolved in the dispersed solution and ultrasonication was continued for another 30 min. Then 2.5 M $FeCl_3$ solution (in 20 mL methanol) was added dropwise to the mixture of pyrrole and GO at the temperature range close to 0-5 °C under vigorous stirring for 6h. The polymer composite so obtained was filtered, washed with water and methanol until the solution become colourless and dried in vacuum.

(vi) Preparation of polypyrrole/graphene oxide (PPy/GO) composites

The PPy/GO composites were prepared by *in-situ* polymerization involving pyrrole and graphene oxide. In a 250 mL three-necked round-bottomed flask, different concentration (0.25, 0.50, and 1.0 % w/v) of GO was dispersed in 50 mL of methanol by ultrasonication for 30 min. Then, pyrrole (0.2 M) was dissolved in the dispersed solution and ultrasonication was continued for another 30 min. Then 2.5 M $FeCl_3$ solution (in 20ml methanol) was added dropwise to the mixture of pyrrole and GO at the temperature range close to 0-5 °C under vigorous stirring for 6h. The polymer composite so obtained was filtered, washed with water and methanol until the solution became colourless and dried in vacuum.

(vii) Preparation of poly(styrene-co-methyl acrylate) (SMA) latex

To a one litre resin kettle equipped with a mechanical stirrer, a nitrogen inlet, a condenser and a thermometer added 120 mL of water was added and purged with nitrogen for half an hour. Then 0.7 g of PVP was added to the kettle and temperature is raised upto 70^0C. When temperature reaches 70 °C, 0.1 g of $K_2S_2O_8$ (in 10 mL water) was added. Maintaining the temperature at 70 °C, a mixture of 5g of styrene and 1.7 g of MA was added with the aid of a dropping funnel in 2 h. Polymerization was continued for further 24 h. Then it was cooled to room temperature to get the core latex.

(viii) Preparation of poly(styrene-co-methylacrylate)-polyaniline/graphite (SMA/PA/G) core-shell composites

In a three necked round bottom flask equipped with a thermometer and dropping funnel an emulsion containing 4g of the SMA latex was added and diluted with 50 mL of water. To this latex 0.1 mol of aniline (in 25 mL of 1.5 M HCl), 25ml of 0.125 mol $K_2S_2O_8$ solution and different amount of graphite (0%, 0.25%, 0.50%, 1% w/v) were added in turn in a nitrogen atmosphere. The mixture was stirred for 24 h at 0-5 °C. The resulting dark green precipitates were isolated by filtration and washed several times with water and ethanol to remove unreacted monomer and unabsorbed graphite particles. The prepared composites were dried at room temperature in a vacuum oven.

2.4 Instrumentations

Samples were characterized by using the following instruments

2.4.1 Fourier Transform Infrared Spectrophotometer (FTIR)

Vibrational spectra of the samples were recorded with Nicolet, Impact 410 in the range of 400 – 4000 cm^{-1}. FTIR is primarily used for the detection of functional groups, but analysis of spectra in the lower frequency finger print region can give evidence of degree of polymerization and the effect of substituents on the electronic properties of the polymer backbone. The polymer and carbon filled polymer composite powder was triturated together with KBr powder to form polymer and composite/ KBr pellet.

2.4.2 X-Ray Diffractometer (XRD)

The X-ray diffraction study of PA, PPy and their composites was carried out at room temperature (ca. 25 °C) on Rigaku X-ray diffractometer with Cu, *K*α radiation (λ= 0.15418nm) at 30 kV and 15 mA using a scanning rate of 0.050°/s in the range of 2θ = (10°–70°). The samples were in powder form and the XRD patterns were recorded on a glass slide. From the 2θ value for the reflections, d values were calculated using Bragg's equation.

$$n\lambda = 2d \sin\theta \qquad (2.1)$$

Where, *n* is an integer, λ is the X-ray wavelength, *d* is the distance between crystal lattice planes and θ is diffraction angle.

2.4.3 Scanning Electron Microscope (SEM)

SEM studies were performed to investigate the surface morphology or microstructure of the samples. JSM-6390LV, JEOL, Japan was used for analysis. The surface of the sample was coated with platinum before SEM analysis.

2.4.4 Transmission Electron Microscope (TEM)

Transmission electron microscope measurements were conducted on a PHILIPS CM 200 microscope at 200kv. The TEM samples were prepared by dispensing a small amount of dry powder in ethanol. Then, one drop of the suspension was dropped on 300 mesh copper TEM grids covered with thin amorphous carbon films.

2.4.5 Thermogravimetric Analyser (TGA)

Thermogravimetric analysis of PA, PPy and their composites were investigated by using Shimadzu TG 50 thermogravimetric analyzer with a heating rate of 10 °C/min under a nitrogen atmosphere. Thermogravimetric analysis reveals the thermal characteristics of polymers including degradation temperature, absorbed moisture content the level of oligomer in polymer etc. It determines the weight loss with respect to temperature. Analysis was performed at 0- 700 °C temperature ranges.

2.5 Results and Discussions

2.5.1 Synthesis of PA and its composites with different carbon fillers

The *in-situ* oxidative polymerization method was employed to synthesis both the polymer PA, PPy and their composites viz., PA/G, PPy/G, PA/EG, PPy/EG, PA/GO, PPy/GO and SMA-PA/G composites.

In case of graphite incorporated into the polymer matrix, the monomer (Ani or Py) may have been adsorbed on the surface of the graphite particles. This adsorbed monomer on the graphite sheet as well as the remaining free monomer got polymerized in the presence of the oxidizing agent to yield the PA/G and PPy/G composites.

In EG, the interlayer spacing is separated by increased distance leading into a porous structure consisting of numerous graphite sheets of thickness in nanometer and micrometer in diameter. The PA or PPy grows on the surface of the EG sheets and formed *in-situ* in the pores and galleries of EG. **Scheme 2.1** shows the schematic representation of formation of PA/EG composite.

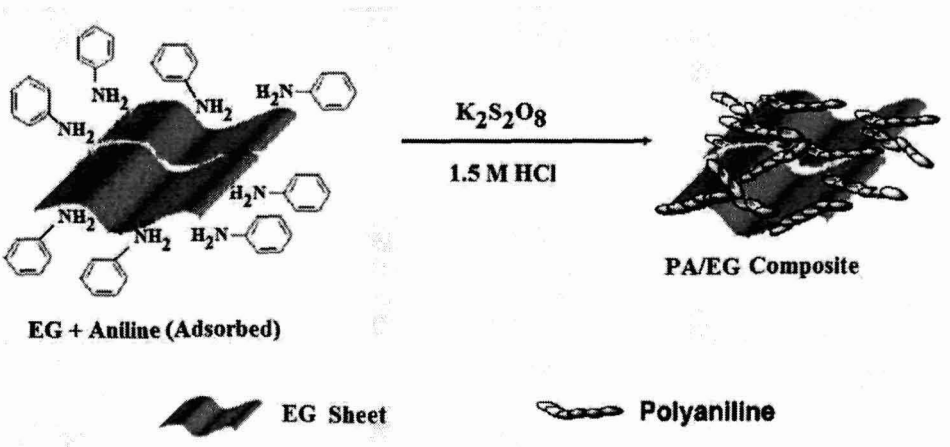

Scheme 2.1 Illustration of the process of preparation of PA/EG composite

In case of GO filler, the functional groups –OH, –COOH, epoxy, exist on the surface and pores of the GO which promote the hydrogen bonds between the GO to amine and imine nitrogen of benzenoid and quinoid moieties of the polymer chain. It is also expected that there would be π-π stacking between the polymer backbone and the GO sheets. The possible H-bonding and π-π stacking between GO and PA in the GO/PA composite is schematically depicted in **Scheme 2.2.**

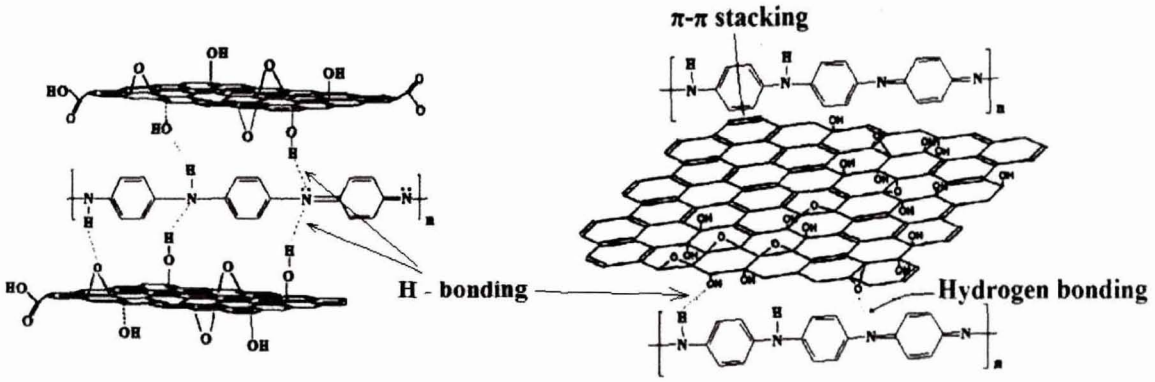

Scheme 2.2 Interactions between PA and GO

In case of SMA-PA/G core-shell composites, copolymer particles of styrene and methylacrylate were formed by mini emulsion polymerization. These latex particles were used as template for the polymerization of aniline. The polymer (either PA or PPy) coated SMA core–shell particles and polymer/carbon filler coated SMA core–shell particles were synthesized by in situ oxidative polymerization technique. The monomer (Ani or Py) and the carbon fillers graphite or EG get adsorbed on the surface of the dispersed SMA particles. These adsorbed aniline and EG on the surface of SMA get polymerized in presence of oxidizing agent. Thus a layer of PA/EG composite is formed over the SMA latex to result core–shell morphology (**Scheme 2.3**).

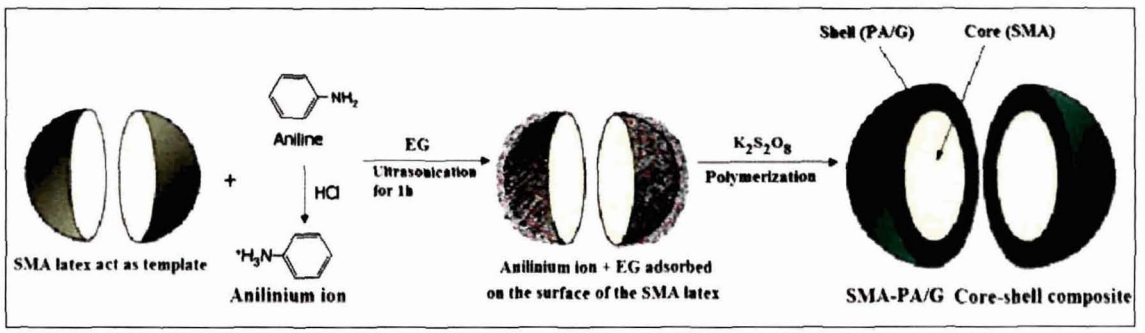

Scheme 2.3 Schematic representation of the formation of the core-shell composite particles

2.5.2 Characterization of the polymer and polymer composites with carbon fillers

2.5.2.1 FTIR study of graphite, expanded graphite and graphene oxide

Figure 2.1 shows the FTIR spectrum of graphite, EG and GO. In graphite, the peak at 1560 cm^{-1} is of the C-C-C symmetric stretching vibration. The peak at 1655 cm^{-1} is of the C=O stretching of ketone group. The broad absorption band at 3400 cm^{-1} indicates O-H stretching vibration, whereas the band at 2924 cm^{-1} is due to the stretching of the C-H bonds (**Figure 2.1a**).

In FTIR spectra of EG (**Figure 2.1 b**), some new peaks are observed at lower wave number in between 400-800 cm^{-1} due to the C–H outer bending vibration, C-H in plane bending and out-of-plane C-H wagging.[17, 18] The peak at 3436 cm^{-1} is attributed to the O-H stretching vibration of phenolic or alcoholic functional groups present on the EG surface. The peak at around 1627 cm^{-1} is of the C=O stretching of carboxyl functional groups. During intercalation of natural graphite by strong acids some of the carbon double bonds are oxidized, which leads to the formation of oxygen-containing functional (carboxylic and hydroxyl) groups on exfoliated graphite surface, that can facilitate the physical and chemical interactions with the functional groups of polymeric matrix.[15]

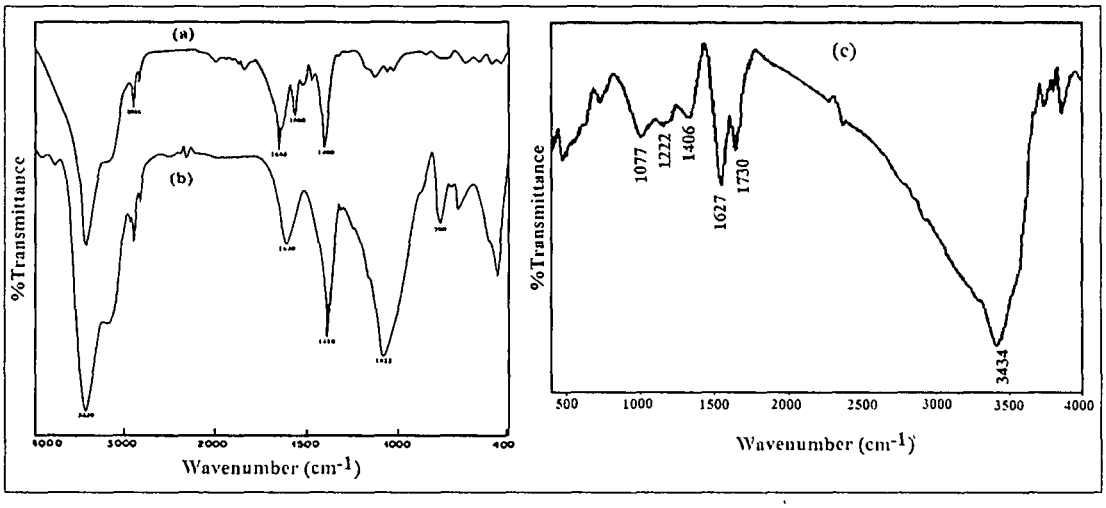

Figure 2.1 FTIR spectra of (a) graphite, (b) EG and (c) GO

In the FTIR spectrum of GO the broad peak at 3434 cm^{-1} and a peak at 1730 cm^{-1} represent the O-H stretching vibration and strong carbonyl (C=O) stretching respectively. The peak at 1222 and 1406 cm^{-1} represent the C-O-C and C-OH stretching

vibration respectively.[19] The peak at 1077 cm^{-1} represents the C-O stretching vibration indicating the presence of epoxide group in the GO layers. The frequency data obtained and their probable assignments are presented in the **Table 2.1**.

Table 2.1 FTIR assignment of graphite, EG and GO

Absorption frequency (cm^{-1})			Assignment
Graphite	**EG**	**GO**	
3400	3436	3434	O-H stretching
2924	2924		C-H stretching
1655	1627	1730	C=O stretching
1560	---		C-C-C symmetric stretching
---	---	1406	C-OH stretching
---	---	1222	C-O-C stretching
---	---	1077	C-O stretching

2.5.2.2 FTIR analysis of polyaniline and its composites

FTIR spectra of PA and graphite incorporated PA/G composites is given in the **Figure 2.2**. The incorporation of graphite in to the polymer chain was confirmed from the IR studies. The frequency data obtained and their probable assignments are presented in the **Table 2.2.**

The FTIR spectrum of synthesized PA gave absorption band at 3430, 2924, 1631, 1461 and 1283 cm^{-1}. Here, the broad absorption band at 3430 cm^{-1} indicates the secondary amine in the polymer backbone whereas band at 2924 cm^{-1} is due to stretching of the C-H bonds in phenyl rings. The presence of characteristic IR absorption due to quinoid and benzenoid rings at 1631 cm^{-1} and 1461 cm^{-1} clearly indicates the presence of these two states in the polymer chain. The presence of C-N-C bonds is confirmed by the absorption band found at 1283 cm^{-1}.

In PA/G composites, the absorption peaks were similar to PA, except that the absorption bands assigned to benzenoid and quinoid rings at 1631 and 1461 cm^{-1} for PA were shifted to 1605 cm^{-1} and 1485 cm^{-1} for PA/G composites. This indicates the interaction between the pi-conjugated structure of the benzenoid and quinoid rings with graphite.

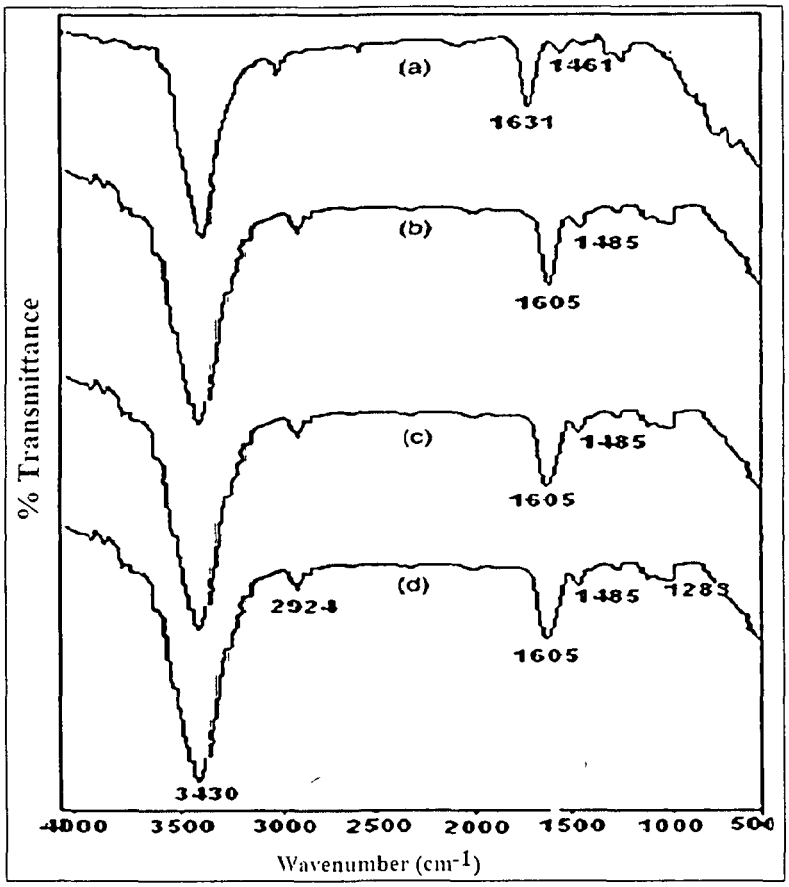

Figure 2.2 FTIR spectra of (a) PA, (b) PA/G (0 2%), (c) PA/G (0 5%), and (d) PA/G (1.0%) composites

Table 2.2 FTIR assignment of PA powders and PA/G composites

Absorption frequency (cm^{-1})				Assignment
PA	**PA/G composite**			
	0.2%	**0.5%**	**1.0%**	
3430	3430	3430	3430	NH
2924	2924	2924	2924	C-H stretching in phenyl rings
1631	1605	1605	1605	Quinoid N=Q=N stretching
1461	1485	1485	1485	Benzenoid N-B-N stretching
1283	1283	1283	1283	C-N-C stretching

The FTIR spectrum of the synthesized SMA-PA/G composite gave absorption bands at 3422, 2923, 1723, 1612, 1432, 1283 and 1132 cm^{-1} (**Figure 2.3**) quite similar with pure PA. The frequency data obtained and their probable assignments are presented in the **Table 2.3**. Here, the broad absorption band at 3422 cm^{-1} indicated the secondary amine in the polymer backbone, whereas the band at 2923 cm^{-1} was due to the stretching of the C-H bonds in phenyl rings. The absorption band at 1612 cm^{-1} was

obtained for the quinoid rings, and that at 1432 cm^{-1} was for the benzenoid ring. The presence of C-N-C bonds was confirmed by the absorption band at 1283 cm^{-1}. The peak at 1723 cm^{-1} and 1132 cm^{-1} refer to C = O and CO stretching of poly (methyl acrylate). It has been observed that the peak at 1631 cm^{-1} and 1461 cm^{-1} for PA shifted to 1612 cm^{-1} and 1432 cm^{-1} in the graphite incorporated core shell particles. This may be attributed to the conjugation effect between the C=C of benzenoid and quinoid ring and the graphite surface. Thus from the IR spectra it may be confirmed that the core-shell particle contains both the SMA latex as well as the graphite incorporated aniline phase.

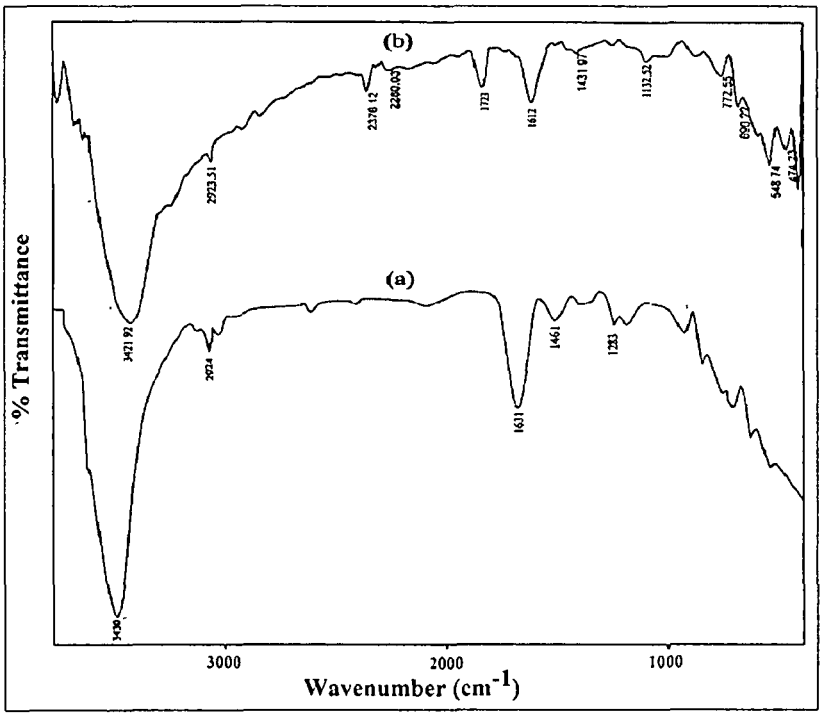

Figure 2.3 FTIR spectra of (a) PA and (b) SMA-PA/G (0.10%) core-shell composite

Table 2.3 FTIR assignment of PA powders and SMA-PA/G core-shell composite

Absorption frequency (cm^{-1})		Assignment
PA	SMA-PA/G composite	
3430	3422	NH stretching
2924	2923	C-H stretching in phenyl rings.
---	1723	C=O stretching
1631	1612	Quinoid N=Q=N stretching
1461	1432	Benzenoid N-B-N stretching
1283	1283	C-N-C stretching
---	1132	CO stretching

The FTIR spectra of GO, PA, and PA/GO is shown in **Figure 2.4.** For the PA powder sample, the absorption peak at 3430 cm^{-1} is attributed to the N–H stretching vibrations of the leucoemeraldine component.[20] The weak peak at 2924 cm^{-1} corresponds to aromatic sp^2 CH stretching. The absorption peaks located at 1631 cm^{-1} and 1461 cm^{-1} are respectively ascribed to the C=C stretching deformation of the quinoid ring in the emeraldine salt and benzenoid rings leucoemeraldine .[21] The peaks at 1283 and 1152 cm^{-1} correspond to C–N stretching of the secondary aromatic amine and C=N stretching, respectively.[22]

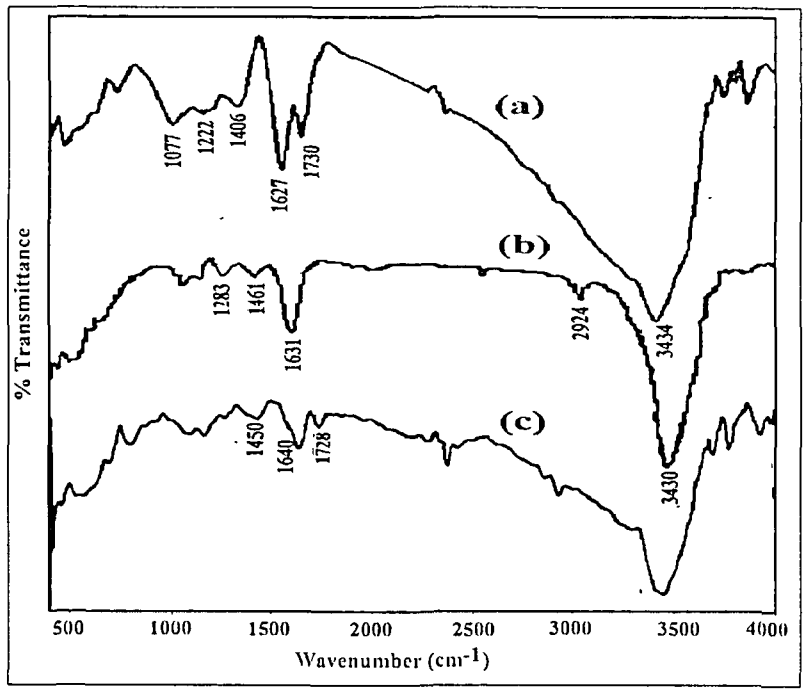

Figure 2.4 FTIR spectra of (a) GO, (b) PA and (c) PA/GO composite

For the GO, the characteristic vibrations include the broad and intense O-H peak at 3434 cm^{-1}, strong C=O peak in carboxylic acid and carbonyl moieties at 1730 cm^{-1}, C-OH peak at 1406 cm^{-1}, C-O-C peak at 1222 cm^{-1}, C-O stretching peak at 1077 cm^{-1}. By comparison, the spectrum of the PA/GO composites, the absorption peaks are similar to PA except that the characteristic peak of C=O group at 1728 cm^{-1} was observed from PA/GO composite. The absorption peaks at ~1640 and 1450 cm^{-1} represent the quinoid and benzenoid structures of the PA in PA/GO composite. The presence of PA characteristic vibrations reveals the successful deposition of PA on the GO surface. The frequency data and probable assignments obtained from PA, GO and PA/GO are presented in the **Table 2.4**.

Table 2.4 FTIR assignment of PA, GO and PA/GO composite

Absorption frequency (cm^{-1})			Assignment
PA	**GO**	**PA/GO**	
3430	---	3422	NH stretching
---	3434	---	O-H stretching
2924	---	2923	C-H stretching in phenyl rings
---	1730	1728	C=O
1631	---	1640	Quinoid N=Q=N stretching
1461	---	1450	Benzenoid N-B-N stretching
---	1406	---	C-OH stretching
1283		1283	C-N-C stretching

2.5.2.3 FTIR analysis of PPy and its composites

The FTIR spectrum of PPy is given in the **Figure 2.5a**. The broad strong bands at 3433 cm^{-1} corresponds to the absorption of N–H stretching of PPy. The frequency at 2926 cm^{-1} refers to the stretching vibration of C–H bond. The absorption at 1578 cm^{-1} was assigned to the C=C ring stretching of pyrrole. The band at 1380 cm^{-1} is due to C-H vibration. The peak at 1187 cm^{-1} is due to C-C stretching. The band at 1042 cm^{-1} is due to in-plane deformation of C–H bond and N–H bond of pyrrole ring.[23] The incorporation of graphite in to the PPy chain was confirmed from the IR studies (**Figure 2.5b**). In PPy/G composites, the absorption peaks were similar to pyrrole, except that the absorption bands assigned to C=C ring stretching of pyrrole at 1578 cm^{-1} was shifted to 1630 cm^{-1} for PPy/G composites, which might be ascribed to the conjugate effect between C=C of pyrrole and surface of the graphite layers.

In PPy/EG composites, the absorption peaks were similar to pyrrole, except that the absorption bands assigned to C=C ring stretching of pyrrole at 1578 cm^{-1} was shifted to 1620 cm^{-1} for the composites (**Figure 2.6**), which might be ascribed to the conjugate effect between C=C of pyrrole and surface of the EG layers. The frequency data obtained and their probable assignments are presented in the **Table 2.5.**

In the spectrum of the PPy/GO composites (**Figure 2.7**), the characteristic absorption peak of C=O group has been downshifted to 1728 cm^{-1} which is probably due to the π - π interaction between the GO layers and aromatic polypyrrole rings. The absorption peaks located at 2930 cm^{-1} and 2857 cm^{-1} are ascribed to the asymmetric stretching and symmetric vibration of CH_2 respectively.[24] The characteristic peaks of PPy at 1587 cm^{-1} and 1450 cm^{-1} indicates the presence of PPy in the PPy/GO composite.

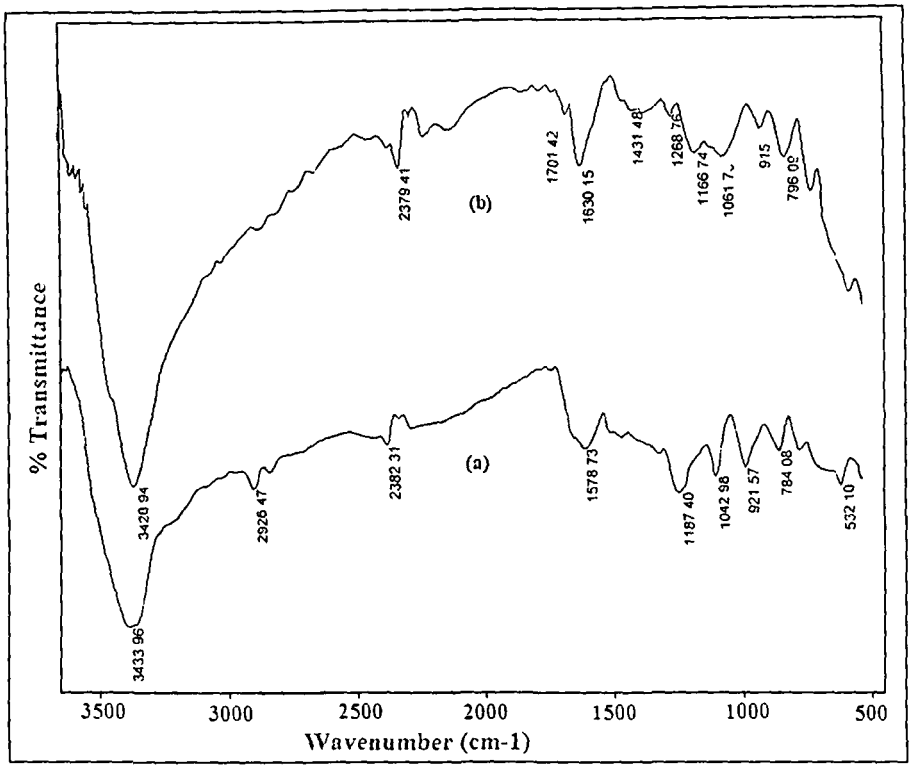

Figure 2.5 FTIR spectrums of (a) PPy and (b) PPy/G composite

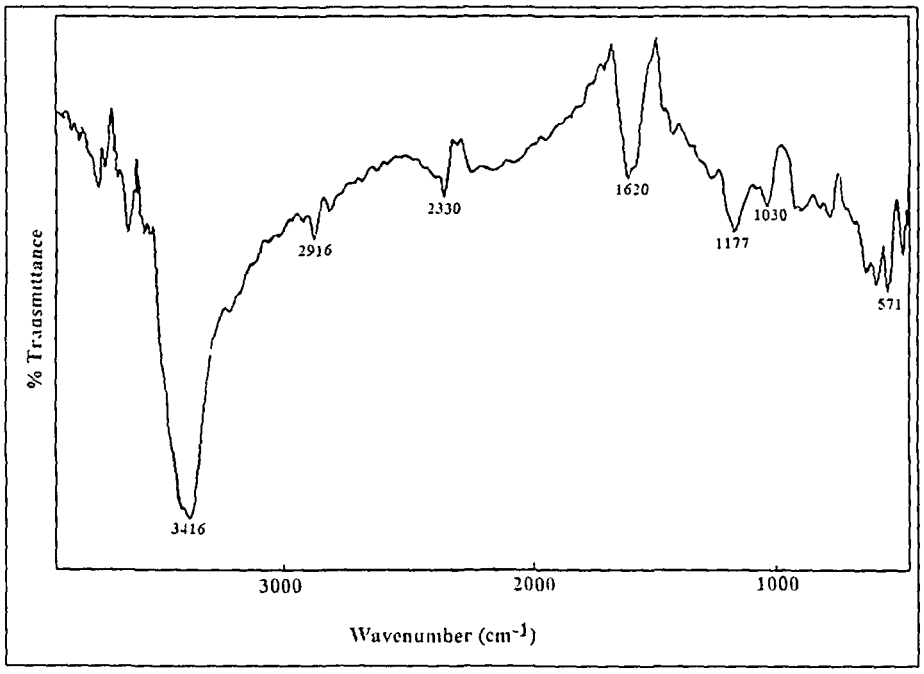

Figure 2.6 FTIR spectrum of PPy/EG composite

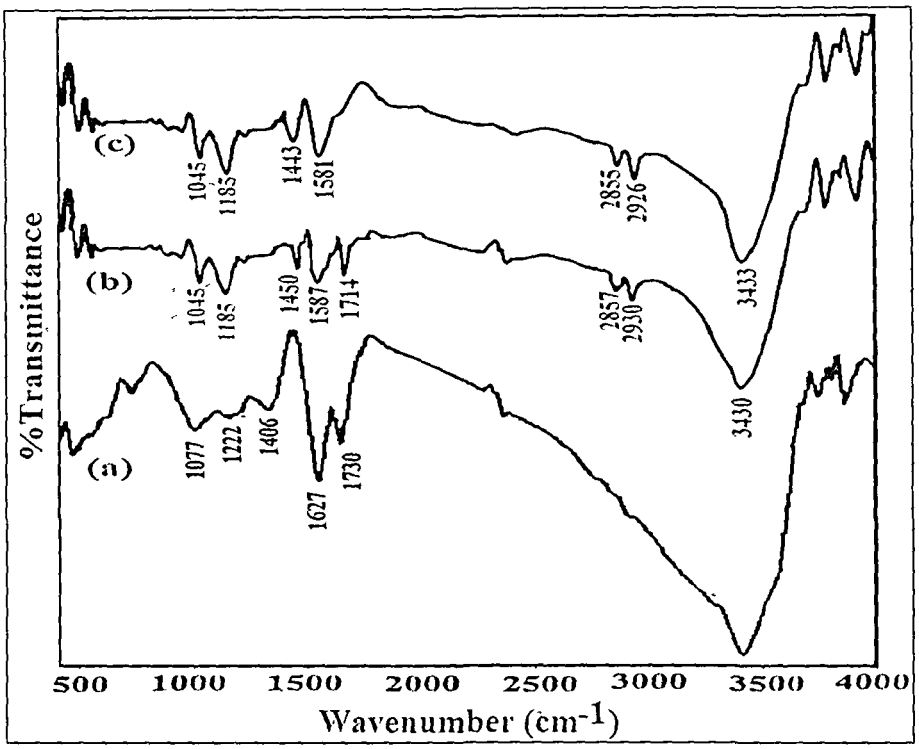

Figure 2.7 FTIR spectrum of (a) GO, (b) PPy/GO composite and (c) PPy

Table 2.5 FTIR assignment of PPy, PPy/G and PPy/EG

Absorption frequency (cm^{-1})				Assignment
PPy	PPy/G	PPy/EG	PPy/GO	
3433	3428	3416	3433	C-H stretching
2926	2926	2916	2930	C-H stretching in polymer rings
1578	1630	1620	1587	C=C ring strtetching
1187	1173	1177	1185	C-C stretching
1042	1045	1030	1045	In-plan deformation of N-H bond

2.5.2.4 XRD studies

The π-conjugated polymers are generally amorphous in nature and have a substantial volume fraction without crystalline order. Structural information and crystallinity of the doped PA, PPy and their composites are very important in order to understand the interchain interaction that could affect the electrical conductivity of the polymer composites. The X-ray diffraction analysis is a powerful tool to determine the structure and crystallization of polymer matrices.

XRD analysis has been performed by preparing the polymer film on the glass substrate. **Figure 2.8** presents X-ray diffraction pattern of graphite, EG and GO. The corresponding peaks of graphite are observed at 26 6°, 44.6° and 54.85° matching with

the (002), (101) and (004) planes of hexagonal system with primitive structure [ref. No. - PCPDFWIN 25-0284]. While in EG, the (002), (101) and (004) diffraction peaks assigned to the EG, interlayer distance between the sheets were gradually shifted to a smaller angle region (i.e., larger distance) the 2θ value were slightly shifted to the lowering value compared to graphite and the corresponding peaks were quite similar with graphite powder.

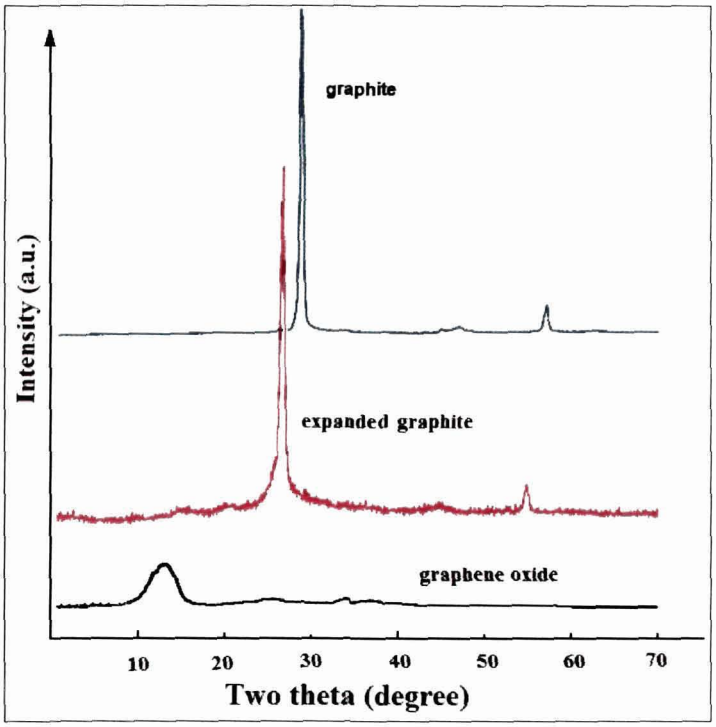

Figure 2.8 XRD of graphite, EG and GO

In GO, a broad reflection with peak at 2θ = 13.1° has been observed, which is correlated to an interlayer spacing of 0.68 nm in the layer-like GO. This value can be assigned to the (001) reflection peak and might depend on the method of preparation and on the number of layers of water in the gallery space of the material.[25, 26]

The respective diffraction patterns of pure PA, PA/G, PA/EG, PA/GO and SMA-PA/G composites are shown in **Figure 2.9** and diffraction data are tabulated in **Table 2.6**. In PA, a broad peak at about 2θ = 25.8°, a characteristic peak of amorphous PA has been observed similar to previous reports.[27-31] The XRD pattern of PA/G composites corresponding peaks were observed at 26.6°, 44.6° and 54.85° respectively matching with the (002), (101) and (004) planes of hexagonal system with primitive structure [ref. No. - PCPDFWIN 25-0284]. This indicates the presence of graphite in PA/G composites. In PA/EG composite three characteristics peaks of EG have been

observed and the gradual shift to a smaller angle region (i.e., larger distance) in comparison to PA/G composite is clearly observed. This may be due to the adsorption and intercalation of the polymer on the surface and between the EG sheets. PA/GO composite exhibits two peaks where the peaks of PA (2θ = 25.82°) can clearly be observed.

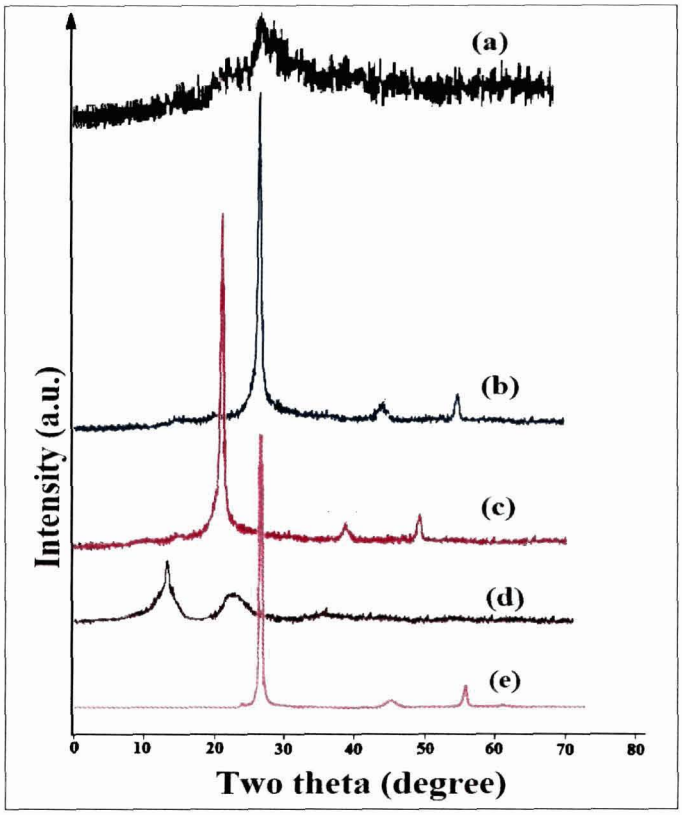

Figure 2.9 XRD of (a) PA, (b) PA/G, (c) PA/EG, (d) PA/GO and (e) SMA-PA/G composites

Table 2.6 XRD data of PA, PA/G, PA/EG, PA/GO and SMA-PA/G composites

Samples	2θ (degree)	*d*-spacing (Å)
PA	25.8	3.3594
PA/G	26.6	3.6171
	44.6	2.1856
	54.85	1.7959
PA/EG	24.02	3.9989
	43.20	2.2536
	53.52	1.8380
PA/GO	13.21	7.2429
	25.86	3.7184
SMA-PA/G	26.65	3.6101
	44.62	2.1846
	54.82	1.7970

Figure 2.10 presents XRD pattern of pure PPy, PPy/G, PPy/EG, PPy/GO, and SMA-PPy/G composites. The pure PPy sample exhibits the most intense peak at 2θ = 26.65°, which indicates the crystalline nature of PPy. However, change in the position of the peak intensities of the PPy composites with the carbon fillers is observed. The characteristic 2θ values and diffraction data of PPy and its composites are tabulated in **Table 2.7**.

XRD pattern of PPy/G, PPy/EG and PPy/GO composites show the similar three characteristic peaks at 24.3° - 26.73°, 43.12° - 45.62° and 53.07° - 55.37°. Incorporation of EG into the PPy matrices, the gradual shift of 2θ values to a smaller angle have been observed. This may be due to the adsorption and intercalation of the polymer on the surface and between the EG sheets. In PPy/GO composite two sharp peaks are observed where the characteristic peaks of PPy (2θ = 26.73°) and GO (2θ = 13.95°) can clearly be observed. This indicates the successful incorporation of GO and PPy.

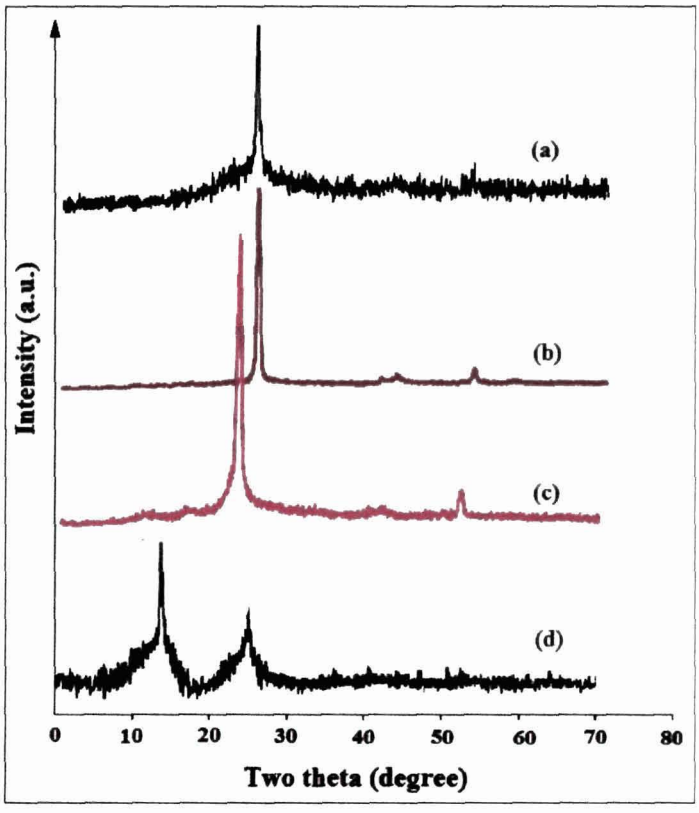

Figure 2.10 XRD of (a) PPy (b) PPy/G (c) PPy/EG and (d) PPy/GO composites

Table 2.7 XRD data of PPy and different PPy composites

Samples	2θ (degree)	*d*-spacing (Å)
PPy	26.65	3.6101
PPy/G	26.35 44.6 54.65	3.6505 2.1856 1.8022
PPy/EG	25.38 43.12 54	3.7878 2.2576 1.8226
PPy/GO	13.95 26.73	6.1618 3.5988

2.5.2.5 Scanning Electron Microscopy (SEM)

The surface morphology of pure PA and PPy has been studied by SEM micrographs of their powdered sample (**Figure 2.11**). In PA, the particles were randomly aggregated, and rough surfaces were observed.

From the SEM micrographs the differences in microstructures between graphite and EG can be clearly observed (**Figure 2.12**). The layer-liked structures of EG which is distinctly observed in higher magnifications (**Figure 2.12 c**). This is due to opening of planar carbon networks wedged at the edge surface of crystallite by surface groups as a consequence of oxidation. In EG, the interlayer spacing is separated by increased distance leading into a porous structure consisting of numerous graphite sheets of thickness in nanometer and micrometer in diameter.

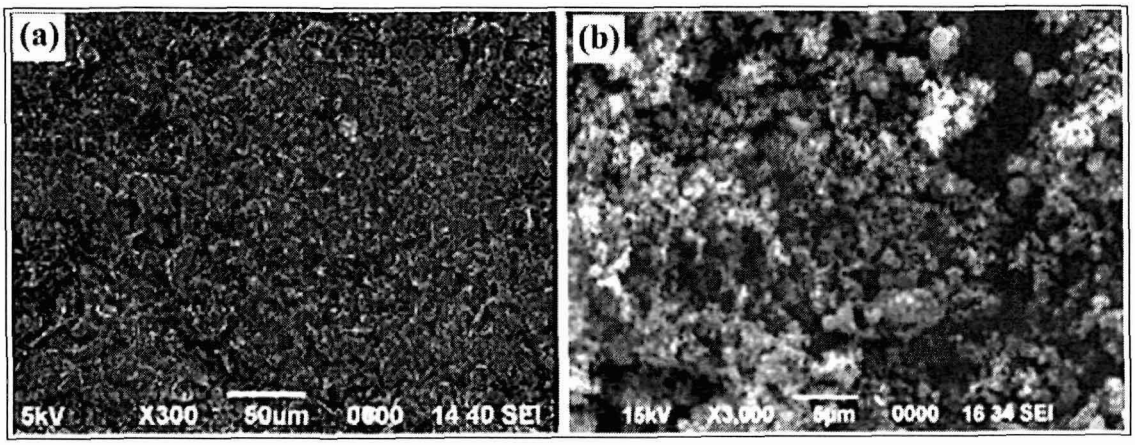

Figure 2.11 SEM images of PA and PPy

The GO inherits the layer-by-layer and network structure but in a denser stacking compared with the randomly aggregate structure having rough surface for the pure graphite is observed (**Figure 2.12 d**).

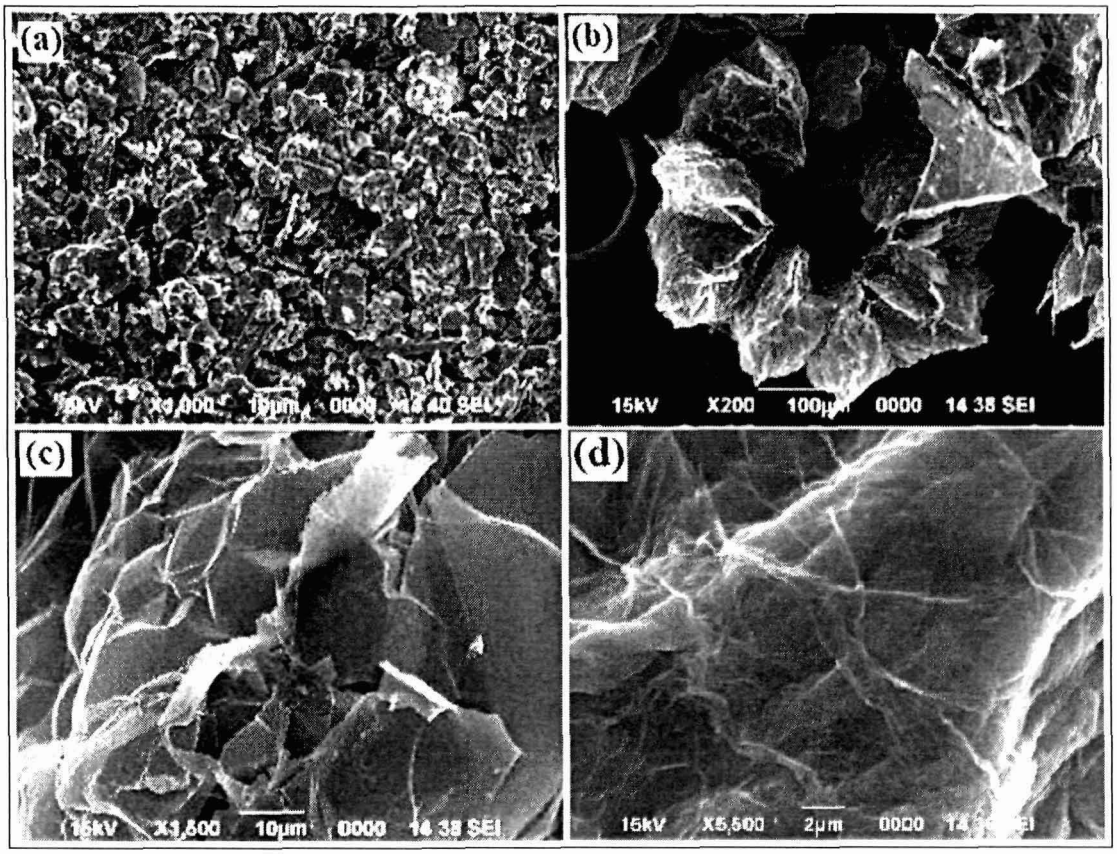

Figure 2.12 SEM images of (a) Graphite, (b) EG and (c) EG in higher magnification and (d) GO

The SEM micrographs of the PA composites with graphite, EG and GO are presented in **Figure 2.13.** The PA/G composites presented a surface with some holes and smooth regions. In the PA/G composites, the particles were bigger in size compared to pure PA. This was possibly because of the adsorption of aniline hydrochloride on the surface of the graphite particles and subsequent polymerization. The PA/G composites showed a higher current, probably because of the rougher surface, as demonstrated by the SEM micrograph of the composites.[32] **Figure 2.13 (b)** shows the SEM images of PA/EG composite (3%). The PA grows on the surface of the EG sheets and rod/fiber shaped PA/EG composites were formed which is possibly due to the subsequent polymerization occured on the surface of the whole sheets of the EG.

The SEM image of PA/GO is shown in **Figure 2.13 (c).** In the SEM micrographs of PA/GO composite, the polymers are grown in the pores and galleries of GO. Thereby it is difficult to distinguish the individual phase, i.e., GO and PA in

PA/GO composite. This imparts the high in-plane conductivity between adjacent GO layers of the composites.

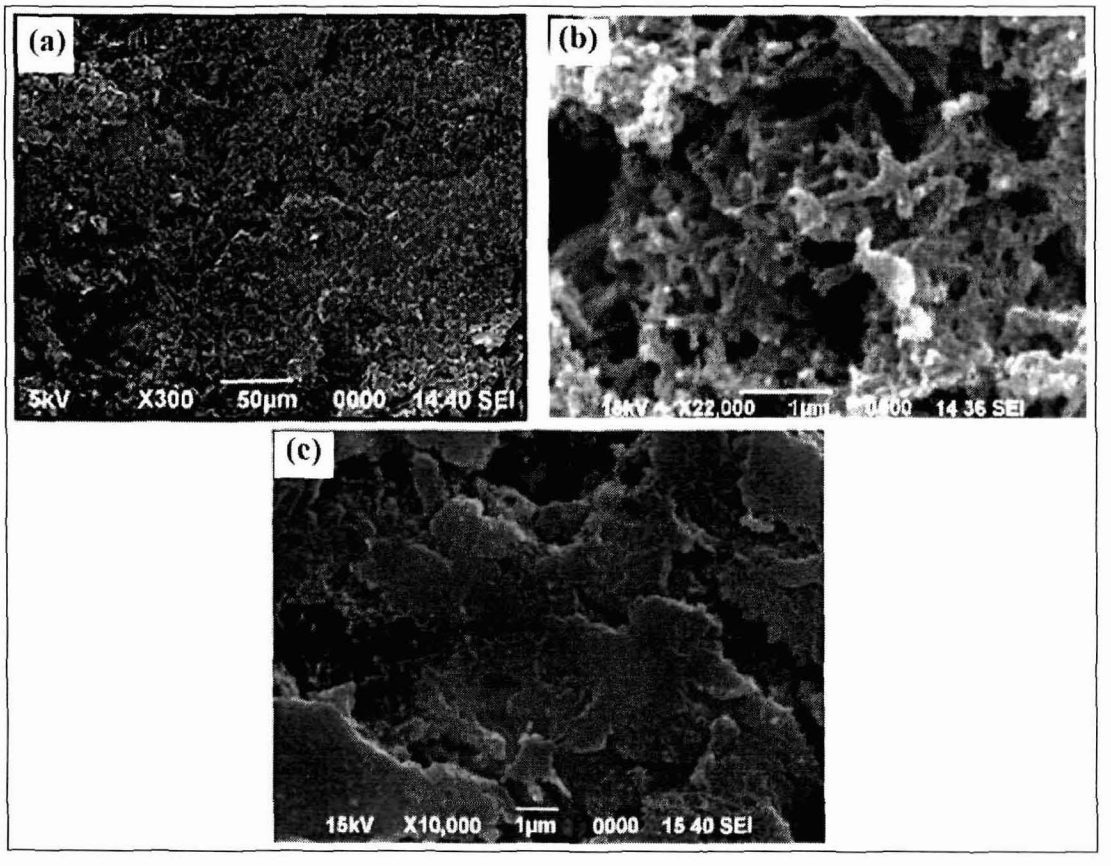

Figure 2.13 SEM images of (a) PA (b) PA/EG and (c) PA/GO composites

The SEM images of the SMA latex, and the graphite incorporated PA coated SMA-PA/G core-shell composites are shown in **Figure 2.14**. From the **Figure 2.14 (a)** it is seen that SMA particles are spherical in shape and nearly mono dispersed. The particles form a continuous array with no bare patch. The core-shell morphology of the SMA-PA/G composite (**Figure 2.14 b**) is also found to be spherical and bigger size than the uncoated SMA latex. This is due to the formation of a thin layer of PA/G over the SMA layer.

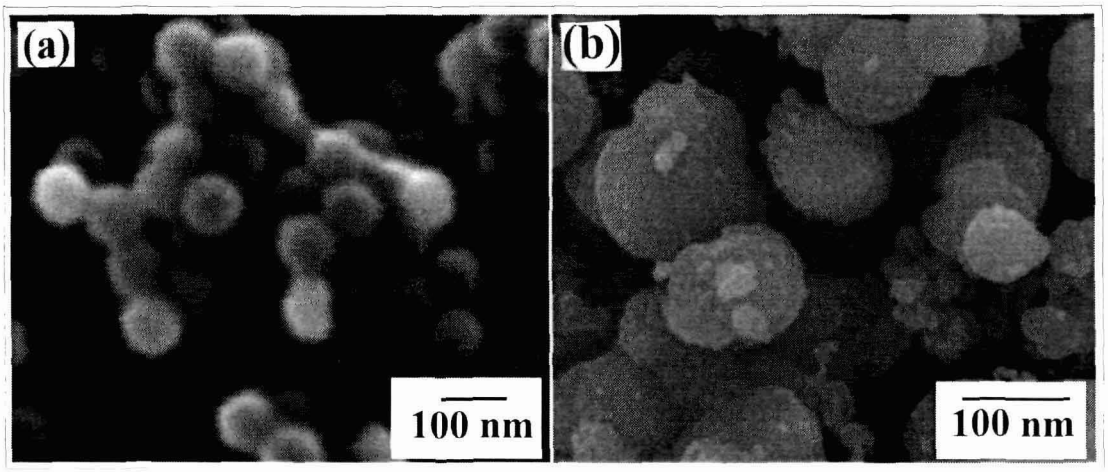

Figure 2.14 SEM images of (a) SMA latex and (b) SMA-PA/G core-shell composite

The SEM micrographs of the PPy/G composites are presented in **Figure 2.15.** A very high magnification of SEM images shows the presence of hemispherical nature of polymer as clusters in the composite. In PPy/G composites the particles are bigger in size. This is possibly due to adsorption of pyrrole on the surface of the graphite particles and subsequent polymerization.

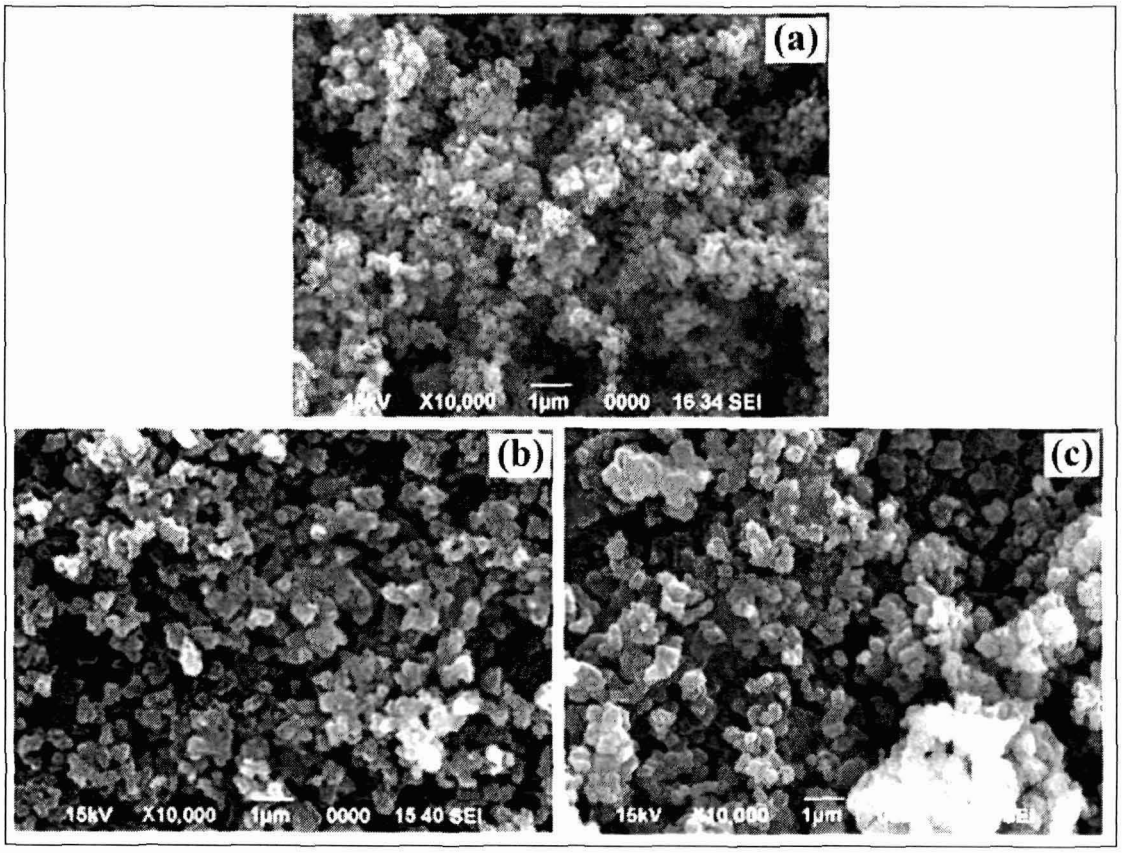

Figure 2.15 SEM images of (a) PPy/G (0.25%), (b) PPy/G (0.50%) and (c) PPy/G (1.0%) composites

In PPy/EG composite, the polymers are absorbed in the pores and galleries of EG, which gives the nanocomposites without distinguishing the individual phase, i.e., EG and PPy polymer. So, there is a possibility for pyrrole monomer to polymerize on the surface and also in the interspaces of EG, resulting into the regular PPy/EG composites (**Figure 2.16a & 2.16b**).

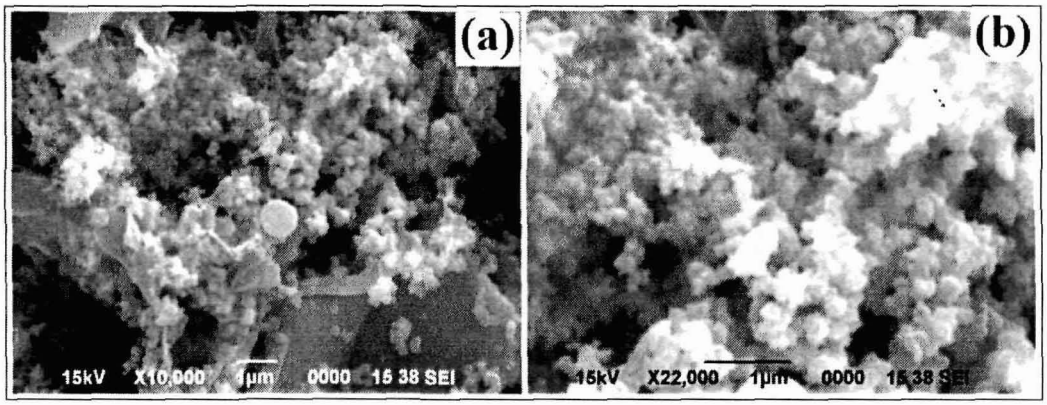

Figure 2.16 SEM images of PPy/EG composite

SEM images of the GO and PPy/GO are shown in **Figure. 2.17.** The GO inherits the layer-by-layer and network structure with denser stacking while SEM image of PPy shows the presence of hemispherical nature of polymer.

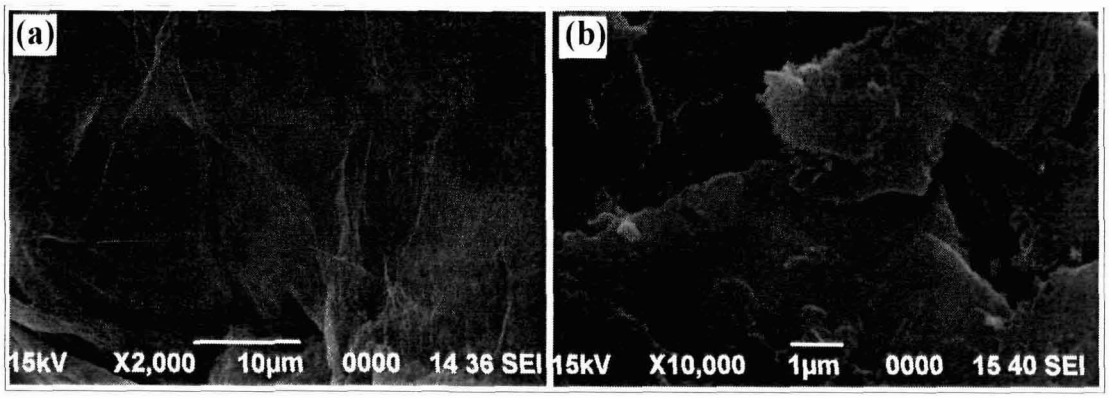

Figure 2.17 SEM images of (a) GO, (b) PPy and (c) PPy/GO composite

In the SEM micrographs of PPy/GO composite smooth surfaces are observed. Since the polymers are grown in the pores and galleries of GO so it is difficult to distinguish the individual phase, i.e., GO and PPy in PPy/GO composite from the SEM micrograph.

2.5.2.6 Transmission Electron Microscopy (TEM)

The morphology investigation of GO and its composite with PA and PPy were carried out using transmission electron microscopy (TEM). Typical morphology of GO is shown in the TEM image of **Figure 2.18 a**. The GO prepared here has a typically curved, layer likeed structure with thickness of ~5–10 nm of thinner. For PA/GO composite (**Figure 2.18 b**) TEM image shows that all the GO sheets are homogeneously coated with PA and the PA mainly grown on the surface or intercalate between the GO sheets. SEM and TEM images reveal that the chemically modified GO and the PA formed a uniform composite with the PA absorbed on the GO surface and/or filled between the GO nanosheets.

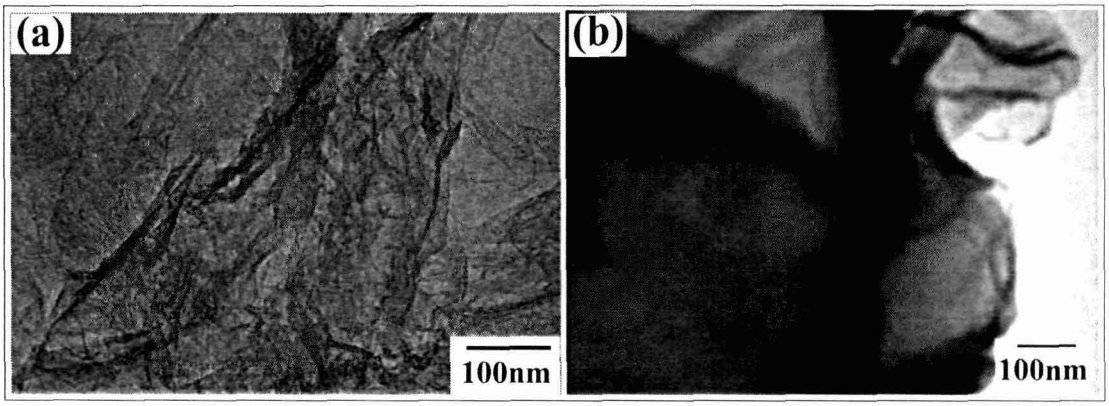

Figure 2.18 TEM images of (a) GO and (b) PA/GO composite

The TEM images of PPy/GO composite (**Figure. 2.19**) TEM image shows that all the GO sheets are homogeneously coated with polymer and the PPy mainly grown on the surface or intercalate between the GO sheets. SEM and TEM images reveal that the chemically modified GO and the PPy formed a uniform composite with the PPy absorbed on the GO surface and/or filled between the GO nanosheets.

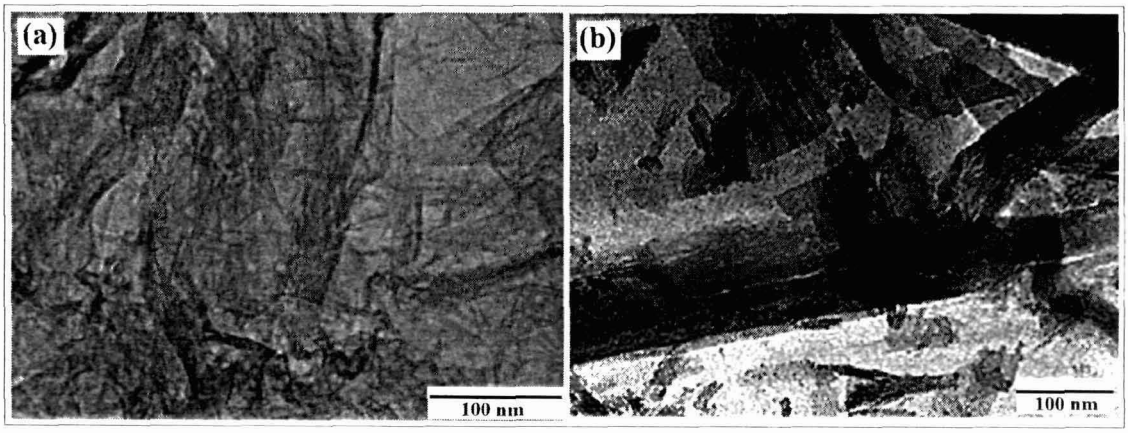

Figure 2.19 TEM images of (a) GO and (b) PPy/GO composite

Figure 2.20 represents the TEM images of the SMA-PA/G core-shell composite particles. The uniform layer of conducting PA/G shell is formed as a layer on the SMA surface. The shell layer seems to be rather continuous with little or no evidence of bare patches. There is a distinct contrast difference between the inner and outer phase of the composite particles. This further confirms the core-shell morphology of the composite particles.

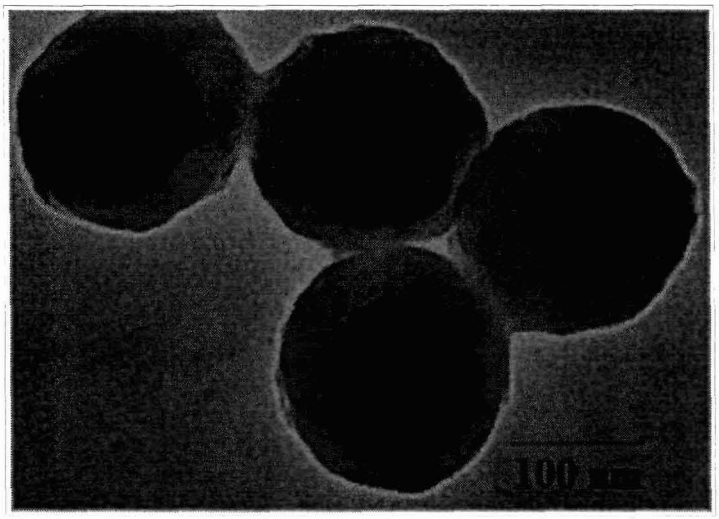

Figure 2.20 TEM images of SMA-PA/G core-shell composite

2.5.2.7 Thermogravimetric analysis

The thermal properties of polymers and their composites are investigated by thermogravimetric analysis under nitrogen atmosphere at the heating rate of 10 °C per minute.

TGA analysis of PA and PPy

The TGA curve of PA and PPy are shown in **Figure 2.21** and **Figure 2.22**.The polymers, PA and PPy are found to have thermal stability upto 225 °C. The first weight loss step i.e. 2-7% weight loss at the temperature range of 80-120 °C corresponds to the loss of moisture and volatilization of solvent. The second step in the TGA curves by gradual weight loss of 40-50% weight loss between 225-600 °C is due to degradation of skeletal chain structure of polymers. Above 600 °C, the results obtained are associated with the residues only. The onset decomposition temperature of PPy is found a little higher (300 °C) than that of PA which may be attributed to the attached rigid pyrrole ring along the main chain.

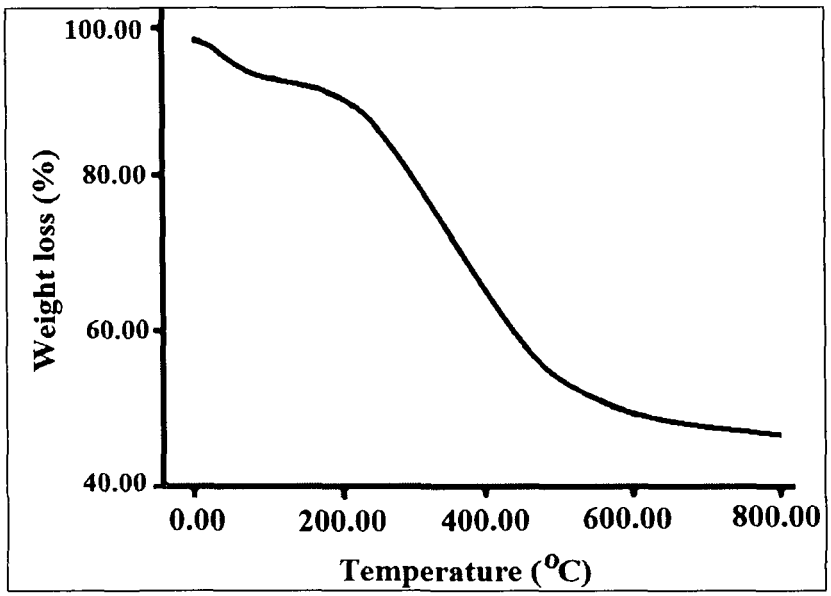

Figure 2.21 TGA of PA

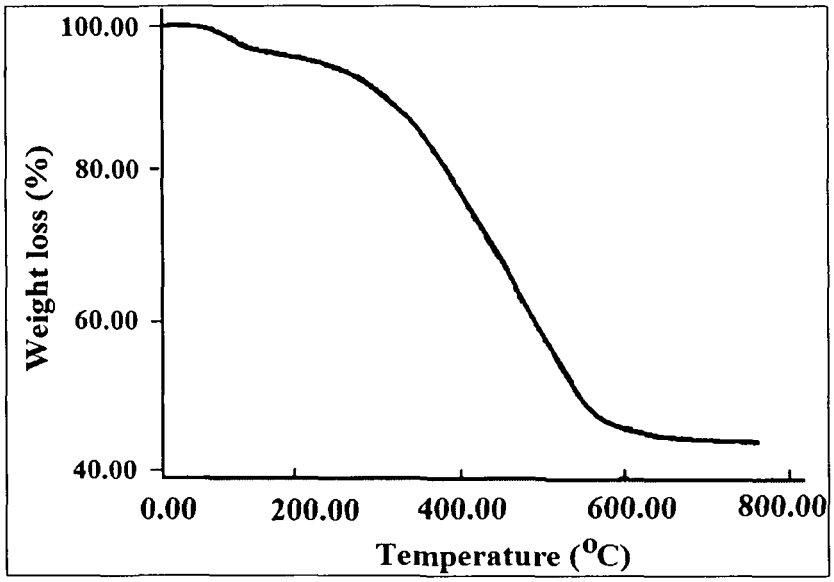

Figure 2.22 TGA of PPy

TGA analysis of EG and GO

The TGA is used to verify the amount of volatile materials and to determine the thermal stability of the functional groups on EG and GO.

Figure 2.23 shows the weight loss of EG and GO as a function of temperature. It is seen that there was not much weight loss for EG. The first 1-2 % of weight loss step in the TG analysis curves around 80-120 °C corresponds to the loss of moisture. A small weight loss at the temperatures around 220-230 °C occurred which is probably due to release of sulphuric acid. The TGA data of EG shows that there are small

amount of functional groups on EG, the amount is at least 1.5 wt%. The final degradation temperature is found to be 508 °C and residual weight of EG is 90.5 wt%.

The sharp weight loss of 2-15% of GO at the temperature range of 210-310 °C reveals the presence of functional group on the surface of GO sheet. During this dramatic weight loss, most of the oxygen containing functional groups is removed from the GO, and the material turned into single graphene and EG sheets.[33, 34] The residual weight of the GO is about 85 wt%, indicating that at least 15 wt% functional groups exist on GO before thermal treatment in the TGA machine.

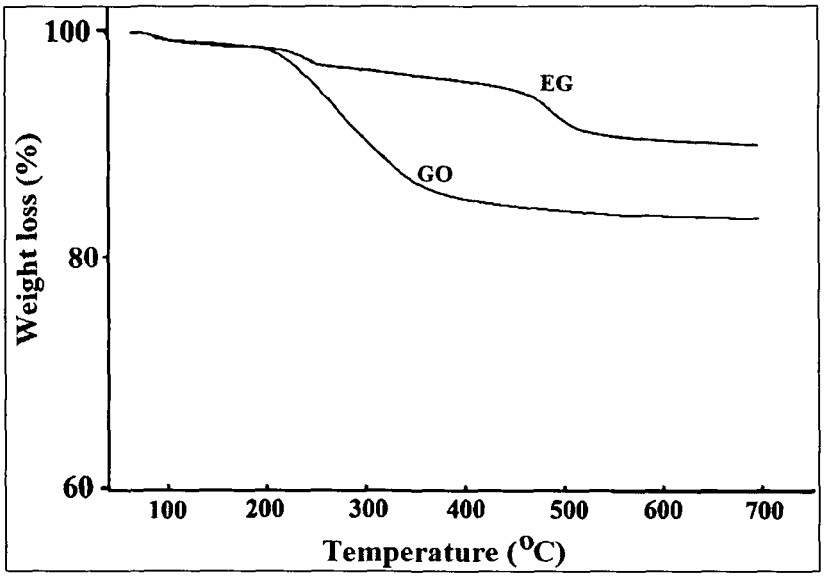

Figure 2.23 TGA of EG and GO

TGA analysis of modified polymer composites

The polymer composites of PA and PPy with graphite, EG and GO show similar patterns with the pure polymers, with a small variation in the degradation temperature. The first weight loss step i.e. 2-7% weight loss in the TGA curves is due to absorbed moisture and solvent upon initial heating upto 120 °C. The polymer composites are found to have thermal stability upto 470 °C (**Figure 2.24 -2.27**).

In PA/G composite, the weight loss at 125 °C reveals the loss of water molecules from the polymer matrix. The weight loss from 125-225 °C was due to the removal of HCl bound to the PA chain and low-molecular-weight oligomers. The final degradation starting from 300 °C was due to the degradation of the polymers. The gradual weight loss over a wide range of temperature indicated the thermal stability of the PA/G composites (**Figure 2.24**).

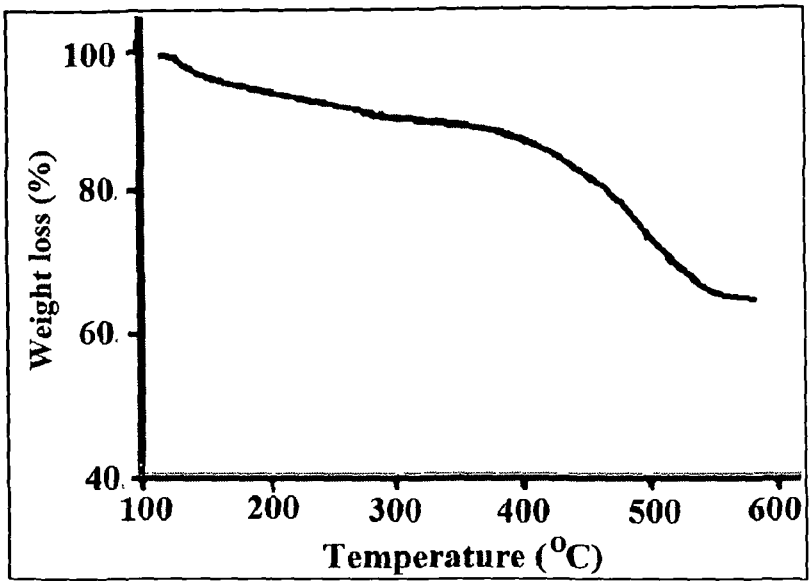

Figure 2.24 TGA of PA/G composite

The major degradation for PA/EG composite occurs at 470 °C which may be inferred that there is a sufficient enhancement in the thermal stability of the PA/EG composites after the incorporation of EG (**Figure 2.25**). Polymers are formed *in-situ* in the pores and galleries of EG, which results in the increase of thermal stability of PA/EG composite. Here in PA/EG composites the polymers are not directly exposed to thermal environment.

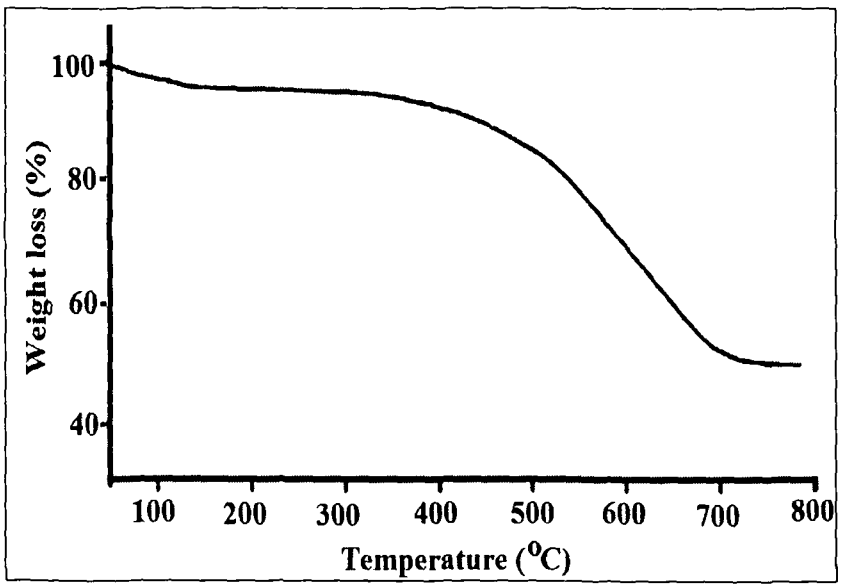

Figure 2.25 TGA of PA/EG composite

Compared with GO, a mass loss of 30% can be observed for PA/GO composites from 125 to 300 °C. The relatively larger mass loss of PA/GO composite than the pure

GO are observed after 300 °C, should be contributed to the decomposition of the PA component in the composite (**Figure 2.26**)..

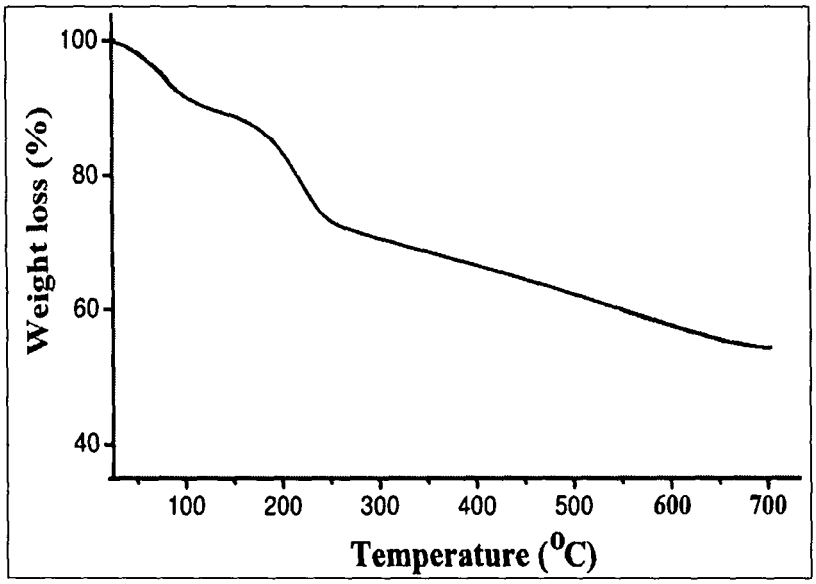

Figure 2.26 TGA of PA/GO composite

The polymer core-shell composites of SMA-PA/G composite showed gratifying thermal stability to the range of 300 - 497 °C (**Figure 2.27**). 60-70% weight loss in the TGA curves between 300-497 °C is attributed to degradation of polymers. Nearly, 25% of residue was left when the polymers are heated to 600 °C.

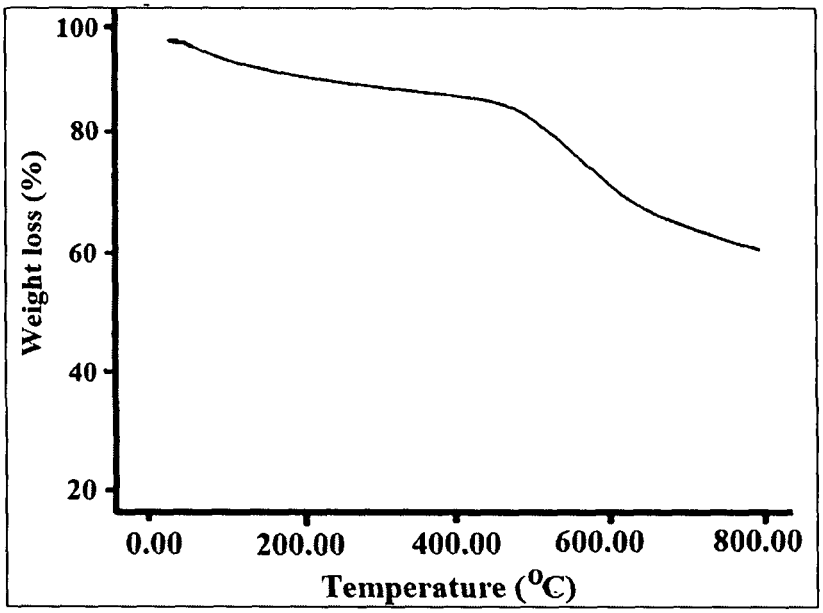

Figure 2.27 TGA of SMA-PA/G composite

The polymer composites of PPy/G, PPy/EG and PPy/GO are found to have thermal stability upto 450 °C (**Figure 2.28** and **Figure 2.29**). The major degradation of PPy/G in the TGA curve occurred by gradual weight loss (40-50%) between 400 - 600 °C is due to degradation of polymers. Whereas, the maximum thermal stability of PPy/EG composites is found to be 450 °C. The onset degradation temperature of PPy/GO (320 °C) is found to be lower in comparison to that of PPy/G and PPy/EG composite.

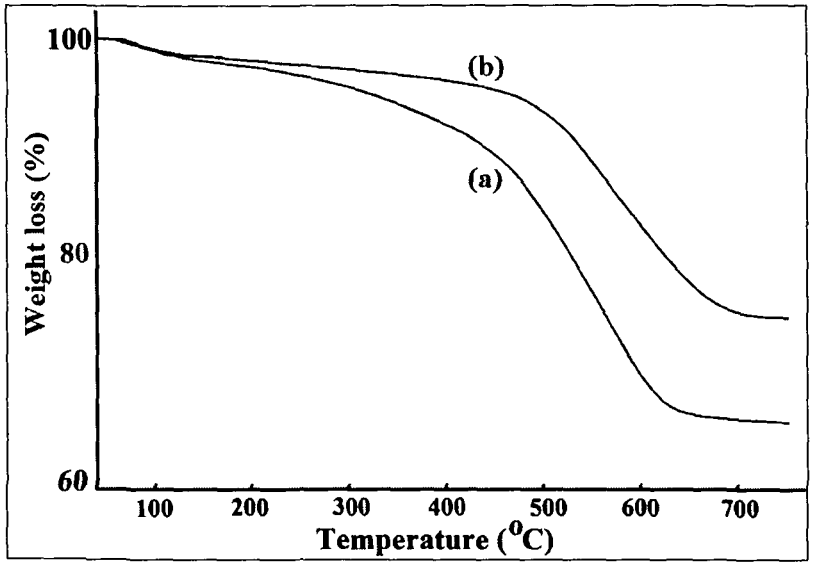

Figure 2.28 TGA of (a) PPy/G and (b) PPy/EG composite

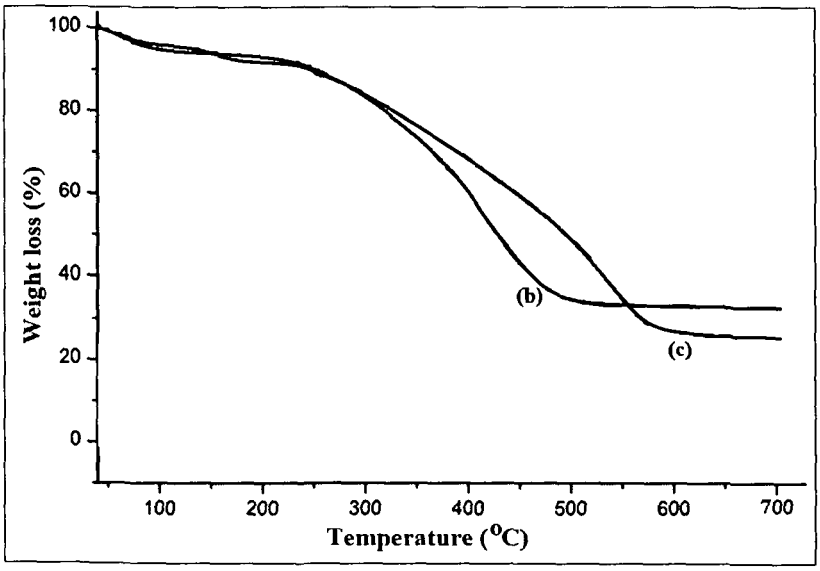

Figure 2.29 TGA curves of (a) GO, (b) PPy/GO and (b) pure PPy

In case of PPy/GO composites nearly a 7-8% weight loss has occurred at 100-120 °C, due to removal of water from the gallery space of the GO framework. The weight loss near 210 °C is probably due to removal of the oxygen-containing functional groups. After 250 °C, major weight loss has occurred due to decomposition of the PPy from the composite. Finally at 450 °C, almost 24% weight loss for GO-based PPy composite has been observed.

2.6 Conclusions

The important findings of this investigation are given below:

- Expanded graphite (EG) and graphene-oxide (GO) have been synthesized successfully from natural graphite flake. The synthesized EG and GO was characterized by FTIR, XRD, TGA, SEM and TEM analysis.
- XRD analysis reveals the hexagonal crystalline structure of graphite and EG. In EG, the interlayer distance between the sheets increases which causes the shifting of diffraction peak (2θ) to lower value compared to graphite. In GO, a broad reflection peak at $2\theta = 13.1°$ is observed, which is correlated to an interlayer spacing of 0.68 nm in the layer-like GO.
- SEM micrographs show the differences in microstructures between graphite, EG, and GO. The graphite particles are randomly aggregated having rough surface whereas in EG layer-liked structures are observed. The GO inherits the layer-by-layer and network structure.
- A series of PA and PPy composites incorporated with different carbon fillers viz., graphite, EG and GO have been synthesized by in-situ chemical polymerization using $K_2S_2O_8$ and $FeCl_3$ as an oxidizing agents.
- XRD and FTIR study reveal the incorporation of carbon filler into the polymer matrices.
- PA and poly (styrene-co-methyl acrylate) core-shell composite particles have also been synthesized successfully. TEM micrographs confirm the formation of core-shell morphology.
- The polymer composites with graphite, EG and GO showed gratifying thermal stability than that of individual polymers.

- The major degradation for PA/G, PA/EG and PA/GO composites occurs at 470 °C, whereas polymer composites of PPy/G, PPy/EG and PPy/GO are found to have thermal stability upto 450 °C. There is a sufficient enhancement in the thermal stability of the polymer composites after the incorporation of the carbon filler.

References

1. Grimsdale, A. C.; Chan, K. L.; Martin, R. E.; Jokisz, P. W.; Holmes, A. B. Synthesis of light emitting conjugated polymers for applications in electroluminescent devices, *Chem. Rev.* **109,** 897-1091 (2009)
2. Akcelrud, L. Electroluminescent polymers, *Prog. Polym. Sci.* **28,** 875-962 (2003)
3. Skotheim, T. A.; Elsenbaumer, R. L.; Reynolds, J. R. *Handbook of conducting polymers* (Marcel Dekker, Inc., New York, 1998)
4. Hu, X.; Xu, L. Structure and properties of 3-alkoxy substituted polythiophene synthesized at low temperature. *Polymer* **41,** 9147-9154 (2000)
5. Ogawa, K.; Stafford, J. A.; Rothstein, S. D.; Tallman, D. E.; Rasmussen, S. C. Nitrogen-functionalized polythiophenes: Potential routes to new low band gap materials, *Synth. Met.* **152,** 137-140 (2005)
6. Levent, A.; Toparre, L.; Cianga, I.; Yagci, Y. Synthesis and characterization of conducting copolymers of (S)-2-methylbutyl-2-(3-thienyl) acetate with pyrrole and thiophene, *Macromol. Chem. Phys.* **204,** 1118–1122 (2003)
7. Yamamoto, T. Conjugated polymers with electronic and optical functionalities: Preparation by organometallic polycondensation, properties, and applications, *Macromol. Rapid Commun.* **23,** 583-606 (2002)
8. McCullough, R. D. The chemistry of conducting polythiophenes, *Adv. Mater.* **10,** 1-23 (1998)
9. Loewe, R. S.; Ewbank, P. C.; Liu, J.; Zhai, L.; McCullough, R. D. Regioregular, head-to-tail coupled poly(3-alkylthiophenes) made easy by the GRIM method: Investigation of the reaction and the origin of regioselectivity, *Macromolecules* **34,** 4324-4333 (2001)
10. Chen, T. A.; Reike, R. D. The first regioregular head-to-tail poly(3-hexylthiophene-2,5-diyl) and a regiorandom isopolymer: nickel versus palladium catalysis of 2(5)-bromo-5(2)-(bromozincio)-3-hexylthiophene polymerization, *J. Am. Chem. Soc.* **114,** 10087-10088 (1992)
11. Rehahn, M.; Schluter, A. D.; Wegner, G.; Feast, W. J. Soluble poly(*para*-phenylene)s. 2. Improved synthesis of poly(*para*-2,5-di-n-hexylphenylene) via Pd-catalysed coupling of 4-bromo-2,5-di-n-hexylbenzeneboronic acid, *Polymer* **30,** 1060-1062 (1989)

12. Bao, Z.; Chan, W.; Lu, L. Synthesis of conjugated polymer by the Stille Coupling Reaction, *Chem. Mater.* **5,** 2-3 (1993)

13. Stejskal, J.; Gilbert, R. G. Polyaniline. Preparation of a conducting polymer. *Pure Appl. Chem.* **74,** 857-867 (2002)

14. Chandrasekha, P. *Conducting Polymers, Fundamentals and Applications, A Practical Approach* (Ashwin-Ushas Corp., Inc.1999)

15. Dhakate, S. R.; Sharma, S.; Borah, M.; Mathur, R. B.; Dhami, T. L. Expanded graphite-based electrically conductive composites as bipolar plate for PEM fuel cell, *Int. J. Hydrogen Energy* **33,** 7146-7152 (2008)

16. Zhang, K.; Zhang, L. L.; Zhao, X. S.; Wu, J. Graphene/polyaniline nanofiber composites as supercapacitor electrodes, *Chem. Mater.* **22,** 1392-1401 (2010)

17. Si, Y.; Samulski, E. T. Synthesis of Water Soluble Graphene, *Nano Lett.* **8,** 1679- 1682 (2008)

18. Wu, X.; Qi, S.; He, J.; Duan, G. High conductivity and low percolation threshold in polyaniline/graphite nanosheets composites, *J. Mater. Sci.* **45,** 483-489 (2010)

19. Jeong, H. K. *et al.* X-ray absorption spectroscopy of graphite oxide, *J. Explor. Front. Phys.* **82,** 67004-67009 (2008)

20. Yan, X. B.; Han, Z. J.; Yang, Y.; Tay, B. K. NO_2 gas sensing with polyaniline nanofibers synthesized by a facile aqueous/organic interfacial polymerization, *Sens. Actu. B* **123,** 107-113 (2007)

21. Cruz-Silva, R. *et al.* Comparative study of polyaniline cast films prepared from enzymatically and chemically synthesized polyaniline, *Polymer* **45,** 4711-4717 (2004)

22. Tiwaria, A. *et al.* Nanofibrous polyaniline thin film prepared by plasma-induced polymerization technique for detection of NO_2 gas, *Polym. Adv. Technol.* **21,** (2010) 615-620

23. Liu, J.; Wan, M. Synthesis, characterization and electrical properties of microtubules of polypyrrole synthesized by a template-free method, *J. Mater. Chem.***11,** 404-407 (2001)

24. Wu, T. M.; Lin, S. H. Synthesis, characterization, and electrical properties of polypyrrole/multiwalled carbon nanotube composites, *J. Polym. Sci. Part A Polym. Chem.* **44,** 6449-6457 (2006)

25. Zhang, K.; Zhang, L. L.; Zhao, X. S.; Wu, J. Graphene/Polyaniline nanofiber composites as supercapacitor electrodes, *Chem. Mater.* **22,** 1392-1401(2010)

26. Liu, Z. H.; Wang, Z. M.; Yang, X.; Ooi, K. Intercalation of organic ammonium ions into layered graphite oxide, *Langmuir* **18,** 4926-4932 (2002)

27. Zhang, Z. M.; Wan, M. X. Composite films of nanostructured polyaniline with poly(vinyl alcohol), *Synth. Met.* **128,** 83-89 (2002)

28. Djurado, D.; Nicolau, Y. F.; Dalsegg, I.; Samuelsen, E. J. X-ray Scattering study of CSA protonated polyaniline films and powders, *Synth. Met.* **84,** 121-122 (1997)

29. Laska, J.; Djurado, D.; Luzny, W. X-ray study of plasticized polyaniline, *Eur. Polym. J.* **38,** 947-951 (2002)

30. Laridjani, M. *et al.* Amorphography -The relationship between amorphous and crystalline order. 1. The structural origin of memory effects polyaniline, *Macromolecules* **25,** 4106-4113 (1992)

31. Zheng, W. Y.; Levon, K.; Laakso, J.; Osterholm, J. E. Characterization and solid-state properties of processable N-alkylated polyanilines in the neutral state, *Macromolecules* **27,** 7754-7768 (1994)

32. Calixto, C. M. F. *et al.* Development of graphite-polymer composites as electrode materials, *Mater. Res.* **10,** 109-114 (2007)

33. McAllister, M. J. *et al.* Single sheet functionalized graphene by oxidation and thermal expansion of graphite, *Chem. Mater.* **19,** 4379-4620 (2007)

34. Zhang, K.; Zhang, L. L.; Zhao, X. S.; Wu, J. Graphene/Polyaniline nanofiber composites as supercapacitor electrodes, *Chem. Mater.* **22,** 1392-1401 (2010)

Chapter 3

Optical, electrical and electrochemical properties of carbon filled π-conjugated polymers

3.1 Introduction

This chapter reports the optical, electrical, and electrochemical properties of synthesized polymer composites. The influence of carbon fillers like graphite, expanded graphite (EG) and graphene oxide (GO) on the electrical conductivity, reduction and oxidation potentials of the PA and PPy composites have been studied thoroughly. Redox stability of polymers is tested by cyclic voltammetry up to 150^{th} cycles. Furthermore, band gap of polymer composites is measured electrochemically and compared with optical method.

3.2 Materials

$LiClO_4$ (Aldrich), ITO coated glass were used as received. All the solvents used were purified and distilled according to the standard procedure. The synthesized polymers and polymer composites reported in Chapter 2 were used for electrical and electrochemical analyses.

3.3 Instrumentations

3.3.1 UV- Visible spectrophotometer

UV-Visible (UV-Vis) spectrophotometer provides information about structure and stability of the materials in solution. Various kinds of electronic excitation may occur in organic molecules by absorbing the energies available in the UV-Vis region. The resulting spectrum is presented as a graph of absorbance versus wavelength. The intensity of the absorption is proportional to the number, type and location of colour absorbing structures (chromophores) in the molecule. UV-Visible spectra were recorded on a Shimadzu UV-2550 UV-VIS Spectrophotometer using THF solvent.

3.3.2 Two-probe 2400 Sourcemeter

The current - voltage characteristics of the π-conjugated polymer composites were measured by using a digital sourcemeter (model 2400, Keithley Instruments, Inc).

The part of this chapter was published in

J. Appl. Polym. Sci. 116, 1138–1145 (2010)

Mater. Chem. Phys. 124, 738–743 (2010)

J. Mater. Sci. Mater. Elect. (Accepted, 2011)

Mater. Chem. Phys. (Accepted, 2011)

Figure 3.1 shows the Keithley 2400 two probe measurement set-up. The current-voltage characteristics of the samples are performed by introducing the pellets between the electrodes followed by a linear sweep of the voltage between -10 to +10 Volts at probe spacing of 1 cm at voltage step of 0.05 V and scan rate in the range of 50 mV/s - 0.1V/s.

Figure 3.1 Two-probe set up

3.3.3 Four-probe resistivity measurement setup

The four probe method is one of the standard and most widely used methods to measure the resistivity of semiconductors. Many conventional methods for measuring resistivity are unsatisfactory for variety of materials such as semiconductors, because-semiconductor contacts are usually ractifying in nature. The error due to contact resistance, which is especially serious in the electrical measurement on semiconductors, is avoided by the use of two extra contacts (probes) between the current contacts. In this arrangement the contact resistance may all be high compare to the sample resistance, but as long as the resistance of the sample and contact resistances are small compared with the effective resistance of the voltage measuring device (potentiometer, electrometer or electronic voltmeter), the measured value will remain unaffected. The arrangement is also especially useful for quick measurement on different samples or sampling different parts of the same sample due to the pressure contacts. The Four-Probe Set-Up is shown in the **Figure 3.2.**

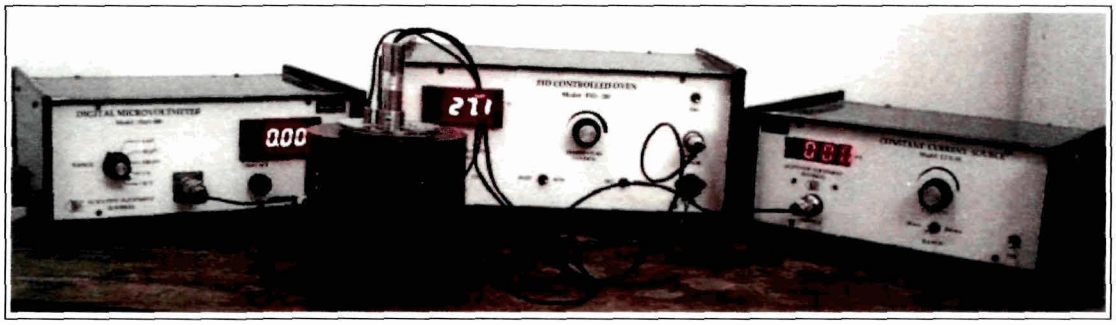

Figure 3.2 The Four-probe set-up

The whole four probes set-up produced by Scientific Equipment & Services, Roorkee was used to measure the resistivity of the pellet samples in various temperatures. The set-up unit consists of three sub-units enclosed in one cabinet, including a digital microvoltmeter (Model CCS-01), constant current source (Model CCS-01) and PID controlled oven power supply. The temperature variation for the oven to achieve is from room temperature to 200 °C. This equipment was calibrated by using standard Germanium slice before measuring the samples.

Some assumptions are necessary to be made in order to use this four probes method in conducting polymer pellet. It is assumed that the resistivity of the material is uniform in the measurement area. The surface on which the probes rest must be flat with no surface leakage. Instead of this, the four probes for resistivity measurements must contact the surface at points that lie in a straight line. Furthermore, the diameter of the contact between the metallic probes and the material should be small compared to the distance between probes.

The Four-probe connection

The basic model for resistivity measurements of all samples is illustrated schematically in **Figure 3.3.** The sample was put on the base plate of the four-probe arrangement and the probes were rested gently on the sample. The four-probe arrangement was then connected with a PID controlled oven. The digital microvoltmeter mode was then adjusted to voltage measuring mode and the voltage between the probes can be read. Lastly the oven was on and the rate of heating can be chosen between low and high as desired. The voltage of sample was collected in the temperature range of 30 - 150 °C. The distance between the adjacent probes is of 2.0 mm.

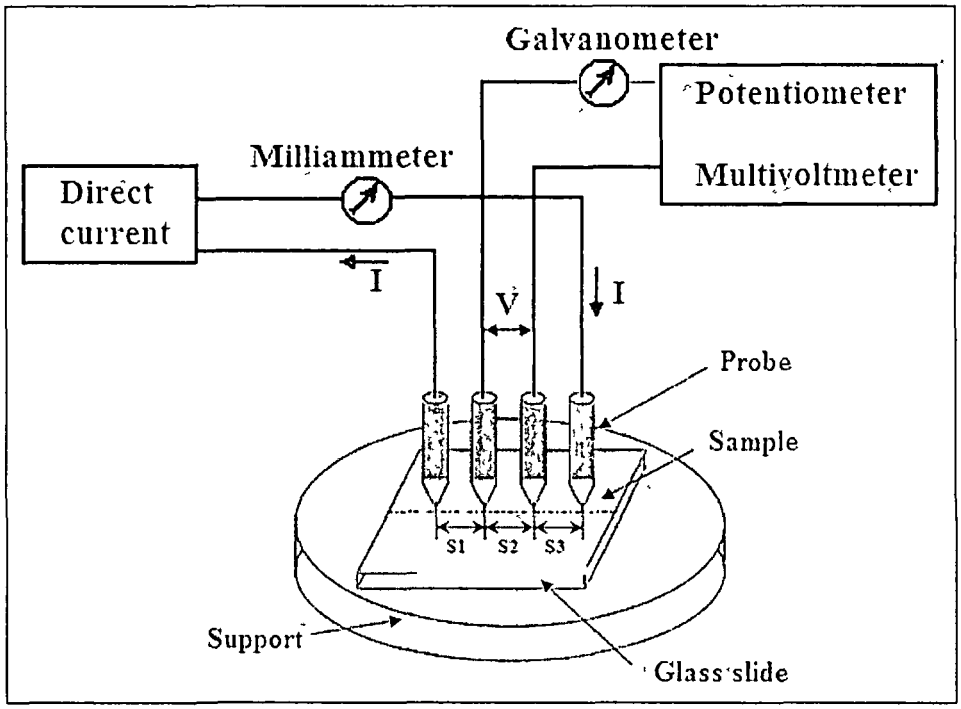

Figure 3.3 Circuit of the four probe resistivity measurements

3.3.4 Cyclic voltammetry

Cyclic voltammetry is a dynamic electrochemical method in which the potential applied to an electrochemical cell is scanned and the resulting change in cell current are monitored to yield a cyclic voltammogram (CV) of the redox properties of the material under study. The CVs reported here were recorded with a computer controlled Sycopel AEW2-10 potentiostat/galvanostat at a scan rate of 50 mV/S. Measurements were performed with a standard one compartment three-electrode configuration cell (Figure 3.4) with the polymer films deposited on ITO coated glass electrode as the working electrode, platinum as the counter electrode, and an Ag/Ag^+ electrode as the reference electrode. Acetonitrile containing $LiClO_4$ (0.1M) was used as the electrolytic medium. The measurements were calibrated using ferrocene as the standard. Electrochemical oxidation and reduction processes take place when potential is applied in the working electrode with respect to the reference electrode and this process is equivalent to control the energy of the electrons within the working electrode.

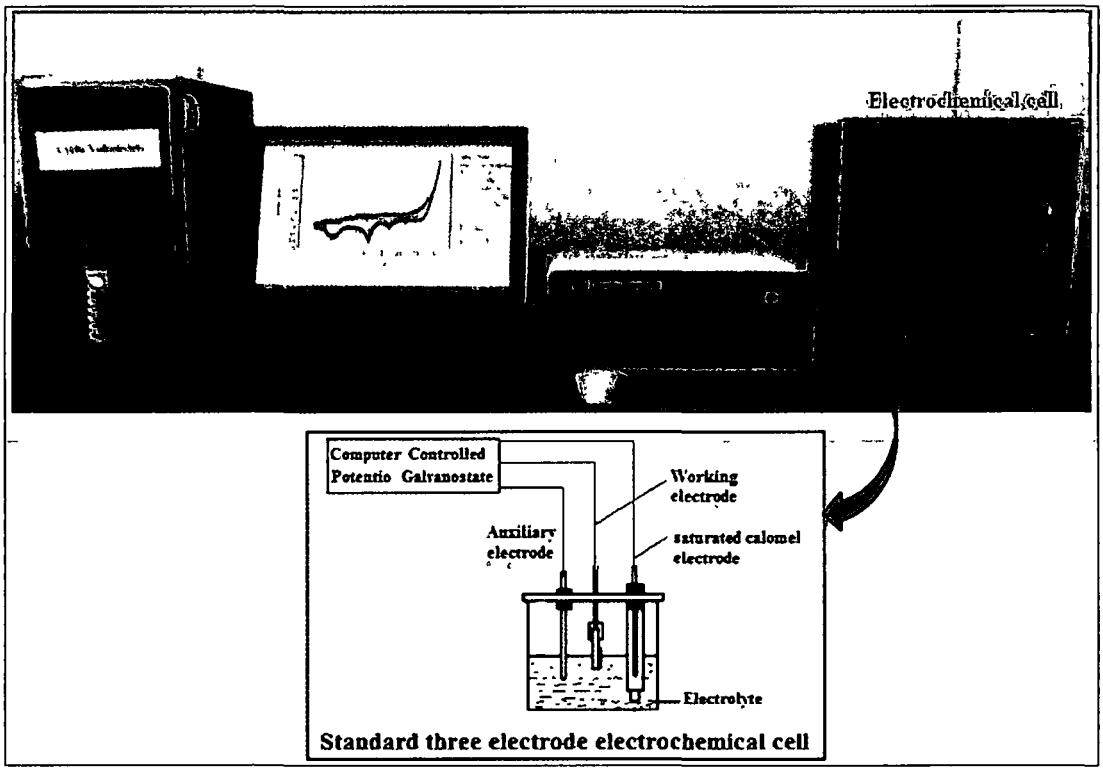

Figure 3.4 The complete electrochemical setup

3.4 Results and discussion

3.4.1 UV-Visible Study of Carbon Filled π-Conjugated Polymers

Conjugated polymers possess intensive and broad absorption bands in the UV-visible (UV-vis) region, indicating an extensive π- conjugation in the polymer backbone. The λ_{max} depends on the effective π- conjugation of the polymer chain and the aggregation state of the polymer. With increase in π- conjugation length, a red shift to λ_{max} is observed.

Absorption spectra of the polymers also enable to provide important information regarding its optical band gap. Optical absorption in conjugated polymers which are mostly amorphous or semicrystalline may be due to the transition of charge carriers, through a forbidden energy gap, called optical band gap. Attempts have been made to determine the optical band gap using the equation[1] 3.1.

$$E_g^{opt}(eV) = 1240 / \lambda edge\ (nm) \qquad (3.1)$$

Where E_g^{opt} is the optical band gap of polymers and λ_{edge} is the absorption edge. The optical band gap of all the polymers composites are summarized in **Table 3.14** and **Table 3.15.**

Figure 3.5 displays the UV–vis spectra obtained from PA and the PA/G composites. In PA, the spectrum shows three distinct absorption bands at 305, 356, and 580 nm for PA. The first and second absorption bands are related to the molecular conjugation (π - π^* transition) while the third absorption peak assigned to the polaron state of PA i.e. charged cationic species.[2] In the PA/G composite, the incorporated graphite interacted with the amine and imine nitrogen in the benzenoid and the quinoid segments resulted in the red shift of the band. However, the other two bands remained unaffected by incorporating graphite particles into the PA matrix.

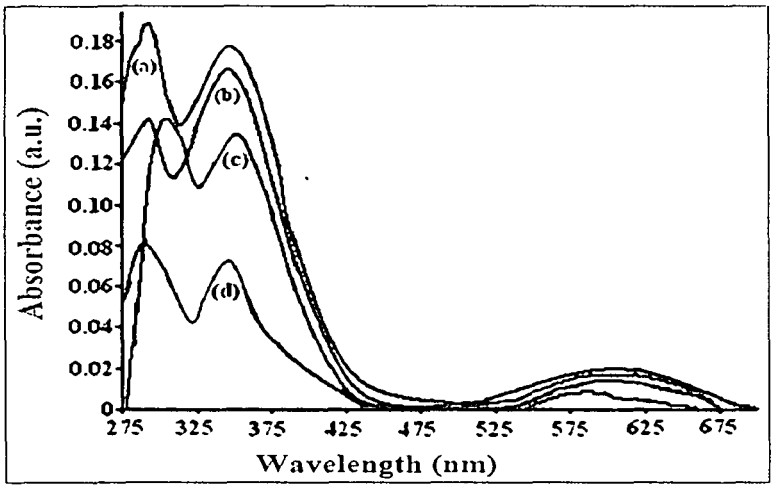

Figure 3.5 UV-vis spectra of (a) PA/G (1%), (b) PA/G (0.5%), (c) PA and PA/G (0.25%) composites

Figure 3.6 represents the UV-vis absorption spectra of the PA/EG (0.25%, 0.50%, 1.0%) solution in NMP. The two absorption bands at 310–320 nm and 330-340 nm are due to the π–π^* transition of benzenoid rings of PA/EG composites. The absorption band at 518-565 nm is attributed to the excitation from the HOMO (highest occupied molecular orbital, π_b) of the three-ring benzenoid part of the system to the LUMO (lowest unoccupied molecular orbital, π_q) of the localized quinoid ring and the two surrounding imine nitrogen in the emeraldine base form of PA (**Scheme 3.1**).

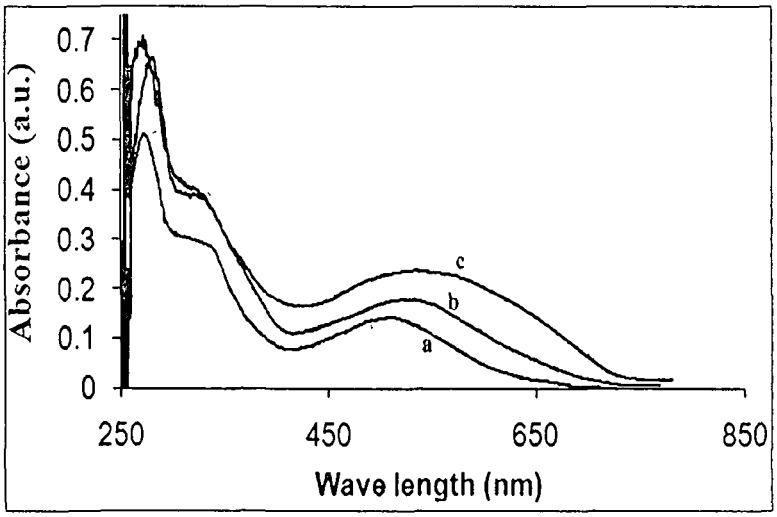

Figure 3.6 UV-vis spectra of (a) PA/EG (0.25%), (b) PA/EG (0.50%) and (c) PA/EG (1.0%) composites

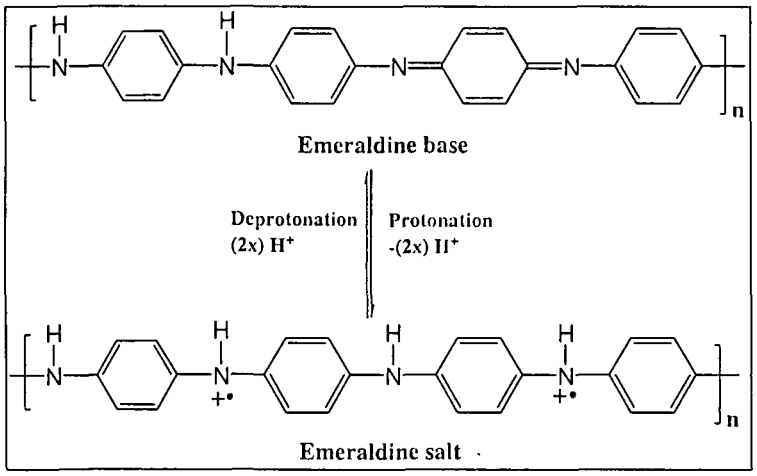

Scheme 3.1 Schematic representation of the formation emeraldine salt from emeraldine base

Figure 3.7 represents the UV-vis absorption spectra of the PA/GO composites (0.25%, 0.50%, 1.0%) recorded in NMP. The PA/GO composite shows an intense absorption peak at 315-320 nm and a broad peak at around 510 - 528 nm. The first absorption bands are related to the molecular conjugation (π - π* transition) while the second absorption peak assigned to the polaron state of PA in the synthesized PA/GO composites. However all the PA band in PA/GO composites, the red shift due to the interaction of increase % of GO into PA matrix have been observed.

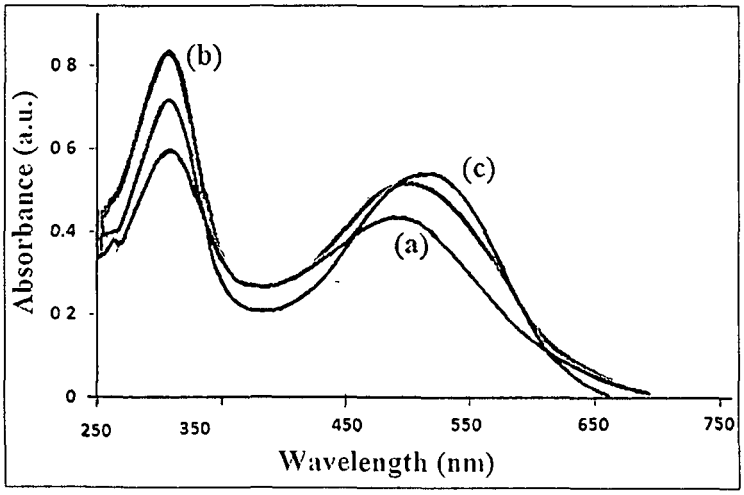

Figure 3.7 UV-vis spectra of (a) PA/GO (0.25%), (b) PA/GO (0 50%) and (c) PA/GO (1 0%) composite

Figure 3.8 shows the UV-Vis spectrum of SMA-PA/G core-shell composites. Similar peaks are observed for the SMA-PA/G composites with pure PA. The peaks at 315-320 nm, due to π-π* transition band and a strong band at around 508-520 nm is observed. The graphite assists the polymerization in such a way that it maintains a higher conjugation length in the chain of the PA itself and there may have some coupling in between the π-electrons of the PA and graphite. The characteristic red shift is due to the extended conjugation length of PA chains and high degree of incorporation of graphite.

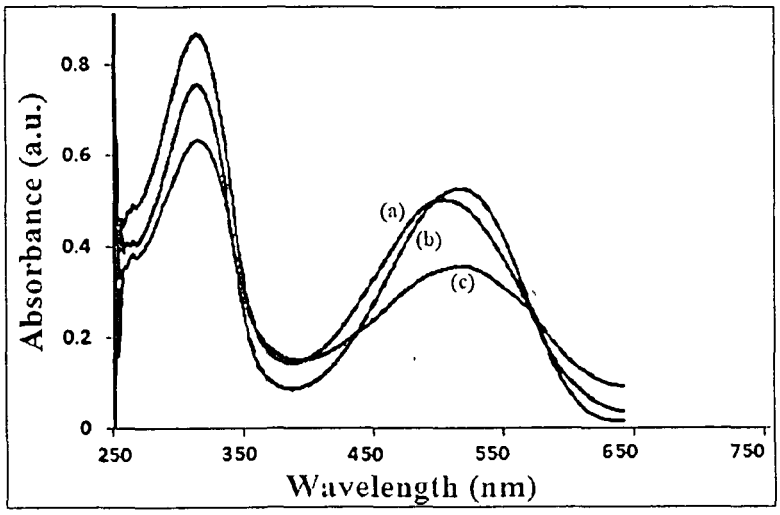

Figure 3.8 UV-visible spectra of (a) SMA-PA/G (0 25%), (b) SMA-PA/G (0 50%), (c) SMA-PA/G (1.0%) core-shell composite

UV-vis spectra of the PPy and PPy/EG correspond are shown in **Figure 3.9.** In PPy, the spectrum shows a weaker absorption at around 330 nm and stronger

absorption at around 570 nm which lead to the optical band gap of 2.17 eV. The first absorption band is associated with the π-π* transition while the second is assigned to the bipolaron state of PPy respectively. Similar peaks are observed for the PPy/EG as shown in the **Figure 3.9**. The peaks at 335-345 nm, due to π-π* transition band is more intense, compared to pure PPy. Significantly, a strong band at around 640-670 nm (1.93 - 1.85 eV) is observed. EG assists the polymerization in such a way that it maintains a higher conjugation length in the chain of the PPy itself and there may have some coupling in betwcen the conjugation length of the PPy and EG. In addition, some functional groups such as –OH, –COOH existed on the surface and pores of the EG at high temperature after acid treatment and they could promote the adsorption of molecular chains and monomers onto the pores. Moreover the π-π stacking between the polymer backbone and the EG sheets may also contribute to extend the conjugation length of the polymer composite. The characteristic red shift of PPy/EG nanocomposites due to the extended conjugation length of PPy chains and high degree of incorporation of EG has clearly be shown. The enhanced dc electrical conductivity of PPy/EG composite also further supports the red-shift behaviour of the composite.

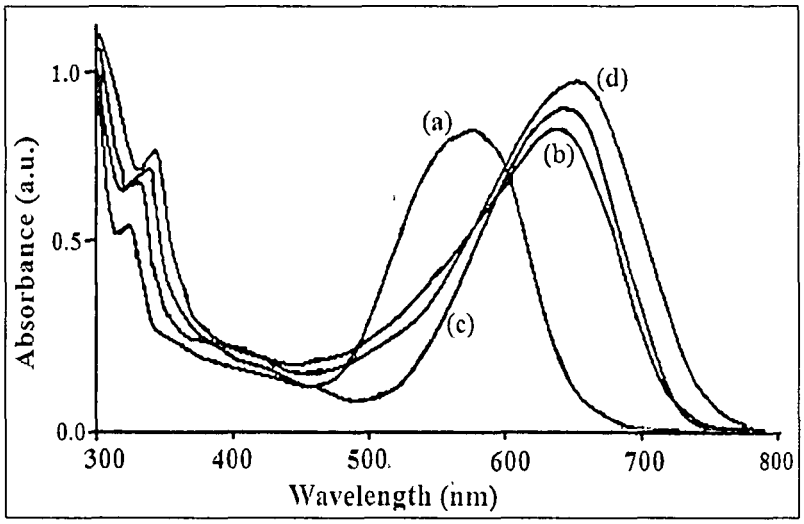

Figure 3.9 UV-visible spectra of (a) PPy, (b) PPy/EG (0.25%), (c) PPy/EG (0.50%) and (d) PPy/EG (1.0%) composites

Figure 3.10 represents the UV-vis absorption spectra of the PPy/G composites. The PPy/G composite shows an weaker absorption peak at 325-340 nm and a broad peak at around 530 - 556 nm. The first absorption bands are related to the molecular conjugation (π - π* transition) while the second absorption peak assigned to the bipolaron state of PPy in the synthesized PPy/G composites. However all the PPy band

in PPy/G composites the red shift due to the interaction of increase content of graphite into PPy matrix has been observed.

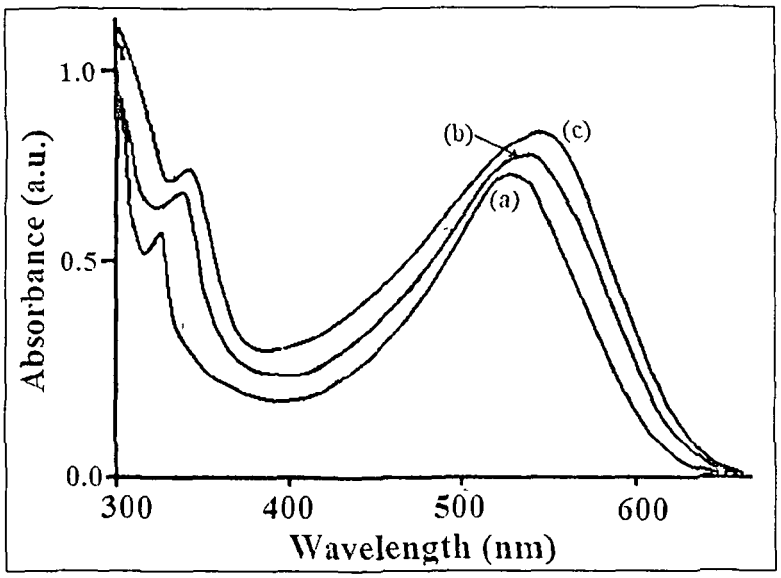

Figure 3.10 UV-visible spectra of (a) PPy, (b) PPy/G (0 25%), (c) PPy/G (0 50%) and (d) PPy/G (1 0%) composites

The PPy/GO composite shows similar spectrum with pure PPy as shown in the **Figure 3.11**. The peaks at 330-338 nm, due to π-π^* transition band and a strong band at around 595-612 nm is observed. This indicates that the PPy is also polaronic state in the synthesized PPy/GO composite. The functional groups such as –OH, –COOH existed on the surface and pores of the GO after acid treatment and they could promote the adsorption of molecular chains and monomers onto the pores. Moreover the π-π stacking between the polymer backbone and the GO sheets may also contribute to extend the conjugation length of the polymer composite. GO assists the polymerization in such a way that it maintains a higher conjugation length in the chain of the PPy itself and there may have some coupling in between the conjugation length of the PPy and GO. The characteristic red shift of PPy/GO nanocomposites due to the extended conjugation length of PPy chains and high degree of incorporation of GO. The enhanced dc electrical conductivity of PPy/GO composite also further supports the red-shift behaviour of the composite.

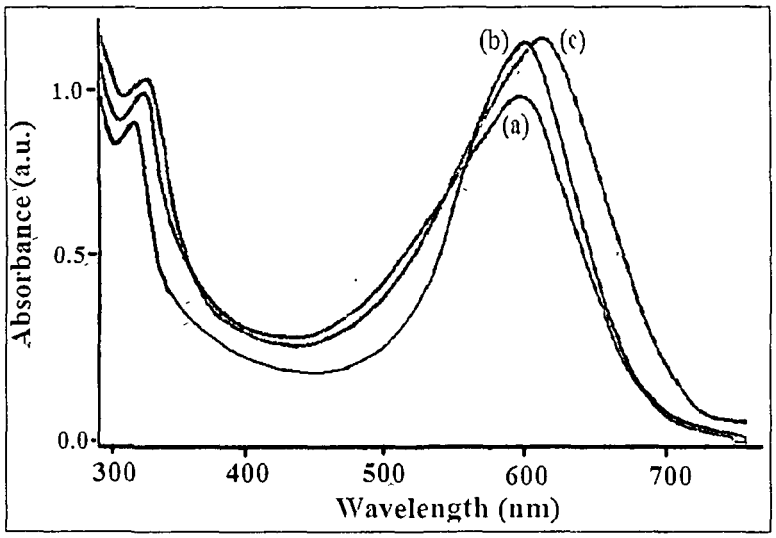

Figure 3.11 UV-vis spectra of (a) PA/GO (0.25%), (b) PPy/GO (0.50%) and (c) PPy/GO (1.0%) composites

3.4.2 Electrical Properties of the polymer composites

3.4.2.1 Preparation of pellet for electrical property measurement

The selected sample of pure polymers and their composites are dried at 60 °C in an oven up to 24 h. The hard round shape pellets of the composite material (220 mg) are made at room temperature using a compression-moulding machine at pressure 1.5 to 2 ton for 10 min. The optimum thickness of pellets is obtained ~2 mm thickness and diameter 1 cm.

3.4.2.2 Current - voltage (I-V) Characteristics Measurements

The effect of graphite, EG and GO filler on the I-V characteristics of PA and PPy composites is a feature of this work. The I-V characteristics of graphite, EG and GO filled PA and PPy composites are shown in figure below. All the synthesized polymer and composites are asymmetric and nonlinear for forward direction of applied voltage. This suggests the semiconducting behaviour and Schottky barrier in the polymer and polymer composites.[3] Here for all the samples, the potential difference (V) increases linearly when the applied current (mA) as well as the % of carbon filler incorporates into the polymer matrices are increased.

Figure 3.12 - 3.14 shows the I-V characteristics of PA/G, PA/EG and PA/GO composites having different graphite, EG and GO content respectively. For all the samples, the potential difference (in Volt) increases gradually with the applied current

(in mA) which clearly indicates the semiconducting behaviour and behaves as Schottky junction The semiconducting behaviour of the PA/G, PA/EG and PA/GO composites gradually increases with respect to the increasing percentage of graphite, EG and GO incorporates into the polymer matrices respectively

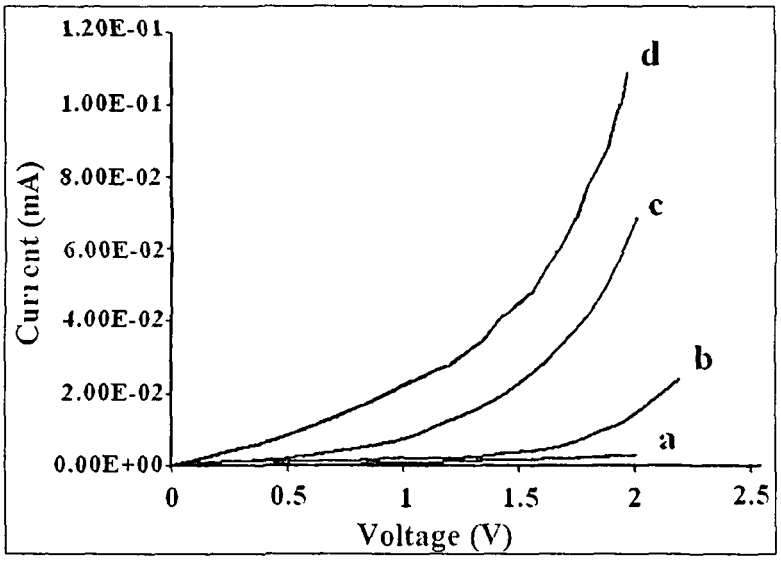

Figure 3.12 I–V plot of (a) PA, (b) PA/G (0 25%), (c) PA/G (0 50%), and (d) PA/G (1 0%) composite

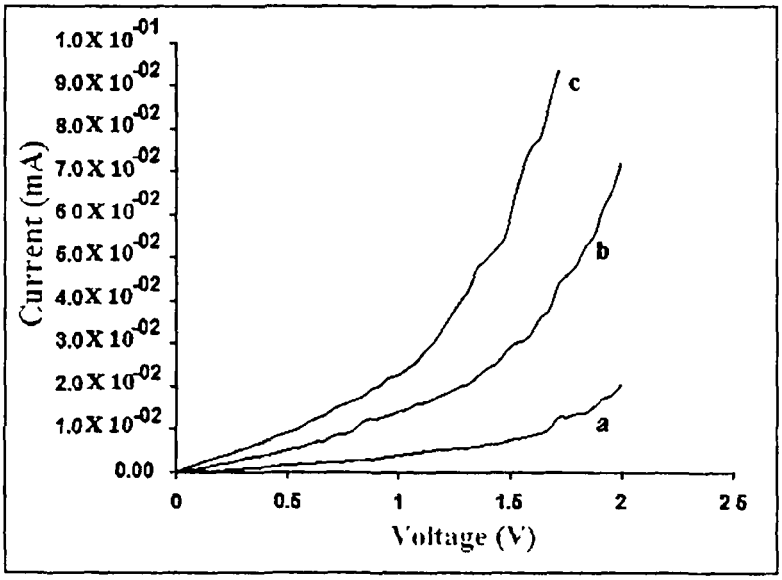

Figure 3.13 I–V plot of (a) PA/EG (0 25%) (b) PA/EG (0 50%) and (c) PA/EG (1 0%)

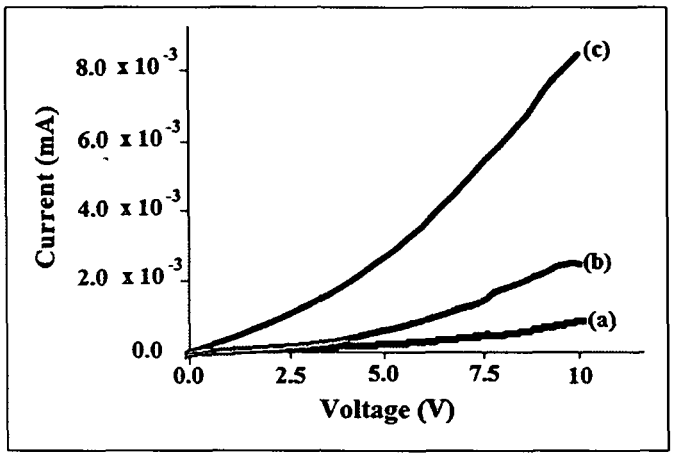

Figure 3.14 I–V plot of (a) PA/GO (0.25%), (b) PA/GO (0.50%) and (c) PA/GO (1.0%)

Figure 3.15 shows the current-voltage relationship of SMA-PA (0% graphite) and SMA-PA/G core-shell composites having different graphite content at room temperature. The SMA-PA/G core - shell composites show better semi conducting behaviour than the SMA-PA composite. For all the samples, the potential difference (in Volt) increases linearly with the applied current (in mA) as well as the % of graphite incorporated into the polyaniline (shell) phase. For SMA-PA/G (1.0%) core – shell composite, maximum semi conducting nature is found compared to the SAM-PA and SMA-PA/G (0.25% and 0.50%) core - shell composites. The drastic jump in current between 0.5% and 1% filler content may be due to the presence of higher amount of graphite incorporated in the PA/G composites which may cause interparticle connectivity resulting in π-electrons coupling in between the PA and graphite.

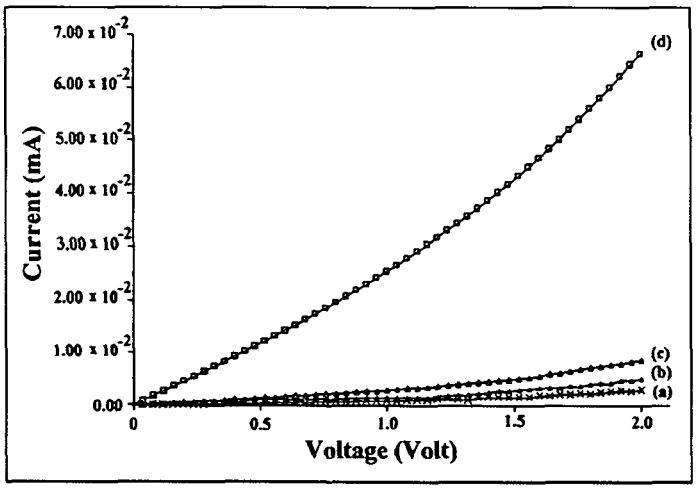

Figure 3.15 I-V plots of the SMA-PA/G core-shell particles with (a) 0% graphite (b) 0.25% graphite, (c) 0.50% graphite and (d) 1.0% graphite

Figure 3.16 - 3.18 shows the current-voltage relationship of PPy/G, PP/EG and PPy/GO composites respectively at room temperature. Here for all the samples, the potential difference (in Volt) increases linearly when the applied current (in mA) as well as the % of graphite, EG and GO incorporated into the polymer matrix is increased.

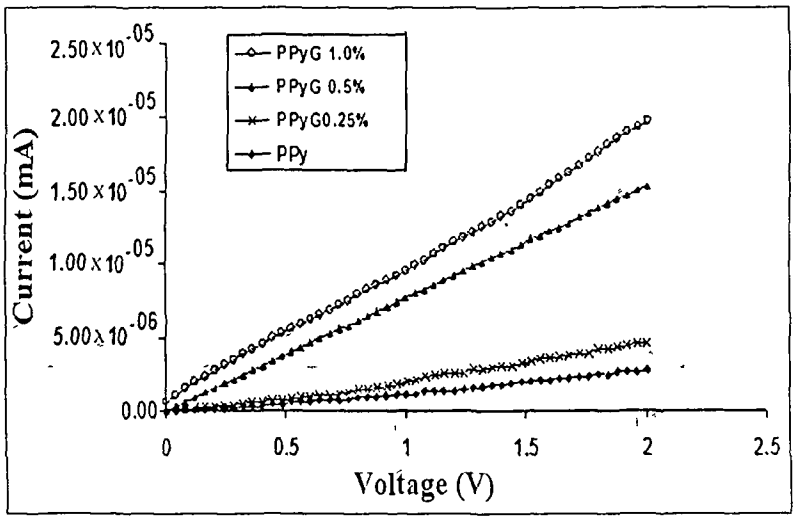

Figure 3.16 I-V plots of PPy and PPy/G composites

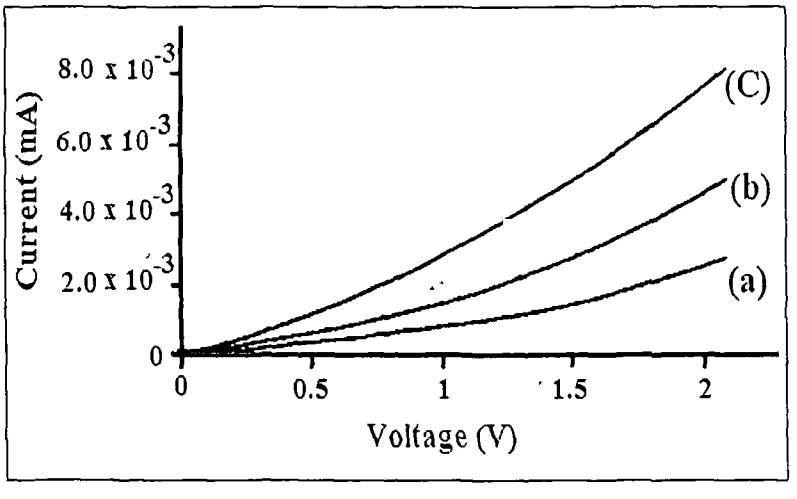

Figure 3.17 I-V plot of (a) PPy/EG (0 25%), (b) PPy/EG (0 50%) and (c) PPy/EG (1%) composites

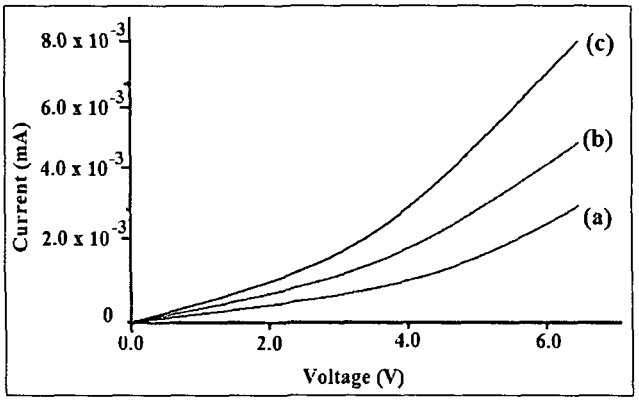

Figure 3.18 I-V plot of (a) PPy/GO (1%), (b) PPy/GO (2%) and (c) PPy/GO (3%) composite

3.4.2.3 DC electrical conductivity

DC electrical conductivity of conducting composite is measured by using a four probe resistivity measurement system. The conductivity (s) was calculated using the following equations-

$$\rho = \rho_o / G_7(W/S) \quad (3.2)$$

$$G_7(W/S) = (2S/W)\ln 2 \quad (3.3)$$

$$\rho_o = (V/I)2\pi S \quad (3.4)$$

$$\sigma = 1/r \quad (3.5)$$

Where $G_7(W/S)$ is a correction divisor which is a function of thickness of the sample as well as probe - spacing; I, V, W and S are current (A), voltage (V), thickness of the pellet (cm) and probe spacing (cm) respectively. The isothermal stability of pellet in terms of DC electrical conductivity retention is carried out on the selected samples at the temperature range of 30 - 140 °C in an air oven. The electrical conductivity measurements are carried out at an interval of 10 min.

3.4.2.4 Conductivity of PA and its composites

The dc electrical conductivity of the PA and PA/G composites vary widely in the range 0.042–238.08 S/cm (**Table 3.1**), depending on the various concentrations of the graphite added and the temperature increase. **Figure 3.19-a** and **Figure 3.19-b** show the variation of the conductivity with temperature as well as activation energy (Ea) of the polymer and composites. From **Figure 3.19-b**, the values of activation energy (*Ea*) is found to be in the range of 15.6-16.6 kJ/mol. In PA, the conductivity first decreases with increasing temperature, which is caused by the removal of acid. PA

shows maximum conductivity at 50 °C (0.50 S/cm), but its conductivity is found in the same range, from 60 to 150 °C.

In the PA/G composite, the conductivity increases with increasing concentration of graphite. We incorporate graphite from 0.2 to 1.0% into the PA matrix, and the maximum conductivity (20.26 S/cm) is found in the 1.0% PA/G composite at room temperature. The increase in temperature results in a decrease in conductivity for the PA/G composites up to 40 °C. The conductivity increases from 40 - 150 °C, showing semiconducting behaviour. The slight increase in temperature may have caused molecular and filler orientation instead of electron hopping from the highest occupied molecular orbital (HOMO) to the lowest unoccupied molecular orbital (LUMO) and, hence, causes the decreases in conductivity observed initially up to 40 °C. The abrupt increase in conductivity for the PA/G composites with different compositions is also observed from 80 °C. This may have been the result of increase intrachain and interchain hopping at high temperatures. An increase in interchain and intrachain hopping results in a high charge carrier mobility within the composite, which leads to an increase in the conductivity at appropriate high temperatures.[4]

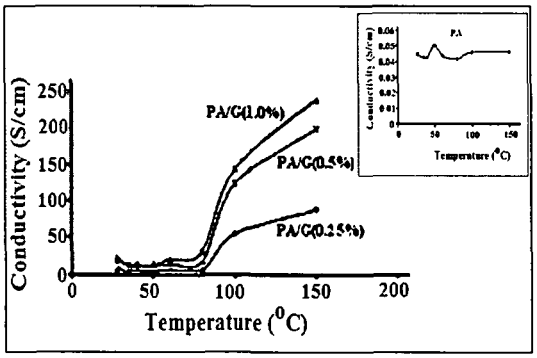

Figure 3.19 -a Conductivity of PA/G composites and PA with respect to temperature

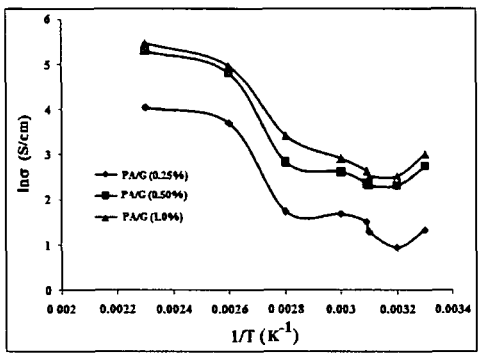

Figure 3.19 -b The dependence of logarithm of specific electrical conductivity on inverse temperature for PA/G composites

Table 3.1 Conductivity and activation energy (E_a) of PA and PA/G composites at various temperatures

Temperature (°C)	Conductivity (S/cm)			
	PA	PA/G (0.25%)	PA/G (0.5%)	PA/G (1%)
27	0.044	3.77	15.45	20.26
35	0.042	2.56	10.07	12.45
40	0.042	3.61	10.07	13.86
50	0.050	4.53	10.57	13.86
60	0.044	5.37	13.61	18.30
80	0.046	5.65	16.86	30.22
100	0.046	40.21	122.54	143.50
150	0.046	56.72	198.01	238.08
Ea	-	23.7 (kJ/mol)	27.7 (kJ/mol)	29.1 (kJ/mol)

The dc electrical conductivity of the PA/EG composites is found to be dramatically increased in comparison to the PA alone. The electrical conductivity get increases with temperature showing semi conducting behaviour and the maximum conductivity is found to be 4 x 10^2 S/cm for PA/EG (1%) at 140 °C (**Figure 3.20-a**). At high temperature, the mobility of the charge carrier increases with the increase in inter-chain and intra-chain hoping. This high charge carrier mobility made the increase in the conductivity.[5,6] From **Figure 3.20-b**, the values of activation energy (*Ea*) is found to be in the range of 15.6-16.6 kJ/mol.

Conductivity also increases with increase in the concentration of EG incorporate to the polymer matrices. We incorporate EG (0.25% to 1.0%) into PA matrices and the maximum conductivity of 71 S/cm is found with 1% PA/EG composites at room temperature (**Table 3.2**). The graphite expansion would certainly influence the overall conductivity of the bulk materials. After expansion, each graphite flake can be exfoliated into many EG layers as conductive fillers. In addition, some functional groups such as –OH, –COOH existed on the surface and pores of the EG after acid and high temperature treatment and they could promote the adsorption of molecular chains and monomers onto the pores.[7] Therefore EG is the most effective in imparting conductivity. This is possibly due to the excess surface provided by the EG compared to the graphite because in EG, only the spacing of the graphite layers was expanded; the conductive characteristics of each EG sheet layer remains the same as graphite flakes themselves by nature.[8]

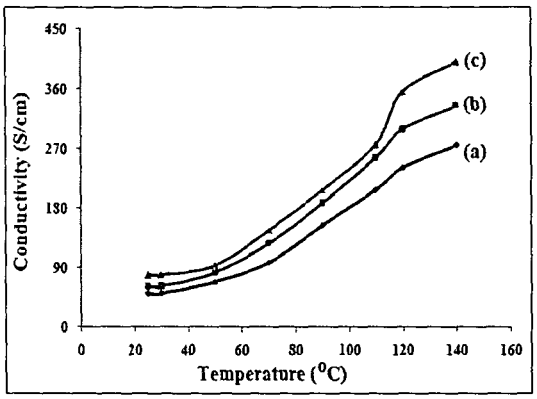

Figure 3.20-a Conductivity of (a) PA/EG (1%), (b) PA/EG (2%), (c) PA/EG (3%) composites with respect to temperature

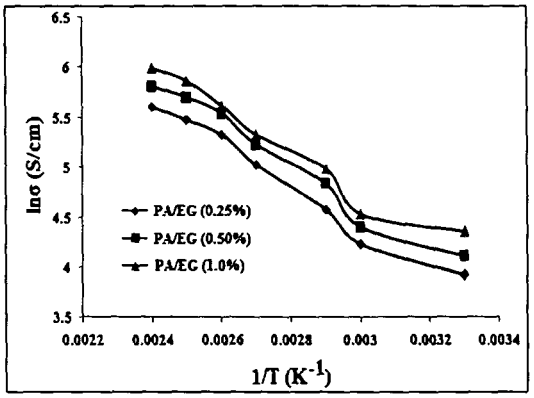

Figure 3.20-b The dependence of logarithm of specific electrical conductivity on inverse temperature for PA/EG composites

Table 3.2 Conductivity and activation energy (E_a) of PA/EG composites at various temperatures

Temperature (°C)	Conductivity (S/cm)		
	PA/EG (0.25%)	PA/EG (0.50%)	PA/EG (1%)
25	51	62	71
30	51	62	71
50	69	82	89
70	98	127	147
90	154	187	208
110	207	256	276
120	241	299	356
140	275	335	400
Ea	16.6 (kJ/mol)	16.4 (kJ/mol)	15.6 (kJ/mol)

The electrical conductivities of the GO and the PA/GO composite materials are listed in **Table 3.3**. The GO sample shows a low conductivity of 0.5 S/m similar to that reported in the earlier literature.[9] The dc electrical conductivity of the PA/GO composite (40.5-292 S/cm) is found to increase dramatically in comparison to the pure PA and GO alone. Such enormous enhancement of the conductivity of PA/GO composite might be attributed to the extended H-bonding between the PA and GO allowing extended π-conjugation in PA chain. Moreover the π-π stacking between the polymer backbone and the GO sheets may also contribute in increase of conductivity in PA/GO composite (**Figure 3.21-a**). The polymerization on the surface and pores of GO sheets restricts the twisting of the polymer backbone away from its planarity which plays a major role to enhance the conductivity. Therefore GO is the most effective in imparting the conductivity. From **Figure 3.21-b**, the values of activation energy (*Ea*) is found to be in the range of 12.0-15.5 kJ/mol.

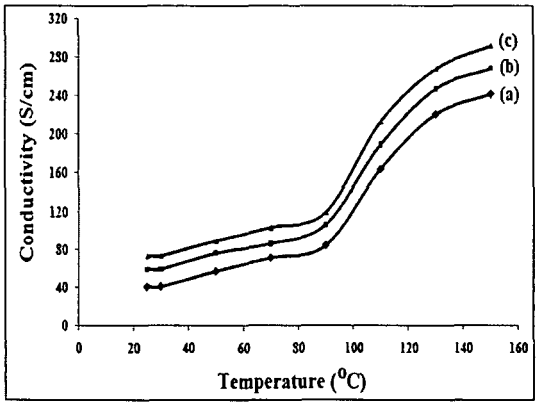

Figure 3.21-a Conductivity of (a) PA/GO (0.25%), (b) PA/GO (0.50%), (c) PA/GO (1.0%) composites with respect to temperature

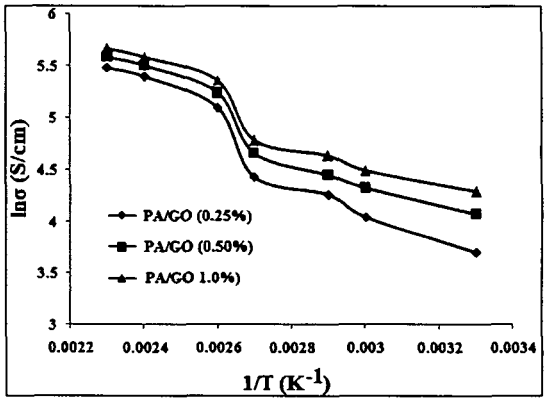

Figure 3.21-b The dependence of logarithm of specific electrical conductivity on inverse temperature for PA/GO composites

Table 3.3 Conductivity and activation energy (E_a) of PA/GO composite at various temperatures

Temperature (°C)	Conductivity (S/cm)			
	GO	PA/GO (0.25%)	PA/GO (0.50%)	PA/GO (1.0%)
25	0.5	40.5	59	73
30	0.5	40.5	59	73
50	0.5	57	76	89
70	0.5	71	86	103
90	0.51	84	106	119
110	0.51	164	189	213
120	0.51	221	247	268
140	0.51	242	268	292
E_a	-	15.5 (kJ/mol)	13.2 (kJ/mol)	12.0 (kJ/mol)

The conductivity of SMA-PA/G core - shell composites vary widely in the range of 8.50 S/cm to 114.70 S/cm (**Figure 3.22**) depending on the various concentrations of the graphite incorporate to the shell phase and the temperature increase. Thus it may be said that in the pellet of SMA-PA/G composite particles, interfacial conductive paths consisting of the PA-graphite shell are formed, and efficient charge transport through the materials can occur without much interference from the electrically insulating SMA component. The conductivity of SMA-PA composite without incorporating graphite particle shows 0.042 S/cm to 0.051 S/cm with variation of temperature. **Figure 3.22** shows the variation of conductivity of the core - shell composites with the temperature range of 30 - 140 °C.

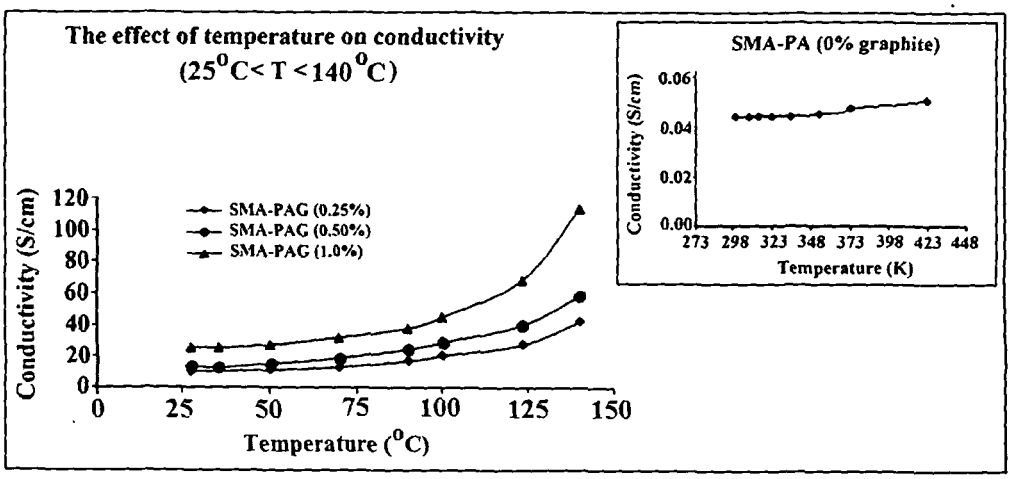

Figure 3.22 Conductivity of SMA-PA and SMA-PA/G core-shell composites with respect to temperature

At higher temperature the inter-chain and intra-chain hopping increases which results in high charge carrier mobility within the composite. This high charge carrier

mobility leads to an increase in the conductivity at high temperatures. Conductivity also increases with increase the concentration of graphite. We incorporate graphite from 0.25% - 1.0% into PA matrix and conductivity increases from 25.30 S/cm at 30 °C to 114.70 S/cm at 140 °C with 1.0% incorporation of graphite. This gives evidence beyond any reasonable doubt that the newly synthesized core-shell composite particles are of semi conducting in nature.

3.4.2.5 Conductivity of PPy and Its Composites

The conductivity of PPy and PPy/G composites vary widely in the range of 0.03 to 60 S/cm (**Table 3.4**) depending on the various concentrations of the graphite added and the temperature increased. **Figure 3.23** showed the variation of conductivity of the PPy and PPy/G composites with temperature range 30-140 °C. In PPy, on heating, the conductivity first decreased with increase in temperature which was due to the removal of solvent. The conductivity got increased from temperature 70-140 °C showing semi conducting behaviour for both the heating and cooling condition. The maximum conductivity for PPy is found 0.055 S/cm at 140 °C.

In PPy/G composites, conductivity increases with increase in the concentration of graphite. We incorporate graphite from 0.25% to 1.0% into PPy matrix and maximum conductivity 22.40 S/cm found with 1.0% PPy/G composite at room temperature. The increase in temperature results in decrease of conductivity for PPy/G composites upto 50 °C. The conductivity got increased from 50 °C to temperature 140 °C showing semi conducting behaviour. The slight increase in temperature may be used up in molecular as well as filler orientation instead of electron hopping from HOMO to LUMO and hence the decrease in conductivity is observed initially upto 50 °C. The increase in conductivity for PPy/G composites with different compositions has been observed from 50 °C. This may be the result of increased intra-chain and inter-chain hopping at high temperature. The increase in interchain and intrachain hopping results in high charge carrier mobility within the composite, which leads to increase in conductivity at appropriate high temperature.[10,11] From **Figure 3.23-b**, the values of activation energy (*Ea*) is found to be in the range of 11-17.8 kJ/mol.

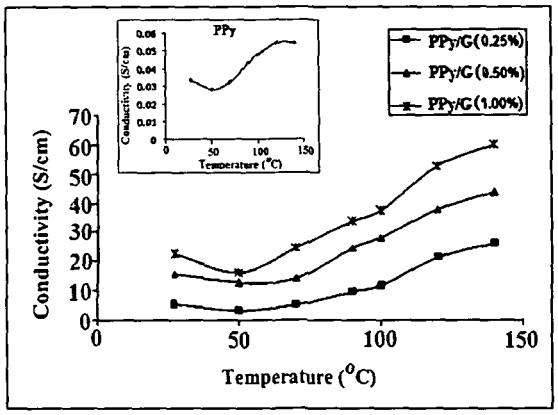

Figure 3.23-a Conductivity of PPy and PPy/G composites with respect to temperature

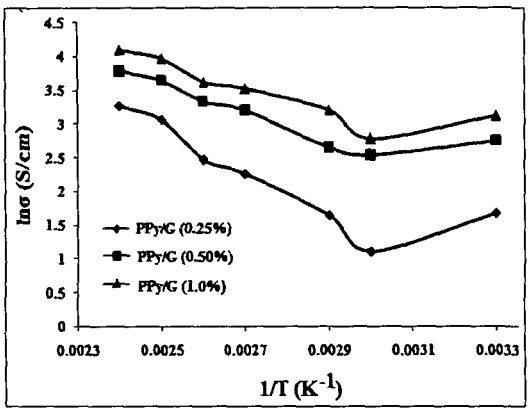

Figure 3.23-b The dependence of logarithm of specific electrical conductivity on inverse temperature for PA/GO composites

Table 3.4 Conductivity and activation energy (E_a) of PPy and PPy/G composites at various temperatures

Temperature (°C)	Conductivity (S/cm)			
	PPy	PPy/G (0.25%)	PPy/G (0.50%)	PPy/G (1.0%)
27	0.031	5.30	15.50	22.40
50	0.028	3.01	12.52	16.08
70	0.040	5.13	14.01	24.50
90	0.044	9.60	24.50	33.60
100	0.045	11.70	28.00	37.30
120	0.050	21.30	37.90	52.80
140	0.055	26.10	43.70	60.00
E_a	-	17.8 (kJ/mol)	14.8 (kJ/mol)	11.0 (kJ/mol)

The dc electrical conductivity of the PPy/EG composites is found to be increased dramatically in comparison to the pure PPy as well as the PPy/G composites (**Table 3.5**). The EG sample shows a very high conductivity of 512 S/m similar to that reported in the earlier literature. The trend of the dc electrical conductivities of PPy/EG composites is similar with the PPy/G composites. Here in PPy/EG composites the electrical conductivity increases with temperature showing semiconducting behaviour and the maximum conductivity is found to be 110.04 S/cm for PPy/EG (1.0%) at 140 °C (**Figure 3.24**). However, the slight increase in temperature results in the decrease of conductivity of the PPy/EG composites which may be due to the removal of solvent bound to the polymer chain and low-molecular-weight oligomers. In addition, the sudden increase in temperature initially upto 50 °C may be used up in molecular as well as filler orientation instead of electron hopping from HOMO to LUMO and hence the decrease in conductivity observed. Then the conductivity got increased from 50 °C to temperature 140 °C showing semiconducting behaviour. The gradual increase in

conductivity for PPy/EG composites with different compositions have been observed from 50-140 °C. This may be the result of increased intra-chain and inter-chain hopping at high temperature. The increase in interchain and intrachain hopping results in high charge carrier mobility within the composite, which leads to increase in conductivity at appropriate high temperature.[12,13] From **Figure 3.24-b**, the values of activation energy (*Ea*) is found to be in the range of 10.4-19.8 kJ/mol.

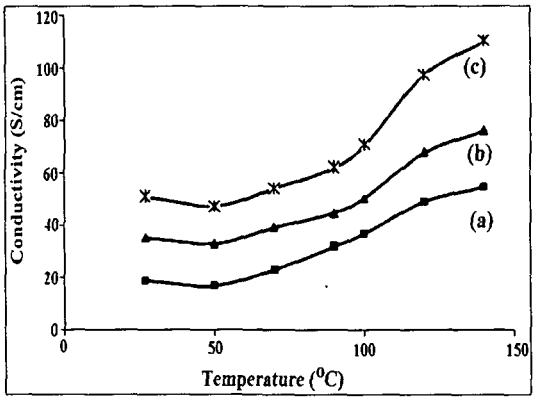

Figure 3.24-a Conductivity of (a) PPy/EG (0.25%), (b) PPy/EG (0.50%) and (c) PPy/EG (1.0%) composites with respect to temperature

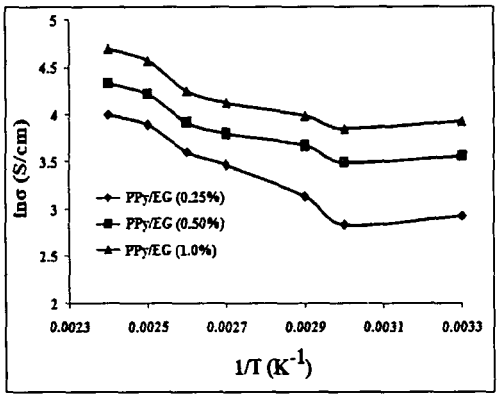

Figure 3.24-b The dependence of logarithm of specific electrical conductivity on inverse temperature for PA/GO composites

Table 3.5 Conductivity and activation energy (E_a) of PPy/EG composites at various temperatures

Temperature (°C)	Conductivity (S/cm)		
	PPy/EG (0.25%)	PPy/EG (0.50%)	PPy/EG (1.0%)
27	18.85	35.24	51.05
50	17.07	33.08	47.25
70	23.01	39.44	54.01
90	32.03	44.76	62.11
100	36.87	50.37	70.65
120	48.92	67.8	97.22
140	54.67	76.12	110.04
E_a	19.8 (kJ/mol)	11.2 (kJ/mol)	10.4 (kJ/mol)

Conductivity also increases with increase in the concentration of EG incorporate to the polymer matrix (**Figure 3.25**). We incorporate EG (0.25% to 1.0%) into PPy matrix and the maximum conductivity of 51.05 S/cm is found with 1% PPy/EG composites at room temperature (25 °C). The graphite expansion would certainly influence the overall conductivity of the bulk materials which leads the dramatic enhancement of the conductivity of PPy/EG composites. After expansion, each graphite flake can be exfoliated into many EG layers as conductive fillers. In addition, some functional groups such as –OH, –COOH existed on the surface and

pores of the EG after acid and high temperature treatment and they could promote the adsorption of molecular chains and monomers onto the pores.[10] Therefore EG is the most effective in imparting conductivity. This is possibly due to the excess surface provided by the EG compared to the graphite because in EG, only the spacing of the graphite layers was expanded; the conductive characteristics of each EG sheet layer remains the same as graphite flakes themselves by nature.

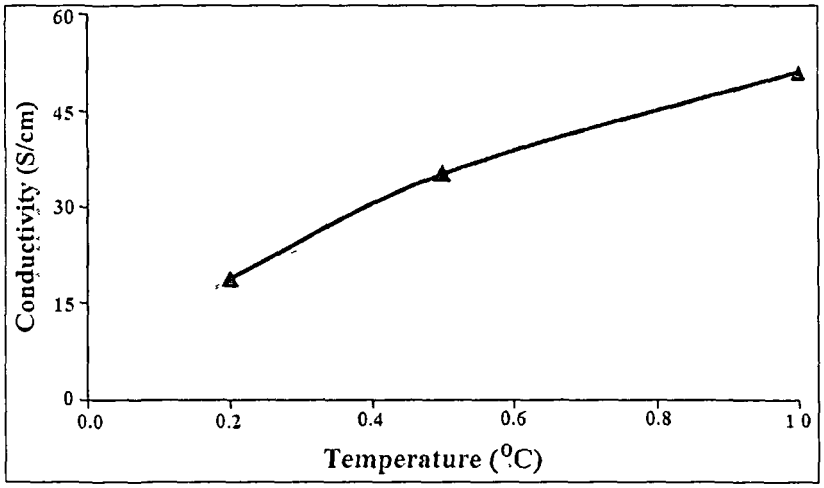

Figure 3.25 Conductivity of PPy/EG composites with varying EG content

The electrical conductivities of the PPy, GO and the composite material is determined and the conductivities are listed in **Table 3.6**. The dc electrical conductivity of the PPy/GO composites (11.5 - 71 S/cm) is increased dramatically in comparison to that of PPy and GO alone (**Figure 3.26**) with respect to increase in temperature and % of GO. Such enormous enhancement of the conductivity of the composite might be attributed to the extended H-bonding between the PPy and GO allowing extended π-conjugation in PPy chain. The polymerization on the surface and pores of GO sheets restricts the twisting of the polymer backbone away from its planarity which plays a major role to enhance the conductivity Therefore GO is the most effective in imparting the conductivity.

We have measured the electrical conductivity of PPy/GO composites in the temperature range of 25-150 °C. The electrical conductivity increases with temperature showing semi conducting behaviour and the maximum conductivity is found to be 71 S/cm for PPy/GO (1%) at 150 °C. At high temperature, the mobility of the charge carrier increases with the increase in interchain and intra-chain hoping. An increase in interchain and intrachain hopping results in a high charge carrier mobility within the

temperatures.[14,15] From **Figure 3.26-b**, the values of activation energy (*Ea*) is found to be in the range of 11.3-14.4 kJ/mol.

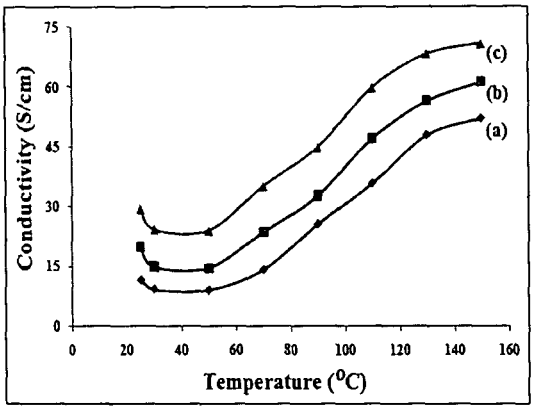

Figure 3.26-a Conductivity of (a) PPy/GO (0.25%), (b) PPy/GO (0.50%) and (c) PPy/GO (1.0%) composites with respect to temperature

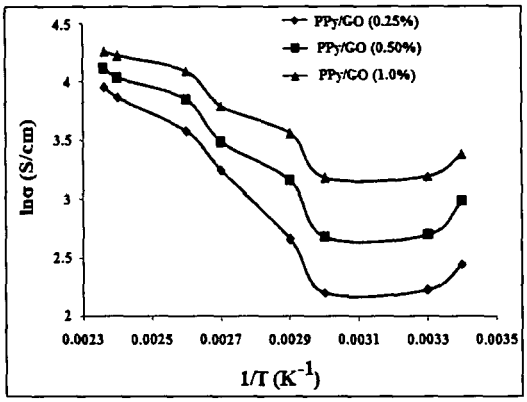

Figure 3.26-b The dependence of logarithm of specific electrical conductivity on inverse temperature for PPy/GO composites

Table 3.6 Conductivity and activation energy (E_a) of the PPy/GO composites at various temperatures

Temperature (°C)	Conductivity (S/cm)		
	PPy/GO (0.25%)	PPy/GO (0.5%)	PPy/GO (1.0%)
25	11.5	19.7	29.4
30	9.2	14.8	24.3
50	9	14.5	24
70	14.2	23.5	35
90	25.6	32.6	44.8
110	35.7	47	59.8
130	47.8	56.5	68.3
150	52.1	61.3	71
E_a	14.4 (kJ/mol)	12.6 (kJ/mol)	11.3 (kJ/mol)

3.4.3 Electrochemical Properties

The study of the electrochemical behaviour of polymers as a function of substitution can shed some light on the understanding of the reduction and oxidation process. The reduction and oxidation processes consist of several simultaneous and / or consecutive chemical and physical processes like swelling of the polymer, charge transfer between the electrode and the polymer, insertion of compensating ions into the bulk of the polymer, conformational changes of the polymer chain and change of conductivity.[16] Nevertheless, some trends can be extracted that may be helpful for design and application of new materials. In addition, the energy position of HOMO and

LUMO of conjugated polymers can be determined by cyclic voltammetric method The relevance and generality of electrochemical characterization of conjugated polymers can be estimated by comparison to other methods. This is frequently done by calculating the electrochemical band gap and comparing it with optical band gap.[17-20]

3.4.3.1 Estimation of energy level and band gap of the polymer composites

The HOMO and LUMO energy levels are estimated from the onset oxidation potentials (φ_{ox}) and the onset reduction potentials (φ_{red}) of the polymers. Energy levels and electrochemical band gap (E_g^{ec}) in turn are calculated using the following empirical equations **3.6 - 3.8.**[21]

$$HOMO = -(\varphi_{ox} + 4.71)\ (eV); \quad (3.6)$$

$$LUMO = -(\varphi_{red} + 4.71)\ (eV); \quad (3.7)$$

$$E_g^{ec} = (\varphi_{ox} - \varphi_{red})\ (eV) \quad (3.8)$$

All the redox potentials are measured against Ag/Ag^+ reference electrode and the energy level calculations are based on ferrocene / ferrocenium (Fc/Fc^+) redox standard in acetonitrile (CH_3CN). The HOMO and LUMO levels are calculated from the onset potentials of oxidation and reduction and by assuming the energy level of ferrocene/ ferrocenium (Fc/Fc^+) to be 4.8 eV below the vacuum level The formal potential of Fc/Fc^+ is measured as 0.09 V against Ag/Ag^+.[22, 23] Hence, the equations 3.6-3.8 are valid for the calculations of HOMO and LUMO energy levels and electrochemical band gap.

The charging of the polymer during the doping process is associated with conformational reorganisation and modification of the energy levels of the polymer. From this point of view only onset potential probes injection of charges to neutral polymers in the ground state. Onset is also advantageous when two or more red / ox peaks are not fully resolved. The onset has been evaluated by drawing two tangents for each peak and is assumed to be where the two tangents cross as indicated by dashed line for E_{pa}^{ox} in **Figure 3.27.**

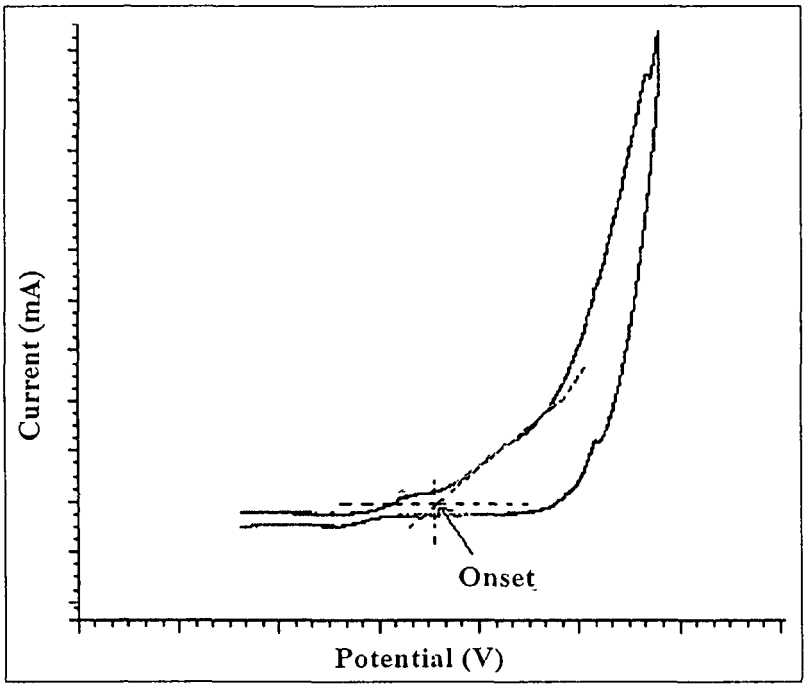

Figure 3.27 Measurement of onset in CV

3.4.3.2 Redox properties of polymers

The redox properties of all the synthesized polymers PA and PPy and their composites with different carbon fillers viz, graphite, EG and GO can be assessed in cyclic voltammetry method. CVs of polymers and their composite films in NMP solvent on to ITO coated glass in 0.1 M $LiClO_4$ in acetonitrile solution are shown in **Figure 3.28 - 3.34.**

The cyclic voltammogram (**Figure 3.28**) for PA and PA/G composites show single irreversible oxidation and reduction peaks. The turn-on potential for the p-doping (onset oxidation potential) for the polymer PA and PA/G composites are very low compared to the turn-on potential of the n-doping (onset reduction potentials) which in turn indicates that the polymers possess very good donor nature. The electrochemical band gap for PA is calculated from the voltammogram and is found to be 3.2 eV, whereas in the PA/G composites, the band gaps are found to decrease (from 1.6 to 1.2 eV) with increasing amounts of incorporated graphite (**Table 3.7**). The incorporation of graphite resulted in a change in the electronic band structure, which manifested as new midgap state being created, and hence, a decrease in the band gap occurred.[24] Thus it can be concluded that PA/G composites possesses higher effective conjugation length compared to Pure PA.

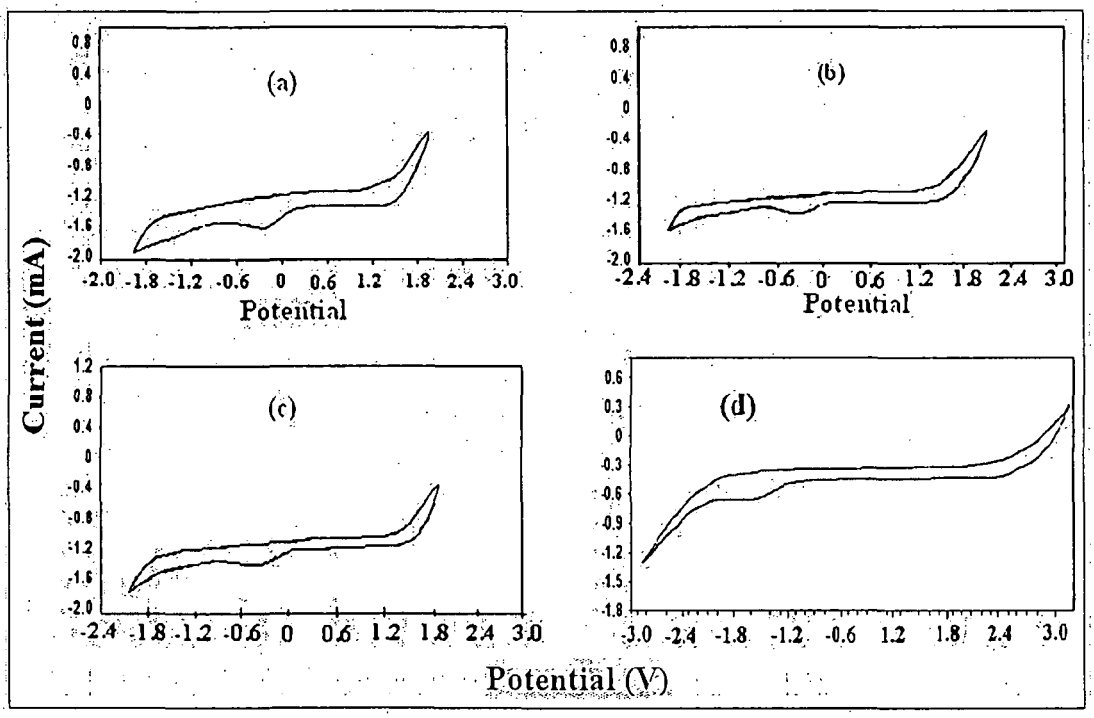

Figure 3.28 CV of (a) PA/G (0.25%), (b) PA/G (0.50%), (c) PA/G (1.0%) and (d) PA

Table 3.7 Electrochemical data of PA and PA/G composites

Sample	$\varphi^{ox}_{onset}/E_{HOMO}$	$\varphi^{red}_{onset}/E_{LUMO}$	E_g^{cc} (eV)
PA	2.10/-6.81	-1.10/-3.61	3.2
PA/G composite			
(0.25%)	1.50/-6.21	-0.10/-4.61	1.6
(0.50%)	1.45/-6.16	0.05/-4.66	1.5
(1.0%)	1.10/-5.81	-0.10/-4.61	1.2

In PA/EG composites, their CV curves are entirely different from pure PA (**Figure 3.29**). This may be due to the increased conjugation comes from the doping of intercalated EG to PA backbone and π-π stacking of PA and EG sheets. The electrochemical band gap for PA (calculated from the voltammogram) is 3.2eV which decreases to 1.24 eV for PA/EG composites (**Table 3.8**).

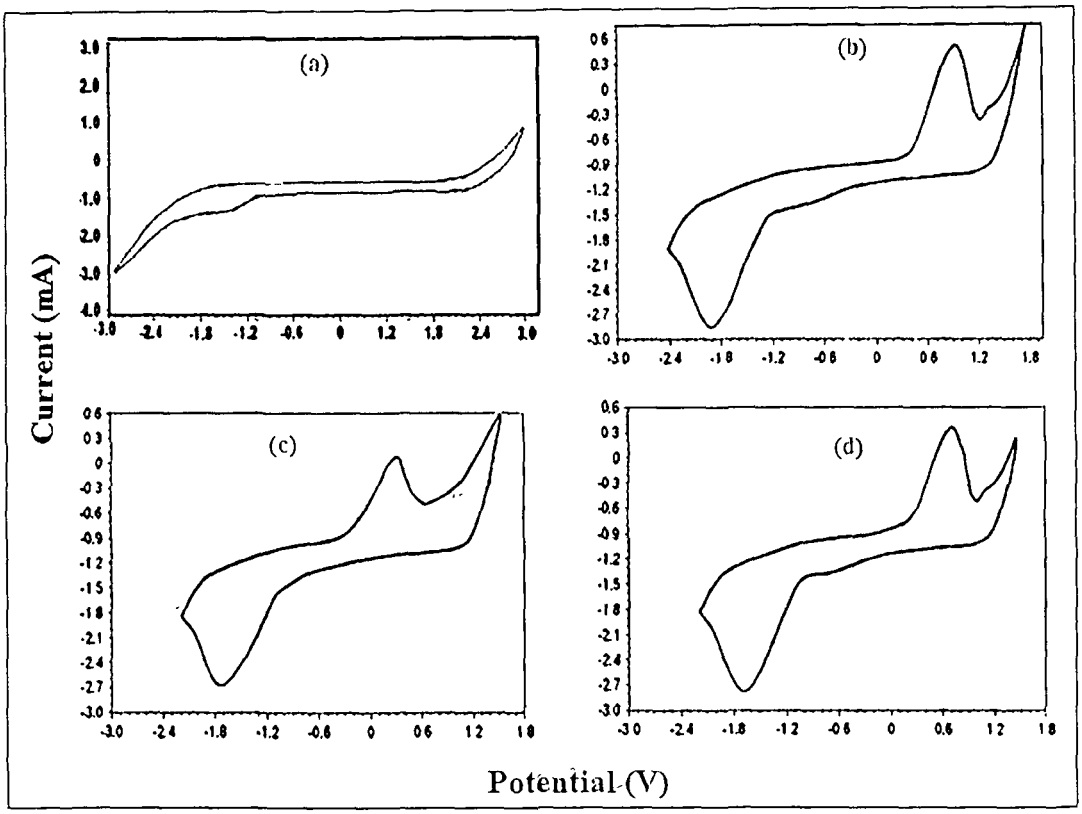

Figure 3.29 CV of (a) PA, (b) PA/EG (0.25%), (c) PA/EG (0.50%) and (d) PA/EG (1.0%) composite

Table 3.8 Electrochemical data of PA and PA/EG composite

Sample	$\varphi^{ox}_{onset}/E_{HOMO}$	$\varphi^{red}_{onset}/E_{LUMO}$	E_g^{ec} (eV)
PA	2.10/-6.81	-1.10/-3.61	3.2
PA/EG			
(0.25%)	0.33/-6 21	-1.50/-4.61	1.65
(0.50%)	0.32/-6.16	-1.38/-4.66	1.35
(1.0%)	0.22/-5.81	-1.40/-4.61	1.24

Figure 3.30 shows the cyclic votammogram of PA and PA/GO composites. The electrochemical band-gap for PA is higher (3.2 eV) than that of PA/GO composites. The band gaps are found to decrease (1.98 to 1.52 eV) in the PA/GO composites, with increasing amounts of incorporated GO (**Table 3.9**). The incorporation of GO changes the electronic band structure of PA/GO composites which manifest a new mid-gap state.

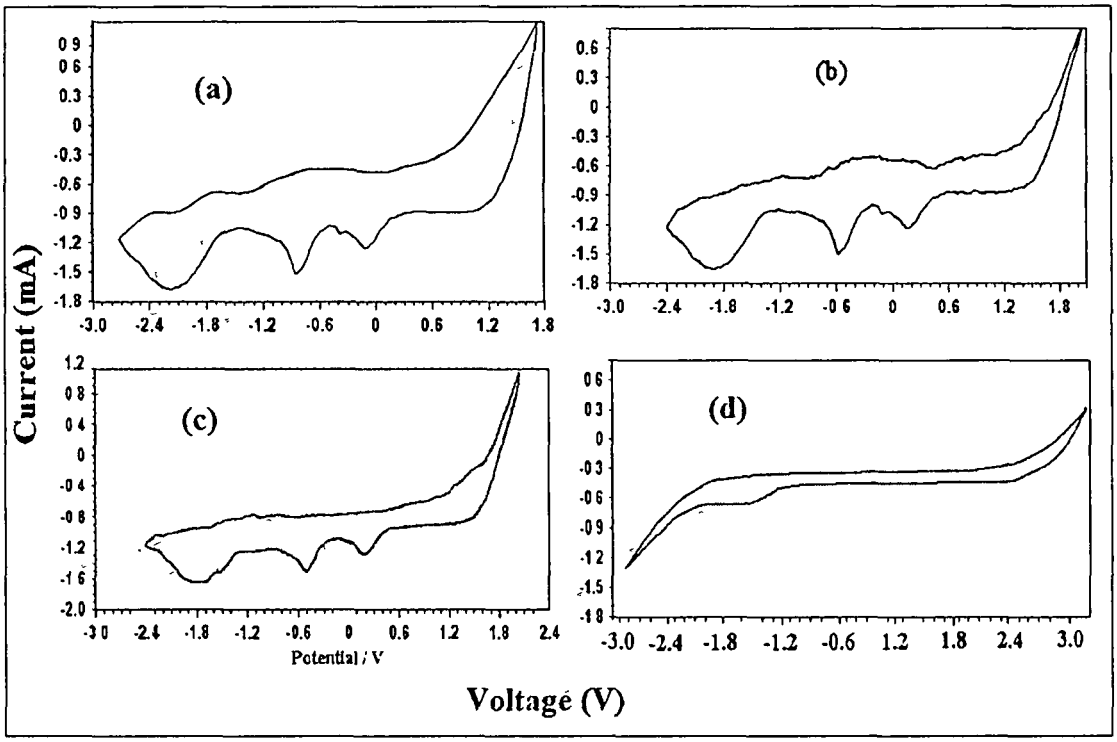

Figure 3.30 CV of (a) PA (b) PA/GO (3%) (c) PA/GO (2%) and (d) PA/GO (1%) composite.

Table3.9 Electrochemical data of PA and PA/GO composites

Sample	$\varphi^{ox}_{onset}/E_{HOMO}$	$\varphi^{red}_{onset}/E_{LUMO}$	E_g^{cc} (eV)
PA	**2.10/-6.81**	**-1.10/-3.61**	**3.2**
PA/GO			
(0.25%)	1.22/-5.93	-0.19/-4.41	1.52
(0.50%)	1.20/-5.91	-0.48/-4.23	1.68
(1.0%)	0.80/-5.51	-0.91/-3.80	1.98

In PA/G and SMA-PA/G composites, their CV curves are entirely different from pure PA (**Figure 3.31**). The electrochemical band gap for SMA-PA/G composites decreases to 1.62 eV as compared to pure PA (3.2 eV). The band gap of the composites decreases with increase in the amount of incorporate graphite into the PA matrix as shown in the **Table 3.10**. Graphite assists the polymerization in such a way that it maintains a higher conjugation length in the chain of the PA itself and π-electrons coupling in between the PA and graphite may also occurred. This increase in conjugation length of SMA-PA/G composites is also reflecting in UV-vis study where the characteristic red shift of the polymer chains is distinctly observed. This indicates the decrease in band gaps which results in the enhancement of dc electrical conductivity of the SMA-PA/G composites.

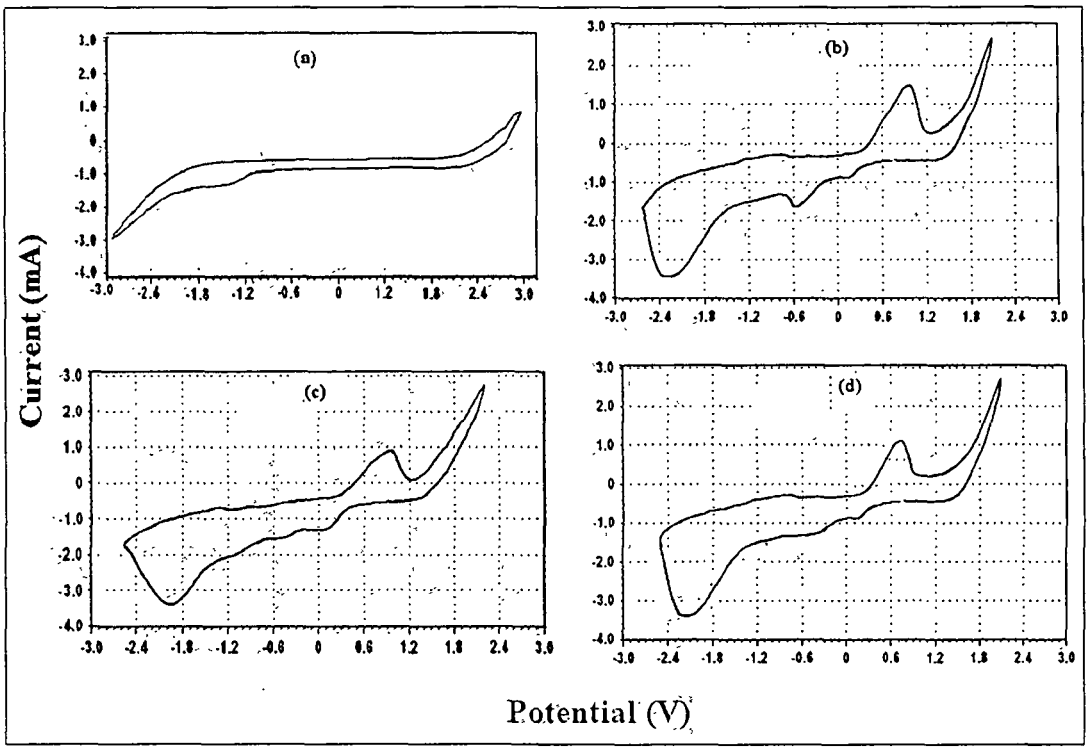

Figure 3.31 CV of (a) PA, SMA-PA/G core-shell composite having (b) 0.25% graphite, (c) 0.50% graphite and (d) 1.0% graphite

Table 3.10 Electrochemical data of PA and SMA-PA/G core-shell composites

Sample	$\Phi^{ox}_{onset}/e_{homo}$	$\Phi^{red}_{onset}/e_{lumo}$	E_g^{cc} (ev)
PA	2.10/-6.81	-1.10/-3.61	3.20
SMA-PA/G			
(0.25%)	0.33/-5.04	-1.50/-3.21	1.83
(0.50%)	0.32/-5.03	-1.38/-3.33	1.70
(1.0%)	0.22/-4.93	-1.40/-3.31	1.62

Figure 3.32 shows the CV of PPy and PPy/G composites. The electrochemical band-gap for PPy was calculated from voltammogram and found to be 2.90 eV whereas in PPy/G composites band gaps were found to be decreased (1.65 to 1.30 eV) with increasing amount of incorporated graphite (**Table 3.11**). The incorporation of graphite resulted in change in electronic band structure manifested as new mid-gap state being created and hence decreasing of band gap occurs.[24]

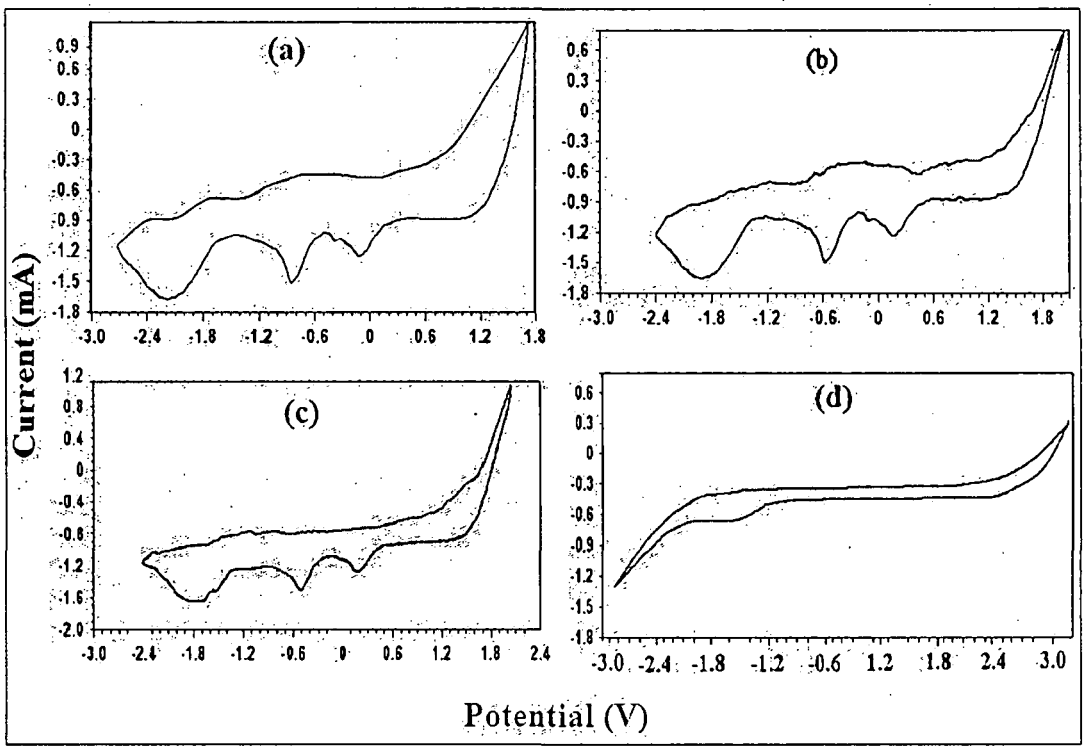

Figure 3.32 CV of (a) PPy (b) PPy/G (0.25%), (c) PPy/G (0.50%) and (d) PPy/G (1.0%) composite

Table3.11 Electrochemical data of PPy and PPy/G composites

Sample	$\varphi^{ox}_{onset}/E_{HOMO}$	$\varphi^{red}_{onset}/E_{LUMO}$	E_g^{ec} (eV)
PPy	1.50/-6.21	-1.40/-3.31	2.90
PPy/G			
(0.25%)	1.25/-5.96	-0.40/-4.31	1.65
(0.50%)	1.25/-1.96	-0.30/-4.41	1.55
(1.0%)	1.20/-5.91	-0.10/-4.61	1.30

Fig. 3.33 shows the CV of PPy and PPy/EG composites. The electrochemical band-gap for PPy is calculated from voltammogram and found to be 2.90 eV which decreases to 1.85 eV for PPy/EG composites. The band gap of the composites decreases with increase in the amount of incorporated EG into the PPy matrix (**Table 3.12**). The incorporation of EG changes the electronic band structure of PPy/EG composites which manifest a new mid-gap state.

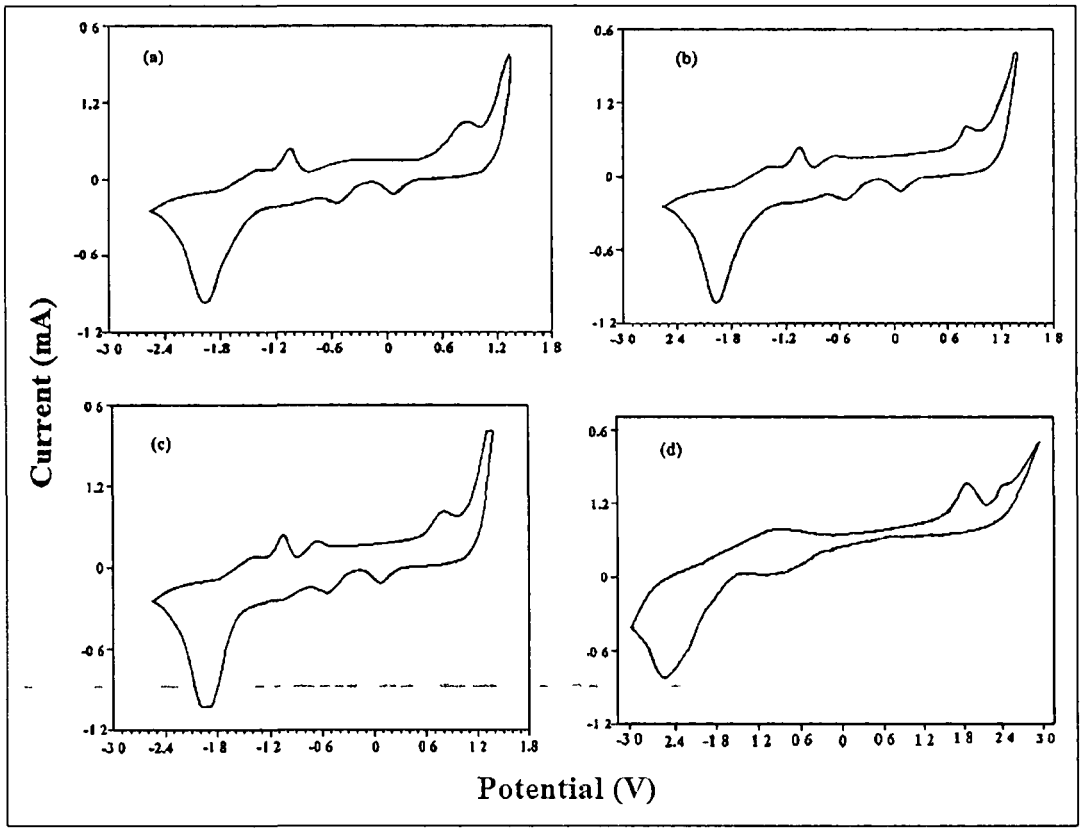

Figure 3.33 CV of (a) PPy/EG (1 0%), (b) PPy/EG (0 50%) and (c) PPy/EG (0 25%) composites and (d) PPy

Table 3.12 Electrochemical data of PPy and PPy/EG composite

Sample	$\varphi^{ox}_{onset}/E_{HOMO}$	$\varphi^{red}_{onset}/E_{LUMO}$	E_g^{ec} (eV)
PPy	1 50/-6 21	-1 40/-3 61	2 90
PPy/EG			
(0 25%)	0 58/-5 29	-1 60/-3 11	2 18
(0 50%)	0 64/-6 35	-1 40/-3 31	2 04
(1 0%)	0 50/-5 21	-1 48/-3 23	1 98

Fig. 3.34 shows the CV of PPy and PPy/GO composites The electrochemical band-gap for PPy is higher (2 9 eV) than that of PPy/GO composites The band gaps are found to decrease (2 23 to 2 02 eV) in the PPy/GO composites, with increasing amounts of incorporated GO (**Table 3.13**) The incorporation of GO changes the electronic band structure of PPy/GO composites which manifest a new mid-gap state

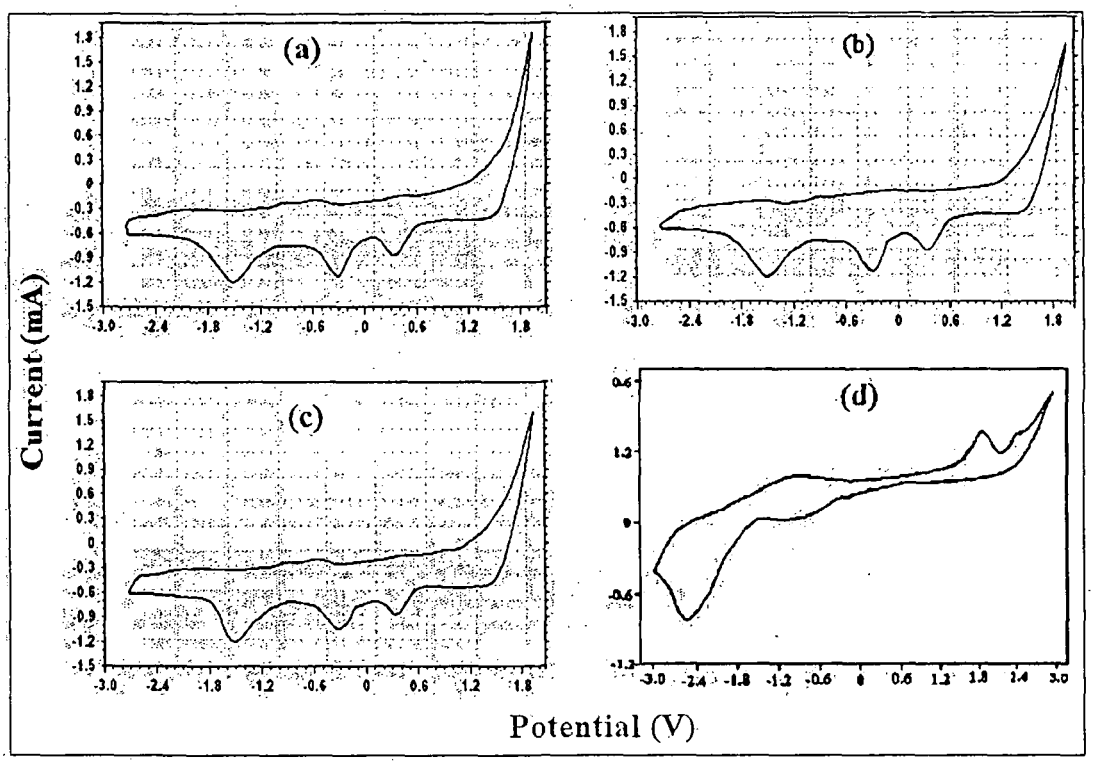

Figure 3.34 CV of (a) PPy/GO (1.0%), (b) PPy/GO (0.50%) and (c) PPy/GO (0.25%) composites and (d) PPy

Table 3.13 Electrochemical data of PPy and PPy/GO composite

Sample	$\varphi^{ox}_{onset}/E_{HOMO}$	$\varphi^{red}_{onset}/E_{LUMO}$	E_g^{cc} (eV)
PPy	1.50/-6.21	-1.40/-3.61	2.90
PPy/GO			
(0.25%)	1.22/-5.93	-1.01/-3.70	2.23
(0.50%)	1.20/-6.35	-0.98/-3.31	2.18
(1.0%)	0.50/-5.21	-0.91/-3.23	2.02

3.4.4 Comparison of band gap estimated from optical and electrochemical method

The band gap is an important parameter whose magnitude governs the intrinsic electronic and optical properties of conjugated polymers. The existence of a finite band gap in conjugated polymers is considered to originate principally from bond length alternation.

The electrochemical determination of band gap actually leads to the formation of charge carriers. On contrary, optical transitions do not reveal the formation of free charge carriers, as the excited state in conjugated polymers may be viewed as a bound exciton. At the same time, optical transitions cannot be directly compared to the

electrochemical doping process.[25] The electrochemical and optical band gap of the PA, PPy and their composites are given in **Table 3.14** and **Table 3.15.** The band gap of graphite, EG and GO containing PA and PPy composites determined by optical and electrochemical method and is found to be 1.2-1.98 eV for electrochemical method and 2.03-2.44 eV for optical method. The band gap of individual PA is found to be 3.2 eV (electrochemically) and 2.47 eV (optically). The band gap of individual PPy is found to be 2.9 eV (electrochemically) and 2.17 eV (optically). It has been found that both the method establishes the same trend of band gap.

Table 3.14 Electrochemical and optical band gap of PA and its composites

Sample	Electrochemical band gap (eV)	Optical band gap (eV)
Pure PA	3.2	2.47
PA/G composites		
0.25%	1.6	2.25
0.50%	1.5	2.10
1.0%	1.2	2.03
PA/EG composites		
(0.25%)	1.65	2.39
(0.50%)	1.35	2.37
(1.0%)	1.24	2.19
PA/GO composites		
(0.25%)	1.98	2.43
(0.50%)	1.68	2.39
(1.0%)	1.52	2.35
SMA-PA/G composites		
0.25%	1.83	2.44
0.50%	1.70	2.40
1.0 %	1.62	2.38

Table 3.15 Electrochemical and optical band gap of PPy and its composites

Sample	Electrochemical band gap (eV)	Optical band gap (eV)
Pure PPy	2.90	2.17
PPy/G composites		
0.25%	1.65	2.33
0.50%	1.55	2.27
1.0%	1.30	2.23
PPy/EG composites		
0.25%	2.18	1.93
0.50%	2.04	1.90
1.0%	1.98	1.85
PPy/GO composites		
0.25%	2.23	2.08
0.50%	2.19	2.06
1.0%	2.02	2.02

3.4.5 Charge capacity or Redox stability of polymers

CV provides information regarding the stability of the product during multiple redox cycles. ITO coated polymers were exposed to cyclic oxidation and reduction upto 150th cycles **Figure 3.35-3.41**. The charge capacity of the polymer composite did not get diminished even after the repeated cycles. This property emphasizes that these synthesized carbon filled π-conjugated PA and PPy composites may be useful and prominent material to be used in various optoelectronic devises.

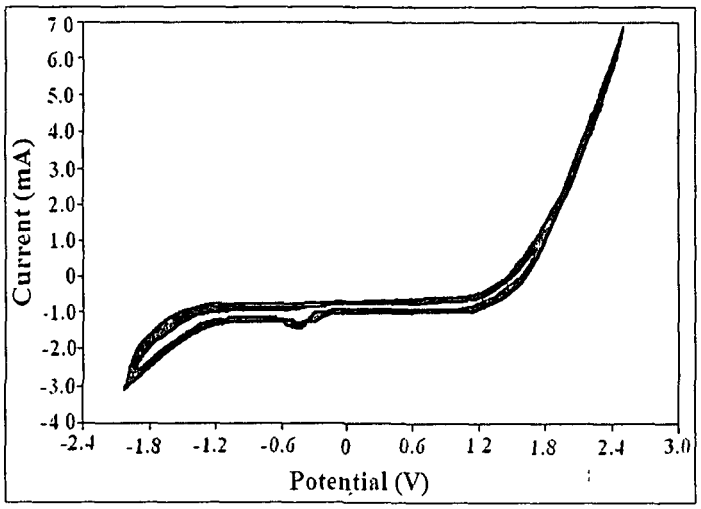

Figure 3.35 CV of PA/G composite up to the 50th cycle

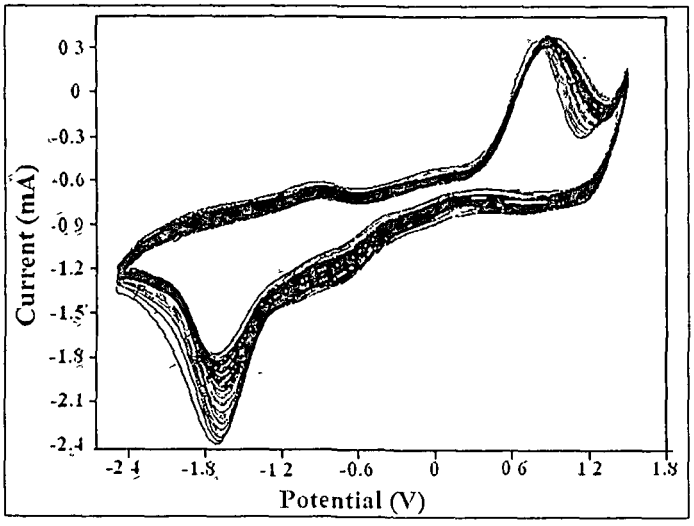

Figure 3.36 CV of PA/EG composite up to the 100th cycle

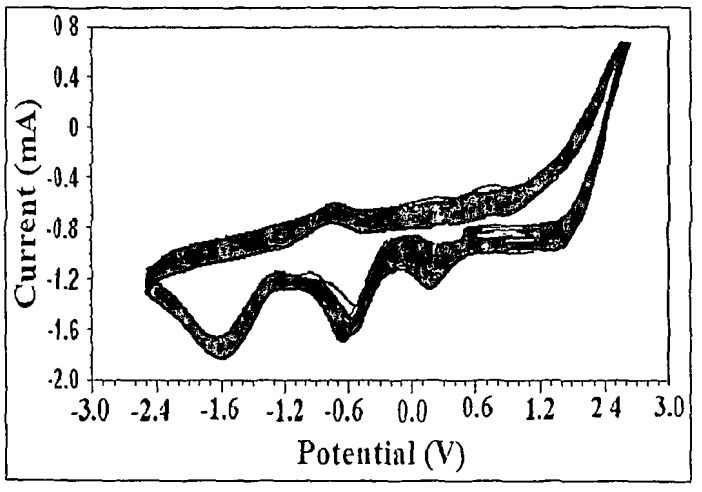

Figure 3.37 CV of PA/GO composite upto the 150th cycle

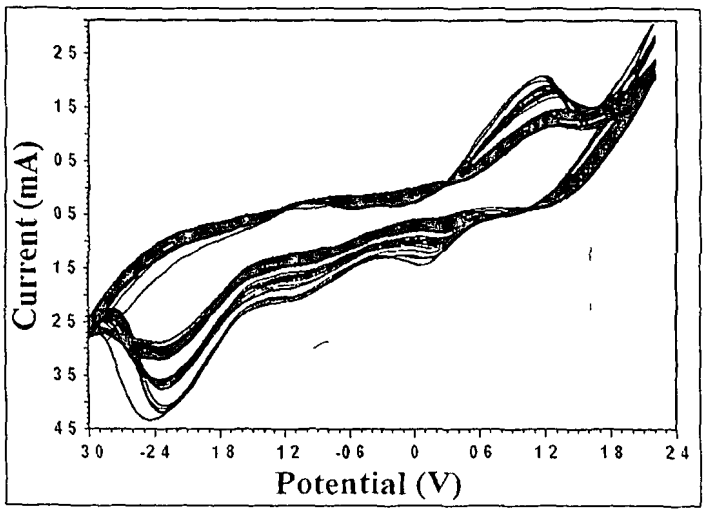

Figure 3.38 CV of SMA-PA/G composite up to the 100th cycle

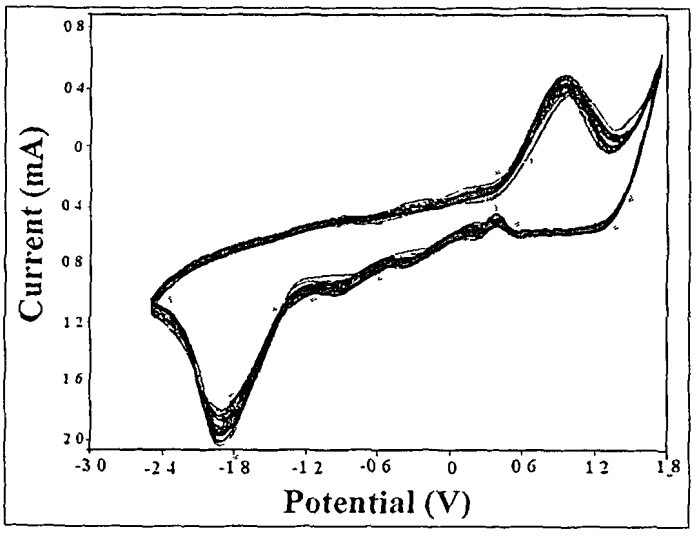

Figure 3.39 CV of PPy/G composite up to the 50th cycle

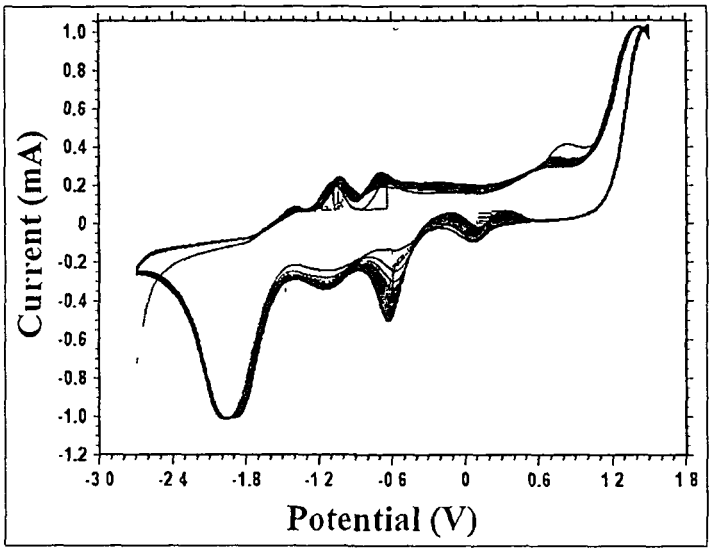

Figure 3.40 CV of PPy/EG composite up to the 125th cycle

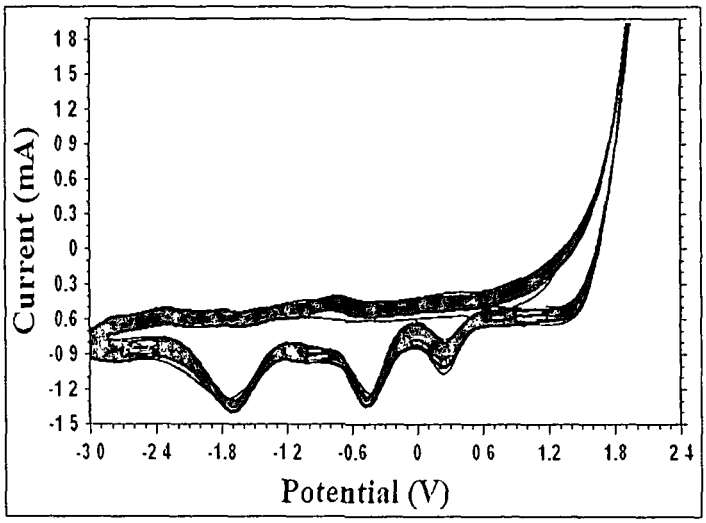

Figure 3.41 CV of PPy/GO composite up to the 100th cycle

3.5 Conclusions

The important conclusions drawn from the above study are compiled below:

- The UV-vis spectrum of PA shows an intense absorption peak at 305 nm, a weak peak at 356 nm, and a broad peak at 580 nm. Whereas the PPy shows a weaker absorption at around 330 nm and stronger absorption at around 570 nm. For both the polymer first bands are related to the molecular conjugation (π - π^* transition) while the final absorption peak assigned to the polaron state of polymer i e. charged cationic species.

- All the carbon filled PA and PPy composites show red shift of UV-visible absorption maximum with respect to their pristine polymers. The carbon filler assists the polymerization in such a way that it maintains a higher conjugation length in the chain of the polymer itself. The incorporated carbon filler interacts with the backbone of the polymer matrices resulted in the red shift of the band.
- Optical band gaps calculated from onset of absorption spectra are in the range of 3.2–1.89 eV for PA composites and 2.90 - 2.02 eV for PPy composites on addition of carbon fillers.
- The I-V characteristics of PA, PPy and carbon filled polymer composites are asymmetric and nonlinear for forward direction of applied voltage suggesting the semiconducting behaviour and Schottky barrier in the polymer and polymer composites.
- The conductivity of the carbon filled PA and PPy composites is found to be dramatically increased in comparison to the bare polymer depending on the content of the carbon fillers. The maximum conductivity of PA and PPy composites are found to be 4 x 10^2 S/cm and 1.11 x 10^2 S/cm respectively on addition of 1% EG at 140 °C.
- Electrochemical properties of the synthesized polymer composites are studied with cyclic voltammogram. HOMO and LUMO energy levels are calculated approximately from the onset oxidation and reduction potential. The difference of these levels gives band gap of the polymers.
- The electrochemical band gap for PA, PA/G, PA/EG and PA/GO composite with 1% content of carbon filler is found to be 3.2 eV, 1.2 eV, 1.65 eV and 1.62 eV respectively. The electrochemical band-gap for PPy, PPy/G, PPy/EG and PPy/GO is found to be 2.90 eV. 1.3 eV, 1.98 eV and 2.02 eV respectively. It has been found that the band gap of the polymer composites decreases with increasing amounts of incorporated carbon fillers.
- The optical and electrochemical band-gaps of polymer composites are found to be different. However both the method establishes the same trend of band gap.
- All the prepared PA and PPy composites show gratifying reversible electrochemical response. The electrochemical behaviour of the polymer composite did not get diminished upto 150^{th} repeated cycles for EG and GO filled PA composites.

References

1. Tsai, F.C.; Chang, C. C.; Liu, C. L.; Chen, W. C.; JenekheTsai, S. A. New thiophene-linked conjugated poly(azomethine)s: Theoretical electronic structure, synthesis, and properties, *Macromolecules* **38**, 1958-1966 (2005)
2. Cao, Y.; Smith, P.; Heeger, A. J. Spectroscopic studies of polyaniline in solution and in spin-cast films, *Synth. Met.* **32,** 263-281 (1989)
3. Dey, A.; De, S.; De, A.; De, S. K. Characterization and dielectric properties of polyaniline-TiO_2 nanocomposites, *Nanotechnol.* **15,** 1277-1283 (2004)
4. Leeuw, D. M.; Simenon, M. M. J.; Brown, A. R.; Einerhand, R. E. F. Stability of n-type doped conducting polymers and consequences for polymeric microelectronic devices, *Synth. Met.* **87,** 53-59 (1997)
5. Leeuw, D. M.; Simenon, M. J.; Brown, A. R.; Einerhand, R. E. F. Stability of n-type doped conducting polymers and consequences for polymeric microelectronic devices, *Synth. Met.* **87,** 53-59 (1997)
6. Kažukauskas, V. *et al.* Conductivity, charge carrier mobility and ageing of ZnPc/C_{60} solar cells, *Opt. Mater.* **32,** 2010, 1676-1680
7. Johansson, T.; Mammo, W.; Seensson, M.; Andersson, M.A.; Inganas, O. Electrochemical bandgaps of substituted polythiophenes, *J. Mater. Chem.* **13,** 1316-1323 (2003)
8. Wenge, Z.; Chung, W. S. Electrical conductivity and dielectric properties of PMMA/expanded graphite composites, *Compos. Sci. Tech.* **63**, 225-235 (2003)
9. Gomez-Navarro, C. *et al.* Electronic transport properties of individual chemically reduced graphene oxide sheets, *Nano Lett.* **7,** 3499-3503 (2007)
10. Liu, J.; Wan, M. Synthesis, characterization and electrical properties of microtubules of polypyrrole synthesized by a template-free method, *J. Mater. Chem.* **11,** 404-407 (2001)
11. Leeuw, D. M.; Simenon, M. M. J.; Brown, A. R.; Einerhand, R. E. F. Stability of n-type doped conducting polymers and consequences for polymeric microelectronic devices, *Synth. Met.* **87,** 53-59 (1997)
12. Yuan, L. *et al.* Synthesis and characterization of SnO_2- polypyrrole composite for lithium-ion battery, *J. Power Sources* **174,** 1183-1187 (2007)
13. Liu, J.; Wan, M. Synthesis, characterization and electrical properties of microtubules of polypyrrole synthesized by a template-free method, *J. Mater. Chem.* **11,** 404-407 (2001)

14. Wu, J.; Pisula, W.; Mullen, K. Graphene as potential material for electronics, *Chem. Rev.* **107,** 718-747 (2007)

15. Yang, C. M. *et al.* Nanowindow-regulated specific capacitance of supercapacitor electrodes of singlewall carbon nanohorns, *J. Am. Chem. Soc.* **129,** 20-21 (2007)

16. Johansson, T.; Mammo, W.; Svensson, M.; Andersson, M. R.; Inganas, O. Electrochemical bandgaps of substituted polythiophenes, *J. Mater. Chem.* **13,** 1316-1323 (2003)

17. Zhou, E.; He, C.; Tan, Z.; Yang, C.; Li, Y. Effect of side-chain end groups on the optical, electrochemical, and photovoltaic properties of side chain conjugated polythiophenes, *J. Polym. Sci.: PartA: Polym. Chem.* **44,** 4916-4922 (2006)

18. Koyuncu, S.; Kaya, I.; Koyuncu, F.B.; Ozdemir, E. Electrochemical, optical and electrochromic properties of imine polymers containing thiophene and carbazole units, *Synth. Met.* **159,** 1034-1042 (2009)

19. Skompska, M.; Szkurlat, A. The influence of the structural defects and microscopic aggregation of poly(3-alkylthiophenes) on electrochemical and optical properties of the polymer films: discussion of an origin of redox peaks in the cyclic voltammograms, *Electrochim. Acta.* **46,** 4007-4015 (2001)

20. Hillman, A. R.; Efimov, I.; Skompska, M. Dynamics of regioregular conducting polymer electrodes in response to electrochemical stimuli, *Faraday Discuss.* **121,** 423-439 (2002)

21. Pokhrel, B.; Dolui, S. K. Synthesis and characterization of 1,1-bis-2-naphthol chromophore containing polyurethanes and study of their electrochemical and photoluminescence proeprties, *J. Polym. Mater.* **26,** 417-426 (2009)

22. Sun, Q.; Wang, H.; Yang, C.; Li, Y. Synthesis and electroluminescence of novel copolymers containing crown ether spacers. *J. Mater. Chem.***13,** 800-806 (2003)

23. Pommerehne, J.*et al.* Efficient two layer LEDs on a polymer blend basis, *Adv. Mater.* **7,** 551-554 (1995)

24. Skotheim, T. A.; Elsenbaumer, R. L.; Reynolds, J. R. Hand book of conducting polymer, (Marcel Dekker Inc. 1998)

25. Johansson, T.; Mammo, W.; Svensson, M.; Andersson, M. R.; Inganas, O. Electrochemical band gaps of substituted polythiophenes, *J. Mater. Chem.* **13,** 1316-1323 (2003)

Chapter 4

Sensors application and capacitance behaviour of carbon filled π-conjugated polymers

4.1 Introduction

Conducting polymer composites formed by the combination of carbon fillers and π-conjugated polymers are attractive for the purpose of creating high–performance or high–functional polymeric materials. In recent years, attention has been given to the potential application of π-conjugated polymer composites in different filled like sensors, supercapacitors, photovoltaic cell etc. by various groups worldwide. In this chapter we investigated the application of synthesized carbon filled π-conjugated polymer composites as sensor and supercapacitor. Polyaniline/graphene oxide (PA/GO) composite has been applied as methanol gas sensing materials. The sensing properties of expanded graphite (EG) filled polyaniline (PA/EG) composites for volatile organic compounds (VOCs) viz. acetone, chloroform and carbon tetrachloride have also been described in this chapter. The study of capacitance behaviour of synthesized polyaniline/graphene oxide (PA/GO) and PA/EG composite electrodes have also been reported in this chapter.

4.2 Materials

Aniline and pyrrole was obtained from Aldrich Co. and used without further purification. Lithium perchlorate ($LiClO_4$) was obtained from Fluka and used as received. The natural graphite flake of size (crystalline, 300 mesh, Alfa Aesar) from Shanker Graphites and Chemical, New Delhi, India, hydrochloric acid (HCl), sulphuric acid (H_2SO_4), nitric acid (HNO_3), sodium nitrate ($NaNO_3$), potassium permanganate ($KMnO_4$), hydrogen peroxide (H_2O_2) and potassium persulphate ($K_2S_2O_8$) were of analytical reagent grade chemicals (Merck) and used as received. Acetonitrile (CH_3CN) and methanol (CH_3OH) was obtained from Merck and purified by standard methods. For all purposes double distilled water was used.

4.3 Experimental

Fourier transform infrared spectroscopy (FTIR) was used to record FTIR spectra by Impact 410, Nicolet, USA, using KBr pellets. The ultraviolet-visible (UV-vis) absorption spectroscopy of the samples in 1-Methyl-2-pyrrolidon solvent was recorded using Shimadzu UV-2550 UV-vis spectrophotometer in the range of 300 nm - 800 nm. Current – voltage (I–V) characteristics of prepared samples were recorded by Keithley 2400 source meter at the room temperature at the scan rate 0.1V/s.

The density functional study have been carried out using B3LYP/6-31+G* level of theory.[1-3] This is a hybrid of Hartree-Fock and density functional theory (DFT) based on Generalized Gradient Approximation (GGA). The advantage of using GGA is that it will not lead to strong bonding of the molecules as in Local Density Approximation. Hence, if GGA shows any bonding, it is confirmed that they will bind in the real system. The DFT calculation was performed using Gaussian 03 suite of program[4] to determine the interaction between the bare polymer and the methanol vapour.

4.4 Carbon Filled π-Conjugated Polymer as gas sensor

In recent years, attention has been given to the potential application of conjugated polymers like polyaniline (PA), polypyrrole (PPy), etc. in chemical and biological sensors due to its high yield in redox process, gas sensing ability, optimum performance at room temperature, response to a wide range of volatile VOCs environmental stability etc.[5-8] The detection of polluted gases, mainly toxic gases are important to get clean the environment. Due to the ability of PA to undergo physiabsorb or chemisorb with the various VOCs and undergo swelling or redox reactions results in change in the resistance. Therefore conducting PA has been used as a sensing material for different gases where the effect of these gases on the electronic properties of these gases has been investigated.[9-11] There have been a great number of reports on the application of PA and its composites in the detection of a wide spectrum of chemical substances including $CHCl_3$, NH_3, CO_2, hydrazine, vapours of common organic solvents, etc. by taking advantage of the variation of its electrical or optical properties on interaction with these chemical substances.[4, 12-25] The PA-based sensors exhibited good sensing properties such as ultrahigh sensitivity, fast response, satisfying reversibility etc.

Recently, modified carbon fillers like expanded graphite (EG) and graphene oxide (GO) have attracted a great interest. The combination of the high surface area (theoretical value of upto 2630 m^2/g,[26] high conductivity, unique graphitized basal plane structure and potential low manufacturing cost makes these fillers a promising candidate for various application in sensors, supercapacitor electrodes etc.[27-34] In addition, the tunable oxygenous functional groups of GO facilitate the modification on the surface[35] and make it a promising material for composites with other materials.

In this part, we investigated the methanol sensing behaviour of the PA/GO composite which is achieved by exposing to methanol, ethanol and propanol vapours. We have also reported the sensing properties of EG based PA composite materials on exposure to oxidising and reducing vapours like acetone, chloroform and carbon tetrachloride which are significant as pollutant and toxic. We have prepared the PA/GO and PA/EG composite by the incorporation of GO and EG into PA respectively through the in-situ polymerization of aniline. The sensitivity of the composite materials has been explained on the basis of the change in resistivity on exposure to various volatile organic vapours.

4.4.1 Sensor Testing Measurements Set-Up

The sensing properties of polymer composites were studied using a gas - sensor set - up as shown in **Fig. 4.1**. The polymer composite pellet was placed in an oven for 24 h at 80 °C to remove excess solvent present in the composite material. The pellet was placed into the glass chamber and the contact between the sensor (as pellets) and the two probes was made with the help of silver paste. The change in resistance was measured using a two probe Keithley 2400 source meter with labtracer software at room temperature at the scan rate 0.1 V/s. Hexane was used as a diluent to obtain different concentration of the alcohol vapours. The distance between sensing material and solvent was kept 3 cm at the time of exposure of different concentration of methanol on the sensing material. The sensing ability of the composite was investigated by recording the electrical responses when exposed alternately to different concentration of alcohol vapour at room temperature and withdrawing the sensor from the analyte molecule to recover the sensor.

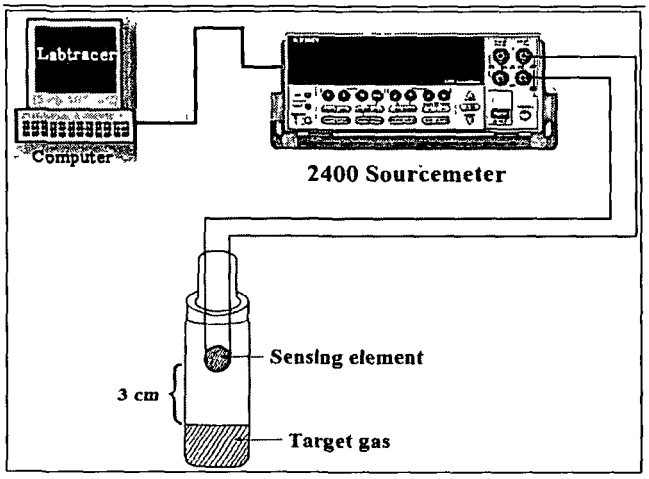

Figure 4.1 Gas sensor set – up

4.4.2 Application of Polyaniline/Graphene Oxide Composite as Methanol Sensor

To carry out the sensing ability of the pure PA and PA/GO composite, we have studied the changes in the electrical response of the pure PA and composite material on exposing to different concentrations of methanol vapours. The electrical response is expressed in terms of sensitivity, $\Delta R/R_0$. Here the sensitivity is defined as

$$\Delta R/Ro = R - R_0/Ro \qquad (4.1)$$

Where, R_0 and R are the initial resistance of sensor in air and in target gas, respectively.

Figure 4.2 depicts the sensitivity ($\Delta R/R_0$), obtained from the pure PA and the PA/GO composite exposed to different concentrations of methanol vapours in the concentration of 100 – 500 ppm. PA is a p-type semiconductor, the exposure to electron-donating gases, such as methanol vapours, will cause an increase in the resistance.[36] When pure PA is exposed to methanol vapour for 2.5 min, it shows a change in the $\Delta R/Ro$ value from 0.03 to 0.35 and on removal of methanol vapour the $\Delta R/R_0$ value decreased to 0.17 i.e., the $\Delta R/R_0$ does not revert to initial state on removal of the analyte methanol. Similarly the changes in $\Delta R/Ro$ values for subsequent cycles are gradually increasing and after each cycle, the base line of $\Delta R/Ro$ *vs.* time curve does not get back to the initial state. This gradual shift indicates the irreversible sensing character of the pure PA. In addition it is found that the recovery time is more than that of response time (**Figure 4.2a**). This may be due to the physical absorption as well as the H-bonding in between methanol vapours and the benzenoid and quinoid moiety of PA backbone. We have carried out DFT study to confirm this assertion of H - bonding with the amine and imine nitrogen of benzenoid and quinoid moieties of the polymer chain and methanol. The sensitivity ($\Delta R/R_0$) of pure PA to methanol is found in the range of 0.35 - 1.47 within 2 - 15 minutes on exposure to methanol vapour.

In PA/GO composite it is observed that the sensing property is better and reproducible than pure PA (**Figure 4.2b-4.2e**). When PA/GO is exposed to the methanol the sensitivity ($\Delta R/R_0$) increased with very short time period (3-120 sec) and on removal of the methanol vapours it get back to its original state with slight deviation indicates the better reversible character. Here the recovery time to release methanol from PA/GO composites is almost same with the response time. This may be due to the physical as well as chemical interaction of the PA, GO and methanol vapours.

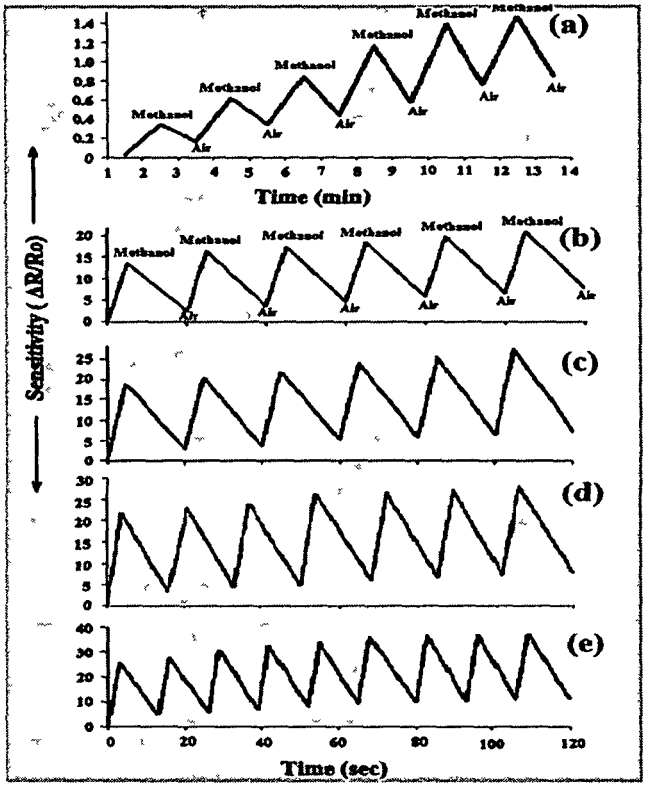

Figure 4.2 Response curves of (a) pure PA and PA/GO exposed to saturated vapours of methanol at different concentrations (b) 100 (c) 200 (d) 300 and (e) 500 ppm

When PA/GO composite is exposed to methanol, strong H-bonding takes place between the methanol vapour with the bare polymer and GO, thereby disrupting the extended H-bonding between GO and PA back bond (**Scheme 4.1**). This results in the enhancement of resistivity. After the removal of methanol vapours, possibly reformation of the extended H-bonding between GO and PA is taking place and restore the original H-bonded PA/GO composite. Thus presence of GO imparts rapid response and reversible character of the sensor. These results are further supported by the FTIR study. In PA/GO composite the sensitivity increases with increase the gas concentration and maximum sensitivity $\Delta R/R_0$ are shown upto 37 for 500 ppm methanol.

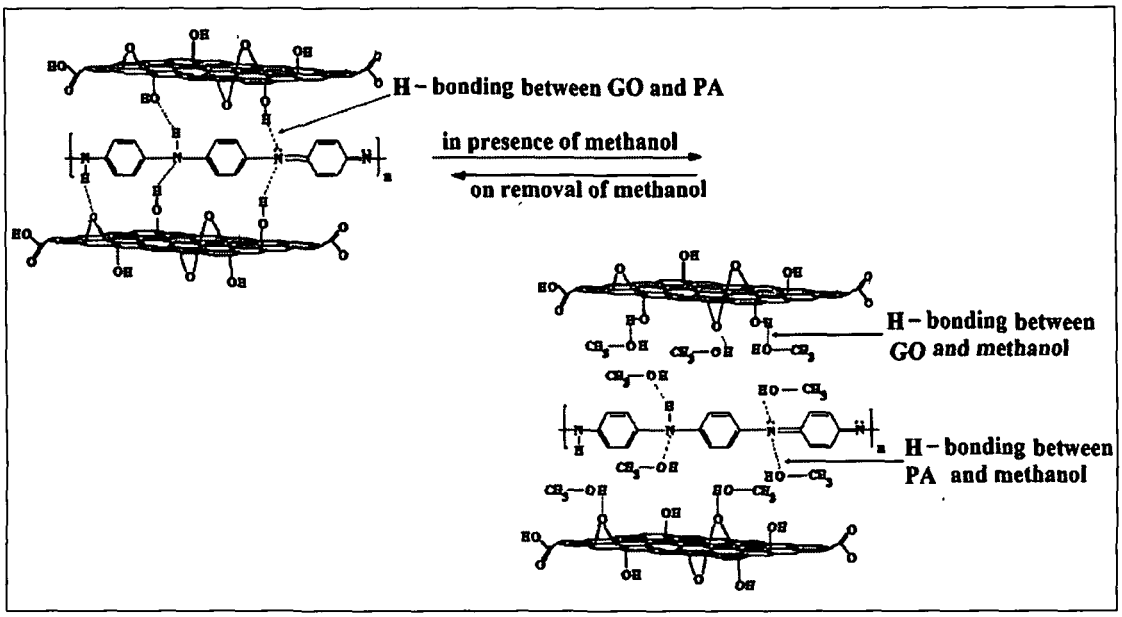

Scheme 4.1 Schematic representation depicting interaction of methanol vapours with PA/GO composite

The responses of PA/GO sensor pellet for the ethanol and propanol are also investigated and shown in **Figure 4.3**. The sensitivities ($\Delta R/R_0$ = 3.77 and 3.1) are less towards ethanol and propanol vapours due to the low polarity nature of these two alcohols compared to the methanol. On the other hand, the response and recovery time for both ethanol and propanol is also increased, this is because the methanol is more polar and small in size than ethanol and propanol; hence it would interact more efficiently than the other two alcohols.

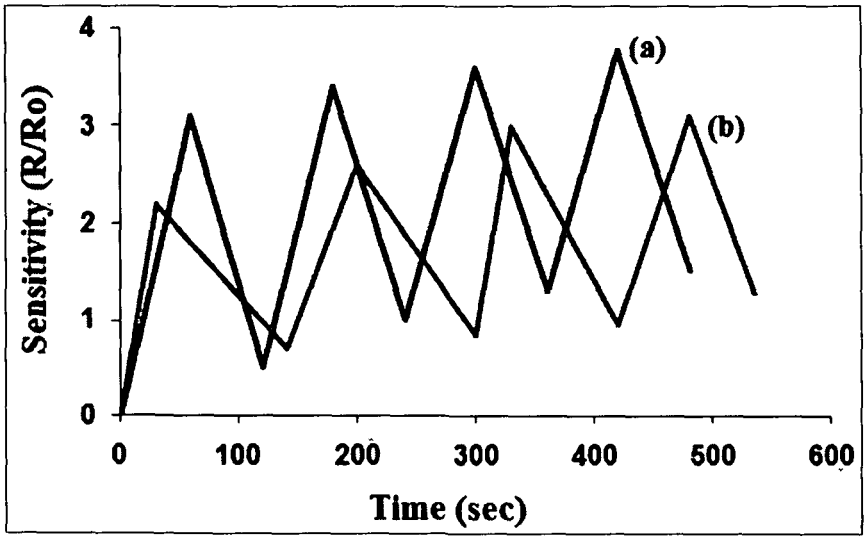

Figure 4.3 Response curves of PA/GO composite exposed to saturated vapours of (a) ethanol and (b) propanol

The selectivity of PA/GO composite with respect to these three alcohols are as Methanol >> ethanol > propanol as shown in the **Figure 4.4**.

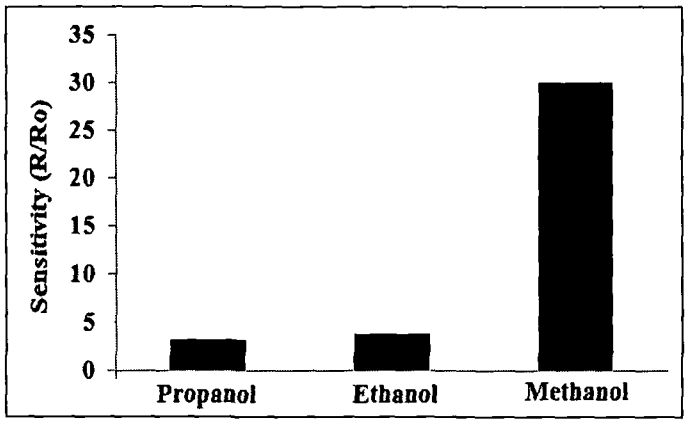

Figure 4.4 Selectivity of PA/GO composite

From the DFT study the binding or the complexation energy between methanol and PA is found to be 3.5 kcal/mol. The optimized geometry of the molecule shows that the distance of the -OH hydrogen of the methanol molecule from the imine nitrogen atom of the quinoid moieties is 2.009Å and the distance of the amine hydrogen atom of benzenoid moieties and the oxygen atom of methanol molecule is 1.976 Å **(Figure 4.5)**, thus confirming the presence of H - bonding between the polymer chain and methanol vapour. This hydrogen bonding shifts the –NH stretching frequencies of benzenoid and quinoid ring of the polymer as is evident from FTIR analysis. Further, the presence of methanol vapour in a close proximity to the polymer twists the PA away from planarity as evident in the optimized geometry which is responsible for the increase in resistivity.

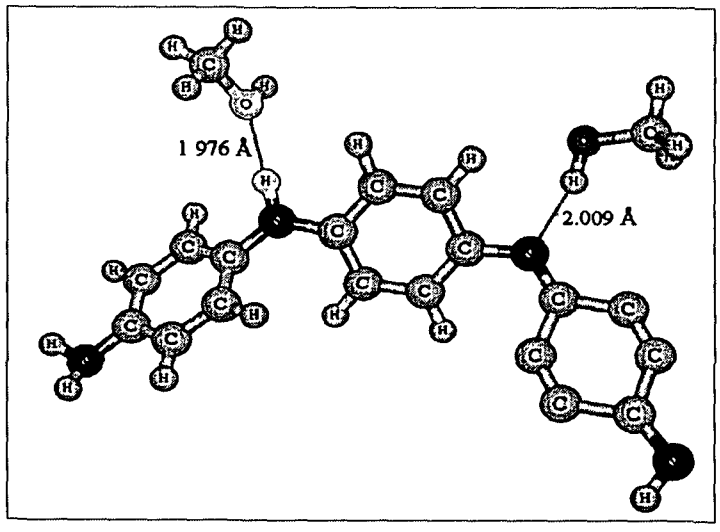

Figure 4.5 DFT optimized geometry of the bare polymer and methanol showing the possibility of H-bonding

The comparison of the sensitivity of PA/GO composite sensor and pure PA sensor is shown in **Figure 4.6 and Figure 4.7.** The PA/GO composite sensors pellet shows the sensitivity limit with methanol vapour concentration upto 500 ppm and thereafter the sensitivity became saturated. The PA/GO composite sensor shows higher sensitivity ($\Delta R/R_0$ = 13.6 - 37) in all range of vapour concentrations than that of pure PA ($\Delta R/R_0$ = 0.35 - 1.47). This may be due to the large specific surface area of GO-sheet present in the PA/GO composite where the maximum surface absorption can be possible.

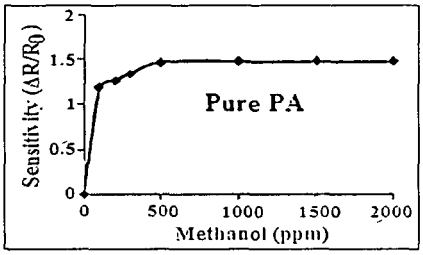

Figure 4.6 Actual response curves of pure PA various concentrations of methanol

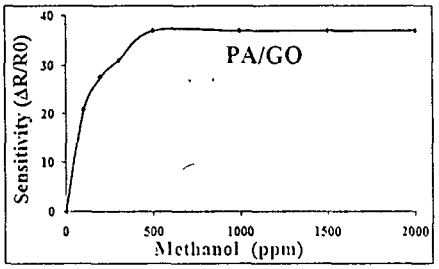

Figure 4.7 Actual response curves of PA/GO with various concentrations of methanol

The FTIR spectra of GO, PA, unexposed PA/GO and methanol exposed PA/GO is shown in **Figure. 4.8**. For the PA powder sample, the absorption peak at 3430 cm^{-1} is attributed to the N–H stretching vibrations of the leucoemeraldine component.[37] The weak peak at 2924 cm^{-1} corresponds to aromatic sp^2 CH stretching. The absorption peaks located at 1631 cm^{-1} and 1461 cm^{-1} are respectively ascribed to the C=C stretching deformation of the quinoid ring in the emeraldine salt and benzenoid rings leucoemeraldine.[38] The peaks at 1283 and 1152 cm^{-1} correspond to C–N stretching of the secondary aromatic amine and C=N stretching, respectively.[39] For the GO, the characteristic vibrations include the broad and intense O-H peak at 3434 cm^{-1}, strong C=O peak in carboxylic acid and carbonyl moieties at 1730 cm^{-1}, C-OH peak at 1406 cm^{-1}, C-O-C peak at 1222 cm^{-1}, C-O stretching peak at 1077 cm^{-1}. By comparison, the spectrum of the GO/PA composites, the absorption peaks are similar to PA except that the characteristic peak of C=O group at 1728 cm^{-1} was observed from PA/GO

composite. The absorption peaks at ~1640 and 1450 cm^{-1} represent the quinoid and benzenoid structures of the PA in unexposed PA/GO composite. A comparison of the FTIR spectra of the methanol exposed PA/GO composite reveals that the benzenoid and quinoid peak is shifted from 1450 to 1439 cm^{-1} and 1640 to 1590 cm^{-1} respectively. This can be attributed to the interaction (probably H-bonding) in between the methanol and benzenoid and quinoid nitrogens of the polymer chain, thereby causing the reducing effect. The presence of PA characteristic vibrations, indicates that PA is successfully deposited on the GO surface.

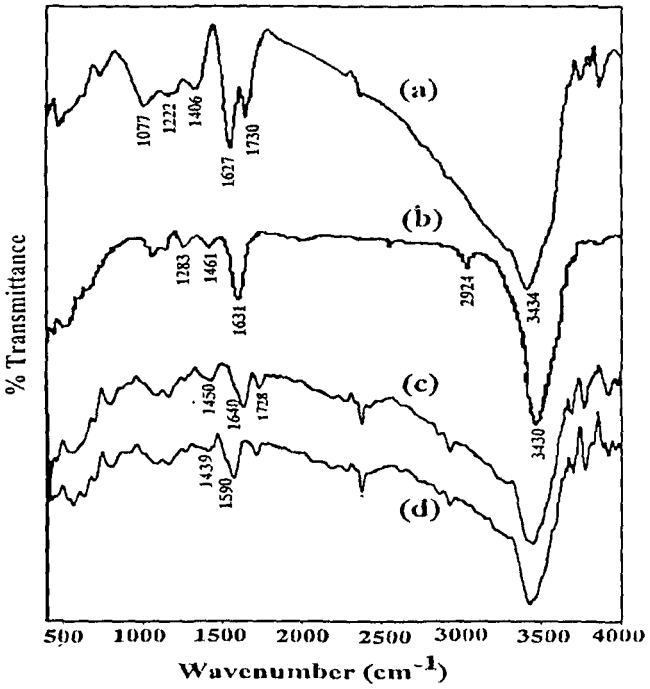

Figure.4.8 FTIR spectra of (a) GO, (b) PA, (c) PA/GO in air and (d) PA/GO with methanol

4.4.3 Sensing Properties of Expanded Graphite Filled Polyaniline Composite for Volatile Organic Compounds

The PA and PA/EG composites are exposed from 0 ppm to 500 ppm of VOCs viz., acetone, carbon tetrachloride and chloroform to study the performance of sensing behaviour of the composites.

Figure 4.9 shows the dynamic responses of pure PA sensor and PA/EG composite sensor upon exposure to acetone gas in the range of 0–500 ppm. PA is a p-type semiconductor, the exposure to electron-donating gases, such as acetone vapours,

will cause an increase in the resistance. The sensitivity ($\Delta R/R_0$) of PA sensor on 2 min exposure to acetone was 0.45 and on removal of acetone vapour the $\Delta R/R_0$ value decreased to 0.09 after 3.5 min. The ΔR/Ro values are gradually increasing with exposure time and after 10 min exposure of acetone the sensitivity was found to 2.5 (**Figure 4.9 a**). In PA, the recovery time is more than that of response time. This may be due the H-bonding between the acetone via oxygen and the N–H site of benzenoid moieties of the PA chain (**Scheme 4.2**).

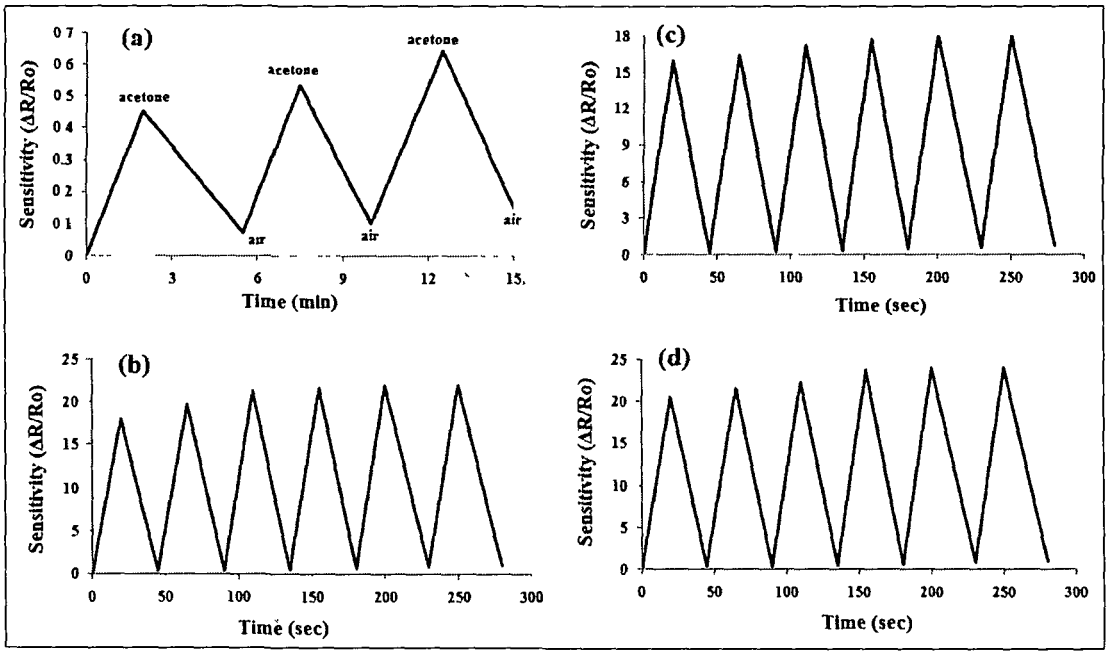

Figure 4.9 Response curves of (a) pure PA and PA/EG exposed to saturated vapours of acetone at different concentrations (b) 100 ppm (c) 200 ppm and (d) 300 ppm

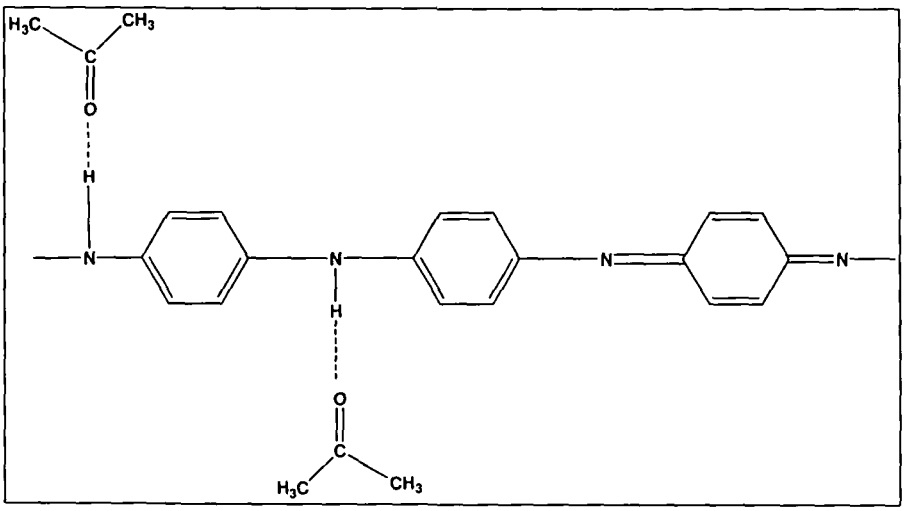

Scheme 4.2 *Schematic representation of the proposed hydrogen bonding interaction between acetone vapour and PA*

In PA/EG composite, the sensor response towards acetone is fast and the sensitivity is higher than pure PA (**Figure. 4.9**). On expose to 100 ppm acetone for 20 sec the sensitivity initially increased to 16 and on removal it again returned back to initial state with slight deviation (ΔR/Ro = 0.15) indicating the better reversible character. The *ΔR/Ro* values are gradually increasing with exposure time and maximum sensitivity is found to 18 after 200 sec. The response magnitude of PA towards the concentration of acetone shows a gradual increase in sensitivity and we have studied up to 300 ppm and it reaches maximum *ΔR/Ro* values upto 32. Here the recovery and release time for PA/EG composites is almost same and very fast compared to pure PA. From this, it is concluded that, there is an increase in the sensitivity towards acetone on exposure to EG into the PA matrix.

Figure 4.10 (a) depicts the sensor response of PA towards chloroform vapour. When chloroform is introduced, the sensitivity (ΔR/Ro) of PA is found to be 1.74 on 2 min exposure and after removal of chloroform the ΔR/Ro value decrease to 0.11 after 3.5 min. The ΔR/Ro values are gradually increased with time and maximum sensitivity is found to 4.2 after 12 min exposure to chloroform.

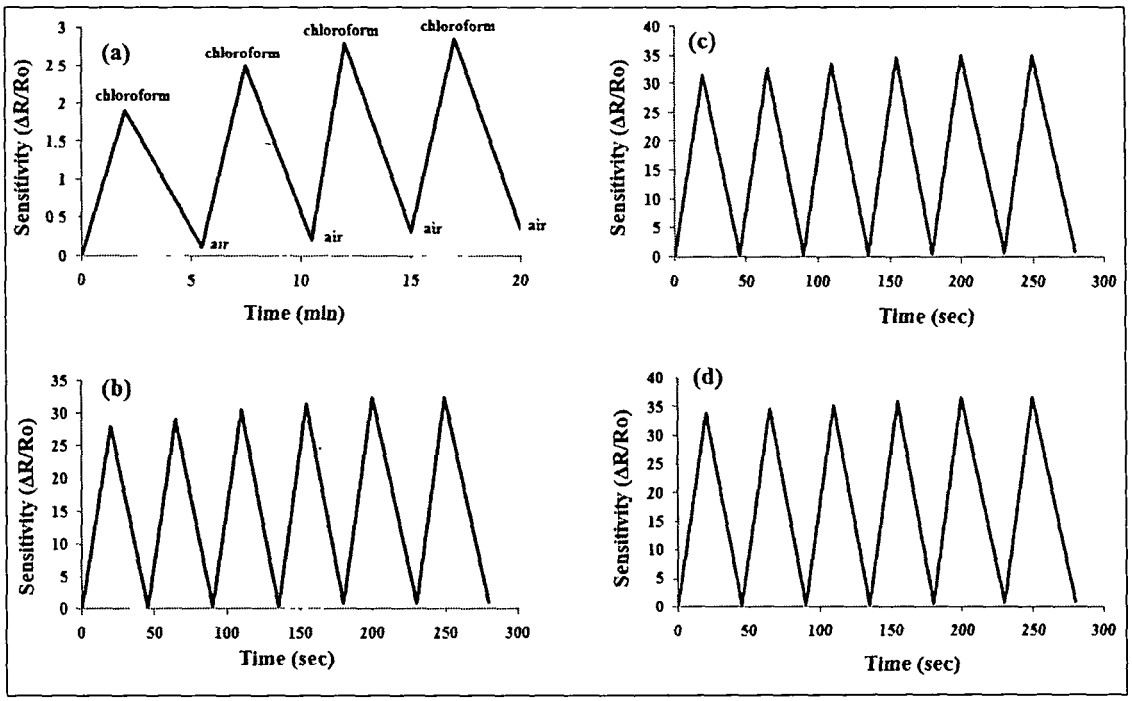

Figure 4.10 Response curves of (a) pure PA and PA/EG exposed to saturated vapours of chloroform at (b) 100 ppm (c) 200 ppm and (d) 300 ppm concentrations

In PA/EG composite, the sensitivity towards chloroform better and reproducible compared to pure PA. The responds and recovery time are faster than pure PA (**Figure 4.10b -4.10d**). On exposure to 100 ppm chloroform for 20 sec, the sensitivity initially increases to 28 and on removal it again returned back to initial state with slight deviation indicating the better reversible character. The response magnitude of PA towards the concentration of chloroform shows a gradual increase in sensitivity up to 250 ppm and it reaches maximum ΔR/Ro values upto 36.5. Due to high vapour pressure (239.75 mm Hg at 30 °C) and small size, chloroform diffuses fast in the polymer matrix. Also, the incorporation of EG into PA matrix shows large variation in resistance even for low concentration of chloroform, making them good sensor materials.

When PA was exposed to chloroform, it reduces the PA matrix from emaraldine salt to emaraldine base by interacting with the NH sites of the polymer resulting the increase in resistivity. **Scheme 4.3** showed the probable interaction between the chloroform and the PA backbone.

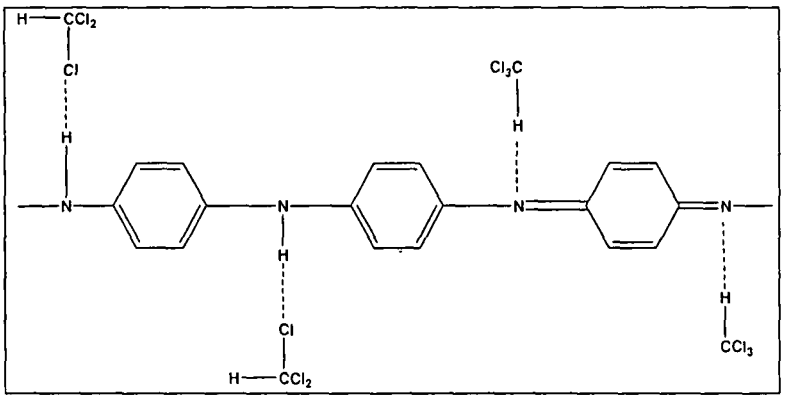

Scheme 4.3 Schematic representation of the proposed hydrogen bonding interaction between chloroform vapour and PA

Figure 4.11 shows the sensor response of PA and PA/EG composites towards carbon tetrachloride vapour. On 2 min exposure of carbon tetrachloride the sensitivity (ΔR/Ro) of PA is found to be 0.57 and on removal of carbon tetrachloride the ΔR/Ro value decreases to 0.09 after 3.5 min. The ΔR/Ro values are gradually increasing with time and maximum sensitivity is found to 3.6 after 10 min exposure of carbon tetrachloride (**Figure 4.11 a**).

Figure 4.11b - 4.11d shows the responds behaviour of PA/EG composite with carbon tetrachloride. The recovery time and sensitivity (ΔR/Ro) towards carbon

tetrachloride of PA/EG composite is better and reproducible than pure PA. On exposure to 100 ppm carbon tetrachloride for 20 sec the sensitivity initially increased to 17.5 and on removal it again returned back to initial state with slight deviation indicated the better reversible character. The response magnitude of PA towards the concentration of carbon tetrachloride showed a gradual increase in sensitivity up to 300 ppm and it reaches maximum ΔR/Ro values upto 32.

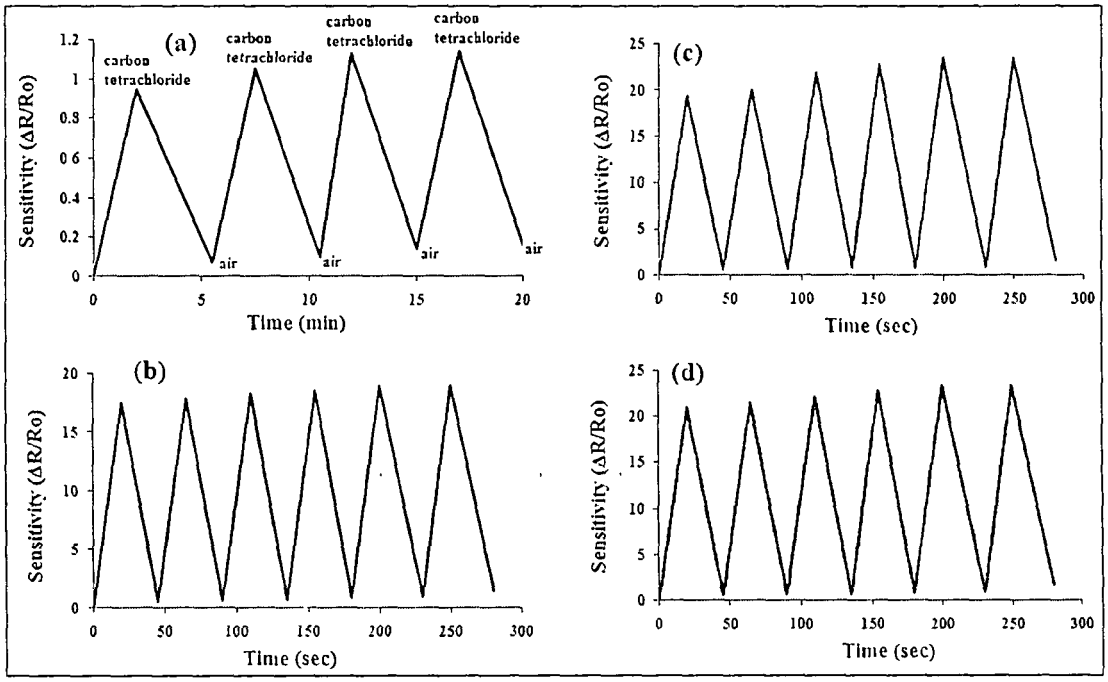

Figure 4.11 Response curves of (a) pure PA and PA/EG exposed to saturated vapours of carbon tetrachloride at (b) 100 ppm (c) 200 ppm and (d) 300 ppm concentrations

Scheme 4.4 shows the probable interaction between the carbon tetrachloride and the PA backbone.

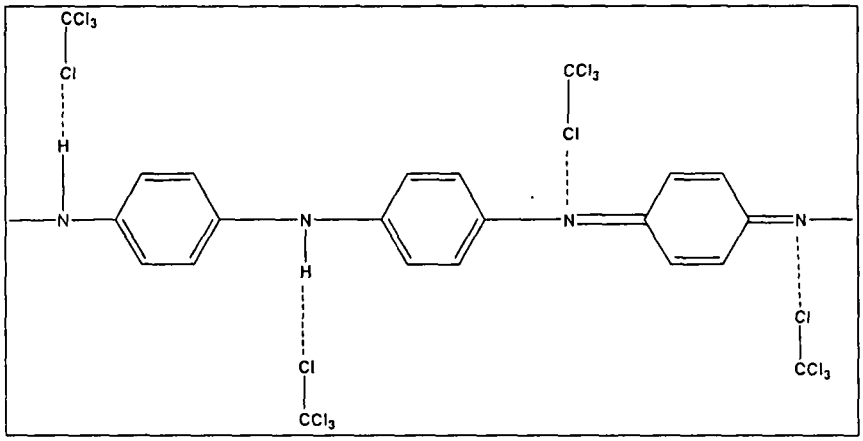

Scheme 4.4 Schematic representation of the proposed hydrogen bonding interaction between carbon tetrachloride vapour and PA

Limit of detection

Figure 4.12 shows the detection limit of PA/EG composite against three different VOCs with their concentration upto 2000 ppm. In acetone, the ΔR/Ro values of PA/EG sensor increases from 18 – 25 in the concentration range of 100 – 500 ppm and thereafter the sensitivity becomes saturated. On exposure to carbon tetrachloride, the limit of sensitivity (ΔR/Ro) shows 19 -24.5 in between the concentration 100 – 300 ppm and then it also becomes saturated. The maximum sensitivity of PA/EG composite showed against chloroform vapour. The maximum ΔR/Ro value is found to be 36.5 on exposure with 300 ppm chloroform.

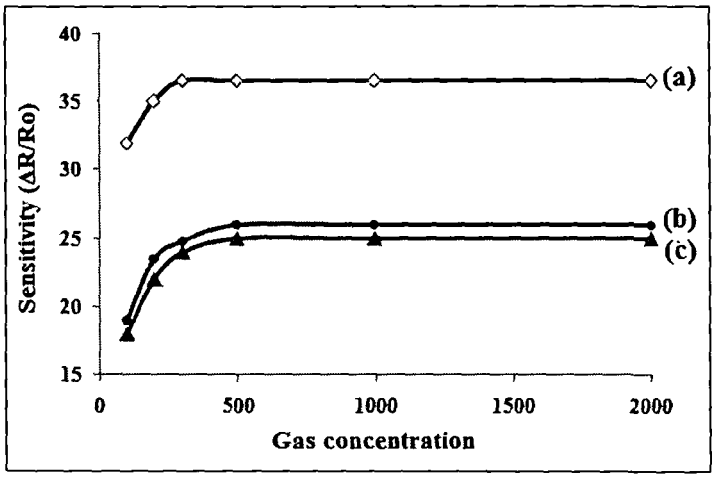

Figure 4.12 Detection limit of PA/EG against the gas concentration (a) acetone (b) carbon tetrachloride and (c) chloroform

The selectivity of PA/EG composite with respect to these three VOCs are as - acetone < carbon tetrachloride << chloroform as shown in the **Figure 4.13**.

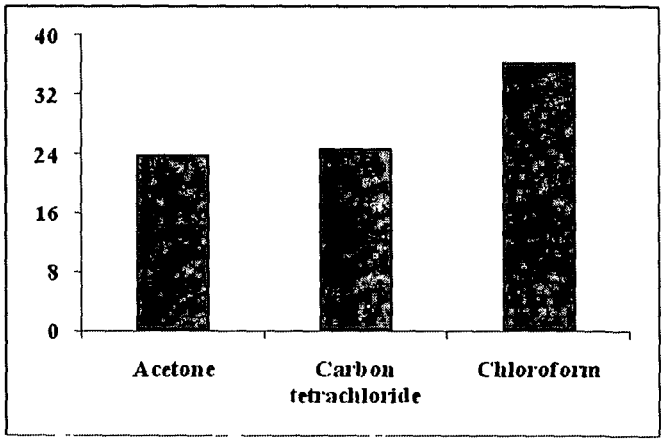

Figure 4.13 Selectivity of PA/EG composite with 300 ppm concentration VOCs

4.5 Capacitance Behaviour of Carbon Filled π-Conjugated Polymers

Supercapacitors are being considered for a variety of applications not only in electric vehicles and uninterruptible power supplies but also in memory protection of computer electronics and cellular communication devices.[40-42] Electrically conducting polymers including PPy, PA, polythiophene show higher capacitance because of the capacitive and Faradaic currents contribute to the charge storage. The cycle-life in charge–discharge for conducting polymer is lower than carbon-based electrodes. This is due to lower stability of the redox sites in the polymer backbone. Some methods have been attempted to improve the capacitance and the conductivity of conducting polymer-based supercapacitors. For example, conducting PPy/graphite fiber composite have been successfully made by using electrochemical polymerization of pyrrole on the surface of graphite fiber and this composite material shows higher capacitance and conductivity.[43,44] The electrochemical method is limited in terms of the mass production of composite electrodes and it is not suitable for preparing controlled polymer films with thicknesses above 100 mm. It is only suitable for preparing very thin films of polymer. If thin polymer film with a very high-specific capacitance per unit mass is converted to specific capacitance per unit area, this value is less than that for a carbon based supercapacitor because of the small deposited polymer mass.

Conducting polymer-based supercapacitors can be classified into three types.[43, 45] Type I is a symmetric system where same *p* - dopable conducting polymers are used at both the electrodes of the capacitor. Type II is an asymmetric system based on two different p-dopable conducting polymers to be used as electrode materials. Type III is a symmetric system based on a conducting polymer, which can be used both as p- and n-doped electrode materials.

In this work we have attempted to build a Type I supercapacitor using two identical electrodes with same conducting polymer composite materials. We have synthesised two composite electrodes PPy/GO by the incorporation of GO into PPy through the in-situ polymerization of pyrrole and PA/EG by the incorporation of EG into PA through the in-situ polymerization of aniline. Structural morphology and characterization were carried out by XRD, SEM and TEM analysis. The effect of GO and EG on the electrical and electrochemical capacitance performance of PPy/GO and PA/EG composite for super capacitor application have been studied.

4.5.1 Electrochemical Measurements

Using a compression-moulding machine, pellets of composite electrodes were made. High pressure was applied (1.5 to 2 ton) to the sample to get hard round shaped pellet (1.5 cm diameter, 2 mm breadth). The two electrode capacitor cells were constructed with electrolyte polyethylene oxide (PEO) as separator using a sandwich type construction (electrode/separator/electrode) with a current-collector silver paste (**Figure 4.14**). The silver paste coating substrate acts as a current collector on both sides of the capacitors. The electrodes were pre-wetted with electrolyte before use. The capacitor performance was characterized by means of galvanostatic charge–discharge tests using an Autolab PGSTAT302N at room temperature. In case of the three-electrode cell, the working electrode was the PPy/GO and PA/EG composites, platinum wire was the counter electrode, and standard calomel electrode (SCE) was used as reference electrode.

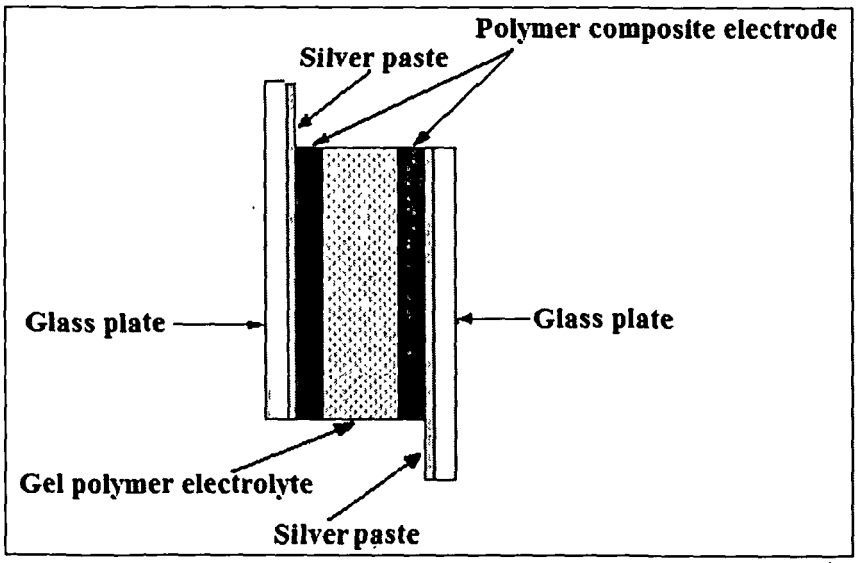

Figure 4.14 Geometrical structure of supercapacitor fabrication

4.5.2 Polypyrrole/Graphene Oxide (PPy/GO) Composites as Supercapacitor Electrode

4.5.2.1 Electrochemical Behaviour

PPy/GO films (5% and 10%) on ITO coated glass, standard calomel electrode (SCE) and Pt wire were used as working electrodes, reference electrode and counter electrode respectively with 0.1M KCl solution as supporting electrolyte prepared in 10ml acetonitrile. All potentials are reported with respect to reference electrode. The

measurements were calibrated using ferrocene as the standard and the scan rate was 50 mV/s.

Figure 4.15 illustrates the cyclic voltammograms (CVs) of PPy and PPy/GO composites electrodes with a potential window from -0.2 to 1.0 V (vs SCE). The PPy/GO composites electrodes show the CV is nearly rectangular in shape (**Figure 4.15b and 4.15c**), which indicating good charge propagation within the electrode compared to the pure PPy electrodes (**Figure 4.15a**). Therefore GO is the most effective in imparting the electrochemical performances of the nanocomposites.

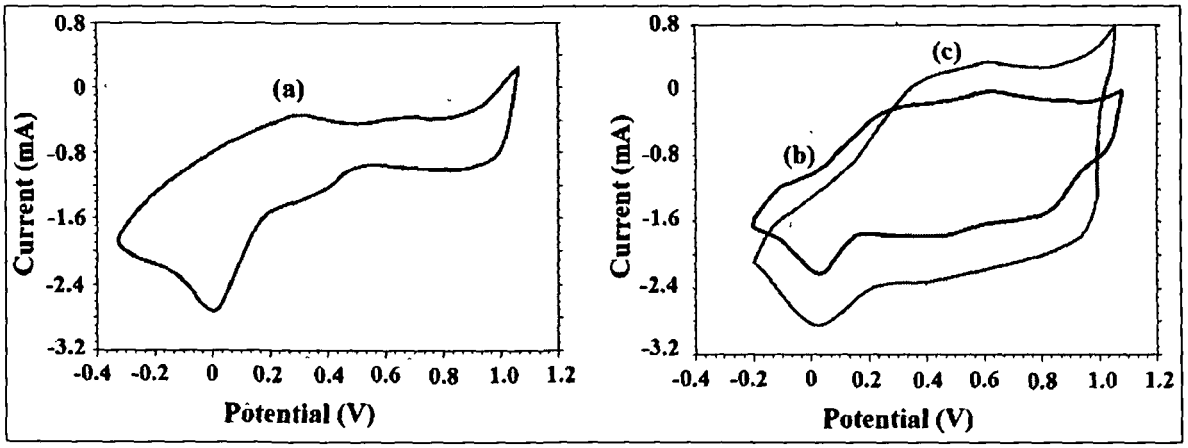

Figure 4.15 Cyclic voltammogram of (a) pure PPy, (b) PPy/GO (5%) and (c) PPy/GO (10%) pellet electrode at scan rate, 50 mV/s

4.5.2.2 Charge–Discharge Studies

The supercapacitor behaviour of the composite electrodes can be directly evaluated by means of the galvanostatic charge–discharge studies. Specific capacitances of different electrode materials were compared at a constant current of 2mA. The average specific capacitance values, C_g (F/g) of the samples were estimated from the discharge process according to the following equation-[46]

$$Cg = \frac{I\Delta t}{\Delta V \times m} \qquad (4.1)$$

Where, I is the current loaded (A), Δt is the discharge time (s), ΔV is the potential change during discharge process, and m is the mass of active material in a single electrode (g).

The Galvanostatic charge/discharge curves of PPy and PPy/GO composites are shown in **Figure 4.16**. The mass of active material used for PPy, PPy/GO (5%) and PPy/GO (10%) electrode is 4.3 mg, 10.8 mg and 11.2 mg respectively. The discharge specific capacitance values of the PPy/GO composite electrodes increases with increasing GO content. The specific capacitance of individual PPy is only 237.20 F/g at 2 mA current in the range from 0 to 0.50 V. The improved specific capacitance behaviour of the PPy/GO composites is due to the presence of GO in the PPy matrix which allows the counter ions to readily penetrate into the polymer matrix and access their internal surface. In addition the enhanced electrochemical performances of PPy/GO may be due to the synergistic effect between GO and PPy. It is noteworthy that PPy/GO (10%) shows a better electrochemical capacitance (421.42 F/g) compared with PPy/GO (5%) (370.37 F/g).

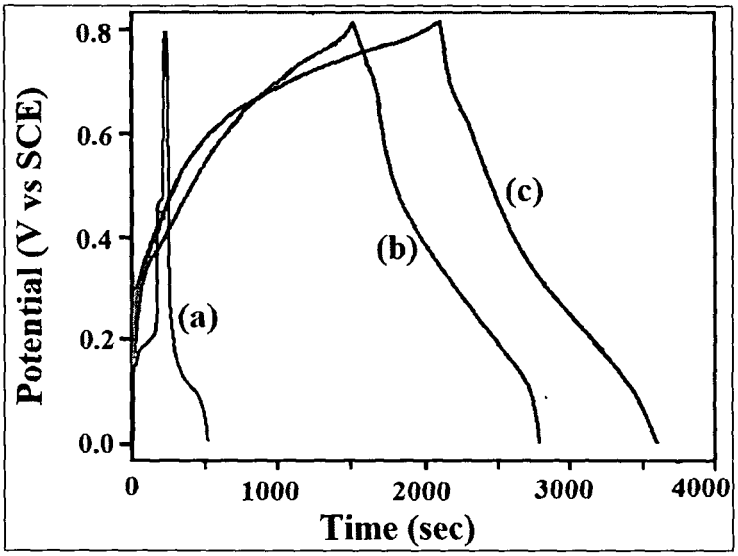

Figure 4.16 Galvanostatic discharge curve, (a) pure PPy (b) PPy/GO (5%) and (c) PPy/GO (10%) pellet electrode at current 2mA

4.5.3 Capacitance Behaviour of Polyaniline/Expanded Graphite (PA/EG) Composites Electrode

4.5.3.1 Electrochemical Behaviour

PA/EG (5% and 10%) composite, SCE and Pt wire were used as working electrodes, reference electrode and counter electrode respectively with 0.1M KCl solution as supporting electrolyte prepared in 10ml acetonitrile. All potentials are reported with respect to reference electrode. The measurements were calibrated using ferrocene as the standard and the scan rate was 50 mV/s.

Figure 4.17 illustrates the CVs of PA and PA/EG composites electrodes with a potential window from -2.4 to +3.0 V (vs SCE). The PA/EG composites electrodes show the CV is nearly rectangular in shape (**Figure 4.17b and 4.17c**), which indicates good charge propagation within the electrode compared to the pure PPy electrodes (**Figure 4.17a**). Therefore EG is the most effective in imparting the electrochemical performances of the nanocomposites.

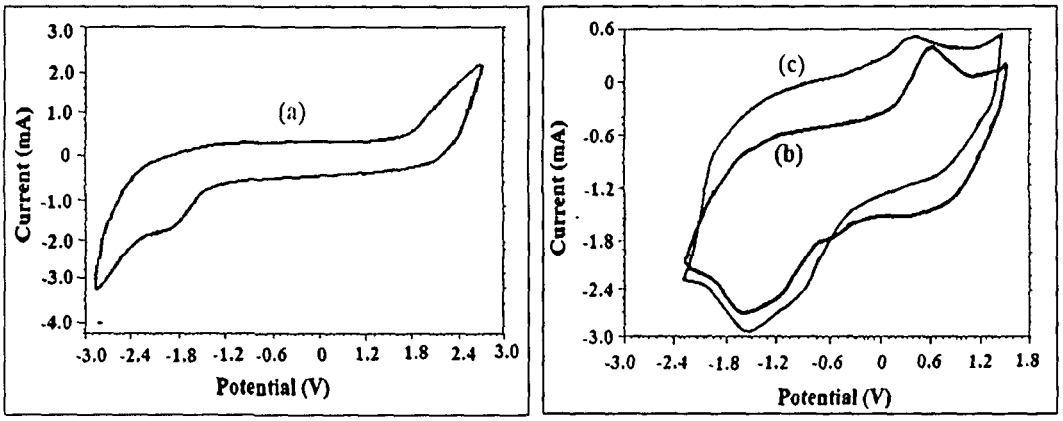

Figure 4.17 Cyclic voltammogram of (a) pure PA, (b) PA/EG (5%) and (c) PA/EG (10%) pellet electrode at scan rate, 50 mV/s

4.5.3.2 Charge–Discharge Studies

The Galvanostatic charge/discharge curves of PA and PA/EG composites are shown in **Figure 4.18**. The mass of active material used for PA, PA/EG (5%) and PA/EG (10%) electrode is 4.5 mg, 3.5 mg and 4 mg respectively. The specific capacitance of PA electrode is 266.66 F/g while for PA/EG (5%) and PA/EG (10%) the specific capacitances are 507.14 F/g and 543.75 F/g at 2 mA current in the range from 0.2 to 0.60 V. The incorporation of EG into the PA matrix enhanced the capacitance behaviour of PA/EG composites. In EG, some functional groups such as –OH, –COOH present on the surface and pores of the EG sheets and at high temperature after acid treatment they could promote the adsorption of molecular chains and monomers onto the pores. Moreover the π-π stacking between the polymer backbone and the EG sheets may also contribute to extend the conjugation length of the polymer composite which allows the counter ions to readily penetrate into the polymer matrix and access their internal surface. Therefore the specific capacitance increases with increase the EG content in PA/EG composite.

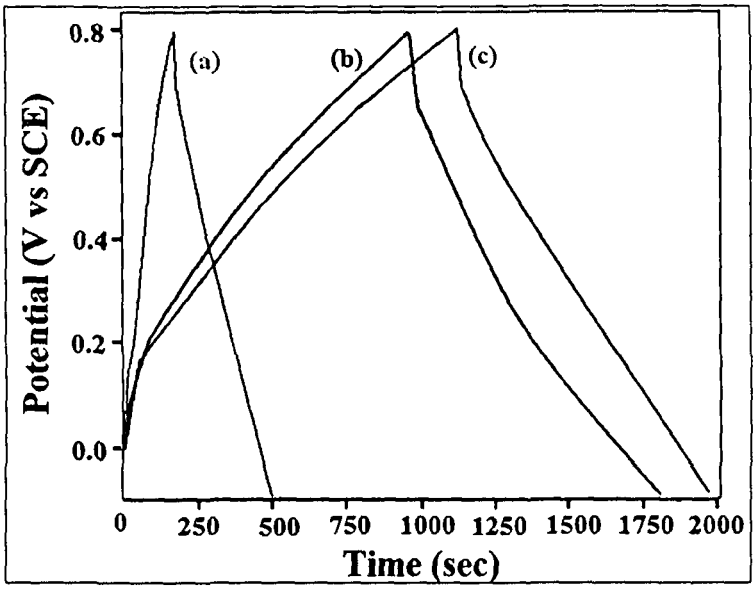

Figure 4.18 Galvanostatic discharge curve of (a) pure PPy (b) PA/EG (5%) and (c) PA/EG (10%) pellet electrode at current 2mA

4.6 Conclusions

The following conclusions can be extracted from this investigation:

Sensor Applications

Methanol sensor

- The PA/GO composite is found to be a highly sensitive (ΔR/Ro = 20.9 - 37) sensor material for methanol vapours (100-500 ppm). However the sensitivity (*ΔR/Ro*) is quite low with ethanol (*ΔR/Ro* = 3.77) and propanol ((ΔR/Ro = 3.1). The response time of PA/GO composite is low shows better reversible characteristics in comparison with the pure PA.
- The basic mechanism of the interaction between methanol and PA is believed to be hydrogen bonding between the methanol and benzenoid and quinoid nitrogen of the polymer chain as revealed by DFT and FTIR studies.

Sensing properties of PA/EG composite for volatile organic compounds

- The PA/EG composite is found to be a highly sensitive (ΔR/Ro = 33.3-36.5) sensor material for chloroform vapours (100-300 ppm) than that of carbon tetrachloride (ΔR/Ro = 21-24.5) and acetone ((ΔR/Ro = 20.5-24). The response time of PA/EG composite is low and shows better reversible characteristics than that of pure PA.

Supercapacitor Application

- Polypyrrole/graphene oxide (PPy/GO) and polyaniline/expanded graphite (PA/EG) composites are tested as super capacitor electrode.
- The specific capacitance of the PPy/GO composite has been found to be 421.42 F/g with 10% of GO content whereas the specific capacitance of individual PPy is found to be only 237.20 F/g in the voltage range 0 to 0.50 V at current 2 mA.
- The specific capacitances of the PA/EG composite is found to be 543.75 F/g with 10% of EG content whereas the specific capacitance of individual PA is found to be only 266.64 F/g in the voltage range 0.2 to 0.60 V at current 2 mA.

References

1. Becke, A. D. Density-functional thermochemistry. III. The role of exact exchange, *J. Chem. Phys.* **98,** 5648-5652 (1993)
2. Lee, C.; Yang, W., Parr, R. G. Development of the Colle-Salvetti correlation-energy formula into a functional of the electron density, *Phys. Rev. B* **37,** 785-789 (1988)
3. Vosko, S. H.; Wilk, L.; Nusair, M. Accurate spin-dependent electron liquid correlation energies for local spin density calculations: a critical analysis, Can. *J. Phys.* **58,** 1200 -1211 (1980)
4. Frisch, M. J. *et al.* Gaussian 03, revision D.02, (Gaussian, Inc.: Pittsburgh, PA, 2003)
5. Huang, J. X.; Virji, S.; Weiller, B. H.; Kaner, R. B. Polyaniline nanofibers: Facile synthesis and chemical sensors, *J. Am. Chem. Soc.* **125,** 314-315 (2003)
6. Khan, A. A.; Khalid, M.; Baig, U.; Synthesis and characterization of polyaniline–titanium(IV)phosphate cation exchange composite: methanol sensor and isothermal stability in terms of DC electrical conductivity, *React. Funct. Polym.***70,** 849-855 (2010)
7. Maiti, J.; Pokhrel, B.; Boruah, R.; Dolui, S. K. Polythiophene based fluorescence sensors for acids and metal ions, *Sens. Actu. B* **141,** 447-451 (2009)
8. Yan, X. B.; Han, Z. J.; Yang, Y.; Tay, B. K. NO_2 gas sensing with polyaniline nanofibers synthesized by a facile aqueous/organic interfacial polymerization, *Sens. Actu. B* **123,** 107-113 (2007)
9. Chithralekha, P.; Balaji, M.; Subramanian, S.; Padiyan, P. D. Sensing properties of polyoxomolybdate doped polyaniline nanomaterials for oxidising and reducing volatile organic compounds, *Cur. Appl. Phys.* **10,** 457–467 (2010)
10. Xie, D. *et al.* Fabrication and characterization of polyaniline-based gas sensor by ultra-thin film technology, *Sens. Actuator B* **8,** 158–164 (2002)
11. Kim, J. S.; Sohn, S. O; Huh, J. S. Fabrication and sensing behavior of PVF_2 coated-polyaniline sensor for volatile organic compounds, *Sens Actuator B* **108,** 409-413, (2005)
12. Nicolas-Debarnot, D.; Poncin-Epaillard, F. Polyaniline as a new sensitive layer for gas sensors, *Anal. Chim. Acta.* **475**, 1-15 (2003)

13. Prasad, G. K.; Radhakrishnan, T. P.; Kumar, D. S.; Krishna, M. G. Ammonia sensing characteristics of thin film based on polyelectrolyte templated polyaniline, *Sens. Actuators B* **106,** 626-631 (2005)

14. Tan, C. K.; Blackwood, D. J.; Interactions between polyaniline and methanol vapour, *Sens. Actuators B* **71,** 184-191 (2000)

15. Dixit, V.; Misra, S. C. K.; Sharma, B. S. Carbon monoxide sensitivity of vacuum deposited polyaniline semiconducting thin films, *Sens. Actuators B* **104,** 90-93 (2005)

16. Ogura, K.; Shiigi, H. A CO_2 Sensing composite film Consisting of Base-Type Polyaniline and Poly(vinyl alcohol), *Electrochem. Solid State Lett.* **2,** 478-480 (1999)

17. Chabukswar, V. V.; Pethkar, S.; Athawale, A. A. Acrylic acid doped polyaniline as an ammonia sensor, *Sens. Actuators B* **77,** 657-663 (2001)

18. Anitha, G.; Subramanian, E. Dopant induced specificity in sensor behaviour of conducting polyaniline materials with organic solvents, *Sens. Actuators B* **92,** 49-59 (2003)

19. Santra, S. *et al.* ZnO nanowires grown on SOI CMOS substrate for ethanol sensing, *Sens. Actuators B* **146,** 559-565 (2010)

20. Barker, P. S. *et al.* Vapour recognition using organic films and artificial neural networks, *Sens. Actuators B* **17,** 143-147 (1994)

21. Ogura, K.; Shiigi, H. M. Nakayama, A. Fujii, Thermogravimetric/mass and infrared spectroscopic properties and humidity sensitivity of polyaniline derivatives/polyvinyl alcohol composites, *J. Electrochem. Soc.* 145 (1998) 3351-3357.

22. MacDiarmid, A. G.; Zhang, W. J.; Feng, J.; Haung, F. (ANTEC' Society of Plastic Engineers, Atlanta, GA, 1330–1334 1998)

23. Sukeerthi, S.; Contractor, A. Q.; Applications of conducting polymers as sensors, *Ind. J. Chem. Sect. A* **33,** 565-571 (1994)

24. Hatfield, J. V.; Neaves, P. I.; Hicks, P. J.; Persuad, K. C.; Travers, P. Towards an integrated electronic nose using conducting polymer sensors, *Sens. Actuators B* **18,** 221–228 (1994)

25. Pradip, K.; Pradhan, N. C.; Adhikari, B. Application of sulfuric acid doped poly (m-aminophenol) as aliphatic alcohol vapor sensor material, *Sens. Actuators B* **140,** 525-531 (2009)

26. Qian, Y.; Lu S.; Gao, F.; Synthesis of manganese dioxide/reduced graphene oxide composites with excellent electrocatalytic activity toward reduction of oxygen, *Mater. Lett.* **65,** 56-58 (2011)

27. Geim, A. K.; Novoselov, K. S. The rise of graphene, *Nat. Mater.* **6,** 183-191 (2007)

28. Wu, J.; Pisula, W.; Mullen, K. Graphene as potential material for electronics, *Chem. Rev.* **107,** 718–747 (2007)

29. Bunch, J. S. *et al.* Electromechanical resonators from graphene sheets, *Science* **315,** 490–493 (2007)

30. Dikin, D. A. et al. Preparation and characterization of graphene oxide paper, *Nature* **448,** 457–460 (2007)

31. Wang, X.; Zhi, L.; Mullen, K. Transparent, conductive graphene electrodes for dye-sensitized solar cells, *Nano. Lett.* **8,** 323–327 (2008)

32. Yan, J.; *et al.* Preparation of a graphene nanosheet/polyaniline composite with high specific capacitance, *Carbon* **48,** 487-493 (2010)

33. Zhang, K.; Zhang, L. L.; Zhao, X. S.; Wu, J. Graphene/Polyaniline Nanofiber Composites as Supercapacitor Electrodes, *Chem. Mater.* **22,** 1392–1401 (2010)

34. Sen, P.; De, A. Electrochemical performances of poly(3,4-ethylenedioxythiophene)–$NiFe_2O_4$ nanocomposite as electrode for supercapacitor, *Electrochim. Act.* **55,** 4677–4684 (2010)

35. Si, Y.; Samulski, E. T. Synthesis of Water Soluble Graphene, *Nano Lett.* **8,** 1679–1682 (2008)

36. Miasik, J. J.; Hopper, A.; Tofield, B. C. Conducting polymer gas sensors, *J. Chem. Soc. Faraday Trans. I.* **82,** 1117–1126 (1986)

37. Yan, X. B.; Han, Z. J.; Yang, Y.; Tay, B. K. NO_2 gas sensing with polyaniline nanofibers synthesized by a facile aqueous/organic interfacial polymerization, *Sens. Actuators B* **123,** 107-113 (2007)

38. Cruz-Silva, R. et al. Comparative study of polyaniline cast films prepared from enzymatically and chemically synthesized polyaniline, *Polymer* **45,** 4711-4717 (2004)

39. Tiwaria, A. *et al.* Nanofibrous polyaniline thin film prepared by plasma-induced polymerization technique for detection of NO_2 gas, *Polym. Adv. Technol.* **21,** 615-620 (2010)

40. Conway, B. E.; Pell, W. *Proceedings of the 8th International Seminar on Double-Layer Capacitors and Similar Energy Storage Devices,* (Florida Educational Seminars, Deerfield Beach, FL, 1998)

41. Arbizzani, C.; Mastragostino, M.; Scosati, B. H. S. Nalwa (Ed.): Handbook of organic conductive molecules and polymers, (Wiley, Chichester, UK, 1997)

42. W.R. Cieslak (Ed.): Selected Battery Topics, PV 98-15, *The Electrochemical Society Proceedings Series,* (Pennington, NJ, 1998)

43. Rudge, A.; Davey, J.; Raistrick, I.; Gottesfeld, S. *J. Power Sources* **47,** 89-107 (1994)

44. Rudge, A.; Raistrick, I.; Gottesfeld, S.; Ferraris, J. P *Electrochim. Acta* **39,** 273-287 (1994)

45. Zhang, K.; Zhang, L. L.; Zhao, X. S.; Wu, J. Graphene/Polyaniline nanofiber composites as supercapacitor electrodes, *Chem. Mater.* **22,** 1392–1401 (2010)

Chapter 5

Conclusion and future scope of the present investigation

5.1 Conclusion

Conjugated polymers are attractive materials for optoelectronic applications such as sensors, super capacitors, light emitting diodes, etc. The electrical and electrochemical properties of polymer composites based on polyaniline (PA) and polypyrrole (PPy) with various carbon fillers like graphite, expanded graphite (EG) and graphene oxide (GO) have been investigated in the present study.

In this thesis we provide an insight into synthesis, characterization of PA and PPy composites incorporated with graphite, EG and GO by *in-situ* polymerization. A considerable effort has been devoted to study the influence of carbon fillers on the optical, electrical and electrochemical properties of polymers. The thesis also provides an account of sensors and supercapacitor applications.

Findings of the thesis are summarised below:

(I) Synthesis and characterization of carbon filled π - conjugated polymers

- EG and GO have been synthesized successfully from natural graphite flake. The synthesized EG and GO was characterized by FTIR, XRD, TGA, SEM and TEM analysis.
- XRD analysis reveals the hexagonal crystalline structure of graphite and EG. In EG, the interlayer distances between the sheets increases which causes the shifting of diffraction peak (2θ) to lower value compared to graphite. In GO, a broad reflection peak at $2\theta = 13.1°$ is observed, which is correlated to an interlayer spacing of 0.68 nm in the layer-liked GO.
- SEM micrographs show the differences in microstructures between graphite, EG, and GO. The graphite particles are randomly aggregated having rough surface whereas in EG, layer-liked structures are observed. The GO inherits the layer-by-layer and network structure.
- A series of PA and PPy composites incorporated with different carbon fillers viz., graphite, EG and GO have been synthesized by in-situ chemical polymerization using $K_2S_2O_8$ and $FeCl_3$ as an oxidizing agent.
- XRD and FTIR study reveal the incorporation of carbon filler into the polymer matrices.

- PA and poly (styrene-co-methyl acrylate) core-shell composite particles have also been synthesized successfully. TEM micrographs confirm the formation of core-shell morphology.
- The polymer composites with graphite, EG and GO showed gratifying thermal stability than that of individual polymers.
- The major degradation for PA/G, PA/EG and PA/GO composites occurs at 470 °C, whereas polymer composites of PPy/G, PPy/EG and PPy/GO are found to have thermal stability upto 450 °C. There is a sufficient enhancement in the thermal stability of the polymer composites after the incorporation of the carbon filler.

(II) Optical, electrical and electrochemical properties of carbon filled π - conjugated polymers

- The UV-vis spectrum of PA shows an intense absorption peak at 305 nm, a weak peak at 356 nm, and a broad peak at 580 nm. Whereas the PPy shows a weaker absorption at around 330 nm and stronger absorption at around 570 nm. For both the polymer first bands are related to the molecular conjugation (π - π* transition) while the final absorption peak assigned to the polaron state of polymer i.e. charged cationic species.
- All the carbon filled PA and PPy composites show red shift of UV-vis absorption maximum with respect to their pristine polymers. The carbon filler assists the polymerization in such a way that it maintains a higher conjugation length in the chain of the polymer itself. The incorporated carbon filler interacts with the backbone of the polymer matrices resulted in the red shift of the band.
- Optical band gaps calculated from onset of absorption spectra are in the range of 3.2–1.89 eV for PA composites and 2.90 - 2.02 eV for PPy composites on addition of carbon fillers.
- The I-V characteristics of PA, PPy and carbon filled polymer composites are asymmetric and nonlinear for forward direction of applied voltage suggesting the semiconducting behaviour and Schottky barrier in the polymer and polymer composites.
- The conductivity of the carbon filled PA and PPy composites is found to be dramatically increased in comparison to the bare polymer depending on the content of the carbon fillers. The maximum conductivity of PA and PPy

composites are found to be 4 x 10^2 S/cm and 1.11 x 10^2 S/cm respectively on addition of 1% EG at 140 °C.

- The electrochemical band gaps for PA, PA/G, PA/EG and PA/GO composite with 1% content of carbon filler are 3.2 eV, 1.2 eV, 1.65 eV and 1.62 eV respectively. The electrochemical band-gap for PPy, PPy/G, PPy/EG and PPy/GO is found to be 2.90 eV. 1.3 eV, 1.98 eV and 2.02 eV respectively. The band gap of the polymer composites decreases with increasing amounts of incorporated carbon fillers.
- The optical and electrochemical band-gaps of polymer composites are found to be different. However both the methods establish the same trend of band gap.
- All the prepared PA and PPy composites show gratifying reversible electrochemical response. The electrochemical behaviour of the polymer composite did not changed upto 150th cycles for EG and GO filled PA composites.

(III) Capacitance behaviour and sensors application of carbon filled π-conjugated polymers

Supercapacitor Application

- Polypyrrole/graphene oxide (PPy/GO) and polyaniline/expanded graphite (PA/EG) composites are tested as super capacitor electrode.
- The specific capacitance of the PPy/GO composite is 421.42 F/g with 10% of GO content whereas the specific capacitance of individual PPy is found to be only 237.20 F/g in the voltage range 0 to 0.50 V at current 2 mA.
- The specific capacitances of the PA/EG composite is found to be 543.75 F/g with 10% of EG content whereas the specific capacitance of individual PA is only 266.64 F/g in the voltage range 0.2 to 0.60 V at current 2 mA.

Sensor Applications

Methanol sensor

- The PA/GO composite is found to be a highly sensitive ($\Delta R/Ro$ = 20.9 - 37) sensor material for methanol vapours (100-500 ppm). However the sensitivity ($\Delta R/Ro$) is quite low with ethanol ($\Delta R/Ro$ = 3.77) and propanol (($\Delta R/Ro$ = 3.1).

The response time of PA/GO composite is low shows better reversible characteristics in comparison with the pure PA.

- The basic mechanism of the interaction between methanol and PA is believed to be hydrogen bonding between the methanol and benzenoid and quinoid nitrogen of the polymer chain as revealed by DFT and FTIR studies.

Sensing properties of PA/EG composite for volatile organic compounds

- The PA/EG composite is found to be a highly sensitive ($\Delta R/Ro$ = 33.3-36.5) sensor material for chloroform vapours (100-300 ppm) than that of carbon tetrachloride ($\Delta R/Ro$ = 21-24.5) and acetone ($\Delta R/Ro$ = 20.5-24). The response time of PA/EG composite is low and shows better reversible characteristics than that of pure PA.

Comparative study

The principal goal of the thesis is to study the effect of carbon fillers like graphite, EG and GO on the properties PA and PPy. The EG-based PA and PPy composites show better thermal stability (upto 470 °C) than graphite and GO-based polymer composite. The effect of fillers on the properties of PA and PPy is quite different. The following observations have been made:

- The expanded graphite filled polymer composites show higher conductivities (4.00×10^2 S/cm) as compared to the graphite (2.38×10^2 S/cm) and graphene oxide (2.42×10^2 S/cm) with 10% of filler content.
- Polyaniline/carbon filled composites show higher conductivity (upto 4×10^2 S/cm) than that of polypyrrole composites (upto 1.11×10^2 S/cm).

5.2 Future scope of the present investigation

- Theoretical study of band gap for carbon filled π – conjugated polymers
- To study the actual mechanism of selectivity of the conjugated polymers to different volatile gases
- Study of the synthesized polymers in other optoelectronic devices e.g. LED, electrochromic devices, transistor etc.

List of publications

Journals

1. Konwer, S.; Pokhrel, B.; Dolui, S.K. Synthesis and characterization of polyaniline/graphite composites and study of their electrical and electrochemical properties, *J. Appl. Polym. Sci.* **116,** 1138–1145 (2010)
2. Konwer, S.; Dolui, S.K. Synthesis and characterization of polypyrrole/graphite composites and study of their electrical and electrochemical properties, *Mater. Chem. Phys.* **124,** 738–743 (2010)
3. Borthakur, L.J.; Konwer, S.; Das, R.; Dolui, S.K. Preparation of conducting composite particles of styrene-methyl acrylate copolymer as the core and graphite incorporated polypyrrole as the shell by surfactant free mini emulsion polymerization, *J. Polym. Res.* (DOI: 10.1007/s10854-010-0242-4, Online)
4. Konwer, S.; Gogoi, J.P.; Kalita, A.; Dolui, S.K. Synthesis of expanded graphite filled polyaniline composites and evaluation of their electrical and electrochemical properties, *J. Mater. Sci. Mater. Elect.* (DOI 10.1007/s10854-010-0276-7, Online)
5. Pokhrel, B.; Konwer, S.; Dutta, A.; Huda, M.K.; Ghosh, B.; Dolui, S.K. Study of photovoltaic performance of host-guest system comprising optically active polyurethane and Rhodamine B dye, *J. Appl. Polym. Sci.,* (accepted)
6. Konwer, S.; Maiti, J.; Dolui, S.K. Synthesis of expanded graphite filled conductive polypyrrole nanocomposites and their optical, electrical and electrochemical behaviour, *Mater. Chem. Phys.* (Accepted)
7. Konwer, S.; Borthakur, L.J.; Dolui, S.K. Synthesis of graphite incorporated core-shell composite particle of styrenemethylacrylate/polyaniline by surfactant free mini-emulsion polymerization and evaluation of their electrical property, *JMSE. Mat. Elect.* (Revision submitted)
8. Konwer, S.; Guha, A.K.; Dolui, S.K. Graphene oxide filled polyaniline composite as methanol sensor, *React. Funct. Polym.* (Revision submitted)
9. Dutta, A.; Konwer S.; Pokhrel B.; Huda, M.K.; Kalita A.; Dolui S.K. Optical and electrical behaviour of Cu/PA nanocomposite, *Synth. Met.* (Under review)
10. Konwer, S.; Boruah, R.; Dolui, S.K. Studies on conducting polypyrrole/graphene oxide composites as supercapacitor electrode, Polym. J. (Under review)

11. Konwer, S.; Dolui, S.K. Studies on graphene oxide filled conductive polypyrrole nanocomposites and their optical, electrical and electrochemical behaviour, *J. Polym. Res.* (communicated)
12. Konwer, S.; Mandal, S.; Dolui, S.K. Synthesis of polyaniline/graphene oxide nanocomposites and their optical, electrical and electrochemical behaviour, *Mater. Chem. Phys.* (communicated)
13. Konwer, S.; Dolui, S.K. Sensing properties of expanded graphite filled polyaniline composites for volatile organic compounds, *Sen. Transd. J.* (communicated)
14. Konwer, S.; Dutta, A.; Pokhrel B.; Kamrupi I.R.; Huda, M.K.; Kalita A.; Dolui, S.K. Capacitance behaviour of polyaniline/expanded graphite composites electrode, *Polym. Mater.* (Communicated)

Patent Filed

1. Konwer, S.; Dolui, S.K. "Graphite filled polyaniline and its suitability in electrode" (Application no. 1293/KOL/2009 dated 28.102009)

Conference Presentations

1. Konwer, S.; Dolui, S.K. "Preparation of polyaniline /graphite composite and its electrical properties" 45th Annual Convention of Chemists, International Conference on Recent Advances in Chemistry, Dharwad University, Karnataka, (2008).
2. Konwer, S.; Dolui, S.K. "Synthesis, characterization of polypyrrole/graphite composite and its electrical properties" National Conference on Frontiers in Polymer Science and Technology (POLY–2009), Saurastra University, Rajkot, (2009).
3. Konwer, S.; Kalita, A.; Dolui, S.K. "Chemical synthesis of expanded graphite filled conductive polypyrrole nanocomposites and their optical, electrical and electrochemical behaviour" DAE-BRNS 3rd International Symposium on Material Chemistry (ISMC-2010), BARC, Mumbai, India. December 7-11 (2010).

   (Awarded as best paper presentation-First Prize)

4. Konwer, S.; Dolui, S.K. "Methanol gas sensing properties of graphene oxide filled polyaniline nanocomposite" National Conference on Smart Nanostructure (NCSN-2011), Tezpur University, Assam, (2011).
5. Konwer, S.; Dolui, S.K. "Preparation of polyaniline/graphene oxide nanocomposite as a Methanol gas sensing material" National Seminar on Green Chemistry for Sustainable World, Gargaon College, Assam, February, 4 & 5 (2011).
6. Konwer, S.; Dolui, S.K. "Preparation of highly conductive expanded graphite filled polypyrrole nanocomposites and their optical, electrical and electrochemical behaviour" National seminar on Polymer science and Technology: Vision and scenario, Chaiduar College, Gohpur, Assam, February,11-12, 2011.
7. Konwer, S.; Dolui, S.K. "Preparation of expanded graphite filled polyaniline composite as methanol sensor" 2nd International Symposium Frontiers in Polymer Science (Poly-2011), Centre de Congres, Lyon, France, May, 29-31 (2011) (accepted).